ANL-99/10

Chemical Technology Division

Annual Technical Report

1998

Applying Chemical Innovation to Environmental Problems

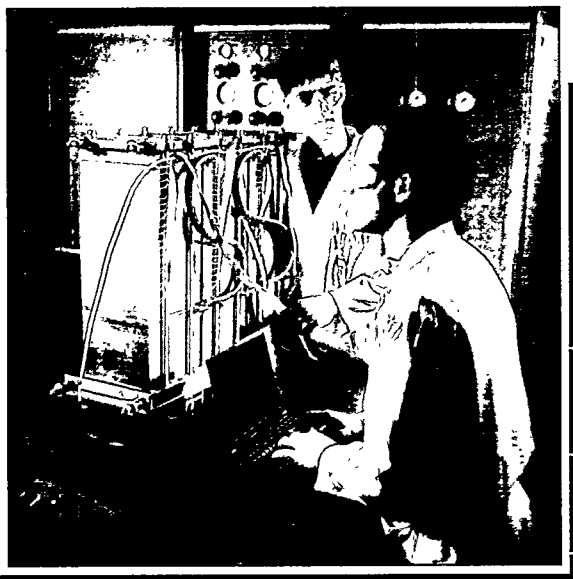

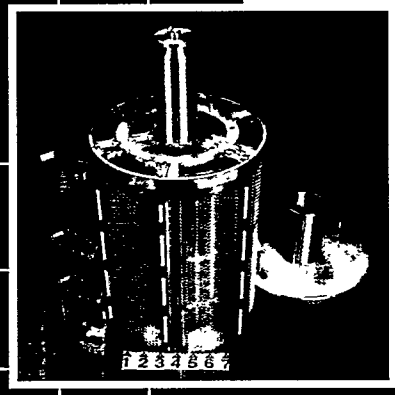

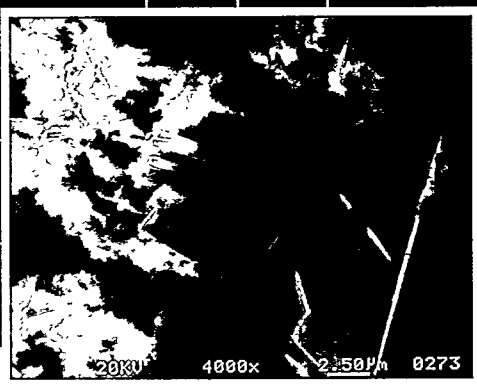

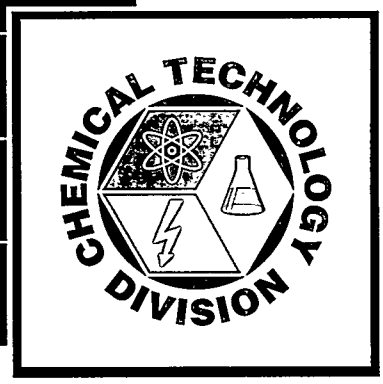

Argonne National Laboratory

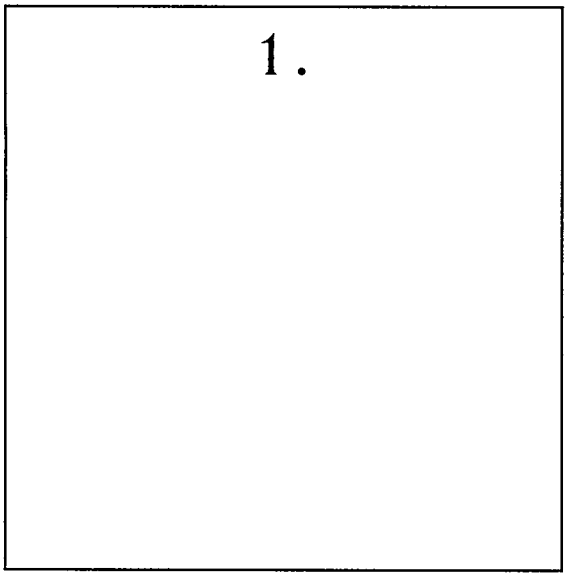

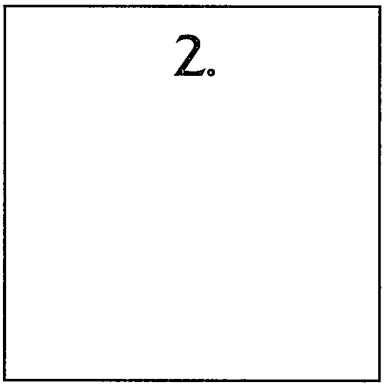

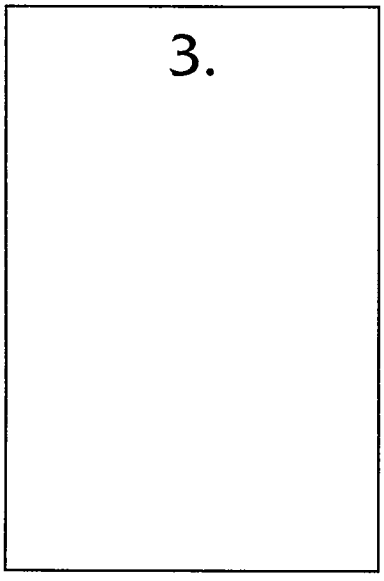

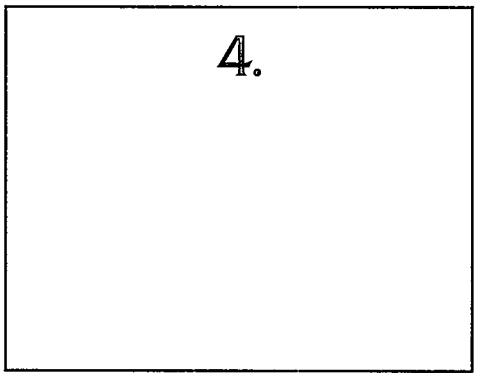

Cover Description

1. Polymer electrolyte fuel cell stack (30 kW) in facility for testing under simulated driving profile.
2. Anode assembly for high-throughput electrorefiner developed for electro-metallurgical treatment of spent nuclear fuel.
3. Environmental sample being prepared for analysis in the Analytical Chemistry Laboratory.
4. Electron micrograph of synthesized crystals that are analogues of the corrosion products formed on spent nuclear fuel exposed to repository-relevant conditions.

Disclaimer

Printed in the United States of America

This report has been reproduced from the best available copy.

Available to DOE and DOE contractors from the Office of Scientific and Technical Information
P.O. Box 62
Oak Ridge, TN 37831
Prices available from (423) 576-8401, FTS 626-8401

Available to the public from the National Technical Information Service
U.S. Department of Commerce
5285 Port Royal Road
Springfield, VA 22161

ANL-99/10

Argonne National Laboratory
9700 South Cass Avenue
Argonne, IL 60439

1998

Chemical Technology Division

Annual Technical Report

J. P. Ackerman — Division Director (Acting)
J. F. Miller — Electrochemical and Basic Science Department
R. E. Einziger — Waste Management Department
E. C. Gay — Nuclear Technology Department (Acting)
D. W. Green — Analytical Chemistry Laboratory

July 1999

TABLE OF CONTENTS

TABLE OF CONTENTS (contd)

TABLE OF CONTENTS (contd)

TABLE OF CONTENTS (contd)

TABLE OF CONTENTS (contd)

1998

Chemical Technology Division

Annual Technical Report

Abstract

The Chemical Technology (CMT) Division is a diverse technical organization with principal emphases in environmental management and development of advanced energy sources. The Division conducts research and development in three general areas: (1) development of advanced power sources for stationary and transportation applications and for consumer electronics, (2) management of high-level and low-level nuclear wastes and hazardous wastes, and (3) electrometallurgical treatment of spent nuclear fuel. The Division also performs basic research in catalytic chemistry involving molecular energy resources, mechanisms of ion transport in lithium battery electrolytes, and the chemistry of technology-relevant materials. In addition, the Division operates the Analytical Chemistry Laboratory, which conducts research in analytical chemistry and provides analytical services for programs at Argonne National Laboratory (ANL) and other organizations. Technical highlights of the Division's activities during 1998 are presented.

Summary

Electrochemical Technology

The CMT Division conducts research, development, engineering, and performance/life evaluation studies of advanced power sources for vehicle propulsion, utility load-leveling, and other energy storage applications. The Division is also responsible for the technical management of industrial contracts for the Department of Energy (DOE) related to the development of fuel cells for transportation applications.

During the past year, the in-house battery R&D has focused on the lithium-polymer and lithium-ion battery systems. Under the U.S. Advanced Battery Consortium (USABC) R&D program, the Division is working with 3M Corp. and Hydro-Québec to develop lithium-polymer batteries for transportation applications. These batteries show promise for meeting the demanding performance requirements of electric vehicles and operate at slightly elevated temperatures (typically 80°C). This effort involves engineering studies, development of electrode materials, and electrochemical characterization of electrodes, cells, and multicell modules.

In 1993, the Partnership for a New Generation Vehicle (PNGV) established a research program with the objective of developing an 80 mpg (34 km/L) passenger vehicle with negligible environmental emissions. A new CMT program was initiated late in 1998 to support this national program. The Division's role in this initiative is to assist DOE and its industrial battery developers in the development of lithium-ion batteries that meet the requirements of an energy storage device for hybrid vehicles. This multi-year program, being managed for DOE by ANL, will include contributions from several national laboratories (Sandia, Lawrence Berkeley, Idaho, and Brookhaven), as well as by the University of Michigan. Key elements of the program include the development of high-power lithium cells with reduced cost, improved calendar life, and abuse tolerance, as well as the development of diagnostic tools to better understand those parameters that currently limit life and abuse tolerance.

A materials research program on lithium batteries is being carried out to develop new and improved electrode materials for lithium-ion batteries. The current program is focused on the development of manganese oxide-based cathode materials as a replacement for the present $LiCoO_2$ cathodes. There are concerns about the use of $LiCoO_2$ because of its high cost and safety hazards. Promising performance has been obtained with composite $LiMnO_2$ structures. In the anode area, α-MnO_2 has shown promise as an alternative to the LiC_6 anodes currently being used. The driving force behind this work is enhanced safety for the lithium-ion battery.

The Electrochemical Analysis and Diagnostic Laboratory in CMT is used to conduct battery and fuel cell evaluations under simulated application conditions. Evaluations during 1998 have included the testing of (1) nickel/metal hydride deliverables from USABC cost reduction programs with GM-Ovonics and SAFT (France) and (2) electric-vehicle batteries from foreign manufacturers for the DOE. These evaluations are expected to continue through 1999. Also,

installation of the Fuel Cell Test Facility was completed during 1998, providing DOE with an independent source for validating the performance of fuel cell stacks (5-50 kW) fabricated by industrial developers. The facility is capable of controlling pressure, temperature, humidity, and flow rate of both the oxidant and fuel supply gas streams. The fuel supply can be either pure hydrogen or simulated reformate from liquid hydrocarbons.

Fuel cells convert chemical energy directly into electricity by electrochemical reaction, thereby eliminating the need for heat engines and rotating machinery. Since fuel cells have very low environmental emissions and high efficiency, interest in their development for stationary and transportation applications continues to grow. To aid in the development of polymer electrolyte fuel cells for transportation applications, CMT researchers are developing a compact, lightweight, fast-response fuel reformer that converts hydrocarbon fuels into a hydrogen-rich gaseous fuel. During the last year, we have developed new catalysts, for use in our partial oxidation reformer, that are fuel flexible. The catalyst has been demonstrated to work effectively in a micro-reactor with the following liquid fuels: methanol, ethanol, and methyl-tertiary-butyl ether, as well as retail gasoline and even diesel fuel. Experiments with this catalyst in an engineering-scale reactor verified its effectiveness with gasoline, which is the near-term fuel of choice for transportation. Additionally, the catalyst works effectively on natural gas, which is the residential fuel of choice.

One of the major contaminants in the reformed fuel is carbon monoxide, which must be reduced below 100 ppm to avoid significant degradation in fuel cell performance caused by poisoning of the platinum-based anode catalyst. The CMT researchers are studying several approaches for converting the CO to CO_2, via a water-gas shift reaction, and removing traces of CO by selective sorption/desorption. Significant advances were made in both areas. Plans include optimization of the sorbent support and dispersion process, followed by integration of the reformer, shift reactor, and CO sorber to demonstrate an integrated fuel processor.

A computer simulation model was developed for fuel cell systems operating in light-duty vehicles. Efforts this past year focused on efficiency trade-off studies for various system designs using gasoline as the fuel. The effects of cell voltage, excess fuel processor water, fuel utilization, reformer heat loss, and gross parasitic power (to operate ancillaries) were calculated for fuel cell systems that employed either a partial-oxidation reformer or a steam reformer. The results indicate a slight efficiency advantage for the system that uses the steam reformer. This model will be refined by (1) adding pressure drops and heat losses for the various components, (2) adding and refining component weights, volumes, and packaging, and (3) adding cost factors.

Efforts continue on developing molten carbonate fuel cells for utility applications. One problem area with this technology is segregation of the molten Li_2CO_3-K_2CO_3 electrolyte, caused by differences in the ionic mobility of Li^+ and K^+. The resulting compositional changes create variations in local melting points, increase cathode solubility, and cause reduced performance. This past year CMT developed electrolyte additives that lower the electrolyte melting point and maintain nonsegregating behavior. Additionally, this electrolyte enhances the performance of molten carbonate fuel cells. A second problem area with this technology is corrosion of the bipolar plates and current collectors. The corrosion behavior of various metal alloys is being determined to identify the best alloy to use for this application.

In the area of solid oxide fuel cells, CMT is performing research for Westinghouse Electric Corp. directed at enhancing the oxide ion conductivity of the $La_{0.8}Sr_{0.2}MnO_3$ ceramic electrolyte. Our approach is to substitute a trivalent element for the manganese, where the substituting element prefers a tetrahedral coordination to an octahedral coordination. Gallium has been shown to be an effective dopant at the 5 mol% level.

The Division continues to provide support to the DOE Office of Transportation Technologies and the DOE Office of Buildings Technology in the form of technical management of R&D contracts with industrial developers of fuel cells and related components. Major ongoing projects managed by CMT include DOE contracts with General Motors Corp., Ford Motor Co., Plug Power, Allied Signal Corp., Energy Partners, and 3M Corp., as well as several other fuel-cell component suppliers.

Waste Management

The primary CMT research in waste management involves the determination of the corrosion behavior of various nuclear waste forms in adverse atmospheres in support of disposal in approved repositories. This includes chemical and physical characterization, testing, and analyses of the results in terms of mechanisms of release. Qualification testing is being conducted on all the major waste forms intended for interment: DOE spent nuclear fuel, spent fuel from commercial light water reactors (LWRs), the ceramic waste form being developed for plutonium disposition, glasses developed for the Defense Waste Processing Facility (DWPF) and the West Valley Demonstration Project (WVDP), and the ceramic waste form resulting from the electrometallurical treatment of spent sodium-bonded fuel from Experimental Breeder Reactor-II (EBR-II). Besides the work on spent fuel and high-level waste, projects are also underway on characterization and testing of low-level waste and the behavior of actinide species in various subsurface environments. Several projects are applying techniques developed in the waste management efforts to new areas.

The DOE has over 200 types of spent fuel from a variety of testing programs and research reactors. These fuels have been divided into groups to facilitate degradation testing. Fuels from four of the major groups have been selected for testing at CMT: namely, N-Reactor fuel, mixed oxide fuel, UAl_x fuel, and graphite fuel. Of these groups, the mixed oxide and aluminum fuels have been characterized and are being tested. The N-Reactor and graphite fuels are expected to be received shortly for characterization and testing. The results of the tests will be compared with the release from LWR spent fuel to determine a relative source term. In a related effort, a nuclear magnetic resonance spectroscopy technique with a toroid cavity probe is being adapted to monitor DOE nuclear material in storage containers. In particular, the technique will provide an indication of the water left in a canister after drying and a measure of the evolution of hydrogen after long storage times. Understanding both of these effects is important for development of a safe storage and disposal system.

The license application will be prepared shortly for the candidate Yucca Mountain repository, which will be used primarily for disposing spent fuel from commercial reactors. Both long-term drip tests and vapor hydration tests are underway in support of that effort. In drip tests for up to 14 years, the uranium release from unirradiated UO_2 samples has been determined to be

rapid during the first one to two years of testing and to remain relatively low after that. Drip tests with nominal-burnup irradiated UO_2 fuels have been underway for nearly 5 years. It was found that several radionuclides in the fuel matrix (U, Np, and Pu) accumulate in the alteration phases on the fuel surface, whereas the technetium is highly soluble. Work has started on vapor tests with clad samples to determine if the alteration phases have the ability to split the cladding. High-burnup fuel has been received and characterized, and is being tested to determine if the altered structure of the fuel caused by prolonged irradiation will affect its dissolution properties. The results from the drip and vapor hydration tests are being incorporated into the performance assessment of the repository behavior.

The DOE is considering several alternatives for the disposal of excess plutonium resulting from the dismantlement of nuclear weapons. A ceramic waste form is one option. For this effort, CMT researchers are fabricating, characterizing, and testing a range of candidates for the ceramic waste form. Argonne was the first laboratory able to produce the waste form in quantity and has produced over 300 samples in the past year. Characterization has concentrated on the determination of the phases, structure, and oxidation states. Corrosion tests (MCC-1, product consistency, vapor hydration) with a Ba-Zr, zirconolite-rich ceramic indicated that the ceramic dissolved incongruently, and that the corrosion rate depends on the test duration and type. The test results will be used in development of a qualitative corrosion model. Other work includes determination of the effects of impurities and the presence of glass on the ceramic corrosion behavior.

Long-term drip tests are continuing with waste glasses representative of those that may be produced at DWPF. The data after nearly 13 years of testing indicate that insoluble elements, including U, Pu, and Am, are incorporated into alteration phases as the glass reacts and are subsequently released with particulate or colloidal matter as the alteration products spall from the glass. Recent trends have shown that the releases of Pu and Am, while initially quite low compared with those of soluble elements (such as B and Np), eventually are accelerated as the alteration phases spall from the glass surface and enter the test solution. Ultimately, the release of these actinides will be determined by the transport of the particulates suspended in solution. A long-term series of drip tests with a WVDP-type glass has indicated that actinides (except neptunium) are released from the glass primarily as solution-borne colloids and particulates when fresh glass is reacted. Pre-hydrated glass, however, rapidly released most elements (including actinides) when first exposed to dripping water.

A glass-bonded sodalite waste form is being proposed to immobilize salt wastes generated during the electrometallurgical treatment of EBR-II fuel. Preliminary testing is in progress to evaluate the response of this waste form in standard tests, determine the mechanisms of corrosion, obtain data to support mechanistic models of its corrosion behavior, and develop a method for monitoring the consistency of the waste form over the range of processing variables. Tests conducted to date suggest that the glass-bonded sodalite dissolves at a rate similar to high-level waste glasses in highly dilute solutions, but has a much lower solubility than waste glasses. Since the long-term durability is determined by solubility, it is expected that the glass-bonded sodalite will be at least as durable as waste glasses in a disposal system. Tests are in progress to determine the long-term durability of the glass-bonded sodalite waste form.

Fundamental studies on actinide behavior have concentrated on the interaction of subsurface microbes with the actinides, actinide stability and solubility in the Waste Isolation Pilot Plant (WIPP) environment, and actinide oxidation states in both the waste forms and alteration products. The microbe interaction with actinides was originally concentrated on the aerobic system but, this past year, was extended to anaerobic situations. The emphasis was on studying the fate of neptunium because its migration and release from waste sites could constitute a long-term health risk. Test results showed that the predominant oxidation state under biotic and abiotic conditions is Np(IV), suggesting that microbiologically reduced Fe(II) or Mn(II/III) may serve as the source of electrons for neptunium reduction. The studies of actinide stability and solubility in WIPP brine indicated that the lower oxidation states of plutonium will predominate under the conditions expected in WIPP. The Advanced Photon Source at Argonne is being used to determine the oxidation state and fate of actinides in both high-level and WIPP waste.

The DOE has contracted British Nuclear Fuels, Ltd. (BNFL), to vitrify tank wastes at the Hanford, Washington, site. Researchers in CMT are evaluating the durability of low-activity waste glasses being developed by BNFL in support of the performance assessment of the proposed low-level disposal system at Hanford. Also, CMT researchers have formulated and tested a standard material that will be used by DOE in acceptance testing of the waste products and are working with the American Society for Testing and Materials to develop standards for waste-form testing procedures.

Several projects are in the startup phase. Two initiatives are developing industrially important processes. In the first, CMT researchers are working with an Illinois startup company to develop means to produce medical implants containing radioactive tracers. This technique will allow more efficient delivery of the isotopes for treatment of prostate cancer with minimal damage to healthy tissue. For the second initiative, CMT researchers are seeking industrial partnerships for developing innovative rheological control aids for use in consumer goods such as paints, inks, and cosmetics.

Finally, techniques have been developed to model fluid flow in fractured media over long distances where the size of the fracture density varies over many orders of magnitude. These techniques may be applicable to vadose zone migrations under the Hanford tanks and elsewhere and to the modeling of the unsaturated zone in the Yucca Mountain repository.

Separation Science and Technology

The Division's R&D in separation science and technology is in three areas: (1) substitution of low-enriched for high-enriched uranium in the production of ^{99}Mo, (2) treatment of radioactive, mixed, and hazardous waste, and (3) novel applications of separation science to industrial processes.

The largest R&D effort presently being pursued is development of low-enriched uranium (LEU) targets and processing methods for production of ^{99}Mo to be used for medical applications. In this activity, CMT is participating in a program to convert all current processes, worldwide, from high- to low-enriched uranium. This international program involves ongoing

and new initiatives with partners in Indonesia, Canada, the United States, Korea, Australia, and Argentina. During 1998, the irradiation and processing of LEU metal-foil uranium targets were demonstrated in tests conducted in Indonesia with CMT participation. This was the first in a series of demonstrations before actual conversion can be undertaken. Now that the concept of a metal-foil target has been proven, activities are underway to design an economical, commercially viable target. During 1999, developing means to convert the Argentine process for ^{99}Mo production will be the primary activity of the effort.

The major activity in the waste treatment area involved R&D on solvent extraction processes for the cleanup of radioactive liquid waste. A solvent-extraction flowsheet for alkaline-side cesium-extraction (CSEX) was developed in cooperation with Oak Ridge National Laboratory, the Savannah River Technical Center, and the Savannah River Site. The CSEX process was then demonstrated in a 2-cm centrifugal contactor consisting of 24 stages. Because the process was not chosen by the Savannah River Site for further development, only minimal activities in this area are scheduled for 1999.

The magnetically assisted chemical separation (MACS) process developed in CMT provides an efficient and cost-effective way of removing radionuclides and hazardous components from a variety of waste streams. A significant effort is underway to apply MACS particles in diverse applications, including removal of ^{137}Cs from contaminated milk, removal of actinides from mixed waste streams, reduction of Fe and Cr in chrome plating baths, and decontamination of stainless steel components in the nuclear power industry. New avenues of development of MACS particles in 1999 are likely to include using them as radionuclide carriers in medical applications. In other separations work, a sol-gel technique is also being developed for treating solids in radioactive alkaline waste. The Division is also continuing its role as the chemical engineer for ANL Waste Management Operations and aiding them in deploying new operations.

Electrometallurgical Treatment Technology

The CMT Division is developing an electrometallurgical process for treatment of spent nuclear fuels. It is capable of handling most types of spent fuel and is especially intended for fuels at risk of chemical reaction with the groundwater in the repository. The central feature of the electrometallurgical treatment is electrorefining of the spent fuel in a molten salt electrolyte at 500°C. After electrorefining of the spent fuel, the fuel cladding and fission products are placed in two stable waste forms (one a ceramic, the other metal), which are suitable for disposal in a geologic repository. There are no other high-level wastes, and only negligible amounts of low-level waste are generated.

An effort has been underway to develop an advanced electrorefiner having high throughput (>40 kg uranium per hour) and large batch size (>100 kg) for treating large quantities of spent fuel. Effort this past year focused on testing a high-throughput electrorefiner with a diameter of 25 in. (0.6 m). The test samples were unirradiated N-reactor fuel elements (Zircaloy-clad uranium) from the Hanford site. Effort this past year was concentrated on testing a new design of scraper for removing uranium deposited on the electrorefiner cathode. In the improved scraper test, uranium was electrotransported from the anode baskets to the cathode tubes at

0.046 A/cm^2, which is twice the current density for sustained operation with the original cathode scrapers. Approximately 30 kg of uranium was anodically dissolved; no uranium holdup or stalling of the anode drive occurred, as had been the case in the past. The improved cathode scraper shows promise of achieving a throughput rate of 30 kg of uranium per day.

An electrorefining test was conducted with the anode-cathode module (ACM) for the Mark V electrorefiner, which will be used to treat the EBR-II blanket fuel at ANL-West. This test was terminated after 15,750 gross ampere-hours of current (electrodeposition plus stripping, where "electrodeposition" is the designation for electrotransport of uranium from the anode baskets to the cathode tubes, and "stripping" is the designation for electrotransport of uranium from the cathode tubes back to the anode baskets). For this test, the stripping current was only 30% of the gross ampere-hours. Sustained operation of the ACM was demonstrated at the rate needed to electrorefine a batch of EBR-II blanket fuel. The weight of cathode product collected during this test was 20 kg (about 16 kg of uranium). The morphology and density of the product are reported, as well as the uranium mass balance for the experiment. The results from this electrorefining test are being used to establish the operating procedure for the planned demonstration at ANL-West. Also, a promising method has been developed for the synthesis of the large quantity of UCl_3 needed for the demonstration of the Mark V electrorefiner. Other work in the past year included development of a flowsheet for the electrometallurgical treatment of aluminum-based fuel and a method for the bismuth-based reduction of Zircaloy-clad UO_2 fuel to metal.

Ceramic and metal waste forms are being developed to contain the high-level waste from the electrometallurgical treatment. In the metal waste form, those components of the high-level waste that are chemically unaffected by the electrometallurgical process—cladding hulls, zirconium alloying additions, and noble metal fission products—are combined with small amounts of particulate materials from electrolyte filters and melted to form a highly durable waste form. Work in the past year was done in support of the demonstration project with spent EBR-II fuel. The baseline metal waste form for this fuel is stainless steel-15 wt% zirconium (SS-15Zr). Synthesis and analysis of various SS-Zr compositions indicated that the SS-15Zr waste form can readily accommodate the noble metal fission products and actinides from the EBR-II fuel. However, fission-product rich phases may be present in alloys containing ≤5 wt% zirconium. The present emphasis is on the qualification of the metal waste form for geologic disposition. Some work is also being done in support of other aspects of the electrometallurgical treatment process, including development of crucible materials for fabrication of the metal waste form and for the uranium melting step.

The ceramic waste form contains the transuranic elements and the most easily oxidized fission products that accumulate in the electrorefiner salt. The reference ceramic waste form is a sodalite-glass composite. To develop coarse zeolites that would improve the flow properties of the raw materials and ease remote handling in the waste form fabrication, waste forms from several sieve cuts of ground zeolite pellet were prepared and tested. So far, they appear to be equivalent to forms made from finer zeolites. In a different set of experiments, representative ceramic waste forms were heated for several months (600°C in air) to determine the allowable long-term storage temperature; this temperature was found to be well above that anticipated in a geologic repository. The minimum acceptable level of glass binder in the waste form, the

minimum acceptable pressing temperature, and maximum allowable moisture levels in the zeolite raw material are also being determined. In support of the qualification of the ceramic waste form, CMT researchers have prepared test specimens of reference waste form containing nonradioactive fission product elements, and specimens containing uranium and/or plutonium. As part of advanced characterization efforts, CMT researchers have determined the corrosion behavior of actinide halides in the ceramic waste form, established an acceptable level of uranium in the waste salt, and showed that there is no need to limit the plutonium content of salt that is disposed of by blending with zeolite to make the ceramic waste form. As part of the process improvement efforts, CMT researchers are developing (1) a zeolite column that will concentrate waste radionuclides in the zeolite phase, thereby reducing the overall waste volume, and (2) a manufacturing method that simplifies fabrication, increases throughput, and decreases space and handling requirements.

Pyrochemical Process Applications

The electrometallurgical treatment of spent oxide fuel requires an initial step to convert the actinide oxides to the metallic form. The Division has developed a lithium reduction process to accomplish this. The process uses lithium dissolved in molten LiCl to reduce the actinide oxides to the corresponding metals, yielding Li_2O. The Li_2O is subsequently electrolytically decomposed to form lithium and oxygen in a salt-recovery step.

During the past year, work continued to develop both the reduction and the salt-recovery portions of the lithium reduction process, with an emphasis on process scaleup. Laboratory-scale experiments indicated that the reduction kinetics is affected by the ratio of the lithium source surface area to the salt volume and by the Li_2O concentration. These results will be used in optimizing the process. Preliminary experiments also indicated that SnO_2 could be used to replace the costly platinum now used as the anode material. Laboratory-scale experiments confirmed that the product from the reduction step, in crushed or clad pellet form, can be easily electrorefined.

An engineering-scale series of experiments is underway to obtain design information and operating experience needed for scaling up the reduction and salt-recovery steps to the plant size required for processing DOE oxide spent fuels. Three engineering-scale experiments of the reduction process were completed in the past year with kilogram quantities of UO_2. The results were very encouraging. In the first experiment, the reduction rate was determined to be similar to that in earlier laboratory-scale experiments. The reduction was essentially complete in 12-20 h. The next experiment employed the same fuel basket assembly (Mark V) currently employed for the electrometallurgical treatment of spent fuel at ANL-West. Reduction was essentially complete after about 78 h. This longer reduction time was attributed to the thickness of the insert for the Mark V basket. A modified insert design was tested in the next reduction experiment, and the reduction time was decreased to 25-30 h.

An engineering-scale experiment was also completed to test the salt-recovery step. In this experiment, the Li_2O concentration was reduced from 3 wt% to 1.8 wt%, slightly less than the starting value in the salt from the previous reduction experiment. The total time required for the salt recovery was 45 h, with 4400 Ah of charge passed. The lithium was recovered in a form

suitable for use in future reductions. The cell ran in a reliable manner, but the calculated current efficiency, 30%, was significantly lower than the 50-80% obtained in laboratory-scale experiments.

In support of design work being performed on the pilot-scale reduction facility planned for ANL-West, a series of tests was performed to evaluate the corrosion resistance of candidate materials for the reduction and electrowinning vessels. Test coupons included tantalum, various stainless steels, and 2¼ Cr-1Mo. In the tests under reduction conditions for 30 days at 725°C, the tantalum suffered minor attack, while none of the other test coupons had any measurable corrosion. For the electrowinning conditions, all coupons were severely corroded. Followup tests with a wide variety of alloys tested under less severe electrowinning conditions for 6 days at 650°C showed Inconel 600 to be the most corrosion resistant.

Basic Chemistry Research

Basic chemistry research is being pursued on fundamental issues that relate to homogeneous and heterogeneous catalysis, ion transport mechanisms in electrochemical devices, high-critical-temperature superconductivity, and the decontamination of radioisotope-impregnated materials.

The research on homogeneous catalysis includes (1) *in situ* spectroscopic investigations of the chemistry associated with the conversion of some key industrial homogeneous processes to more energy efficient and more environmentally benign supercritical ones, and (2) the synthesis of extremely electrophilic polyfluorinated metallophthalocyanine catalysts and the exploration of their chemistry at extreme conditions of temperature and pressure to achieve the controlled functionalization of methane and other hydrocarbons.

The various processes designed to achieve the commercial hydroformylation of olefins comprise the largest scale use of homogeneous catalysts and are the subject of the program's current efforts in supercritical fluid catalysis. During the past year, the $HCo(CO)_4$-catalyzed hydrogenation of carbon monoxide was conducted in a supercritical fluid for the first time. Reaction rates measured in supercritical carbon monoxide using a toroid-pressure probe agreed well with earlier autoclave measurements for liquid-heptane solutions.

Research in hydrocarbon activation is underway with the goal of achieving the controlled catalytic functionalization of methane and other hydrocarbons via activation of their C-H bonds. Current research focuses on developing catalytic strategies based on the extremely robust phthalocyanine nucleus. During the past year, nuclear magnetic resonance structural studies were used to show that the reductions of several highly fluorinated metallophthalocyanine catalysts involved addition of electrons predominantly to the ligand and much less so to the metal center.

An advanced battery project is in progress to investigate the mechanism(s) of ion transport in lithium-polymer electrolyte battery materials. Research in this area in the past year has focused on using a new *in situ* magnetic resonance imager developed in the catalysis research to investigate the ^7Li quadrupolar interaction in a polymer electrolyte composed of $LiN(SO_2CF_3)_2$ dissolved in polyethylene oxide. Although the quadrupole interaction also manifests itself along

the chemical shift dimension, the spectral features that are produced by this interaction are distinct from those produced by chemical shielding and provide unique information about the local electrostatic environment of the ^{7}Li nuclei. The ability of the near-electrode imager to detect a quadrupole powder pattern makes it possible to investigate the spatial distribution in an electrochemical cell of lithium ions that are contained in crystalline or amorphous phases. The distribution of these phases in the electrochemical cell is of importance because it has been determined that only the amorphous phase is conductive.

A new program within CMT has been initiated with the objective of developing heterogeneous catalysts for the selective desulfurization of diesel fuel and the etherification of synfuel-derived phenolics. The latter effort is being directed toward formulating, evaluating, and establishing catalytic solids that promote the etherification of alkyl hydroxyl groups with alcohols.

Other basic chemistry research projects in CMT are addressing forefront issues in energy and environmental science that relate to electric power technology and the decommissioning and decontamination of nuclear facilities. In the area of electric power technology, we are continuing to explore novel processing methods for improving the performance of high-critical-temperature superconducting (HTS) ceramics. Our efforts are focused on the silver-sheathed $(Bi,Pb)_2Sr_2Ca_2Cu_3O_x$ (Ag/Bi-2223) composite superconductor, the leading HTS embodiment for high current applications. In the past year we have completed research that has shed new light on phase evolution and microstructure development in Ag/Bi-2223 composites during thermal processing to form the Bi-2223 phase. The influence of oxygen pressure, temperature, processing time, and HTS filament dimensions/architecture has been correlated with current-carrying capacity. A controlled-environment scanning electron microscope has been used to perform *in situ* examinations of the Bi-2223 microstructure during heat treatment. The analysis results have provided graphic visual evidence of important process-relevant phenomena for which only indirect speculative evidence had heretofore been reported. Also, in the course of the work on HTS materials, CMT researchers have pioneered the exploitation of Raman microspectroscopy and imaging Raman microscopy as tools for the identification and spatial mapping of all the important chemical phases in HTS materials.

Work in the area of radionuclide decontamination research is aimed at developing a detailed understanding of the mechanism(s) by which radioactive elements and heavy metal contaminants are incorporated into the surfaces of common construction materials. Synchrotron-based X-ray absorption spectroscopy methods are being used to investigate the structure of Cr and U complexation in passive films on nickel. Oxidation states and coordination geometry, including the near-neighbor elements bonded to each metal, have been determined. These results are providing important insights concerning the leachability of hazardous metals from surface films and the types of decontamination methods that are likely to be effective for removal of specific surface contaminants.

Analytical Chemistry Laboratory

The Analytical Chemistry Laboratory (ACL) is administratively within CMT, its principal client, but collaborates as a full-cost-recovery service center with many technical divisions and

programs at ANL. In addition, the ACL conducts research in analytical chemistry and provides analytical services for governmental, educational, and industrial organizations.

During the past year, ACL was involved in a diverse array of analytical activities. These included analyses in support of the Argonne projects to develop an electrometallurgical treatment for spent nuclear fuels; chemical analyses of samples retrieved from a simulated reactor accident; determination of leach resistance in samples being tested for use as phosphate-ceramic-stabilized hazardous waste; analysis of lithium aluminate prepared for use in tritium production targets, as well as development of improved methods for this analysis; participation in a comprehensive program to provide DOE with information on data quality from laboratories analyzing environmental and waste samples; preparation and characterization of simulated waste samples in support of the Waste Isolation Pilot Plant; support in construction of a mobile laboratory for analysis of soil contaminated with volatile organic compounds at Argonne; characterization of high-temperature superconducting samples; characterization of residues from pitchblende ore processed to extract uranium at a weapons production site; development of automated methods for real-time analysis of chemical sensor data from environmental samples; preparation of osmium-189 targets for photon excitation studies; analysis of environmental samples submitted for the determination of hazardous or radiological components; characterization of particulate debris in the cooling system of a commercial nuclear reactor; and identification of volatile and semivolatile byproducts produced by top-of-rail lubricants.

I

Electrochemical Technology

The ANL Electrochemical Technology Program in CMT undertakes (1) in-house research, development, testing, post-test analysis, and technical evaluation studies of advanced battery and fuel cell systems and (2) support research, technology transfer, and technical management for industrial R&D contracts to develop these systems. During the past year, in-house battery R&D has focused on lithium-polymer and lithium-ion systems. The testing, evaluation, and post-test analysis of a variety of advanced batteries fabricated by industrial firms are performed in CMT's Electrochemical Analysis and Diagnostics Laboratory. Potential uses of these battery systems include vehicle propulsion, utility load-leveling, and other energy storage applications. In-house R&D is also being conducted on fuel cells, where the CMT Division continues to be the premier DOE laboratory in fuel-cell technology development. We are engaged in R&D on the solid oxide fuel cell and the molten carbonate fuel cell, which are targeted for utility applications, and we are heavily involved with fuel processing development for the polymer electrolyte fuel cell for transportation applications.

A. Advanced Battery Research and Development

The advanced battery program in CMT is involved in the development of the lithium-polymer battery for electric vehicles, the lithium-ion battery for hybrid vehicles, and new materials for electric- and hybrid-vehicle batteries, as well as batteries for consumer products such as laptop computers and cellular phones. This program uses a complementary experimental and theoretical approach to study the structures and electrochemical properties of various electrode materials for nonaqueous lithium batteries.

1. Lithium-Polymer Electrolyte System

The lithium-polymer battery (LPB) is a lightweight, high-energy system that can operate at moderate temperatures (typically 60-80°C). With a polymer electrolyte, this all-solid-state battery can be manufactured using high-speed film-laminate technology. The battery's low

weight translates into high specific energy. The Li/Li^+ redox reaction (negative electrode, -3.0 V) gives the battery its high power. The positive electrode is a reversible chemical host for intercalating lithium cations. Thus, during discharge, the lithium cations insert into the host material with simultaneous electrochemical reduction of the host's closest-neighbor redox sites. The host structure is highly reversible to both redox and insertion reactions; this allows the lithium cations to exit upon recharge.

The LPB for electric-vehicle applications is being developed under a Cooperative Research and Development Agreement (CRADA) with 3M Corp. and Hydro-Québec. Under the CRADA, Argonne presently provides technical support in three main areas: electrochemical characterization and modeling, testing and evaluation of prototype cells and multicell modules, and development of alternative electrode materials.

a. Electrochemical Characterization and Modeling

Electrochemical modeling of lithium-polymer cells is being conducted to elucidate the phenomena occurring in the cells during operation. This work involves simultaneously solving differential mass, charge, energy, and momentum equations on every species in each phase and component of the fundamental electrochemical cell. The time constant for the lithium transport in lithium-polymer cells is relatively large when compared to liquid-electrolyte battery systems. This is a result of the slow ionic transport in the polymer electrolyte and the positive active material. These phenomena are difficult to separate and examine experimentally because of the composite positive-electrode structure—containing carbon, electrolyte, and active material—and the thin cell geometry.

The electrochemical model developed in this effort has been very effective in identifying the limitations of the lithium-polymer cell, particularly, the metal-oxide active material for the positive electrodes. To date, this model is the only available tool with which one can effectively examine concentration, potential, and current distributions in the cell. The flexibility, quality, and reliability of the model have continued to be improved, and the resulting model has provided insights into cell operation. During the past year, work concentrated on improving the oxide diffusion section of the model and examining surface potentials in the metal-oxide positive electrode at high currents near the end of discharge. Also, an improved set of transport parameters for the electrolyte was developed and integrated into the model. Recently, the model has been used to examine concentration, potential, and current distributions in the cell during simulated driving profiles, such as the Dynamic Stress Test (DST).

Testing and characterization of individual cell components and full cells are carried out using various electrochemical techniques, such as DC methods (e.g., constant current or power discharge, peak power measurements, and current interruptions), and variable power studies, such as the DST and AC impedance methods. The purpose is to develop a better understanding of the cell characteristics and to provide the critical information needed to focus the future research efforts on improving and optimizing the LPB performance. In addition, thermal effects during the operation of lithium-polymer cells are being examined through electrochemical microcalorimetry studies. This work has provided simultaneous thermal and electrochemical information on the cells that is highly accurate.

b. Prototype Testing and Evaluation

Argonne provides 3M and Hydro-Québec with high-quality, reliable, and independent testing of full-size prototype cells and multicell modules. Efforts during this last year concentrated on testing LPB modules, one of which is shown in Fig. I-1. Modules like this one will eventually make up an electric-vehicle battery pack (16 modules/pack), which will also be tested at ANL.

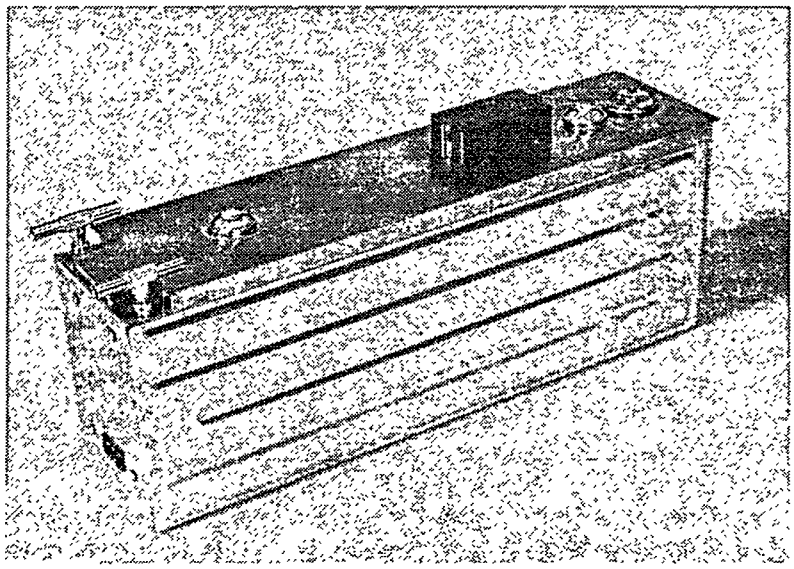

Fig. I-1. Lithium-Polymer Battery Module for Electric Vehicles

The prototypes are tested under a rigorous set of conditions intended to evaluate their performance under simulated electric-vehicle operation. An example is the DST discharge shown in Fig. I-2, which was obtained with a 95-Ah module containing a positive electrode material developed at ANL. The testing protocols are established by Hydro-Québec and 3M, and they generally follow test procedures established by the U.S. Advanced Battery Consortium. The protocols are designed to examine all aspects of electrochemical performance, including cycle life and peak power evaluations. The test results contribute to a statistical data base on the present LPB technology.

c. Development of Electrode Materials

Work continues on improving the LPB technology. Rechargeable lithium batteries with either metallic lithium or lithium carbon as the negative electrode use transition metal oxides as the positive electrode, for example, oxides of V, Mn, Co, or Ni. These transition metal oxide electrodes have host structures into which lithium can be inserted during electrochemical discharge; the insertion of lithium is accompanied by a concomitant reduction of the transition metal ion. The reverse process occurs during charge.

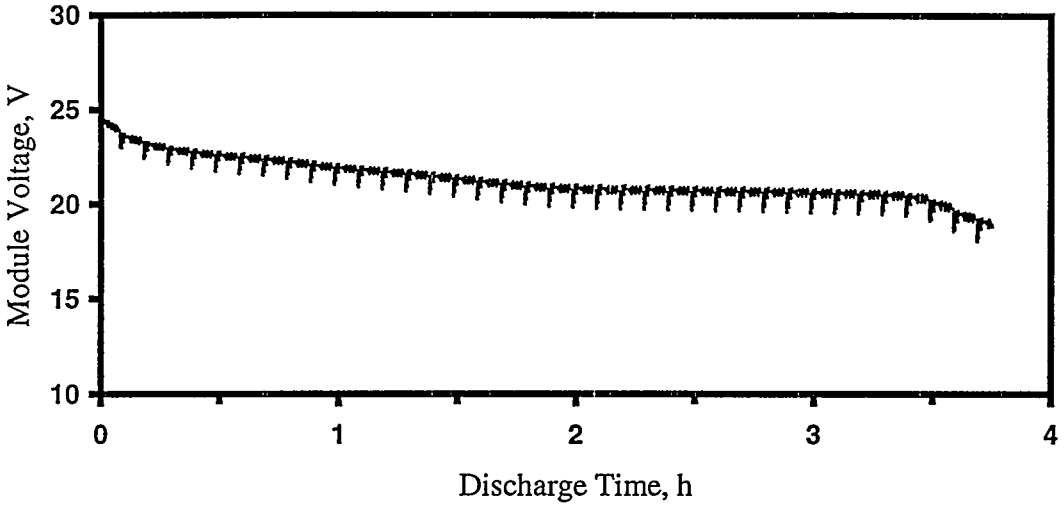

Fig. I-2. Discharge Characteristics of 95-Ah Lithium-Polymer Battery Module under Dynamic Stress Test to 80% Depth of Discharge

Materials development within the LPB project is focused on the synthesis and characterization of metal oxide electrodes that offer superior electrochemical behavior to state-of-the-art materials. Emphasis is placed on the structural stability of the host electrode to the repeated insertion and extraction of lithium because it is undoubtedly one of the key properties for ensuring that a lithium cell operates with good electrochemical efficiency and cycle life. In transition metal oxides, both stability of the oxygen-ion array and minimum displacements of the transition metal cations in the host are required to ensure good reversibility. Also, structures of transition metal oxide insertion electrodes are, in general, not tolerant to overcharge or overdischarge. It is, therefore, critically important to carefully control fabrication conditions so that the composition of the electrode corresponds to that of the most stable host structure of the metal oxide system. Furthermore, cell operating conditions, such as voltage limits and current drain, must be carefully controlled to ensure that the structural integrity of the electrodes is not destroyed on cycling. Results from this project will be reported at a later date.

2. *High-Power Lithium-Ion Battery System*

The lithium-ion battery operates at room temperature and is receiving increased attention as a power supply for consumer electronics and, in the longer term, for electric and hybrid vehicles. Because these batteries possess high specific energy (>100 Wh/kg) and offer the potential for high power (>1000 W/kg), they are attractive as energy storage devices for hybrid vehicles.

The DOE Partnership for a New Generation Vehicle (PNGV) has established a research program with the objective of developing an 80 mpg (34 km/L) passenger vehicle with negligible environmental emissions. The PNGV is focusing its R&D efforts on hybrid vehicles that employ high-power lithium-ion batteries to meet its energy storage requirements for leveling the load on the prime power source and for capturing regenerative braking energy. The PNGV is sponsoring

industrial R&D projects on this technology with SAFT America, Varta Batteries Ltd., and PolyStor Corp. The industrial developers have demonstrated that the lithium-ion battery is capable of meeting the performance and cycle-life requirements for this application, but barriers to commercialization remain in the areas of calendar life, abuse tolerance, and cost. To reduce the R&D risk associated with overcoming these barriers, DOE's Office of Advanced Automotive Technologies has collaborated with the PNGV to establish a technical support program at DOE laboratories. This program is called the Advanced Technology Development (ATD) Program, and DOE has selected ANL to manage the effort.

The ATD Program has two major objectives. First is to develop and demonstrate the application of national laboratory diagnostic tools to identify factors that limit calendar life and abuse tolerance for the lithium-ion battery technology, with a view to assisting in the development of practical solutions. Second is to reduce cell costs. This program has five projects. Two projects focus on the development, characterization, and initial demonstration of diagnostic tools. These tools will be tested with commercial lithium-ion cells from Sony Corp. and ANL baseline cells that employ commercially available materials (Gen 1). These cells are considered 18650 type because they are 18 mm in diameter and 65 mm long. They have an output voltage of 3.7 V, the same as three nickel-cadmium or nickel/metal hydride cells connected electrically in series. The first major goal is to provide the PNGV industrial developers with an initial demonstration of the application of the diagnostic tools by November 1999. Two other projects involve sequential iterations on the baseline cell technology (Gen 2 and Gen 3) that incorporate feedback from the earlier diagnostic evaluations, with the aim of providing further validation of the diagnostic tools. Additionally, development of lower cost materials and processing is a secondary goal for the Gen 2 and Gen 3 cell. A fifth project targets the development of novel approaches for reducing the costs associated with the packaging of full-size lithium cells.

As the first step in developing Gen 1 cells, ANL has screened a variety of electrode active materials, electrode additives, electrode binders, and current collection designs to arrive at a cell that possesses reasonably high power capability. Six candidates for the positive electrode materials ($LiNi_{0.8}Co_{0.2}O_2$) and four candidates for the negative electrode materials (graphites) were screened. All materials considered had to possess a relatively small particle size to be used in making these thin-film, high-power electrodes. Each positive and negative electrode material was characterized in terms of its particle size and shape, surface area, capacity density (mAh/g) with regard to reversible and irreversible lithium insertion, rate capability as a function of depth of discharge, and thermochemical stability with the electrode at both 50 and 100% states of charge. Figure I-3 illustrates the relative quantities of heat generated, as determined by differential scanning calorimetry, from two of the positive electrode materials in contact with an electrolyte of 1 M $LiPF_6$ in ethylene carbonate (EC) and diethyl carbonate (DEC). The exotherm of the Sumitomo material is considerably smaller in magnitude and occurs at a slightly higher temperature than the alternative material, indicating that it possesses enhanced thermochemical stability. Also, the positive electrode materials were blended with additives and binders to achieve optimal combinations of high-rate performance and thermochemical stability. The optimal blend was determined to be Sumitomo material with 4 wt% acetylene black, 4 wt% SF6-6 graphite, and 8 wt% polyvinylidene fluoride (PVDF) binder. Similar studies led to an anode containing MCMB-6 graphite blended with a second graphite and PVDF binder.

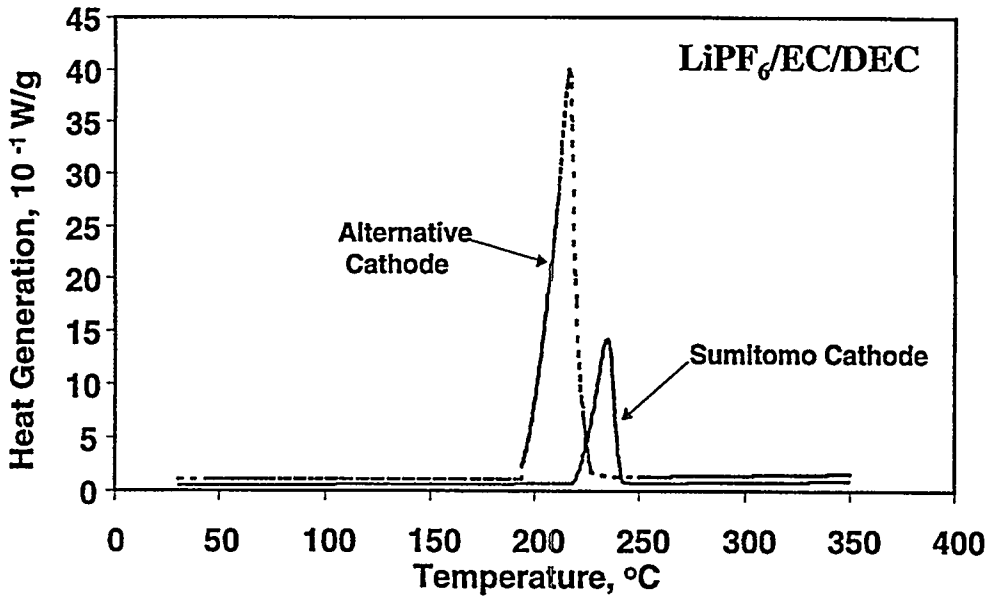

Fig. I-3. Differential Scanning Calorimetry Data on Two $LiNi_{0.8}Co_{0.2}O_2$ Positive Electrode Materials Lithiated to 50% State of Charge. Materials in contact with 1 M $LiPF_6$ in EC/DEC (1:1 ratio) electrolyte.

Argonne is working with PolyStor Corp. (an industrial manufacturer of lithium-ion cells) to incorporate the proposed cell chemistry and design into high-power 18650 cells. PolyStor will build and supply 300 cells, incorporating the Gen 1 chemistry, and DOE laboratories will characterize their performance, tolerance to thermal abuse, and life (cycle and calendar) at elevated temperatures (50-60°C). Gen 1 cells at the beginning, middle, and end of life, as well as thermally abused cells, will be subjected to tests to determine the most useful diagnostic tools for identifying the factors that limit the abuse tolerance and calendar life of this technology. Additionally, PolyStor will supply positive and negative electrode laminates, which will be used in diagnostic tests that do not permit the use of 18650 cells.

Results of these studies on Gen 1 cells will be shared with domestic developers of lithium-ion cells so that they will become thoroughly informed about the practical application of these diagnostic tools to the resolution of technical barriers for their own lithium-ion cell technology. The results of the studies on Gen 1 cells will be used to refine the technology that goes into Gen 2 and Gen 3 cells and to provide further validation of the diagnostic tools. Gen 2 and Gen 3 cells will undergo similar characterization and diagnostic evaluations, and the results of these studies will again be shared with the industrial development community. At any point in this process, the industrial developers can negotiate with individual national laboratories to employ selected diagnostic tools to help identify and understand limiting factors with their specific lithium-ion cell chemistry, under proprietary agreements.

3. Materials Research

The objective of this effort is to find and develop new or improved electrode materials for a variety of rechargeable lithium battery systems. Over the past year, the research at ANL has focused on the manganese oxide positive electrode and titanium oxide negative electrode. The driving force behind this work is achieving enhanced safety and lower costs for lithium batteries.

a. Manganese Oxide Materials

To achieve a good cycle life in lithium-ion cells, both positive and negative insertion (host) electrodes must maintain their structural integrity when cycled over a wide compositional range. Host electrodes with cubic symmetry that can "breathe" isotropically during lithium insertion and extraction with minimal volume expansion provide structures that can withstand many discharge and charge cycles.[1] One of the best host structures is the lithium titanium oxide spinel, $Li_4Ti_5O_{12}$, which can accommodate three lithium ions per formula unit without any significant lattice expansion.[2] This material can be cycled hundreds of times without structural decay and is discussed further in Sec. I.A.3.b.

The cubic spinel $Li[Mn_2]O_4$ is a cathode material of interest for both 3-V and 4-V lithium batteries. For lithium insertion, i.e., over the range $1 \leq x \leq 2$ in $Li_x[Mn_2]O_4$, the electrode operates at 3 V vs. metallic lithium, whereas lithium extraction occurs over the range $0<x<1$ at 4 V.[3] The reactions emphasize the stability of the stoichiometric $A[B_2]O_4$ spinel composition: (1) lithium insertion causes an immediate first-order transition in which the tetrahedral-site lithium ions are displaced into neighboring octahedral sites to change the structure type, in a two-phase reaction, from spinel to a rock-salt phase $Li_2[Mn_2]O_4$; (2) lithium extraction requires a high potential; and (3) the reaction creates a metastable, defect spinel structure with high chemical activity (reduction potential). The stability of the stoichiometric spinel composition $Li[Mn_2]O_4$ is, perhaps, not surprising because the spinel structure occurs in nature as the prototypic mineral *spinel*, $Mg[Al_2]O_4$, which is extremely stable and has gem-like qualities. In the $Li_x[Mn_2]O_4$ system, the electrochemical reaction at 4 V provides good charge/discharge cycling behavior because the crystal structure remains cubic over the whole range $0<x<1$, whereas the reaction at 3 V induces a distortion in the lithiated spinel structure that reduces the crystallographic symmetry from cubic in $Li[Mn_2]O_4$ to tetragonal in the rock-salt phase $Li_2[Mn_2]O_4$. Such a severe change in the lattice parameter ratio is too large for the spinel electrode particles to maintain their structural integrity on cycling.[1] Recent data obtained at ANL have shown that improved cycling over the 3- and 4-V plateaus can be achieved by using composite structures rather than single-phase $Li_x[Mn_2]O_4$ spinel materials, as shown by the voltage vs. capacity plots.

The stability of the stoichiometric spinel structure is manifest by the fact that many Li-Mn-O compounds with Li:Mn ratios varying between 1:2 and 4:5 transform to a spinel structure either on heating or during electrochemical reactions. For example, orthorhombic-

[1] M. M. Thackeray, *J. Electrochem. Soc.* **142**, 2558 (1995).

[2] K. M. Colbow, J. R. Dahn, and R. R. Haering, *J. Power Sources* **26**, 397-402 (1989).

[3] M. M. Thackeray, *Prog. Solid State Chem.* **25**, 1 (1997).

$LiMnO_2$ and layered-$LiMnO_2$ structures are unstable to lithium extraction and electrochemical cycling.[4] Our electron diffraction (and X-ray diffraction) analyses of cycled electrodes have shown that these materials transform to spinel-type structures (Fig. I-4). These structures show superior cycling behavior when cycled over both the 3- and 4-V plateaus, compared to the standard spinel $Li[Mn_2]O_4$ (Fig. I-5). Lattice images of cycled electrodes indicated that the increased stability to cycling over a wide voltage window may be attributed to a composite matrix consisting of spinel domains intergrown with the residual orthorhombic- or layered-$LiMnO_2$ structures. The electrochemical stability at 3 V suggests that the transformations of these $LiMnO_2$ structures do not lead to spinel domains with the ideal $[Mn_2]O_4$ spinel framework, but rather to spinel domains having a $[Mn_{2-x}Li_x]O_4$ framework within the spinel system $Li_{1+x}Mn_{2-x}O_4$ ($0 < x \leq 0.33$); such frameworks are known to display superior cycling behavior at 3 V compared to standard $Li[Mn_2]O_4$.[3] It is known that cation substitution into the spinel

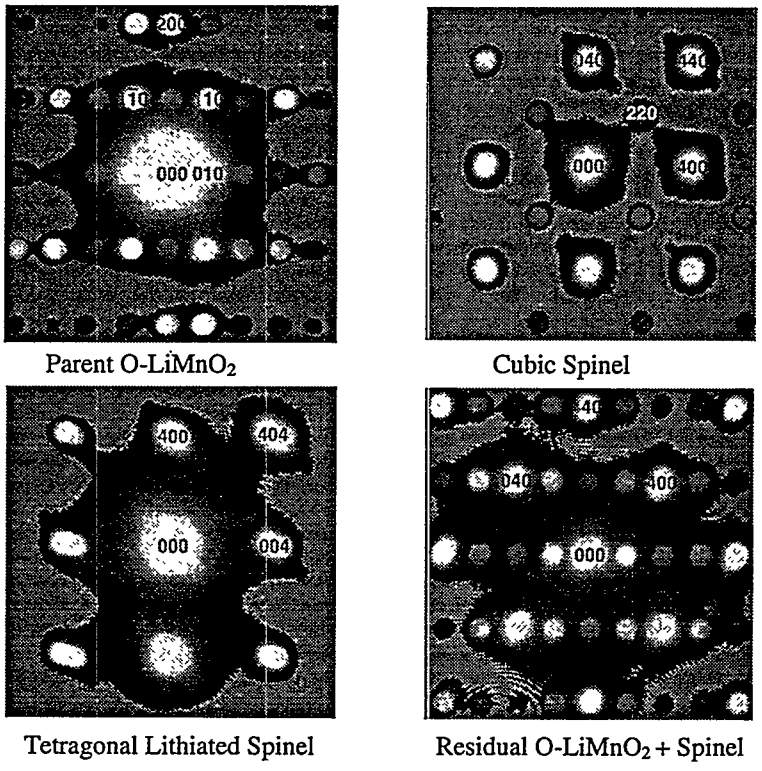

Fig. I-4. Electron Diffraction Patterns of Parent Orthorhombic-$LiMnO_2$ Crystallite, Cubic Spinel Derived Electrochemically at 4 V, Tetragonal Spinel Derived Electrochemically at 3 V, and Oriented Crystallite from a Cycled Electrode Showing Diffraction Spots Coincident with Residual Orthorhombic-$LiMnO_2$ Component and a Spinel Component. (All projections along 001 zone axes.)

[4] R. J. Gummow and M. M. Thackeray, *J. Electrochem. Soc.* **141**, 1178-1182 (1994); A. R. Armstrong and P. G. Bruce, *Nature* **381**, 499-500 (1996); F. Capitaine, P. Gravereau, and C. Delmas, *Solid State Ionics* **89**, 197-202 (1996); G. Vitins and K. West, *J. Electrochem. Soc.* **144**, 2587-2592 (1997).

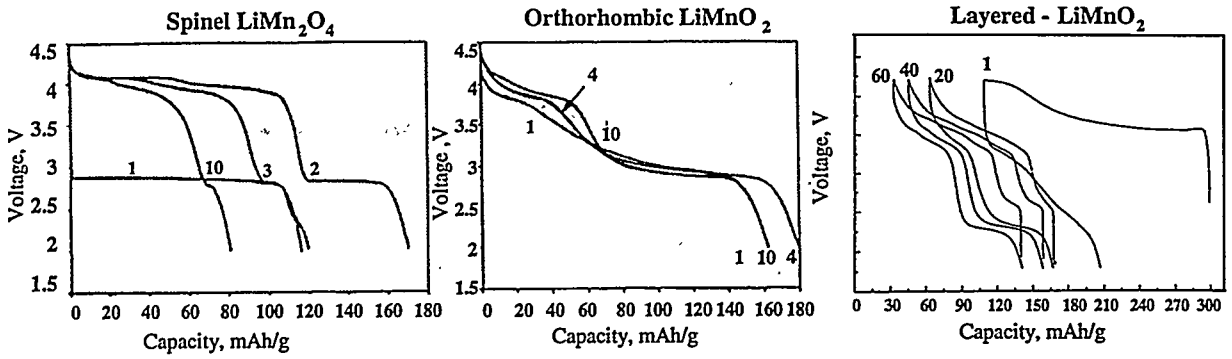

Fig. I-5. Cycling Behavior over the 3- and 4-V Plateaus of Spinel $Li_x[Mn_2]O_4$, Orthorhombic-$LiMnO_2$, and Layered $LiMnO_2$

structures $Li[Mn_{2-x}M_x]O_4$ (e.g., M = Li, Co, Ni) can also increase the stability of a pure spinel electrode to cycling over both 3- and 4-V regions. Future work will investigate substituted orthorhombic-$LiMnO_2$ and layered-$LiMnO_2$ structures and will evaluate the electrochemical behavior of these substituted materials.

b. Titanium Oxide Materials

Lithium titanium oxides, such as the spinel phase $Li_4Ti_5O_{12}$ and the ramsdellite phase $Li_2Ti_3O_7$, have been investigated in the past as possible insertion electrodes for lithium batteries.[2,5] The spinel phase is of particular interest because three lithium ions can be inserted reversibly into the $Li_4Ti_5O_{12}$ structure at 1.5 V vs. metallic lithium.[2,5] When coupled with $LiMn_2O_4$ or $LiCo_{1-x}Ni_xO_2$ positive electrodes that offer ~4 V vs. lithium, $Li_4Ti_5O_{12}$ can be used effectively as a negative electrode to provide a 2.5-V cell. Although $Li_4Ti_5O_{12}$ shows excellent reversibility and stability to lithium insertion/extraction, it has a relatively low theoretical capacity (175 mAh/g) compared with TiO_2 (335 mAh/g). The application of TiO_2 compounds as electrode materials, such as rutile, anatase, and the spinel $LiTi_2O_4$ (which reaches a TiO_2 stoichiometry on complete extraction of lithium), has been limited either by their inability to accommodate much lithium or by structural instability to lithium insertion/extraction reactions.[6,7] Also known to exist is TiO_2 with a hollandite-type structure. This compound is normally stabilized by large cations, such as potassium, in the (2 x 2) channels of the structure, as is also the case for the mineral *hollandite* ($Ba_xMn_8O_{16}$). These large cations restrict lithium diffusion within the hollandite structure, thereby limiting their usefulness as insertion electrodes. The stabilizing cations can be removed from the hollandite-TiO_2 structure by acid treatment or by reaction with hydrogen peroxide. Recently, we demonstrated that an isostructural α-MnO_2 material could be synthesized without any stabilizing cation, and that H_2O or Li_2O molecules could be introduced into the (2 x 2) channels of the structure instead. The lithia-stabilized compound, $0.15Li_2O{\cdot}MnO_2$, in particular, has shown promising electrochemical behavior; it can provide a rechargeable capacity of approximately 180 mAh/g for many tens of cycles. The

[5] E. Ferg, R. J. Gummow, A. de Kock, and M. M. Thackeray, *J. Electrochem. Soc.* **141**, L147 (1994).

[6] M. E. Arroyo y de Dompablo, E. Morán, A. Várez, and F. García-Alvarado, *Mater. Res. Bull.* **32**, 993 (1997).

[7] Y. Yagi, M. Hibino, and T. Kudo, *J. Electrochem. Soc.* **144**, 4208 (1997).

possibility of using a hollandite-type TiO_2 structure without any large stabilizing cation within the (2 x 2) channels has, therefore, been explored in an attempt to find an electrode with a higher electrochemical capacity than the spinel $Li_4Ti_5O_{12}$.

Neutron-diffraction data showed that an acid-leached K_xTiO_2 sample contained a minimal amount of potassium (<0.02 K^+ per TiO_2 unit), in agreement with X-ray diffraction data and an energy dispersive X-ray analysis of the sample. The structure of the TiO_2 phase with empty (2 x 2) channels is shown in Fig. I-6a; it is stable in air. Neutron diffraction analysis of a sample with a small amount of inserted lithium, $Li_{0.125}TiO_2$, showed that the lithium ions were disordered over crystallographically equivalent sites in the (2 x 2) channels and coordinated in a distorted tetrahedral arrangement to the oxygen ions at the corners of the channels (Fig. I-6b). Although such structures will probably not exhibit long-range order, a superstructure or a deviation from the tetragonal symmetry of the parent unit cell could not be detected. A more highly lithiated sample of composition $Li_{0.57}TiO_2$ showed monoclinic symmetry; the decrease in symmetry can be attributed to a structural distortion in response to coulombic interactions between the inserted lithium ions in the (2 x 2) channels, as shown in Fig. I-6b. Highly lithiated samples were unstable, particularly when exposed to air; this structural instability has prevented a detailed structure analysis of these samples by neutron diffraction. Nevertheless, we have been able to demonstrate that lithium can be extracted chemically by water-washing or by treatment with bromine in a nonaqueous solvent from freshly prepared samples of $Li_{0.57}TiO_2$ to yield the original TiO_2 phase.

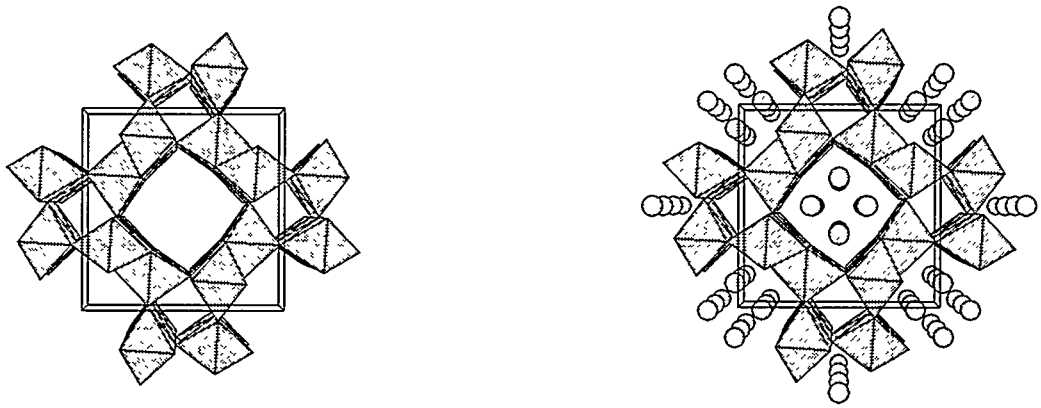

(a) (b)

Fig. I-6. Crystal Structures of (a) Hollandite-TiO_2 and (b) $Li_{0.125}TiO_2$ Showing the Disordered Lithium Ions in (2 x 2) Channels of Structure. The lithium atoms are open spheres, and the TiO_6 units are shaded octahedra.

The electrochemical discharge curve for a Li/Li_xTiO_2 cell indicates that at low current rate, lithium is inserted into the TiO_2 structure in two single-phase processes between 1.0 and 2.0 V; the capacity that is delivered on the initial discharge (~160 mAh/g) corresponds to a discharged electrode composition $Li_{0.45}TiO_2$, which is in reasonably good agreement with the composition $Li_{0.57}TiO_2$ obtained chemically with *n*-butyllithium. Of particular note is a point of inflection at 1.42 V in the electrochemical curve (at approximately 30% depth of discharge), which seems to correspond to the transition of the tetragonal unit cell to monoclinic symmetry

during chemical lithiation. The composition of the electrode at this inflection point is $Li_{0.15}TiO_2$. With the small amount of residual potassium in the structure, this composition corresponds to the typical amount of stabilizing cation that is found in the (2 x 2) channels of hollandite-TiO_2 structures, such as $K_xTi_8O_{16}$ ($1 < x < 2$). Although lithium can be extracted chemically from lithiated TiO_2 structures with bromine, it is not easily extracted by electrochemical methods, as was evident by the relatively small capacity that could be recovered on charging the Li/Li_xTiO_2 cell to 2.0 V (15 mAh/g).

The poor rechargeability of hollandite-TiO_2 electrodes contrasts strongly with the behavior of isostructural α-MnO_2 electrodes.[8] In the manganese oxide system, the hollandite structure is also stabilized by large cations in the (2 x 2) channels, as in $Ba_xMn_8O_{16}$ (hollandite) or $K_xMn_8O_{16}$ (cryptomelane), in which x has a value typically between 1 and 2. However, unlike hollandite-type TiO_2, the α-MnO_2 structure can be stabilized by water (H_2O) or lithia (Li_2O) molecules in the channels. In these stabilized structures, the negatively charged oxygen ion resides close to the site normally occupied by stabilizing cations; this site also corresponds to an oxygen vacancy in a defect close-packed oxygen array.[8] Lithium insertion into lithia-stabilized α-MnO_2 electrodes, notably $0.15Li_2O{\cdot}MnO_2$, occurs far more readily than it does in the titanium analog because the inserted lithium ions can be coordinated to both the oxygen ions of the α-MnO_2 framework and to the oxygen ion at the center of the (2 x 2) channels, thus minimizing the coulombic repulsion between the lithium ions. Future work is being focused on α-MnO_2 positive electrodes rather than the α-TiO_2 negative electrodes.

B. Electrochemical Analysis and Diagnostics Laboratory

The Electrochemical Analysis and Diagnostics Laboratory (EADL) was established at ANL in 1976 to study advanced battery systems for applications such as electric vehicles and utility load management. Its capabilities have recently been expanded to include fuel cells (see Sec. I.C.5). Evaluations are performed for DOE, the Electric Power Research Institute (EPRI), the U.S. Advanced Battery Consortium (USABC), and others to provide insight into those factors that limit the performance and life of advanced battery and fuel cell systems. The results of these evaluations help identify the most promising R&D approaches for overcoming these limitations and provide battery and fuel cell users, developers, and program managers with a measure of the progress being made in R&D programs, a comparison of various technologies, and basic data for modeling.

Performance and life evaluations of advanced batteries were continued under a CRADA with the USABC. The tasks under a second CRADA (initiated in March 1997) were expanded and the scope of work increased to include testing of systems from other battery development contracts. Activities under the second CRADA included evaluation of nickel/metal hydride (Ni/MH) cells and modules from USABC contracts with GM-Ovonics and SAFT (France). This work has been expanded to involve numerous SAFT deliverables, including full-size electric-vehicle battery packs. The EADL has also assisted 3M Corp. and Hydro-Québec by providing

[8] C. S. Johnson, D. W. Dees, M. F. Mansuetto, M. M. Thackeray, D. R. Vissers, D. Argyriou, C.-K. Loong, and L. Christensen, *J. Power Sources* **68**, 570 (1997).

additional cell and module testing and characterization efforts to their program on lithium-polymer battery development with the USABC (Sec. I.A.1.b). The results of these tests and analyses will be released by the USABC at a later date.

Also continued during 1998 was an assessment of foreign EV battery technologies for DOE. During this past year, two Ni/MH modules from Yuasa Corp. (Japan) were evaluated. In addition, leasing and data disclosure agreements were executed with AEG (Germany) to evaluate their $Na/NiCl_2$ "Zebra" battery. A Zebra battery was obtained in July 1998, tested, and returned to AEG in December 1998. A data disclosure agreement was also executed with Matsushita Battery Industrial Co. and Panasonic EV Energy Co. to evaluate several Ni/MH modules for an electric- and hybrid-vehicle battery pack. The electric-vehicle modules were received in September 1998, and their performance characterization studies have been started. The hybrid-vehicle battery modules are expected in January 1999. The results of these tests and analyses will be released by the DOE at a later date.

In 1999, evaluations will be continued for the USABC's Battery Cost Reduction Programs with GM-Ovonics and SAFT and for the Lithium-Polymer Battery Development Program with 3M and Hydro-Québec. In addition, the study to assess foreign electric-vehicle battery technologies for the DOE will be continued, and testing of a polymer-electrolyte fuel cell stack will begin.

C. Fuel Cell Research and Development

Fuel cells convert chemical energy directly into electricity by electrochemical reaction mechanisms, eliminating the need for heat engines and rotating machinery. Since such systems have very low environmental emissions and offer high efficiencies, interest in their application continues to grow. The polymer electrolyte fuel cell (PEFC), in particular, is attracting significant private investment for transportation applications and residential use.

Because of the low operating temperature of the PEFCs, only 80°C, the fuel has to be free of carbon monoxide, which absorbs on the surface of the platinum catalyst and "poisons" the electrode. Making a CO-free hydrogen gas from liquid hydrocarbon precursors is a challenge, especially when volume and weight are major considerations, as they must be for automotive use. More than half of our effort is devoted to development of fuel processing technology. We also continue to lead the field in PEFC systems analysis and modeling. In the development of more traditional molten carbonate and solid oxide fuel cells for stationary applications, we are working closely with industrial developers on specific issues related to technology improvement.

1. Fuel Processing

At the present time, gasoline is the commodity fuel for passenger cars, and natural gas predominates in stationary applications. To operate a fuel cell system on either of the two fuels requires converting a hydrocarbon to a hydrogen-rich stream that must be virtually CO-free. Industrially, natural gas is processed by steam reforming and shifting. Although highly developed, the steam reforming process is too bulky and has unacceptable slow response to

changing fuel processing rates. Argonne was first to propose partial oxidation reforming as a better alternative. We continue to develop this process and also to seek better shift catalysts.

a. Partial Oxidation Reforming

The objective of this work is to develop catalytic partial oxidation reformers for the generation of hydrogen from methanol and hydrocarbon fuels for use with the low-temperature fuel cells (polymer electrolyte and phosphoric acid fuel cells) being developed for transportation applications. Such fuel processors need to be compact, lightweight, efficient, and capable of rapid startup and good dynamic response to changing fuel-processing rates. We are addressing the reforming of methanol and hydrocarbons separately.

For the partial oxidation reforming of any hydrocarbon fuel $C_nH_mO_p$, the idealized general reaction is

$$C_nH_mO_p + x(O_2+3.76N_2) + (2n-2x-p)H_2O = nCO_2 + (2n-2x-p+m/2)H_2 + 3.76xN_2 \qquad (1)$$

where x is the oxygen/methanol molar ratio. This reaction can be conducted most efficiently in a catalytic reactor because catalysts can provide high conversions and product selectivity at relatively low temperatures. A new Argonne catalyst (proprietary) was found to have the ability to convert the different types of hydrocarbons (paraffins, olefins, etc.) present in gasoline. Experiments in a micro-reactor (2 g of catalyst in a 12-mm-dia reactor tube) with retail gasoline produced a gas that contained 60% hydrogen (dry, nitrogen-free basis) at 760°C. Similar experiments with oxygenated hydrocarbons, such as methanol, ethanol, and methyl-tert-butyl-ether, have also shown that the catalyst is very active and selective for hydrogen production.

Experiments were conducted to study the effectiveness of the catalyst for more complex fuels, such as diesel. We found that the catalyst could convert hexadecane (used as a surrogate for the paraffins in diesel) at similar space velocities, but at a higher temperature of 800°C. The experimental and calculated equilibrium compositions of the product gas are plotted in Fig. I-7. As shown in this figure, the reforming reaction produced a gas that contained roughly 60% hydrogen (dry, N_2-free), as did diesel fuel. Compared with the calculated equilibrium composition under the same conditions, the experimental hydrogen percentage is slightly higher. These results are very promising because they indicate that the catalyst is effective with the longer and heavier hydrocarbons that are present in diesel fuels.

To verify the performance of the Argonne catalyst in a larger, self-sustaining reactor, we built an 89-mm-dia tubular reactor and filled it with 1.7 L of the new reforming catalyst. Fuel, steam, and air were fed in at one end, and the hydrogen-rich reformate gas came out at the other end. The product was then analyzed with on-line instruments and a gas chromatograph.

Figure I-8 shows the product gas compositions obtained from the partial oxidation reforming of retail gasoline in this engineering-scale reactor. The product contained 38%

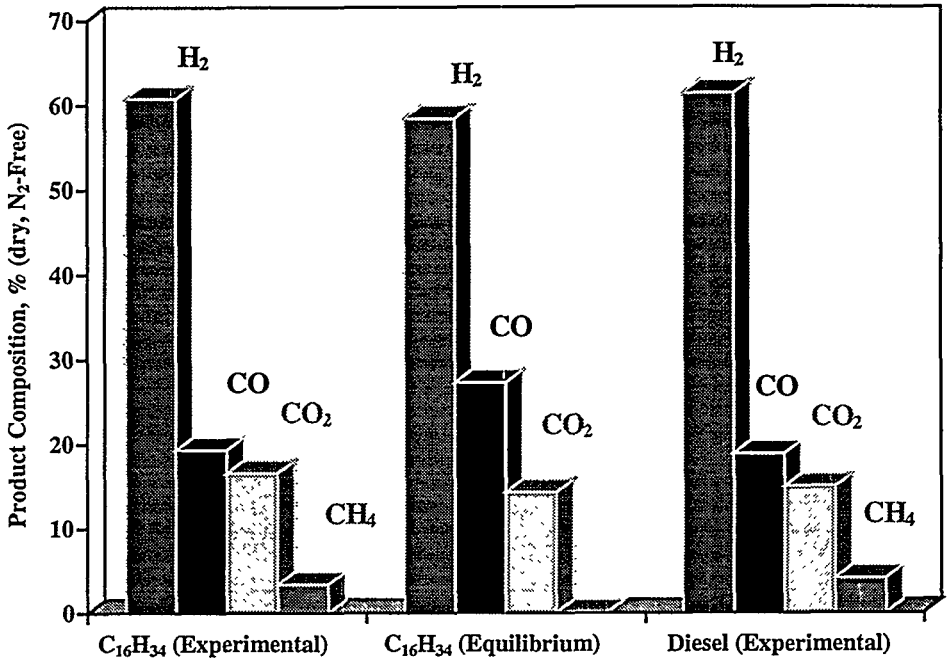

Fig. I-7. Experimental and Equilibrium-Predicted Product Gas Compositions from the Partial Oxidation Reforming of Hexadecane. Also included are experimental results for the products obtained from the partial oxidation reforming of diesel fuel.

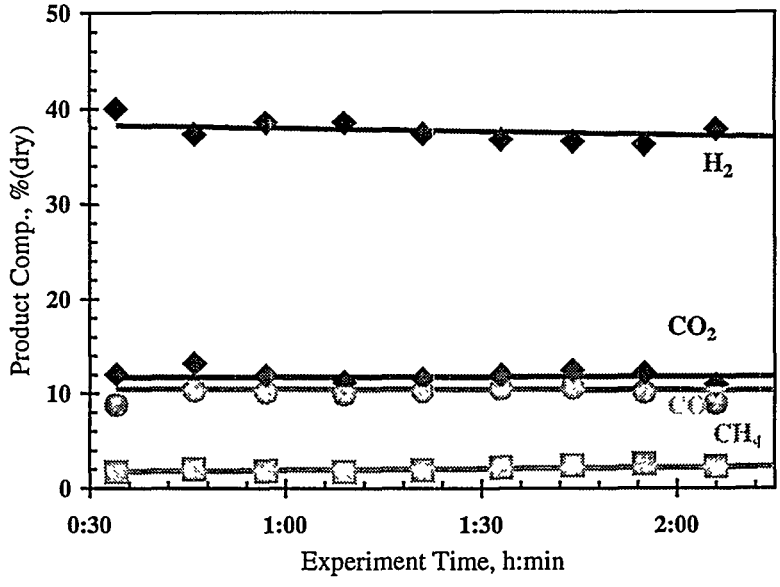

Fig. I-8. Product Gas Compositions Obtained from the Partial Oxidation Reforming of Gasoline in Engineering-Scale Reactor

hydrogen, 12% carbon dioxide, 10% carbon monoxide, and 2% methane (remainder air). The 1.7-L catalyst bed produced a gas stream that contained sufficient hydrogen to sustain a 3-kW fuel cell stack. These results indicate that a full-scale partial oxidation reformer based on this catalyst will be able to convert gasoline on board the anticipated fuel-cell powered cars, which will require a 50-kW fuel cell system.

Experimental results with the engineering-scale reactor also showed that the Argonne catalyst is capable of converting natural gas into a product stream containing about 45% hydrogen. Such reformers are desirable for various fuel cell systems that might operate on natural gas, such as the residential fuel cell power plants that are being developed by the utility companies.

The catalyst development work is continuing at the micro-reactor level to optimize the catalyst composition for the specific fuels and operating conditions. At the engineering scale, a compact, lightweight fuel processor that integrates the reformer and shift reactor is under development.

b. Shift Catalysis

As discussed above, the fuel reforming produces carbon monoxide along with hydrogen. The platinum-based anode catalyst of the fuel cell, however, is readily poisoned by even low levels of CO. Concentrations as little as 0.001% severely degrade the fuel cell performance. The concentration of CO in the fuel gas may be reduced via the water-gas shift reaction:

$$CO + H_2O \leftrightarrow H_2 + CO_2 \qquad (2)$$

This shift reaction is commonly carried out in two stages: a high-temperature stage (HTS) using an iron-based catalyst, and a low-temperature stage (LTS) using a copper-based catalyst. The LTS catalyst is synthesized as a mixture of copper oxide and zinc oxide and must be "activated" by reducing the copper oxide to copper metal in the reactor. Once the catalyst has been reduced, it must be kept in an inert or reducing environment to prevent re-oxidation, which leads to deactivation of the catalyst and sintering. Our research is aimed at finding a more active and thermally rugged catalyst than the copper-zinc oxide. A more active catalyst would reduce the size and weight of the CO cleanup portion of the fuel processor.

Three materials were investigated for finding an alternative LTS catalyst: (1) a support for copper that isolates the individual copper particles and prevents sintering and deactivation, (2) a metal that is more active and more resistant to sintering upon repeated oxidation/reduction, and (3) a two-component catalyst, where one component adsorbs and dissociates the reactant water, and the other component adsorbs and oxidizes the carbon monoxide. Several platinum-based catalysts were tested during the past year. The data shown in Fig. I-9 illustrate the activities of these catalysts. The platinum-on-carbon catalyst falls in the class of replacing the copper with a more active and sinter-resistant metal. With the platinum-in-zeolite catalyst, the function of the support is to isolate and disperse the metal particles to obtain

and maintain a high metal surface area. Finally, the platinum-on-mixed oxide is an example of a bi-functional catalyst, where the intended role of the mixed oxide support is to adsorb and dissociate the reactant water. As shown in Fig. I-9, the activity of the catalyst is strongly influenced by the support used.

Platinum supported on a mixed oxide was the best LTS catalyst found. Tests on the durability of this catalyst showed that its activity is stable to temperature cycling from the reaction temperature of 230°C up to 350°C and down to room temperature under *oxidizing conditions*. (For comparison, the commercial copper-zinc oxide catalyst degrades upon thermal cycling from 230°C to room temperature, even under *reducing conditions*.) Since it does not deactivate at higher temperatures, this platinum/mixed oxide catalyst opens up the possibility of using a water-gas shift reactor with only one stage. To reduce the total amount of catalyst needed, we are exploring various techniques for supporting the new catalyst on a high-surface-area substrate. Using one of these techniques, we have been able to reduce the catalyst loading by 74% while maintaining the same water-gas shift activity as the unsupported powder. We will evaluate this catalyst in a larger reactor.

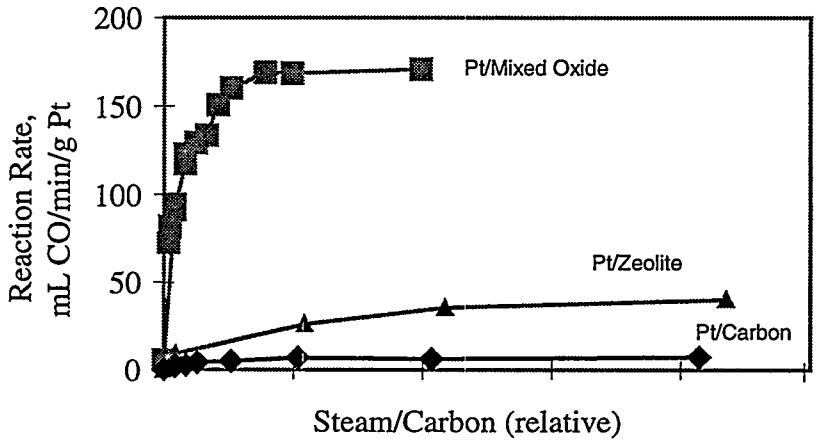

Fig. I-9. Water-Gas Shift Activity of Platinum with Alternative Supports. Temperature is 250°C; gas contains 0.6 vol% CO in nitrogen at flow rate of 500 mL/min.

c. Carbon Monoxide Cleanup

As discussed above, the CO concentration in the fuel gas provided to the fuel cell stack must be reduced to trace levels (<100 ppm). Catalytic preferential oxidation, anode air bleed, or a combination of the two can be used for this purpose, but their use in a dynamically varying system is problematic. We are developing a sorption process based on the reversible complex-forming and dissociation reactions of CO with Cu(I). This approach was discussed in the previous report of this series.[9] During the past year, we have studied the CO

[9] J. J. Laidler et al., *Chemical Technology Division Annual Technical Report, 1997,* Argonne National Laboratory Report ANL-98/13, pp. 28-30 (1998).

sorption/desorption characteristics of two supports with high surface area (activated bauxite and H-ZSM-5 zeolite), on which CuCl is dispersed or reacted. The sorbent was tested at atmospheric pressure and at temperatures ranging from 25 to 250°C using a thermogravimetric analyzer (TGA). The tests were conducted with a synthetic gas mixture containing 30-50% H_2, 12-19% CO_2, 3-14% CO, and the balance N_2. The TGA thermogram showed rapid sorption of CO by the sorbent, as well as CO desorption from the sorbent by a similar gas mixture containing no CO. Figure I-10 summarizes the CO sorption capacity as a function of temperature for both sorbents tested with 3% CO. For the activated bauxite, two CuCl dispersion methods were used. One sample had significantly higher CO sorption capacity than the other, indicating the influence of the technique used to disperse CuCl on the surface of the substrate. However, both samples showed that the amount of CO uptake decreased with increasing temperature, and that the sorbent lost its CO sorption capability at about 200°C. In contrast, the CO sorption capacity of the zeolite sorbent increased with increasing temperature up to 150°C, and then decreased slightly at higher temperatures. These results indicate that a combination of the two types of sorbents may be useful to cover a wide range of temperature, from room temperature to 250°C. Further, within experimental error, the sorption capacity of the zeolite-based sorbent remained essentially constant over ten sorption/desorption cycles.

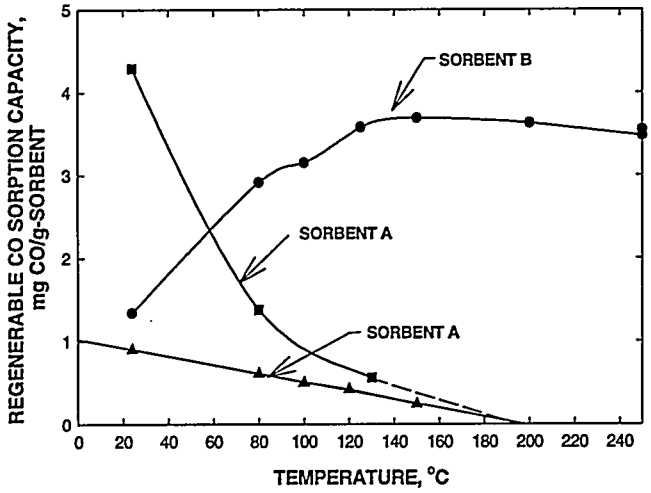

Fig. I-10.

Carbon Monoxide Sorption Capacity as Function of Temperature for Two Activated Sorbents (A) and H-ZSM-5 Zeolite (B). The two activated sorbents were prepared by different CuCl dispersion methods.

Following these TGA tests, a dynamic column was tested at 25 and 110°C to obtain CO breakthrough data for verifying the sorption process. This column (19-mm OD x 1170-mm long) was packed with extrudates of the zeolite-based sorbent. Figure I-11 shows the CO breakthrough and desorption curve at 25°C, with a gas flow rate of 250 mL/min. The CO in the test gas (49% H_2, 19% CO_2, 1% CO, balance N_2) was totally captured for 105 min before the CO started to appear in the column exit. After breakthrough, the CO concentration increased rapidly to the inlet value of 1%. Then, the gas flow was switched to a regeneration gas containing no CO, and the captured CO started to release from the column, as shown in the desorption portion of Fig. I-11. This test demonstrated that the column offers instantaneous cold-start capability at room temperature to reduce 1% CO to <100 ppm in the reformate. In a subsequent test, the column was tested at 110°C with a wet (25 vol% water vapor) test gas containing 1% CO. At a flow rate of 560 mL/min (more than twice the flow rate in the earlier test), the CO was totally captured for 80 min. This test further demonstrated that the sorbent can remove CO to <100 ppm in the temperature range of the polymer electrolyte fuel cell.

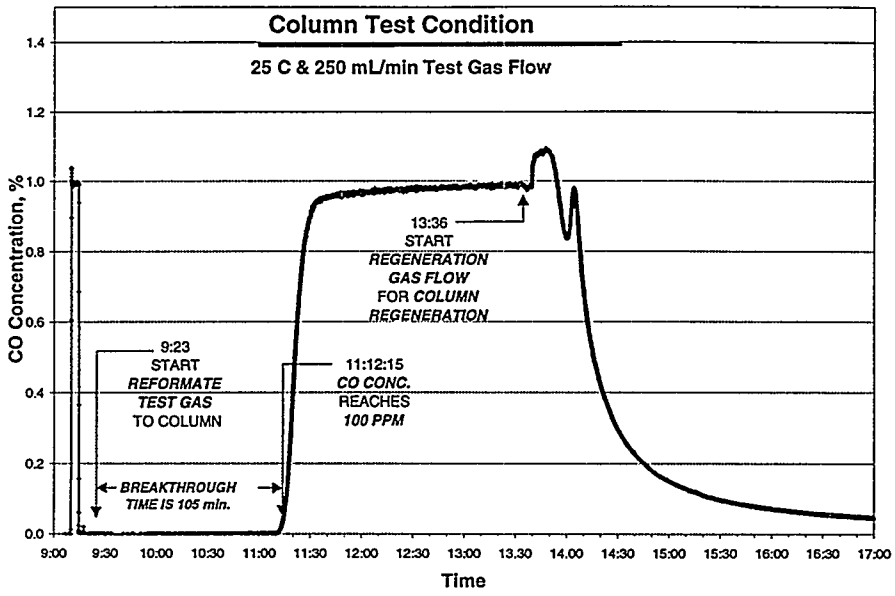

Fig. I-11. Breakthrough/Desorption Curve for Carbon Monoxide Concentration as Function of Time of Day

Results of these studies show that the CuCl-CO complexing concept is valid in the sorption process because CO is easily captured and released from CuCl-based sorbents. In future work, we will investigate alternative supports and dispersion techniques for the CuCl to increase CO sorption capacity and copper utilization. We will also test the process with actual reformate and will design and test a prototype CO sorber unit that is integrated with a reformer and shift reactor.

2. Systems Analysis

In this activity, we are developing computer simulations of fuel cell systems for use in light-duty vehicles. The objective is to use these simulations for determination of key design parameters and operating efficiencies, as well as the influence of component design on startup and dynamic performance. We have developed software for system design and analysis called GCtool, which consists of models of the components in fuel cell systems (as C data structures), mathematical utilities, physical property utilities, and thermodynamic data.[10] This software permits analysis of variable configurations of fuel cell systems, including recycle loops, and is capable of performing parameter sweeps, constrained and unconstrained optimizations, and integrations over time.

Work this past year focused on the analysis of polymer electrolyte fuel cell (PEFC) systems fueled by gasoline. A simplified block diagram of a pressurized PEFC system is shown in Fig. I-12. The blocks in the figure represent the major components in the system. For this

[10] H. K. Geyer and R. K. Ahluwalia, *GCTool for Fuel Cell Systems Design and Analysis: User Documentation,* Argonne National Laboratory Report ANL/98-8 (March 1998).

analysis, gasoline was assumed to consist of 50% iso-octane, 30% toluene, 15% pentene, and 5% cyclohexane (by weight). It was further assumed that the individual constituents of this gasoline are reformed by idealized partial oxidation reactions:

Iso-octane

$$C_8H_{18}(l) + xO_2 + (16-2x)H_2O \rightarrow 8CO_2 + (25-2x)H_2$$

Toluene

$$C_7H_8(l) + xO_2 + (14-2x)H_2O \rightarrow 7CO_2 + (18-2x)H_2$$

Pentene

$$C_5H_{10}(l) + xO_2 + (10-2x)H_2O \rightarrow 5CO_2 + (15-2x)H_2$$

Cyclohexane

$$C_6H_{12}(l) + xO_2 + (12-2x)H_2O \rightarrow 6CO_2 + (18-2x)H_2$$

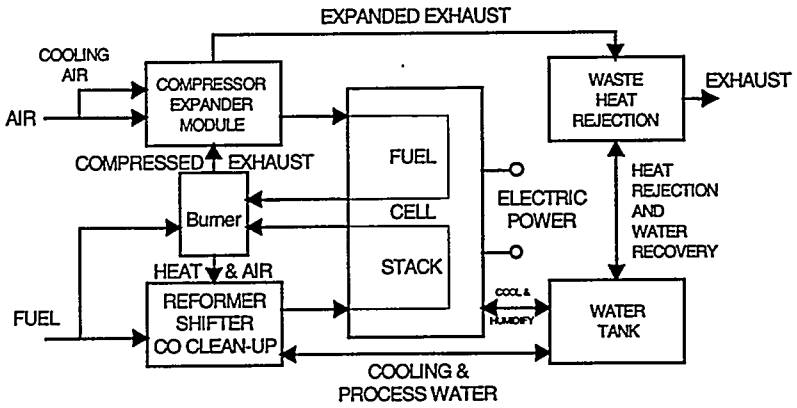

Fig. I-12. Schematic Diagram of Pressurized Polymer Electrolyte Fuel Cell System with Fuel Reforming

The overall system efficiency was calculated as a function of the operating cell voltage for various performance losses in a gasoline fuel cell system with partial oxidation reforming. One set of calculations was for the efficiency of a "perfect" system, i.e., one in which the ideal amount of water is used in the fuel reformer, the electrochemical fuel utilization is 100%, and there is no heat loss at the reformer and no parasitic power consumption. For such a perfect system to achieve a net efficiency of 45% or greater (on a lower heating value basis), we determined that the fuel cell stack must be operated at a cell voltage in excess of 0.65 V. Separate calculations were made to determine the following effects: 30% excess water in the fuel processor, a fuel utilization of 90%, a reformer heat loss of 10% (of the energy in the input fuel), and a parasitic power loss of 5% of the gross power (to operate the various fans, pumps, blowers, compressors, etc.). We concluded that, for practical partial oxidation systems with gasoline,

operating cell voltages must be in the range of 0.75-0.85 V to achieve system efficiencies of 45% or greater.

A similar analysis was conducted for a steam-reformed gasoline system. In this case, however, as the fuel utilization decreases from 100%, the unused fuel is burned at the reformer burner to recover the chemical energy in the spent anode gas. In addition, since the steam reformer entails heat exchange between the burner and the process gas, the heat transfer effectiveness is taken as 90%. The calculated data indicate that, with the gasoline fuel, the steam-reformed system may have a slight advantage in system efficiency over that of the partial oxidation system. Operating cell voltages would only have to be in the range of 0.65-0.75 V to achieve system efficiencies of 45% or greater.

The major thrust of system design and integration is to minimize the various losses so that the cell voltages needed to obtain the desired system efficiency are not prohibitively high. For detailed simulation, a "reference" system configuration was defined to determine efficiency and component sizes and to identify the parameters for a high-performance system. The key design values were net power of 50 kW, oxidant utilization of 50%, partial oxidation temperature of 1027°C, HTS temperature of 427°C, and LTS temperature of 177°C. The design variables included equivalence ratio, water-to-fuel ratio, water flow to LTS catalysts, air-to-fuel ratio, and fuel feed rate.

The following conclusions were reached from the assessment of a system containing a fuel cell stack, gas turbine, compressor, radiator, condenser, water pump, and fuel pump. First, the reference configuration yields 35.1% system efficiency under near-term operating conditions (0.685 V, 85% fuel utilization, 50% oxidant utilization). Second, a reactor operating at a fuel equivalence ratio of approximately three uses 260% excess water. Third, no internal or external humidification is needed for the fuel cell stack. Fourth, if the cathode exhaust contains entrained water, a separator can recover two-thirds of the necessary process water, and the other one-third must be recovered from the turbine exhaust. Finally, the air flow rates for the radiator and condenser (2.7 and 1.2 kg/s, respectively) are high.

In the coming year, we plan to investigate the effect of operating pressure on system performance. We will add pressure drops and heat losses to the various system components and include or refine component weights, volumes, and packaging. We are also adding cost factors to the model.

3. Molten Carbonate Fuel Cells

The CMT Division has a program on development of the molten carbonate fuel cell (MCFC) for utility applications, which offers the possibility of higher efficiency compared with other technologies. At present, the molten carbonate fuel cell consists of a porous nickel anode, a porous nickel oxide cathode, a semi-fluid $(Li,K)_2CO_3 + LiAlO_2$ electrolyte, and a metal bipolar plate. The operating temperature is 650°C. The focus of the MCFC program is developing a nonsegregating electrolyte and improving the corrosion resistance of the cell components.

a. Nonsegregating Electrolyte

Differences in the ionic mobility of the lithium and potassium ions in the Li_2CO_3-K_2CO_3 electrolyte have long been known to lead to changes of the composition between the positive and negative side of the fuel cell. As a result, the melting point and other physical properties of the electrolyte can vary at different locations in the fuel cell.

As described previously,[11] we screen electrolyte compositions for nonsegregation using 12-cm-long strips that are wetted with carbonate and exposed to 5- to 20-V potential gradients. These conditions simulate the gasketing strip of an externally manifolded MCFC. In our case, strips of carbonate-wetted $LiAlO_2$ were made from cold-pressed powders (150 MPa). The strip was purged with a 1:2 O_2:CO_2 gas mixture (500 mL/min) at 655°C. After 72 h at 20 V, the potential distribution in the strip reached equilibrium. The strips were quenched under load and later examined by metallography. These strips were sectioned for chemical analysis by inductively coupled plasma/atomic emission spectroscopy (ICP/AES). The analytical results of electrolyte segregation were correlated to the Li/Na carbonate composition. It was evident that fairly substantial segregation occurs at the eutectic composition of 52% Li_2CO_3, but between 60 and 75% Li_2CO_3, segregation is minimal.

Such lithium-rich salts may not be practical, because their melting points are too high. By adding calcium and barium to Li_2CO_3-Na_2CO_3, however, we were able to lower the melting point by about 70°C and maintain nonsegregating behavior. To explore the relationship between electrolyte composition and electrochemical behavior in the fuel cell, we ran cell tests for various quaternary electrolytes, Li_2CO_3-Na_2CO_3 compositions with Ba/Ca additions (Fig. I-13). Bench-scale (100-cm^2) MCFC tests using these electrolytes show increased performance at 160 mA/cm^2 (the typical operating current density), as much as 150 mV compared with the baseline cell containing the 52 mol% Li_2CO_3-48 mol% Na_2CO_3 eutectic. We have identified a range of quaternary electrolyte compositions (Li/Na/Ca/Ba carbonate) which yield general improvement of MCFC operation and performance. These improvements include high current-density operation (250-360 mA/cm^2), reduced temperature sensitivity, and anticipated extended life.

The nonsegregating property of the carbonate and the composition of the carbonate at the electrodes seem to play a significant role in the MCFC performance. At this point, we are not certain whether the improvement in cell potential is due to higher electrolyte conductivity or lower overpotentials, but we have ascertained the stability of the cell potentials over at least 2000 h of testing with the Li/Na/Ca/Ba carbonate electrolyte. Remarkably, the potentials remain stable even at current densities of 240 mA/cm^2. Transfer of this technology to commercial developers will aid its adaptation. In the next year, we will examine other properties of the alternative electrolytes, such as wettability.

[11] T. D. Kaun, I. D. Bloom, S. P. Nied, and M. Krumpelt, "Non-segregating Electrolytes for Molten Carbonate Fuel Cells," Presented at Fuel Cells '97 Review Meeting, Federal Energy Technology Center, August 26-28, 1997, Morgantown,VA (1998).

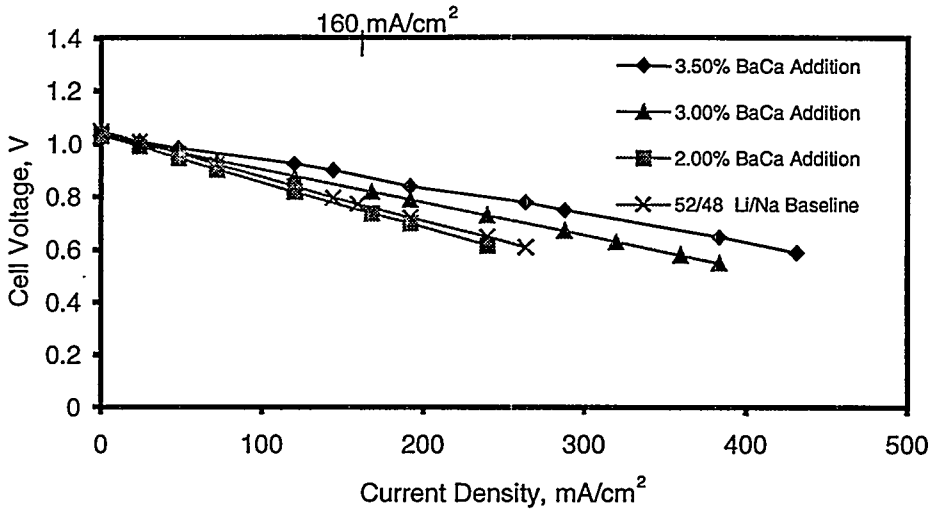

Fig. I-13. Cell Polarization Curves from Molten Carbonate Fuel Cells Containing Different Electrolyte Compositions

b. Resistivity of Bipolar Plate Materials at the Cathode Interface

Molten carbonate fuel cells are promising sources to generate power for stationary power plants with a high efficiency and low emission coefficients. Corrosion of the bipolar plates and current collectors, however, is caused by the severe conditions due to the high operating temperature (650°C) and the highly aggressive molten salts of the electrolyte. This limits the lifetime of the MCFC significantly. Materials for separator plates must satisfy different requirements. They must form a dense, protective layer of corrosion product. Additionally, this corrosion scale must have a high electrical conductivity. The base metal composition strongly affects the oxide scale composition, the thickness of the scales, and the electrical conductivity.[12] The chromium content plays an especially important role in the corrosion behavior.

Tests were undertaken to relate the interfacial electrical resistance of different stainless steels (316L, 310S, and Nitronic 50) and nickel-base alloys with oxide scale composition as a function of exposure time and chemical composition of the electrolyte. Two electrolyte were tested: Li_2CO_3-K_2CO_3 and Li_2CO_3-Na_2CO_3 . The Li/K-carbonate electrolyte is commonly used in the MCFC, while the Li/Na-carbonate electrolyte shows promising properties for improved cell stability and minimal segregation.[13]

The electrical resistivity of the candidate materials was measured at 650°C under simulated MCFC conditions in a cathodic environment (30% CO_2/70% air). Periodically, some samples were taken out of the furnace to investigate the evolution of the microstructural

[12] P. Biedenkopf, M. Spiegel, and H. J. Grabke, *Mater. Corros.* **48**, 477-488 (1997).

[13] M. S. Yaziki, and J. R. Selman, "Electrochemical Response of Stainless Steels 310, 316L, and Nickel-Rich Alloy in Molten Carbonate," Proc. of Electrochem. Soc. Meeting, Los Angeles, CA, May 5-10, 1996, Vol. 96-7, pp. 423-438 (1996).

composition of the formed oxide scales. Scanning electron microscopy (SEM) and energy dispersive X-ray spectrometry (EDX) were used to determine the thickness and composition of the oxide scale. Additionally, X-ray diffraction (XRD) measurements were undertaken: a special polishing device was used to remove microscopic amounts of the surface (about 5 μm) and examine the chemical composition of the oxide layer in the outer and inner area of the scale. After each "polishing" step, the phase distribution of the exposed surface was determined by XRD.

Different alloys developed a wide range of oxide-scale thicknesses and phases. The stainless steel 316L consists of a relatively thick oxide scale (40 μm after 3000 h) with an outer layer of $LiFeO_2$ and a $LiFeO_2/LiFe_5O_8$ inner layer. These corrosion products were formed in both electrolytes. The $LiFeO_2$ was nearly insoluble in the carbonate melt and retarded further corrosion attack. No corrosion products containing Na or K were identified. Calculations showed that the diffusion coefficient for nickel in stainless steels is much higher than that for chromium. Nickel diffuses through the oxide scale to the electrolyte interface and dissolves in the melt. As shown in Fig. I-14, the resistivity of 316L as a function of time displays a saw-toothed pattern. First, the resistivity reaches about 25 $m\Omega \cdot cm^2$. After 500 h the resistivity increases to 130 $m\Omega \cdot cm^2$, then returns to about 25 $m\Omega \cdot cm^2$ by about 2500 h. Others have observed this behavior, but lacked an explanation for it. Horizontal cracking and porosity, a result of oxide scale spallation caused by stresses related to oxide growth, can explain the fluctuations. After long exposure times, we observed crystallite precipitations, which have been analytically determined to be Fe-Ni solid solution. This is a result of a reaction between the NiO and the $LiFeO_2$ layer. Because of the formation of a solid solution of Fe-Ni, the resistivity decreases after long exposure times.

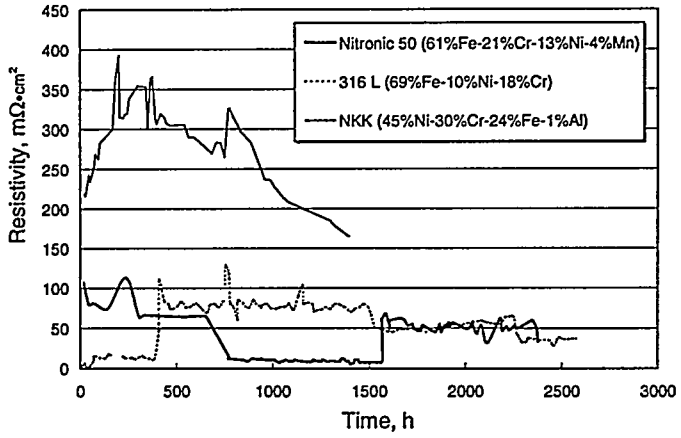

Fig. I-14.

Oxide Scale Resistivity of 316L, Nitronic 50, and NKK in Li_2CO_3-K_2CO_3 Electrolyte at 650°C vs. Time

Type 310S, which has a higher Cr and Ni content than 316L, also forms an outer $LiFeO_2$ layer, but a $LiCrO_2$ layer under the surface. This oxide appears only at chromium contents higher than 20 wt%. Neither 316L nor Nitronic 50 forms $LiCrO_2$ as an inner scale in contact with the metal. Type 310S generally shows a higher corrosion resistance than 316L (oxide scale thickness of 20 μm), although the electrical resistivity of 310S is higher than that of 316L and Nitronic 50. Lower electrical conductivity of the oxides forming the scale would explain this apparent contradiction. Nitronic 50 is a promising material, with similar chromium content and comparable electrical resistivities to 316L.

A nickel-base alloy (designated NKK) developed much thinner oxide layers than the stainless steels (10-15 μm). By XRD analysis, $LiFeO_2$ was determined as the corrosion product on the outer layer. Data from SEM revealed that the outer layer is a $LiFeO_2$-NiO solid solution. In the inner areas of the scale, $LiCrO_2$ was also detected. The NKK has a substantially higher electrical resistivity (increase of 100-300 m•·cm^2), although the oxide scales are much thinner than those of 316L. We found porosity between the base metal and the oxide scale, which additionally increases the interfacial resistivity.

In general, we have found that the electrical conductivity of the oxides forming the layers strongly determines the interfacial resistance. Scale spallation and oxide layer buckling can explain the resistivity fluctuations for 316L. Porosity increases the oxide scale resistivity of NKK. No further work in this area is planned.

4. *Solid Oxide Fuel Cells*

The standard air electrode material for solid oxide fuel cells is $La_{0.8}Sr_{0.2}MnO_3$ (LSM). At the request of Westinghouse Electric Corp., the principal industrial developer of such cells, we are exploring how to improve the oxide ion conductivity of this material. The LSM is a good electronic conductor and has the right thermodynamic and mechanical properties for SOFC applications, but because of the fairly low ionic conductivity, the air electrode reaction is limited to the triple-phase boundaries of electrode, electrolyte, and gas phase.

Earlier attempts by others to increase the oxide vacancy concentration followed the standard method of doping with a lower valent cation. However, in LSM, the substitution of lower valent elements for either the lanthanum or the manganese leads to charge compensation via the manganese ion, which converts to the IV oxidation state. Our approach of solving the problem has involved substituting for the manganese with a III valent element that prefers tetrahedral instead of octahedral coordination. Substitution of an octahedral for a tetrahedral cation causes the neighboring polyhedra to adopt a square pyramidal coordination, which is a common motif for Mn(III) cations.

We chose to begin by testing Ga(III) cations as a dopant for manganese. Figure I-15 shows the cathodic overpotentials of doped LSM for 1-10 mol% gallium substitution in half-cell tests. At a current density of 250 mA/cm^2, the overpotential without gallium is about 60 mV,

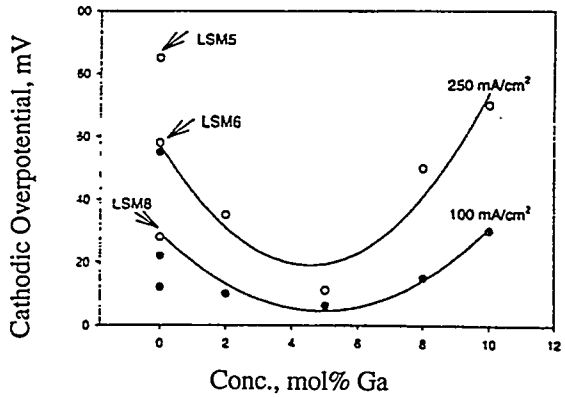

Fig. I-15.

Effect of Gallium Dopant Concentration on Cathodic Overpotential of Three LSM Cathodes at Current Densities of 100 mA/cm^2 (open circles) and 250 mA/cm^2 (closed circles)

which corresponds to literature values. As gallium is added, the overpotential decreases to only 20 mV for 5 mol% doping and then rises again. At 100 mA/cm^2, the overpotential decreases by 20-40 mV and shows similar variance with dopant concentration to the higher current density. The excellent performance at ~5 mol% gallium needs to be confirmed in actual fuel cell tests.

5. Technical Management

The CMT Division, through the ANL Electrochemical Technology Program, provides support to the DOE Office of Transportation Technologies and to the DOE Office of Buildings Technology in the form of technical management of R&D contracts with industrial developers of fuel cells and related components. In this capacity, we prepare work statements, evaluate proposals, and conduct progress reviews. Major ongoing projects managed by CMT include DOE contracts with General Motors Corp., Ford Motor Co., Plug Power, Allied Signal Corp., Energy Partners Inc., the 3M Co., and other fuel-cell component suppliers.

The DOE/General Motors project managed by the Electrochemical Technology Program successfully developed a polymer-electrolyte fuel cell system that operates on methanol fuel and is intended for automotive applications. During 1998, a 50-kW polymer-electrolyte fuel cell stack, built by Ballard Power Systems under a subcontract to General Motors, was integrated with a methanol reformer and other subsystems, all operating with an automotive-based control system. Following the DOE contract, GM installed the fuel cell power system in an Opel Zafira minivan, which was displayed at the Paris auto show in September 1998.

Plug Power, completed the first year of a contract to develop an integrated 50-kW fuel cell system incorporating a fuel-flexible reformer. A major accomplishment during the first year of the program was the integration of fuel cell stacks from Plug Power and Ballard with a partial oxidation reformer developed by Epyx Corp., a major subcontractor to Plug Power. The system produced electricity from gasoline as the starting fuel.

Allied Signal and Energy Partners completed the first year of their respective contracts to develop proton-exchange-membrane fuel cells that tolerate carbon monoxide contaminant in the reformate. Allied Signal developed and fabricated a 10-kW fuel cell stack incorporating advanced stack components; testing began in December 1998. Energy Partners developed an advanced composite bipolar plate and demonstrated the highest performance published to date for a single fuel cell operating on hydrogen (0.72 V at current density of 1.0 A/cm^2).

During the first year of its contract, 3M demonstrated the ability to produce three-layer membrane electrode assemblies (MEAs) that are free of defects. The MEAs were produced with proprietary-catalyst loadings of 0.02 to 0.2 mg/cm^2 on commercial membrane material at continuous line speeds up to 18 m (720 in.) per hour. The catalyst was deposited on nanostructure support whiskers, and when tested in single fuel cells, showed tolerance to 100 ppm CO.

The CMT Division completed the installation of a Fuel Cell Test Facility during 1998, fulfilling DOE's need for an independent source for validating the performance of fuel cells fabricated by industrial developers under DOE sponsorship. The facility consists of a test cell

with specially installed safety systems; an outdoor site for bulk hydrogen storage; and a gas management system to control the pressure, temperature, humidity level, and flow rate of both the fuel and oxidant gas supplies to the fuel cell. The capability exists for testing fuel cell stacks and stack systems with an electrical power output of up to 50 kW. The Fuel Cell Test Facility and the attendant safety systems are in the process of being commissioned. A 30-kW fuel cell stack built by Ballard Power Systems under a DOE contract with General Motors has been delivered and installed. Testing is scheduled to begin in January 1999.

II

Waste Management

In 1999, DOE will start to prepare the license application for the proposed geologic repository at Yucca Mountain, Nevada. This repository is intended for the disposal of spent nuclear fuel (SNF) and high-level radioactive waste. Five CMT projects are contributing data and mechanistic understanding to the licensing effort. First, the ongoing Yucca Mountain Project continues to provide data on the release behavior from commercial spent fuel under conditions similar to those anticipated in the potential repository. Recently added to this project are studies on the release behavior of high-burnup and clad fuel. A second project is conducting corrosion testing on a representative variety of spent fuels in DOE's inventory, with compositions considerably different from those of commercial light water reactor fuel. Two other projects are developing, characterizing, and testing ceramic waste forms: one for plutonium immobilization and the other for salt-bearing waste from the electrometallurgical process described in Sec. IV. These ceramics are proving to be superior to glass. In the fifth project, the glass waste form continues to be tested for the Defense Waste Processing Facility at the Savannah River Site for the West Valley Demonstration Project. Testing durations run from a few days to more than a decade in these five projects. Test methods include the Materials Characterization Center (MCC)-1 Test, Product Consistency Test (PCT), Vapor Hydration Test (VHT), and unsaturated drip tests. Samples of the waste solid and leachate solution are periodically taken for analyses to monitor reaction progress.

Besides this work on spent fuel and high-level waste, projects are also underway on low-level waste disposal, actinide speciation in the subsurface, and contaminated soil cleanup. In addition, two projects are applying techniques developed in the waste management efforts in new areas: one to provide the superior delivery of radioisotopes to cancer sites, and the other to simplify the structural analysis of proteins.

A. Testing of DOE Spent Nuclear Fuel

The Department of Energy has over 200 types of spent fuel in its inventory, which are proposed for disposal at Yucca Mountain. For these fuels to be accepted for disposal, it must be

demonstrated that their disposition in the repository does not create unacceptable risks to human or environmental health. However, determining the potential radionuclide release rate, pyrophoricity potential, and criticality potential of each type of fuel would not only be experimentally redundant, it would also be prohibitively expensive and lengthy. Thus, a more realistic testing scenario was devised by grouping the fuels into 13 categories based primarily on fuel type and cladding composition. Further selection of fuels was achieved by prioritizing the 13 categories based primarily on fissile content, curie content, and expected radionuclide release rates. Four fuel types were thus selected as highest priority for testing, and two additional fuel types were selected for the next tier of testing. The four high-priority fuels are a mixed oxide (MOX) fuel, uranium metal (Hanford N-Reactor) fuel, UAl_x alloy fuel (Savannah River), and graphite fuel (Peach Bottom 2 core). The two second-tier fuels are an aluminum-matrix uranium silicide fuel (Savannah River) and a hydrided U-Zr alloy (TRIGA) fuel.

During 1998, test plans, quality assurance plans, and experimental apparatus for fuel characterization and corrosion testing were prepared and approved for the four high-priority fuels. Corrosion experiments and specimen characterization have been initiated on MOX fuel. Testing of metallic uranium, UAl_x alloy, and graphite fuels is scheduled for next year.

1. Sample Characterization

During 1998, irradiated MOX fuel samples were chemically and mineralogically/metallographically characterized prior to corrosion testing and will be periodically examined throughout the corrosion experiments. Chemical characterization consisted of a destructive dissolution of a small quantity of fuel followed by isotopic analysis using inductively coupled plasma/mass spectrometry (ICP/MS). Additional isotopic information will be obtained from alpha and gamma spectrometry. From these analyses, the isotopic inventory of the fuel prior to corrosion testing will be established, and the fuel burnup will be determined. Nondestructive solid-state examinations of slices of the fuel using macrophotography and photomosaic techniques were made to determine the physical characteristics of the fuel (grain size, void volume and distribution, crack distribution, fuel-cladding interaction zone, etc.). Future characterization work will include electron microprobe examination, scanning electron microscopy (SEM), and transmission electron microscopy (TEM) to determine the location and identity of fission products and redistributed plutonium and to identify fuel/cladding interaction phases.

The release of specific elements from fuel samples in corrosion tests is controlled, in part, by the sample surface area exposed to the leachant. Surface area determinations will thus be performed for all four fuel types, but the methods used depend on the nature of the fuel and the corrosion test. For example, the Brunauer-Emmett-Teller (BET) method is appropriate for powdered samples and thus is used to determine the surface area of MOX fuel used for batch corrosion tests. For this purpose, a BET surface area analyzer was purchased and modified to enable remote hot-cell operation. The surface area of larger samples is determined from geometric considerations of sieved samples. Geometric estimation of surface area has been performed for MOX fuel used in unsaturated corrosion tests and will be used for tests with metallic fuel specimens.

2. Radionuclide Release Testing

The release rate of radionuclides from the spent fuel samples is determined by two approaches: unsaturated (drip and vapor) tests and batch (Petri dish) tests. These tests were initiated for MOX fuel during FY 1998 and will continue through 1999. In addition, unsaturated and batch tests are planned for metallic uranium, UAl_x alloy, and graphite fuels.

Since unsaturated conditions are anticipated in the repository at Yucca Mountain, results from unsaturated tests will be used to (1) measure the release and redistribution of fissile material, (2) estimate the release rate of fission products and the alteration rate of the fuel matrix under the test conditions, (3) identify important processes that will affect spent fuel performance and radionuclide release rates under unsaturated conditions, (4) provide data that can be used to support models that predict the long-term behavior of spent fuel within the repository, and (5) provide information regarding the distribution of radionuclides in solution. It is anticipated that the data will be useful in characterizing fuel corrosion behavior, as well as identifying important degradation modes and aiding in development of a relevant thermodynamic data base. The information derived from these tests will provide a technical basis for the determination of the source term for radionuclide release from exposed fuel contained in failed cladding in a repository, and will support the licensing process. After initial license application to the Nuclear Regulatory Commission, the unsaturated tests will continue to provide data to confirm corrosion models.

The batch (Petri dish) tests were developed to accelerate the formation of alteration phases observed in the unsaturated tests so that relevant observations can be made in six months or less. These tests provide just enough water to maintain a constant film of water on a small quantity of fuel. The compositional changes to the water can be closely monitored as the water reacts with the fuel and eventually with the alteration phases. Thus, the approach to equilibrium chemical composition of the water can be monitored and used to enable predictive modeling of fuel corrosion and secondary phase paragenesis. A series of batch tests on each fuel type is expected to be completed within one year of start.

3. Moisture Detection in Spent Nuclear Fuel Canisters

The toroid cavity probe for use with nuclear magnetic resonance (NMR) was developed in CMT for catalysis studies[1] and is being adapted for the analysis of radioactive materials. The cylindrical geometry of the NMR toroid cavity detector makes it an ideal candidate for monitoring the total moisture content in cylindrical containers. Approximately 2000 metric tons of N-reactor spent fuel clad with Zircaloy is in water storage in the K-basins at the DOE Hanford site. Some of the fuel and storage canisters in the K-basins have degraded and are corroding from reactions with the basin water. Multi-canister overpacks have been designed to hold canisters of fuel during transportation and storage. They will be approximately 0.6 m in diameter and 4.5 m in height. Hanford N-reactor fuel elements will be stored in appropriate overpacks once the fuel has been "dried."

[1] J. J. Laidler et al., *Chemical Technology Division Annual Technical Report, 1994,* Argonne National Laboratory Report ANL-95/24, pp. 126-129 (1995).

One major concern, after sealing the storage overpacks, is the presence of residual moisture and generation of uranium hydrides or hydrogen, species known for their high-chemical reactivity. These species could form through potential reactions between the uranium metal and the water. This NMR technique would allow the determination and monitoring of moisture and H_2 gas in canisters stored at Hanford.

Three modified toroid cavity probes were produced and tuned. One modified toroid probe consisted of a sealed metal canister with a central conductor that serves as a radiofrequency antenna. The waste capacity of this probe is ~100 g. The other two probes have ~5 and ~50 kg capacity, respectively (Fig. II-1). The largest probe is a factor of 2500 times larger than the original patented design for the toroid cavity. The 100-g probe was filled with SiO_2 or UO_2, and the radial distribution of moisture was determined to concentrations as low as 100 ppm. Future

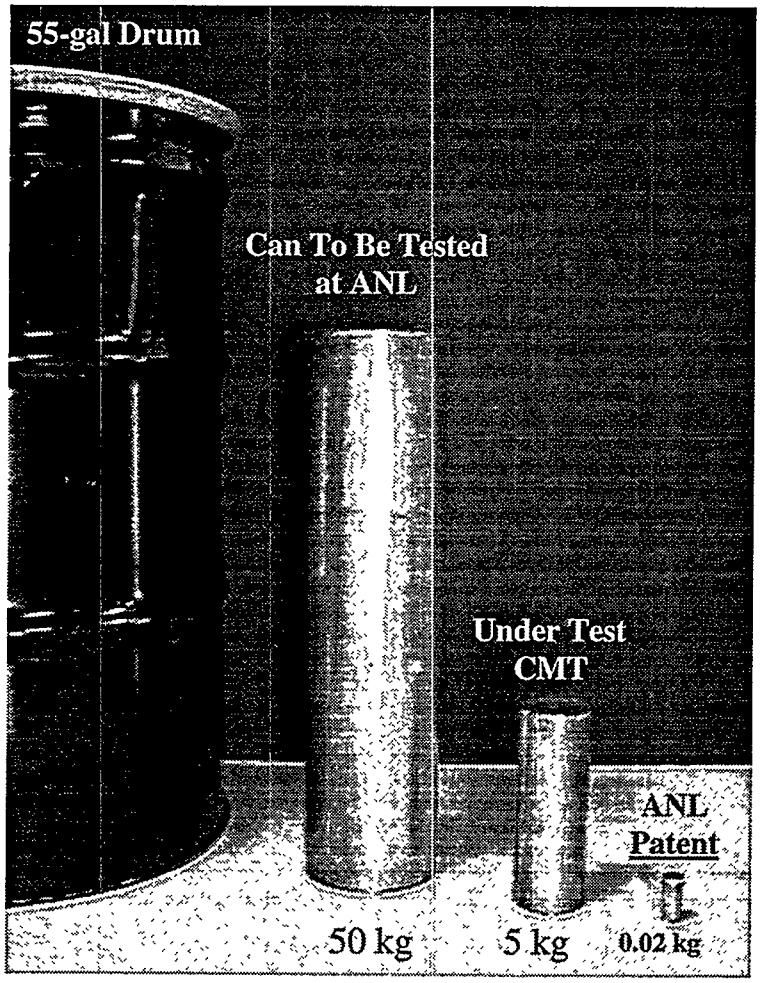

Fig. II-1. Toroid Cavity Probes Constructed for NMR Analysis Compared to 55-Gallon Drum

experiments will focus on extending the NMR spectroscopy to characterize fuel microstructure and follow chemical transformations at elevated temperatures in canisters with complex inner geometry.

B. Testing of Spent Fuel for Yucca Mountain

Spent fuel from commercial nuclear reactors will comprise approximately 90% of the waste to be disposed of at the candidate Yucca Mountain repository. When the sealed waste packages, in which the spent fuel is to be disposed, eventually fail, the fuel is expected to be exposed to hot humid air and dripping groundwater, which will cause the fuel to corrode and release radionuclides. Understanding and modeling the physical and chemical processes that control the fuel corrosion and consequent radionuclide release are important for assessing the repository's performance. We are, therefore, conducting studies to characterize the properties of spent UO_2 fuels and to test their corrosion and radionuclide release behavior under conditions that simulate those expected in the repository. Part of this research includes experiments with unirradiated UO_2. Because commercial spent fuels are greater than 90% UO_2, these experiments provide valuable insight into the corrosion behavior of the predominant component of the spent fuel matrix. Tests are also underway with spent UO_2 fuel samples.

1. *Unsaturated Tests with UO_2 Samples*

Unsaturated experiments, in which simulated groundwater is dripped onto test samples, are used to investigate the corrosion of unirradiated UO_2 and spent UO_2 fuel in an unsaturated oxidizing environment, such as that expected in the proposed repository at Yucca Mountain. In drip experiments, simulated groundwater is injected onto solid samples in stainless steel (SS) reaction vessels maintained at 90°C and 100% relative humidity. The UO_2 dissolves and corrosion products form on the surfaces of the reacted UO_2 or fuel. Two series of drip tests are in progress with unirradiated UO_2: one series with a Teflon support stand, and another series with a perforated 304L SS support stand.

The Teflon-supported tests have been ongoing for 14 years, though four of the seven tests in the series have been terminated (Fig. II-2). Three stages of uranium release (i.e., all uranium transported to the vessel bottom) were identified in these tests. Stage I displays initially low uranium releases during the first one-half year or so. A sharp increase in uranium release characterizes Stage II, which lasts one to two years. This is followed by stage III, during which slower uranium releases are re-established and persist. Initial rapid releases correlated with UO_2 dissolution along grain boundaries and spallation from pellet surfaces of micrometer- to sub-micrometer-sized UO_2 particles. Subsequent slowing of uranium release was accompanied by formation of a mat of U(VI) phases precipitated on UO_2 surfaces.

Trends in cumulative uranium releases that were established during the previous several years have continued into the fourteenth year. One possible exception is experiment PMP8U-6, with a uranium-release rate over the last four years that is approximately one-third that observed during the previous eight (Fig. II-2). Experiment PMP8U-3 is the only experiment with crushed

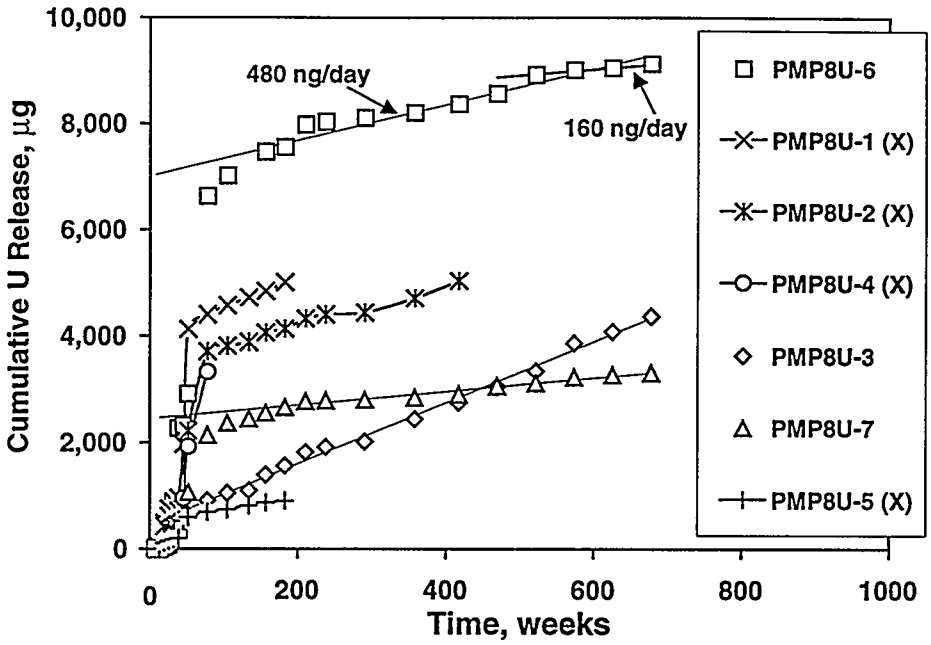

Fig. II-2. Cumulative Uranium Releases for Teflon-Supported Drip Tests. Curves indicate least-squares fit to cumulative releases after the first two years. The (X) indicates a terminated test.

UO_2 powder instead of pellets, and the cumulative release fraction of uranium in PMP8U-3 recently surpassed that of PMP8U-7 (Fig. II-2). Corrosion products of U(VI) were first apparent on UO_2 surfaces after approximately 3.5 years, and spread out to cover much of the upper surfaces of the pellets in the Teflon-supported experiments. There have been no obvious changes to pellet surfaces over the last several years, with the mat of corrosion products remaining relatively thick (~1 mm) on the uppermost surfaces of the UO_2 pellets.

Four SS-supported tests have been running continuously for nine years. Configurations of UO_2 pellets used in these experiments are identical, so that uranium releases are directly comparable. Uranium release rates are much lower in SS-supported experiments (5-120 ng/day) than in Teflon-supported ones (160-910 ng/day). Release rates are comparable to Stage I and III release rates of Teflon-supported experiments. The current release rate in PMP8U-10 is the same magnitude as for current Teflon-supported experiments (Figs. II-2 and II-3), whereas the rates for the other three SS-supported experiments are substantially lower. Uranium releases have remained approximately constant in SS experiments for nearly nine years. The UO_2-pellet surfaces in these tests remain remarkably free of visible alteration products.

Observed differences between the Teflon- and SS-supported experiments are not fully understood. We believe that fluoride, released from the Teflon support stands, may be a factor in the early, rapid uranium releases in the Teflon-supported experiments. Fluorine is known to be an effective complexing ligand for U(VI) in solution. Testing will continue.

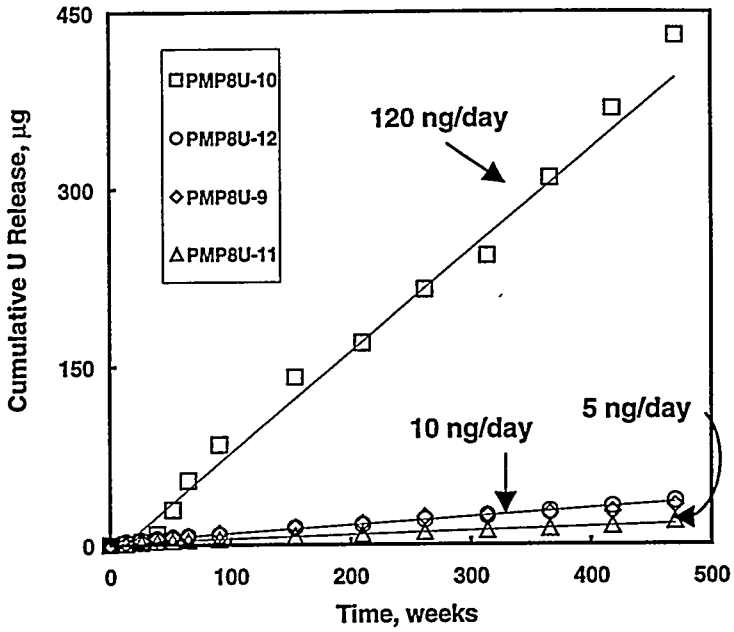

Fig. II-3. Cumulative Uranium Releases for Stainless Steel-Supported Drip Tests with Unirradiated UO_2. Current mass-release rates shown are calculated from a least-squares fit to uranium releases measured during the last 12 sample periods.

2. *Tests with Nominal-Burnup Spent Fuel Samples from Commercial Reactor*

Drip and water vapor tests are underway with two nominal-burnup irradiated UO_2 fuels, ATM-103 and ATM-106, from a pressurized water reactor. Under these test conditions, as the fuel matrix corrodes (i.e., oxidizes and dissolves), uranyl alteration product phases precipitate on, and accumulate at, the surface. As these processes occur, the radionuclides that are embedded in the fuel matrix release incongruently. One of the important objectives of these tests is to understand the role of the alteration phases in sequestering radionuclides and inhibiting their release. For example, it is important to establish and understand the role of the uranyl alteration phases in controlling radionuclide release as the fuel corrodes.

Figure II-4 shows the fractional release rates for Tc, Pu, U, and Np as measured in drip tests with ATM-103. These tests have been in progress for almost 5 years. Because technetium is highly soluble under the test conditions and is believed to be fairly uniformly dispersed in the fuel matrix, its fractional release rate indicates the rate of corrosion of the fuel matrix.[2-4] The lower release rates for the other radionuclides in Figs. II-3 and II-4 indicate that these

---

[2] R. J. Guenther et al., *Characterization of Spent Fuel Approved Testing Material–ATM-103*, Pacific Northwest Laboratory Report PNL-5109-103 (1988).

[3] R. J. Guenther et al., *Characterization of Spent Fuel Approved Testing Material–ATM-106*, Pacific Northwest Laboratory Report PNL-5109-106 (1988).

[4] E. C. Buck, R. J. Finch, P. A. Finn, and J. K. Bates, *Mater. Res. Soc. Symp. Proc.* **506**, 87 (1998).

radionuclides are accumulating in the alteration phases that form at the surface of the corroding fuel (see Sec. II.B.3). Similar results were obtained with ATM-106.

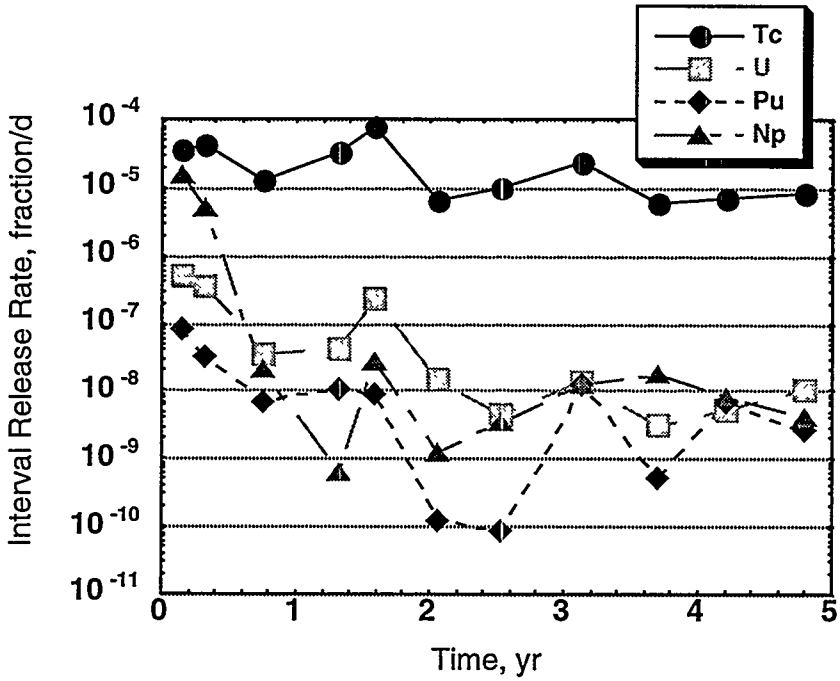

Fig. II-4. Release Rate (fraction per day) for Tc, U, Np, and Pu from ATM-103 during Drip Rate Tests

The release fractions for neptunium at the end of each test interval have been compared to the interval release fractions for technetium. After 5 years of reaction, approximately 4.4% of the technetium has been released from the ATM-103 fuel. Except for the earliest test intervals, the neptunium interval release fraction is 10^3 to 10^4 less than that of technetium. Although neptunium phases are expected to be soluble under the test conditions, they appear to have been incorporated into the uranyl corrosion products. Evidence for the incorporation of neptunium in uranyl phases is the identification of neptunium in dehydrated schoepite, the major alteration phase in the vapor tests.[5] However, because dehydrated schoepite appears to be replaced by more stable uranyl silicate phases (e.g., sodium-boltwoodite) as the fuel corrosion progresses, we are continuing to investigate the role of the uranyl silicates in the observed sequestering of neptunium.

The reacted fuel samples from the drip and vapor tests have been examined by analytical electron microscopy (AEM). Several conclusions have been reached. As illustrated in Fig. II-5, oxidative dissolution of spent UO_2 fuel in vapor and drip conditions occurs via general corrosion at fragment surfaces. Dissolution along fuel-grain boundaries is also evident. Dissolution of fuel along defects is apparent in samples that have been contacted by the largest volumes of water. The outer surfaces of reacted fuel fragments develop fine-grained layers of U(VI) corrosion products adjacent to the fuel (5-15 μm thickness). The thickest and most porous corrosion layers

[5] P. A. Finn, R. J. Finch, E. C. Buck, and J. K. Bates, *Mater. Res. Soc. Symp. Proc.* **506**, 123 (1998).

develop on fuel fragments that have been exposed to the greatest volumes of groundwater (tests at high drip rate). The compositions of corrosion layers depend strongly on water flux, with U(VI) oxy-hydroxides predominating in vapor experiments, and alkali and alkaline earth U(VI) silicates predominating at high drip rates. Lower drip rates give rise to a complex assemblage of corrosion products, including phases identified in both vapor and high-drip-rate experiments.

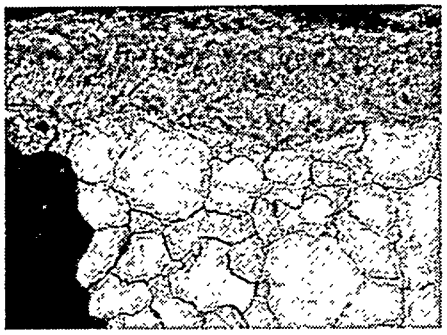

Fig. II-5.

Spent Fuel (bright) Showing Grain Bouandries and Defects along Grain Boundaries. Corrosion layer at top is predominantly Na-boltwoodite.

Analyses of solutions and colloid samples have shown that most plutonium is not released to the leachate in the bottoms of the reaction vessels. We have been unable to detect plutonium enrichment within corrosion layers on the fuel by scanning electron microscopy combined with energy dispersive X-ray spectroscopy (SEM/EDS). However, by combining electron energy-loss spectroscopy (EELS) with AEM, we have obtained evidence that plutonium is accumulating at the interface between the oxidized fuel and U(VI) corrosion products on the surface. These plutonium-rich regions may be residues left after most of the fuel matrix has dissolved. The AEM examinations also revealed cryptocrystalline plutonium-rich regions (100-nm thickness) that contain U, Ru, Zr, and several lanthanide elements. Electron-energy loss spectra indicate that these regions are enriched in both plutonium and lanthanide elements (Fig. II-6). Higher-energy regions of EELS spectra revealed americium enrichment in this region as well, an observation that may have important implications for the long-term disposal of commercial nuclear fuel.

Fig. II-6.

Electron Energy-Loss Analysis of Plutonium-Rich Region in Corroded Fuel

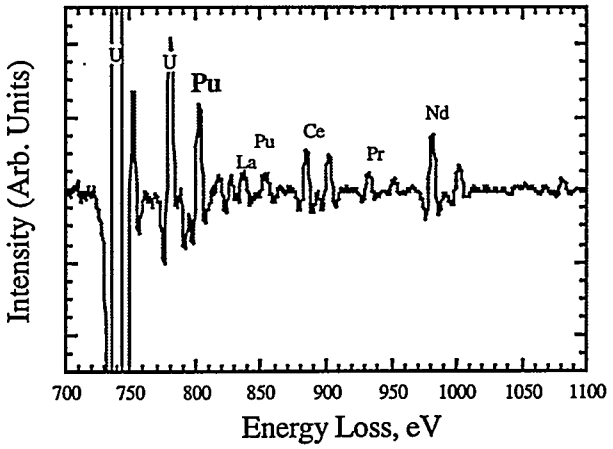

3. Characterization of High-Burnup Spent Nuclear Fuel

In order to interpret the corrosion behavior of high-burnup spent fuel, it is necessary to characterize the distribution of radionuclides within the fuel. We are characterizing samples of fuel (designated as ATM-109) that received high burnups, 60-75 GW days per metric ton uranium, in the Quad Cities boiling water reactor. An AEM examination of ATM-109 samples detected ε-ruthenium phase particles in the fuel matrix. Two types of ε-ruthenium phase particles were identified. One type is about 20 nm in diameter, and the other is approximately 0.25 μm in diameter. The composition of these particles varied between being Mo- and Pd-rich. The most common ε-ruthenium phase in the ATM-109 fuel has a composition close to $Mo_{0.4}Tc_{0.08}Ru_{0.35}Rh_{0.01}Pd_{0.16}$. We found that the ε-phases are more common than those observed in lower burnup fuels. Characterization of these fuel samples is continuing.

4. Tests on Clad Segments of Spent Nuclear Fuel

We are performing two series of long-term tests (vapor hydration and drip) with clad, irradiated UO_2 fuel. The vapor hydration tests are designed to investigate whether exposure of a perforated segment of clad fuel to air saturated with water produces secondary phases sufficient to compromise the integrity of the cladding. If the cladding splits, then the surface area of fuel potentially available for reaction with liquid water would increase, and this increase would need to be taken into account in performance assessment calculations for any potential high-level waste repository.

We are performing four vapor hydration tests with clad spent fuel at 175°C to accelerate the reaction process. Reaction progress is monitored with periodic visual examination and measurement of the diameter of the clad fuel samples. Reacted samples have been observed after 30 and 60 days of testing. Analysis of the samples has revealed no observable deformation of the cladding. Testing will continue.

The drip tests are the clad-fuel analog to drip tests being performed on unirradiated UO_2 fuel fragments (Sec. II.B.1). The clad-fuel drip tests are designed to simulate processes that might occur when groundwater is allowed to percolate through an axial length of fuel. To date, we have prepared five samples for the clad-fuel drip tests and are setting up equipment so that testing may be initiated.

C. Immobilization of Plutonium

The DOE is considering several alternatives for the disposal of surplus plutonium resulting from the dismantlement of nuclear weapons. One such alternative is immobilization, and a titanate-based ceramic has been selected as the preferred waste form. This ceramic contains several phases, including pyrochlore ($A_2Ti_2O_7$), zirconolite ($ABTi_2O_7$), Hf-bearing rutile (TiO_2), and brannerite (BTi_2O_6), where A = Ca and B = actinides, rare earths, Zr, and Hf. A backscatter SEM image of this ceramic is shown in Fig. II-7. This sample also contains zirconolite, but this mineral is not visible in Fig. II-7. Argonne has a program with the objectives of producing the waste form to specification, then characterizing and testing it.

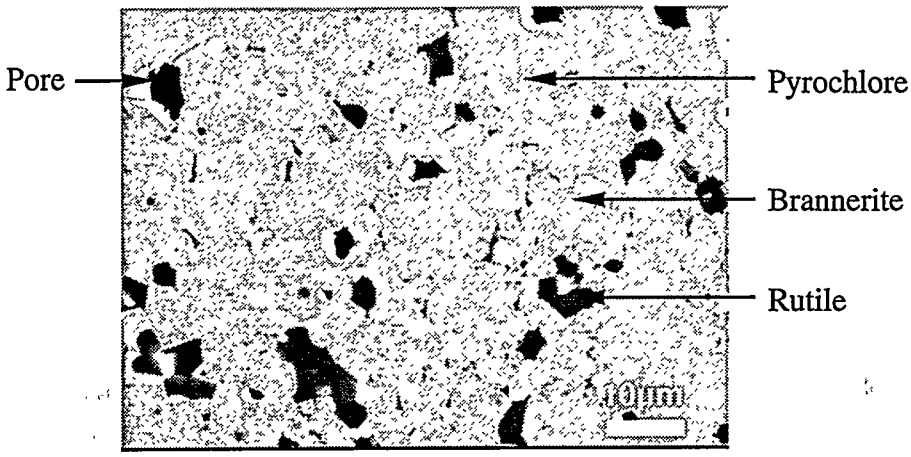

Fig. II-7. Scanning Electron Micrograph Backscatter Image of Hf-Ce-U Baseline Ceramic

1. Ceramic Fabrication

Ceramics are being fabricated at ANL to (1) better understand phase formation and phase boundaries and (2) prepare samples for corrosion testing. Fabrication this year has focused on the preparation of eight compositions of plutonium titanate ceramics. These compositions were designed to yield a range of phases that result from reactive sintering at 1350°C. Each of the ceramics was made by standard procedures. Fine-grained raw materials were wet ball milled to produce well-mixed slurries. The slurries were dried in air at approximately 110°C, then broken into granules to enhance reactivity and to ease handling. This material was calcined to drive off absorbed water and to decompose possible hydroxide and carbonate species. The highly activated, calcined powders were uniaxially pressed, then reactive sintered at 1350°C.

The sintered ceramics were about 90% theoretical density; green densities averaged 40% theoretical density. The phase assemblage of the baseline ceramic was mostly pyrochlore with minor amounts of rutile, zirconolite, and brannerite. Depending on the amount of impurities present, other phases such as perovskite and amorphous silicate phase(s) were also found. These ceramics were then used for further characterization and corrosion testing.

Over 300 ceramic specimens were successfully produced this year for corrosion testing. During this period, the proposed processing techniques were refined and subsequently employed at the other DOE fabrication sites. Additional ceramic compositions will be made to map out isothermal sections of the equilibrium phase diagram and will be used for characterization and corrosion testing.

2. Ceramic Characterization

A number of ceramic formulations were investigated with electron microscopy to identify phase compositions, structure, and oxidation states. This information is needed to interpret

corrosion data and to help in the formulation activities. Samples examined this year included the Hf-Ce-U baseline composition and a range of impurity-bearing formulations.

In these ceramics, zirconolite appears to be present primarily as the 2M structure type. The {001} planes of this zirconolite-2M are preferentially oriented on the {111} planes of pyrochlore, which is the most abundant phase in many of the ceramics examined. In Fig. II-8, diffraction patterns of zirconolite-2M and pyrochlore are shown. The d_{111} spacing in pyrochlore is about 0.57 nm (Fig. II-8a) and is approximately the same as the d_{002} spacing in zirconolite. A TEM multibeam image of pyrochlore taken along the B[110] axis is shown in Fig. II-9a. At lower TEM magnifications, we observed lamellae within the pyrochlore (see Fig. II-9b and II-9c); X-ray analysis suggested that these possessed a zirconolite-like composition. The lamellae may possibly be of the zirconolite-4M type and, in the Hf-Ce-U ceramics, are always enriched in hafnium and depleted in uranium relative to the surrounding pyrochlore. Energy dispersive spectroscopy indicated that the intergrowths are depleted in uranium and enriched in hafnium. More convincing evidence came from filtered images of the intergrowths. Electron energy-loss image maps of uranium showed that these lamellae are depleted in uranium.

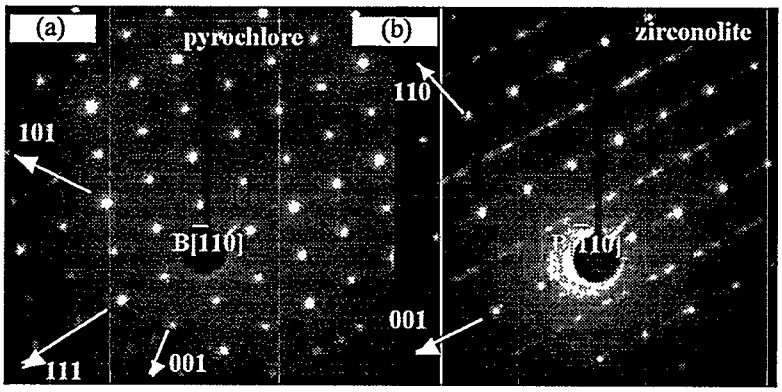

Fig. II-8. Electron Diffraction Patterns from Neighboring Grains of (a) Pyrochlore and (b) Zirconolite

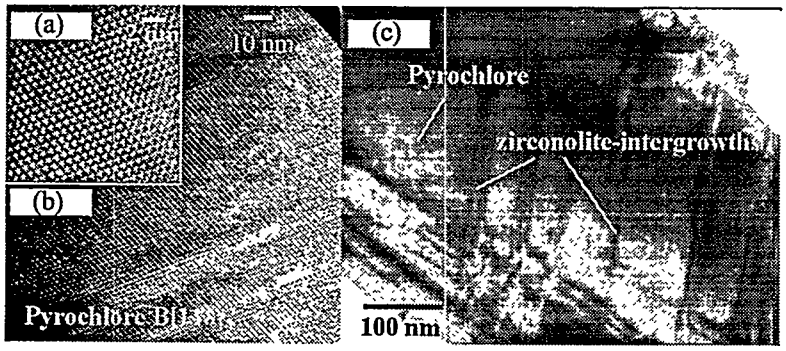

Fig. II-9. High (a), Medium (b), and Low (c) Magnification Images of Zirconolite Intergrowth Structures within Pyrochlore

As zirconolite may be considered a derivative of the cubic pyrochlore structure, the intergrowth of these two phases in the ceramic is not surprising. However, these lamellae may be formed as a result of the large amounts of hafnium introduced into the formulation of the titanate ceramic: the small hafnium ion is more easily accommodated by the seven-fold coordinated B site in zirconolite than by the large eight-fold coordinated A site in pyrochlore.

3. Ceramic Corrosion Testing

Corrosion tests with a Ba-Zr, zirconolite-rich ceramic were initiated to provide input for corrosion models that are under development. The ceramic studied contains Ba, Zr, and Pu and is dominated by the titanate mineral zirconolite. While the ceramic proposed for plutonium disposition contains Hf, Pu, and U and is dominated by the mineral pyrochlore, we expect the corrosion behavior of these two ceramics to be similar. An additional benefit of this work is that it will aid in planning the testing strategy for the Hf-U-Pu ceramic scheduled to begin in 1999.

The ceramic samples tested contained primarily (about 85%) zirconolite and lesser amounts of rutile, PuO_2, Pu-brannerite, and perovskite. Tests conducted include MCC-1, PCT-A, PCT-B, and VHT. The MCC-1 and PCT-A tests are used to compare the corrosion behavior of this ceramic to previously published results for other waste materials and to compare the corrosion behavior of different ceramic compositions. Results from MCC-1 tests are also used to estimate the maximum corrosion rate in highly dilute solutions. The PCT-B tests provide data pertaining to the corrosion of the ceramic in relatively concentrated solutions. Finally, the VHT is designed to generate solid alteration phases on the glass surface in a short time and to determine the effects of those alteration phases on the corrosion rate of the ceramic.

The test results led to two important conclusions regarding the corrosion of this ceramic. First, the ceramic dissolved incongruently. The corrosion data suggest that the incongruent dissolution resulted from preferential dissolution of some phases (especially perovskite) and the release of material from grain boundaries. Second, the measured corrosion rate was dependent upon the test duration and test type. The change in corrosion rate is likely due to solution saturation effects or the formation of a transport barrier. While the data obtained did not allow us to distinguish between these two mechanisms, experiments have been proposed which should allow such a distinction. Overall, the results obtained from testing this zirconolite-rich ceramic provide a basis for development of a qualitative corrosion model and important input for quantitative models.

Because of the presence of impurity elements in the expected plutonium feeds, eight ceramics fabricated at Lawrence Livermore National Laboratory (LLNL) were tested to determine the effects of impurities on the corrosion behavior of the titanate ceramic. It was expected that the addition of impurity elements would lead to the formation of additional phases and, therefore, would affect corrosion behavior. Typical impurity elements include Al, Mg, Fe, Cr, Ni, K, Na, Si, Ta, B, W, Ga, Zn, F, and Cl. The baseline ceramic (containing no impurities) contains four phases: pyrochlore, zirconolite, rutile, and brannerite. The ceramics in this study were characterized with SEM and AEM. The results indicated that the presence of impurities in the base ceramic leads to the formation of two additional phases, a silicate phase and perovskite. Results from MCC-1 tests showed that the presence of the silicate phase leads to increased

release of both Ca and Ce. Calcium is present in both the silicate and the phosphate phase; cerium is present only in the phosphate phase. The presence of brannerite led to increased release of uranium. In the absence of brannerite, the uranium was primarily present in the pyrochlore and zirconolite. The presence of perovskite resulted in relatively high leachate pH and a significant increase in the release of calcium.

Integrated VHTs are being completed to evaluate the effect of glass on the corrosion behavior of the ceramic. These tests are being conducted because the plutonium ceramic will be disposed of in the same container with glass ("can-in-can" method). A series of vapor hydration tests at 200°C was initiated with the baseline Hf-Pu-U ceramic and a nonradioactive glass similar to that expected to be produced in the Defense Waste Processing Facility. In addition, separate tests were initiated with the glass and ceramic alone to provide information on their corrosion behavior. Preliminary results from a 28-day integrated VHT showed an alkali-depleted layer covering the glass surface, with a small amount of the glass alteration product on the ceramic surface. At the interface between the glass and ceramic and at the outer ceramic surface, silica-rich regions up to 10 μm deep appeared to form in ceramic matrix defects. Corrosion testing with the individual ceramic waste form revealed the presence of a very thin layer on the ceramic surface; using SEM/EDS techniques, we found that the composition of this layer was indistinguishable from that of the ceramic matrix. In the glass-only test, the same alkali-depleted alteration layer formed that was observed in the integrated test. Further characterization of the test monoliths is ongoing.

In addition to the integrated VHTs, we initiated drip tests with both U- and Pu-bearing ceramic monoliths. In drip tests at 90°C, a small amount of water that has been reacted with a glass frit is slowly dripped on a ceramic monolith. Tests with these samples have been in progress for 98 days. The drip test monoliths have developed a white alteration product on the ceramic surface. This layer is likely a silicate phase; however, this identification cannot be confirmed at this time. Testing will continue.

D. Testing of Savannah River and West Valley Glasses

Tests have been conducted under the auspices of the DOE Office of Environmental Waste Management to characterize the corrosion behavior of several glasses developed for the Defense Waste Processing Facility (DWPF) at the Savannah River Site and the West Valley Demonstration Project (WVDP). The goal of the tests is to gain insight into the corrosion mechanism and long-term behavior of waste glasses under unsaturated repository conditions, such as those of the proposed Yucca Mountain site. A mechanistic understanding of how radionuclides are released from vitrified waste forms (and from other waste forms, as well) is needed because materials cannot be evaluated for the time scale over which radionuclides must be contained or under the range of environmental conditions that may exist during the service life of the disposal system. Therefore, tests are being conducted to study both the intrinsic corrosion behavior of reference waste glasses and the corrosion behavior under conditions similar to those anticipated in the disposal system over a time scale on the order of 10,000 years. These tests provide insights regarding the glass corrosion mechanism, the modeling of corrosion behavior, the important uncertainties that remain, and the relationship between test results and corrosion progress.

The samples that have been tested include glasses made with actual waste sludge and glasses made with chemical simulants for radionuclides. Some glasses were provided by the Savannah River Technology Center (DWPF reference glasses) and the Catholic University Vitreous State Laboratory (WVDP reference glasses), while other glasses were made at CMT.

The test methods fall into three categories: dissolution tests, vapor hydration tests, and drip tests. Dissolution tests are conducted to measure the intrinsic dissolution behavior of the glass and the disposition of radionuclides. Tests are conducted in an aqueous solution (demineralized water or tuff groundwater) and usually at 90°C. Test durations range from a few days to several years. Tests are conducted as batch tests, and the solution and solids are analyzed to characterize the extent and nature of corrosion. Most tests are variations of the MCC-1 test conducted with monolithic samples or variations of the PCT conducted with crushed material. Depending on the test conditions used, insight is provided into corrosion behavior when water first contacts the glass or after the glass has corroded for many years. Vapor hydration tests are conducted to identify alteration phases that form at advanced stages of corrosion relevant to disposal times exceeding several thousand years. Tests are conducted at elevated temperatures (typically 125-200°C) for durations of a few days to several years. The altered surface is examined at the end of the test to characterize the physical and chemical changes in the glass and to identify any alteration phases that form and determine if they contain radionuclides. Changes in the surface provide insight into the corrosion mechanism and the identity of alteration phases that must be known for performance assessment calculations. The drip test characterizes glass corrosion under a likely contact scenario in which groundwater drips through a pinhole breach of the canister and drips onto the waste form. The dripping water interacts with the glass as it runs over its surface until it drips off. Leachate solution is periodically removed from the test vessel to track sample dissolution, while the reacted sample is examined at the end of the test. The drip tests confirm whether the corrosion mechanism determined from dissolution and vapor hydration tests is operative under repository-relevant conditions. Some results of recent dissolution and drip tests are presented below.

1. Dissolution Tests

Dissolution tests with crushed material have been in progress for test durations of several years with glasses made with DWPF sludge, glasses doped with important radionuclides, and glasses made chemically similar to sludge-containing glasses but with nonradioactive additives. Tests were conducted at a high ratios of glass surface area to solution volume (S/V) so that the solutions became highly concentrated within a short time. This was done to be representative of glass corrosion over very long periods in a disposal system. Highly concentrated solutions simulate long disposal times because the dissolution behavior of glass depends on the amount of dissolved silica rather than time. The most important past finding in these tests is that the long-term dissolution rate increases after certain alteration phases precipitate from the solution.[6,7] The same effect has been seen in vapor hydration tests.[8] In general, rate-affecting phases form within a shorter test duration for less durable glass than for more durable glasses. Until recently, the

[6] W. L. Ebert and J. K. Bates, *Mater. Res. Soc. Symp. Proc.* **176**, 339-346 (1990).

[7] W. L. Ebert, J. K. Bates, and W. L. Bourcier, *Waste Manage.* **11**, 205-221 (1991).

[8] W. L. Ebert and J. K. Bates, *Nucl. Technol.* **104**(3), 372-384 (1993).

effect of alteration-phase formation was only observed in tests with simulated and doped glasses; it had not been observed in tests with sludge-based glasses. Feng et al.[9] have speculated that radiolysis effects or the presence of anions in the radioactive glass somehow delays or prevents rate-affecting alteration phases from forming.

Recent calculations have shown that neither pH effects nor the presence of anions can account for the different behavior. Moreover, alteration phases have formed in tests with a sludge-based glass after about 6 years and led to an increase in the glass dissolution rate. Figure II-10 shows the normalized release results of dissolution tests (PCT type) conducted with a glass made with frit SRL 200 plus sludge from the Savannah River Site, referred to as SRL 200R glass, and with a simulated waste glass having essentially the same composition plus chemical additives, referred to as SRL 200S glass. Alteration phases formed in tests with SRL 200S glass after about 300 days and led to complete dissolution within a few weeks later. This is indicated by the normalized mass loss for boron increasing to greater than 40 g/m^2. [The

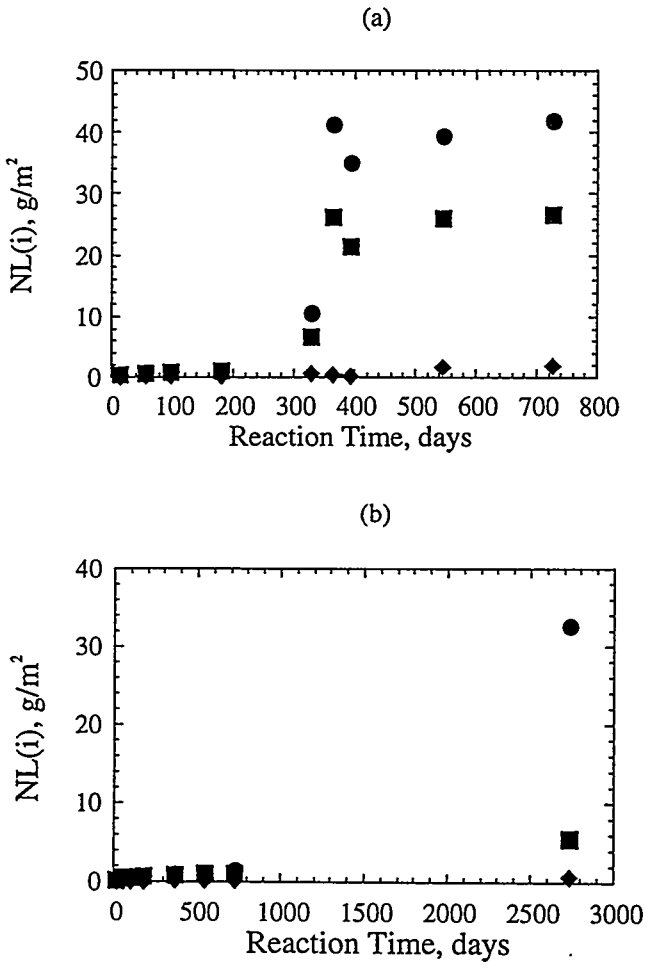

Fig. II-10.

Results of Dissolution Tests Conducted at S/V = 20,000 m^{-1} with (a) SRL 200S Glass and (b) SRL 200R Glass. Normalized mass losses, NL(i), shown for boron (circles), sodium (squares), and silicon (diamonds)

[9]X. Feng, J. K. Bates, E. C. Buck, C. R. Bradley, and M. Gong, *Nucl. Technol.* **104**(2), 193-206 (1993).

normalized release is defined by $NL(i) = M_i/(c_i A)$, where M_i is the measured mass of element i in the leachate solution, c_i is its element fraction in the source glass, and A is the surface area of the glass.] Rate-affecting alteration phases had not formed after 728 days in tests with SRL 200R glass but had formed in tests conducted for 2749 days. One additional test with SRL 200R glass remains in progress; it will be run for about 3000 days to confirm the behavior observed in the 2749-day test. The difference in the time when rate-affecting alteration phases formed was attributed to differences in nucleation of the phases.

Similar tests are being conducted with sludge-based SRL 51R glass and a compositionally identical glass made with simulants, SRL 51S. Results available to date are shown in Fig. II-11. Rate-affecting alteration phases have not been detected in tests with either glass. However, these results with SRL 51S differ from tests with other glasses in that normalized mass losses for boron continue to increase with each test duration. This may indicate that alteration phases have formed between 539 and 1115 days but are too small to be detected. Tests with longer durations are in progress.

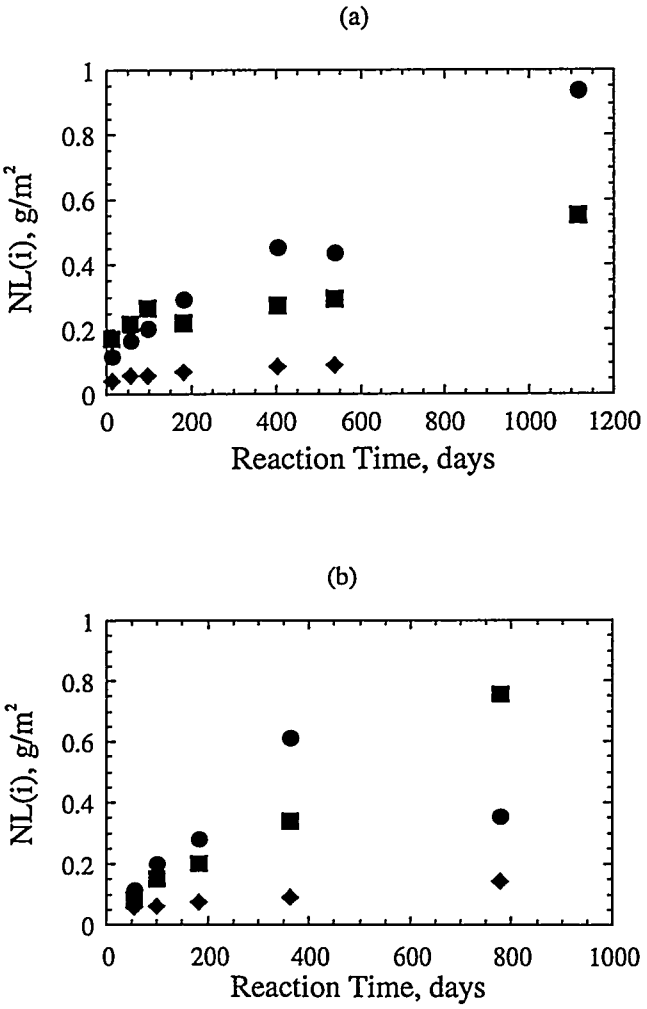

Fig. II-11.

Results of Dissolution Tests Conducted at S/V = 20,000 m^{-1} with (a) SRL 51S Glass and (b) SRL 51R Glass. Normalized mass losses, NL(i), shown for boron (circles), sodium (squares), and silicon (diamonds).

2. Drip Tests

Unsaturated glass tests, designated the N2 tests, were initiated in February 1986 on actinide- and technetium-doped SRL 165 glass. These tests are still in progress and have been sampled intermittently over the ensuing period of nearly 13 years, with regular sampling at 26-week intervals since December 1993. Designed to simulate potential conditions at the proposed Yucca Mountain repository, these 90°C tests combine slowly dripping, tuff-equilibrated groundwater (EJ-13 water) with a monolithic waste glass sample, sensitized 304L stainless steel, and water vapor to determine synergistic interactions possible in a compromised pour canister under unsaturated conditions. Semiannual analyses of the leachate are performed to monitor release of glass components, including actinides. Details of the test procedure and test results can be found elsewhere.[10,11] Particulate and colloidal materials released to solution are also analyzed by analytical transmission electron microscopy and sequential filtering with alpha spectroscopy (for transuranic content). These combined data indicate that insoluble elements, including U, Pu, and Am, are incorporated into alteration phases as the glass reacts and are subsequently released with particulate or colloidal matter as the alteration products slough from the glass. Recent trends have shown that the releases of Pu and Am, while initially quite low compared to those of soluble elements (such as B and Np), eventually are accelerated as the alteration phases in which they are entrained slough from the glass surface and enter the test solution.[11] Ultimately, the release of these actinides will be determined by the transport of the particulates suspended in solution.

In another test series, termed the N4 tests, sludge-based SRL 200R waste glasses have been exposed to unsaturated test conditions for as long as 7 years. This test series included both as-cast glass and glass that had been pre-hydrated by exposure to 200°C water vapor. The 200°C temperature was used to accelerate the hydration reaction and to impart a degree of aging to the glass by an amount that would occur at ~90°C for long periods. When the glass is pre-hydrated, the relationship between the rate of reaction and temperature is of concern. In particular, the high temperature and humidity combination used is not representative of a particular scenario possible in the repository but is meant as a means for accelerating the aging effects.

The test results showed that actinides (except neptunium) are retained in alteration products and released primarily as solution-borne colloids and particulates when fresh glass is reacted. Pre-hydrated (aged) glass, however, rapidly released most elements (including actinides) when first exposed to dripping water. Normalized boron release from the aged glass was more rapid than that of any other element by an order of magnitude. The response of aged glass, as determined by cumulative boron release, follows a power-law behavior with time, corresponding roughly to $t^{1/4}$. This is consistent with diffusional transport through clay alteration phases on the glass surface.

Figure II-12 shows the normalized mass release of Li and B in the vessel rinse from the N4 tests into solution as a function of time. As shown, the release of both Li and B is roughly two orders of magnitude higher in pre-hydrated glass versus as-cast glass. The release of these

[10] J. A. Fortner and J. K. Bates, *Mater. Res. Soc. Proc.* **412**, 205-211 (1996).

[11] J. A. Fortner, S. F. Wolf, E. C. Buck, C. Mertz, and J. K. Bates, *Mater. Res. Soc. Proc.* **465**, 165-172 (1997).

elements is an important gauge of the glass corrosion, as they are not expected to form secondary phases, are not major components of the EJ-13 groundwater, and are not present in the steel reaction vessels. Negligible amounts of Li and B were measured in acid strip solutions. Future efforts will seek to establish a measure of the effect of pre-hydration upon the corrosion behavior of waste forms, as well as to gain a fundamental understanding of what the aging process itself may entail, whether it is hydration or other effects, such as radiation damage.

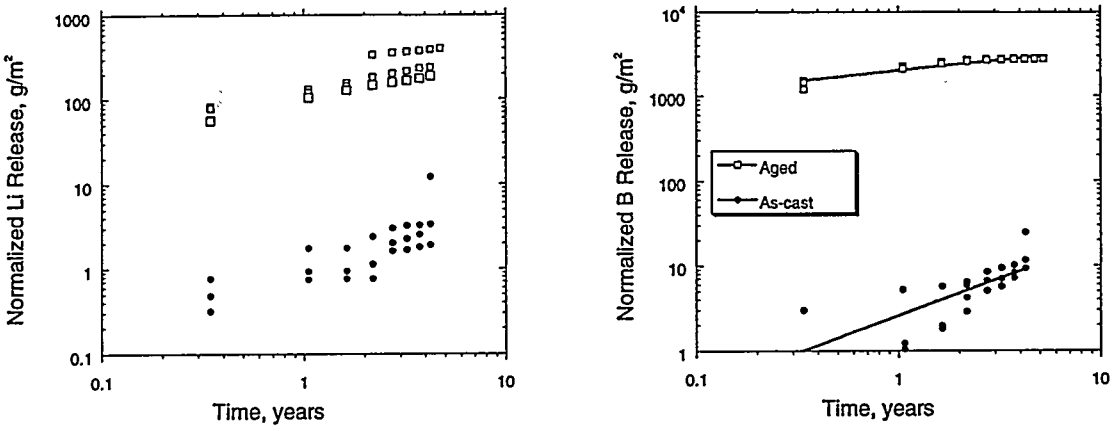

Fig. II-12. Normalized Cumulative Release of Lithium (left) and Boron (right) from the N4 Tests as a Function of Elapsed Time. Open symbols are from samples pre-hydrated in water vapor prior to testing, while solid symbols represent as-cast glass samples. The lines on the boron plot are power-law fits to the data, with slopes of ~1/4 and ~1 for the aged and as-cast glasses, respectively.

3. *Critical Review and Testing of Natural Analogues*

A critical review has been completed on the present state of knowledge regarding the applicability of natural glasses as analogues for the long-term behavior of nuclear waste glasses. Information has been critically analyzed on corrosion processes obtained in studies of a variety of naturally reacted glasses (tektite, obsidian, and basalt) from a wide range of geologic environments and under controlled laboratory conditions. This review has shown how natural glasses provide insight into the corrosion mechanism of nitrate glasses and glass areal distribution rates. Naturally reacted glasses can also be used to calibrate accelerated laboratory tests.

We have also characterized the interface between glass and alteration phases formed on subaerially altered Hawaiian basalt glasses (700 years old) with analytical transmission electron microscopy. The objective was to study the compositional and structural changes that occur and identify alteration phases. Such characterization provides insight into the processes involved in the long-term corrosion of basalt and, by analogy, high-level waste glasses.

Our study provided the first evidence that a gel layer forms at the basalt/alteration layer interface. This observation provides evidence that the alteration mechanism for waste glass corrosion which has been observed in short-term laboratory tests[12] is the same for basalt corrosion in nature. The surface of naturally altered basalt glass is shown in Fig. II-13. The glass is on the right-hand side of the figure, and the alteration layer (palagonite) is on the left-hand side. The glass chattered during sample preparation. A gel layer of up to 0.5-μm thick can be seen at the glass surface. The glass, gel, and palagonite are compositionally distinct. A high density of small, dark, iron-rich precipitates (approximately 10 nm) can be seen embedded in the palagonite and gel layer. Compositional analysis indicated that the gel layer was nearly free of alkali and alkaline earth elements (Na, Ca, and Mg), which had presumably been leached from the glass as the gel formed. The layer was also enriched in Fe, Ti, and Al and depleted in Si relative to the glass.

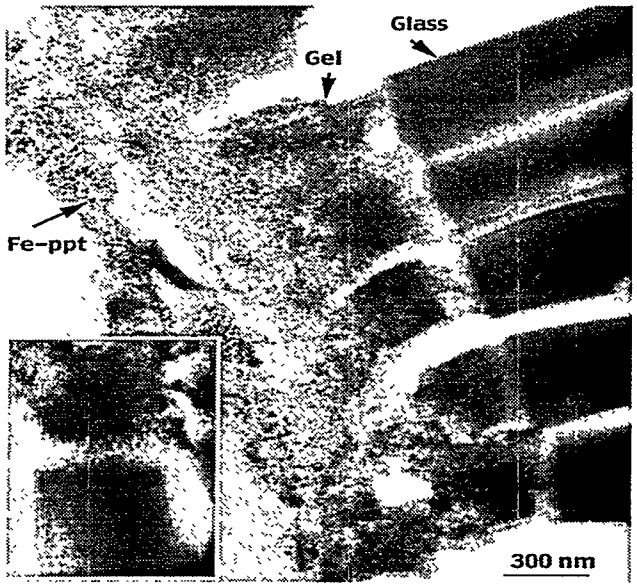

Fig. II-13.

Transmission Electron Photomicrograph of the Altered Surface of Natural Basalt

E. Qualification Testing of Ceramic Waste Forms

Argonne is developing an electrometallurgical process to put spent nuclear fuel in a favorable form (Sec. IV) for repository disposal. Easily oxidized fission products and transuranic elements accumulate in the molten LiCl-KCl electrolyte used in the process and must be removed periodically and, eventually, disposed of as high-level radioactive waste. The process for producing a waste form to immobilize the salt involves first blending it with dehydrated zeolite A to incorporate the salt and radionuclides into the crystal structure of the zeolite. The salt-occluded zeolite is then mixed with a borosilicate glass and processed at high temperature and pressure to produce a ceramic waste form (CWF). Work had been done previously to study the effects of the mass ratios of salt, zeolite, and glass used to make the CWF; the particle size and type of zeolite used; and the benefits of various additives on the chemical durability of the

[12] W. L. Ebert and J. K. Bates, *Ceram. Trans.* **61**, 479-488 (1996).

waste form.[13] A reference waste form that is made with about 75 mass% clay-bonded zeolite 4A and 25 mass% glass is being used in the testing program. During processing, zeolite 4A converts to sodalite, and the reference waste form is referred to as a "glass-bonded sodalite." Sodalite is more dense than the zeolite that is used to occlude the salt and has smaller pore size. Some of the occluded waste material is released during the transformation of zeolite to sodalite, and small amounts (a few mass percent) of various oxides, rare earth oxychlorides, and salts are produced.

Work is in progress to generate a data base and corrosion model that can be used to support qualification of the CWF for disposal in a high-level radioactive waste disposal system. Our approach is based on the requirements established by the DOE Office of Civilian Radioactive Waste Management for high-level waste glass and insight regarding how corrosion of this glass may be treated in the Total System Performance Assessment that will be conducted for the disposal system. Early scoping tests showed that ceramic waste forms made with zeolite 4A are more durable than reference high-level waste glasses in tests commonly used to characterize high-level waste glasses, such as MCC-1 and PCT. However, direct comparison to glass in specific tests will probably not be sufficient to qualify the CWF. Instead, a mechanistic understanding is needed to explain why the CWF performs better than waste glasses in those tests and to be able to predict the long-term performance of the CWF in a disposal system. Therefore, tests are being conducted to (1) characterize the corrosion behavior of the CWF, (2) measure the release rates of waste form matrix components and radionuclides, (3) develop a mechanistic model of waste form corrosion behavior that can be used in performance assessment calculations for the disposal system, and (4) develop a methodology for measuring the consistency of waste forms that are produced.

The scoping tests indicated that corrosion of the CWF is controlled primarily by matrix dissolution. Ion exchange was observed not to be important in the release of occluded material from sodalite contacted by demineralized water. Tests conducted with a NaCl-KCl-MgCl brine solution did show that cesium and other occluded salts will exchange with magnesium. However, this will not be an important release mechanism under disposal conditions, since tuff groundwater contains only a low concentration of magnesium and, to the best of our knowledge, there will not be a significant source of magnesium in the disposal system. A model developed to describe the dissolution of aluminosilicate minerals[14] has been modified to describe the dissolution of high-level waste glasses[15] and will likely be used in performance assessment calculations for the disposal system.[16] Tests are being conducted to verify that the same rate expression can also be used for the sodalite and glass phases of the CWF. If it can, qualification of the CWF would be greatly simplified, since that expression is well established and already incorporated into the performance assessment model. Values of model parameters would simply

---

[13] J. J. Laidler et al., *Chemical Technology Division Annual Technical Report, 1997*, Argonne National Laboratory Report ANL-98/13, pp. 111-113 (1998).

[14] P. Aagaard and H. C. Helgeson, *Am. J. Sci.* **282**, 237-285 (1982).

[15] B. Grambow, *Nuclear Waste Glass Dissolution: Mechanism, Model, and Application*, JSS Report 87-02 (1987).

[16] TRW Inc., "Waste Form Degradation, Radionuclide Mobilization Preliminary, and Transport Through the Engineered Barrier System," in *Total System Performance Assessment-Viability Assessment (TSPA-VA) Analyses Technical Basis Document,* Chapter 6, TRW Environmental Safely Systems report B00000000-01717-4301-0006 REV 01 (1998).

be needed for the sodalite and glass phases of the CWF. The dissolution of other phases (particularly those phases that contain radionuclides) must be addressed separately.

The rate expression for glass dissolution includes three key terms that must be measured experimentally: the forward rate, the saturation concentration of orthosilicic acid, and the long-term rate. The forward rate is the dissolution rate of the material when the solution concentration of orthosilicic acid is near zero and depends on the temperature and pH; the saturation concentration is the concentration of orthosilicic acid at which the dissolution rate becomes near zero; the long-term rate is an *ad hoc* term included to account for the fact that the dissolution rate of glass must always be greater than zero. To apply the rate expression to the CWF, these values must be measured for the sodalite and glass phases of the CWF. Short-term scoping tests have shown that the forward rates of the sodalite and glass phases of the CWF are similar to those of high-level waste glasses measured under the same test conditions. The forward rates determined from MCC-1 tests conducted for 1 and 3 days at 90°C and near-neutral pH values were about 1.5 and 0.5 g/(m^2·day) for nearly pure sodalite and pure glass, respectively. [The actual forward rate for sodalite is probably less than 1.5 g/(m^2·day) if the surface roughness of the samples used in the tests is taken into account.] The forward rate calculated for the CWF with 75% sodalite and 25% glass is 1.25 g/(m^2·day). The forward dissolution rate of the reference ceramic waste form was measured to be about 1.3 g/(m^2·d) in MCC-1 tests. For comparison, the forward rates for high-level waste glasses measured with the same method range between about 1 and 2 g/(m^2·d).

Tests are in progress to measure the temperature and pH dependencies of the forward rates for sodalite, glass, and the CWF. These must be known to calculate the dissolution rate as conditions in the disposal system change over time. We are working with colleagues at ANL to develop a computer model that can be used to predict the long-term behavior of the CWF based on a mechanistic corrosion model. Scoping calculations have shown that the lower solubility of the CWF compared to waste glasses will result in greater long-term durability, even if the forward rate of the CWF is higher than that for waste glasses. The calculations also show the large impact of the long-term rate term. Work is in progress to determine that value for the CWF and to develop a model for the change in the accessible surface area of the sodalite phase as the waste form corrodes.

Static tests with crushed glass at a high S/V ratio are being conducted to measure its saturation concentration. Saturated solutions have not yet been attained in tests completed through 91 days. The results available to date, however, indicate that the saturation concentration will be less than about 50 mg/L Si. (Tests scheduled for up to 2 years are in progress to verify the saturation concentration.) This is significantly less than the saturation concentrations for high-level waste glasses, which are typically 100-120 mg/L Si. This indicates that a solution will become saturated with the CWF faster than with a waste glass. The long-term rate for the CWF is being measured. We anticipate that it will be lower than the long-term rate for glass, since sodalite can equilibrate with the solution and the dissolution rate can be zero.

Tests are being conducted with reference CWF material produced in 32 separate hot isostatically pressed cans to address the development of a product consistency test for the ceramic. The consistency of the material in the different cans was evaluated with release results from 3-day MCC-1 tests and 7-day PCTs, along with measurement of the amount of accessible

free salt. The latter is defined as salt that can be dissolved in two consecutive washes with demineralized water at room temperature. The MCC-1, PCT, and accessible free salt measurements all show significant scatter in the concentrations of Cl, I, Cs, and to a lesser extent, Na. These elements are present as accessible free salts. The release of elements that are contained primarily in the sodalite and glass phases (Al, B, Li, K, Si, etc.) is less scattered. However, the scatter in the PCT results of all elements is greater than the testing uncertainty, which is measured by the variability in replicate tests with the consolidated material. These tests indicate significant variability in the materials processed in different cans under identical processing conditions. Tests will be conducted with materials produced under different conditions to gauge the significance of the variability measured with the materials processed under identical conditions.

We have completed PCTs with consolidated, crushed CWF material at two S/V ratios, 2000 and 20,000 m^{-1}, for 7, 28, and 91 days. The corrosion behavior at both S/V ratios was similar. A large amount of Cl, Na, and Cs was released in the 7-day tests. The Cl and Na concentrations remained nearly the same after 28 and 91 days, but the solution concentration of cesium decreased with test duration. The release of B, Li, and Si increased with test duration. The initial release of Cl, Na, and Cs is likely due to dissolution of accessible salt, while B, Li, and Si are released as the sodalite and glass phases dissolve. The decrease in the cesium concentration with time probably results from its incorporation into alteration products, although this has not been confirmed experimentally. The lower release of silicon compared with that of B and Li indicates that silicon is also being incorporated into alteration phases. It is unlikely that cesium is entering the sodalite cages (for example, by ion exchange with lithium) because the ionic diameter of cesium is larger than the opening in the sodalite cage (0.334 nm compared with 0.22 nm).

Somewhat different behavior is observed in MCC-1 tests conducted for 1, 3, 28, and 91 days than was observed in the PCT. The release of Cl, Cs, Li, Na, Si, and to a lesser extent B increased through 28 days, but not between 28 and 91 days. It is possible that the solution had become saturated with respect to sodalite within 28 days under these test conditions.

In addition to tests being conducted to measure parameter values in the rate expression for the sodalite and glass phases and characterize the long-term corrosion behavior, work is in progress to identify and characterize minor phases generated during waste form processing. The dissolution behavior of important phases (i.e., phases containing radionuclides) will be measured and incorporated into the model for CWF corrosion.

F. Fundamental Studies of Actinide Behavior

1. Microbiological-Actinide Interactions in Subsurface Environments

The behavior of radionuclides is being investigated under conditions relevant to subsurface groundwaters on DOE sites. Emphasis is on factors that affect

mobilization/immobilization of actinides. Results of this work will establish key factors concerning the chemistry of actinide/organic mixtures in the presence of microbes, inorganic substrates, and metal cations.

The interactions between actinides and microorganisms in subsurface environments play an important role in determining the fate of actinide species during bioremediation efforts of organic contaminants. They also help predict the fate of radionuclides in proposed nuclear waste repositories. Improving our ability to predict the effects of chelate biodegradation on the fate of actinides in the subsurface has broad applicability, since many natural organic compounds and microbially derived byproducts found in the subsurface mimic the behavior of anthropogenic complexants.

Our research in this area, which was initially focused on aerobic systems, was extended to the study of actinide reduction under anaerobic conditions. Emphasis was on the fate of neptunium in biologically active anaerobic systems. The migration of neptunium isotopes, especially ^{237}Np, away from nuclear waste sites and repositories presents a significant long-term health risk.

To evaluate the effect of anaerobic microbial activity on the fate of neptunium in natural systems, Np(V) was added to live and sterilized microcosms inoculated with anaerobic sediments from a metal-contaminated freshwater lake. The samples included metal-reducing, sulfate-reducing, and methanogenic microorganisms. In a few days, the soluble neptunium in the microcosm decreased by approximately two orders of magnitude. Similar decreases in neptunium solubility were observed in abiotic controls. Using X-ray absorption near edge structure (XANES) analysis at the ANL Advanced Photon Source (APS), we showed that the predominant neptunium oxidation state under biotic and abiotic conditions is Np(IV), suggesting that microbially reduced Fe(II) or Mn(II/III) may serve as the source of electrons for neptunium reduction in this system.

Several groups of microorganisms are known to utilize uranium and other metals directly as electron acceptors for anaerobic respiration. Sulfate-reducing bacteria (SRB) are among the most ubiquitous metal reducers in natural systems. To assess the ability of SRB to reduce Np(V) directly, we inoculated a minimal growth medium containing pyruvate with a consortium of SRB in sealed bottles. After several days of growth, Np(V) and various electron donor substrates were added to the vessels, and neptunium solubility was monitored periodically. Figure II-14 shows the fraction of neptunium precipitated from solution in the presence of H_2, pyruvate, and a combination of H_2 and pyruvate. Also included was a "blank" run (sterile control), which showed essentially no loss of neptunium from solution. Although precipitation occurred in all cases except the blank, it was most rapid when H_2 was supplied as the electron donor substrate. Preliminary XANES analysis has suggested that the oxidation state of the precipitated neptunium is +4, indicating that SRB are directly reducing Np(V). Because previous work with SRB at Northwestern University[17] has shown that H_2 availability plays an important role in SRB metabolism, in future work we will investigate this reduction mechanism in more detail. Plans

[17] C. P. Lienemann, M. Taillefert, D. Perret, and J. F. Gaillard, *Geochim. Cosmochim. Acta* **61**, 1436 (1997).

are also to continue with the study of actinide interactions in anaerobic systems and investigate the reduction of higher oxidation states of actinides in aerobic systems.

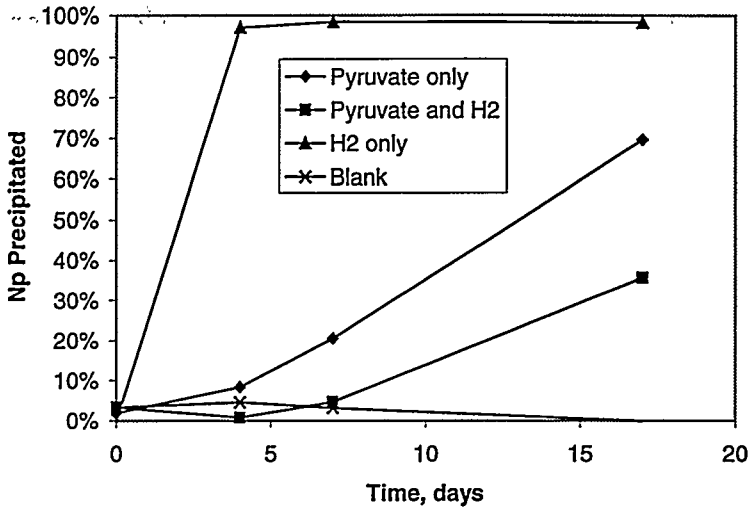

Fig. II-14. Fraction of Neptunium Precipitated during Growth of Sulfate-Reducing Bacteria Using Different Electron-Donor Substrates. Neptunium added as Np(V).

2. *Studies of Actinide Stability/Solubility*

The Waste Isolation Pilot Plant (WIPP) in Carlsbad, New Mexico, has been selected as a possible disposal site for transuranic radioactive wastes. The goal of the Actinide Stability/Solubility Project in CMT is to provide experimental data for WIPP on actinide solubility and oxidation state distribution in WIPP brine. These data are being used to test and challenge the Actinide Source Term (AST) model developed by Sandia National Laboratories.

In prior work,[18] we had shown that Pu(VI) is stable in WIPP brine when no reducing agents are present. To extend these results to repository-relevant conditions, the interactions between dissolved Pu(VI) species in WIPP brine with waste constituents were re-evaluated. The addition of reducing agents (e.g., iron coupons, dissolved Fe^{2+}, and organics) expected to be present in the WIPP resulted in the reduction of plutonium concentration under most conditions tested. These results are consistent with what we have seen in the prior experiments and re-confirm that the reducing agents present in the WIPP will destabilize the high oxidation states of plutonium, leading to lower plutonium solubility.

The most important case, for the WIPP, is high pH brine (pH = 8) when iron is present. This is the expected scenario under repository conditions. When iron was present, as shown in Fig. II-15, the concentration of dissolved plutonium decreased rapidly in all cases considered. At

[18] J. J. Laidler et al., *Chemical Technology Division Annual Technical Report, 1997*, Argonne National Laboratory Report ANL-98/13, pp. 50-51 (1998).

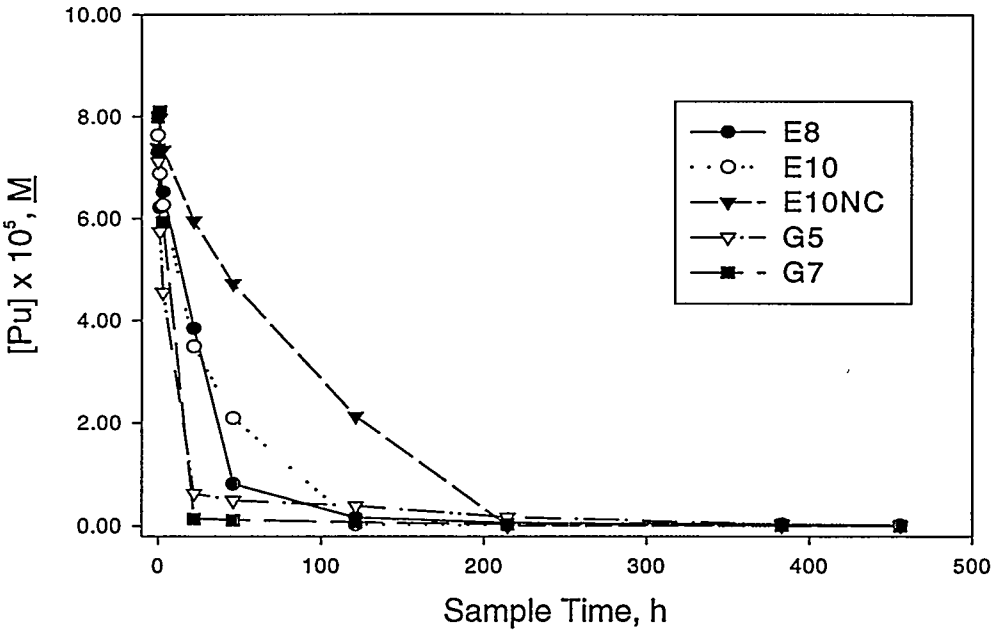

Fig. II-15. Concentration of Plutonium as a Function of Time in WIPP Brine in the Presence of Iron Coupons. The experimental designations are the following: G5 and G7, G-Seep brine at pH 5 and 7, respectively; E8 and E10, ERDA-6 brine with carbonate at pH 8 and 10, respectively; E10NC, ERDA-6 brine at pH 10, no carbonate.

the more repository-relevant condition of higher pH (e.g., pH 7 to 10), the plutonium concentration decreased by approximately three orders of magnitude. This occurred even where Pu(VI) was strongly complexed by carbonate and/or hydroxide. In these experiments, the solids were recovered, and the coupons were separated for XANES analysis to establish the oxidation state of the plutonium. For both absorbed plutonium and precipitated plutonium phase, the plutonium was identified as Pu(IV). This finding indicates that reduction, not sorption of the higher oxidation states, was the key process leading to the reduced plutonium concentrations. Calculations made by the AST also showed that the dissolved plutonium concentrations were consistent with the expected solubility of plutonium oxide in the presence of carbonate. These results help validate the modeling approach being used by the WIPP project and confirm that, under the conditions expected in the WIPP, the lower oxidation states of plutonium will predominate. These will define the solubility, hence release to the accessible environment, of the actinide. There are no plans to continue the experimental work in this area.

3. *Synchrotron-Based Studies of Actinide Species*

Studies are in progress to extend and develop X-ray synchrotron radiation (XSR) techniques to determine the chemical structure of aqueous, adsorbed, and solid actinide species of importance to environmental and nuclear waste issues. This will help resolve a number of fundamental structural issues related to the speciation (e.g., complexation, oxidation state, and

aggregation) of actinides. Emphasis is on both the collection of XSR data on actinide systems and modeling of these data with improved calculational methods and theory.

Progress has been made in both the theoretical and experimental aspects of this project. Theoretical efforts were focused on calculating the best-fit geometry for the Pu^{3+} aquo ion. This is needed to provide a test case for XANES and extended X-ray absorption fine structure (EXAFS) analyses. The most stable configuration was calculated as between 8 and 9 water molecules with a length of 2.51 Å for the Pu-O bond distance. These calculations compare well to existing experimental studies and show that the analyses of the experimental results are on the right track.

The objective of the experimental work is to establish the range of conditions that XANES edge position can be used to identify the oxidation state of actinide species. Synchrotron work was initiated at the ANL Advanced Photon Source (APS), where we were the first to develop methods suitable for the study of radioactive materials. The XANES spectra of four plutonium-bearing solids, taken at the APS, are shown in Fig. II-16. These curves clearly show a correlation between the oxidation state and XANES edge position. Preliminary work on a series of Pu(III) solids also indicated that the oxidation state, not geometry of the actinide phase, defines the XANES edge position, although the EXAFS region of the spectrum is greatly

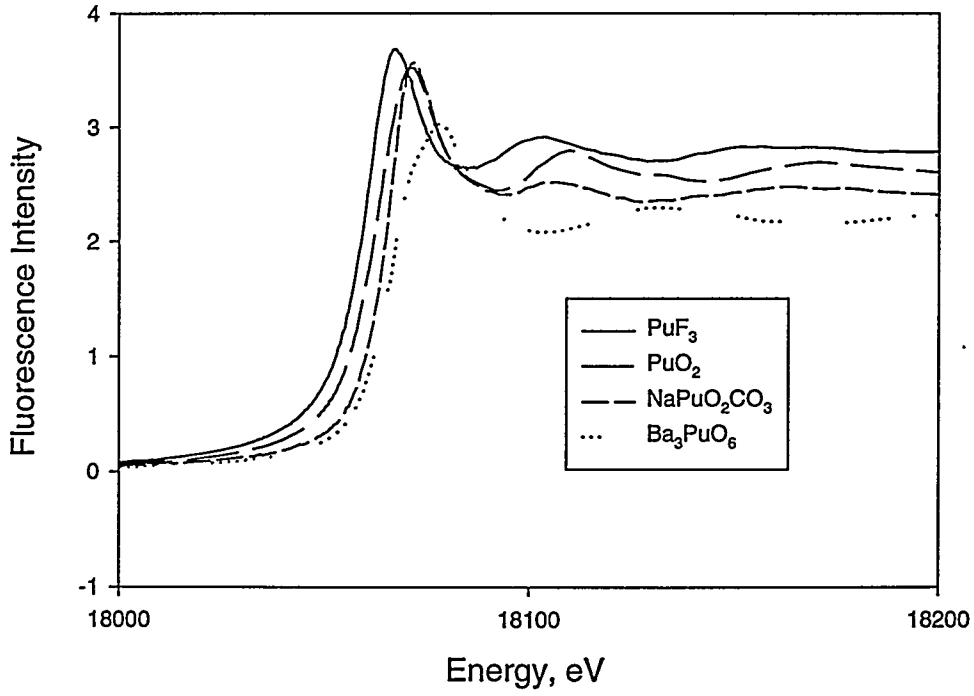

Fig. II-16. X-Ray Absorption Near Edge Structure for Four Oxidation States of Plutonium: (PuF_3) [Pu(III)], PuO_2 [Pu(IV)], $NaPuO_2CO_3$ [Pu(V)], and Ba_3PuO_6 [Pu(VI)]

affected. In all, these results show that the XANES edge position, for plutonium species, can be used to identify the oxidation state in unknowns. This is very encouraging for utilizing synchrotron-based methods to the study of complex environmental systems where it would be difficult to determine the oxidation state.

Plans are to continue the work on characterizing the near-edge XANES spectra of both solid and aqueous actinide species of Pu, Np, and U. The ongoing theoretical work will be emphasizing calculation of near-edge structure for plutonium species and extending the aquo ion calculations to Pu^{4+} and Np species.

G. Development, Characterization, and Testing of Various Waste Forms

1. Development of Test Methods for Low-Activity Product Acceptance

A reference glass has been formulated and characterized for use in acceptance testing of low-activity waste forms made by a private contractor with Hanford tank wastes. Acceptance tests have been identified in the contracts to determine if chemical, physical, and radiological requirements for the waste form that are specified in the contract have been met. The reference material that we have developed will be used to certify laboratories to conduct some of the acceptance tests. We have used the reference glass to conduct replicate tests and analyses with the objective of determining if the tests specified in the contracts are adequate and measuring the mean response and variability. Tests included PCTs at various temperatures, glass/water mass ratios, and durations; the American Nuclear Society 16.1 leach test; the Toxicity Characteristic Leach Procedure; and the vapor hydration test. We also measured the chemical composition, density, and compressive strength of the reference glass and characterized its microstructure. The glass was found to meet the contractual requirements in all tests and analyses.

A large number of PCTs were conducted to measure the precision under different test conditions. The solution concentrations of B, Na, and Si were monitored as test responses. While the responses increased with temperature, glass/water mass ratio, and duration as expected, the standard deviation of replicate tests was not affected by these parameters. Instead, the precision was found to be dominated by uncertainties in the solution analyses. One objective of this work was to recommend test conditions for use in calculating the radionuclide release rates for use in performance assessments. On the basis of the PCT results, we recommended test conditions of 40°C, a glass/mass ratio of 1/10, and a test duration of 7 days. These conditions were recommended because they generated solution concentrations that could be quantified reliably with several analytical techniques and provided enough solution so that it would not have to be diluted for analysis.

We have procured about 1000 pounds of the reference glass for use in acceptance testing. Some of this glass will be used in round-robin testing to measure the inter-laboratory precision for tests conducted under the recommended conditions. Participating laboratories will also be

asked to analyze the glass composition so that the glass can be used as a composition standard. The measured precision will be used to establish the range of acceptable results for laboratory qualification. We anticipate formulating and testing a radioactive standard in the future that can be used to certify analyses of radionuclides for which concentration limits are specified.

2. Transmutation Effects in Crystalline Waste Forms

The objective of this study is to determine the effect of transmutation of ^{137}Cs to ^{137}Ba on crystalline waste forms by examining archived samples of pollucite ($CsAlSi_2O_6$) in stainless steel capsules. These samples have been stored at ambient temperatures for up to 20 years, making their ages comparable to the half-life of ^{137}Cs (~30 years). This project is a joint endeavor between Pacific Northwest National Laboratory and Argonne National Laboratory.

The original intent in this project was to use high-energy EXAFS to obtain information on the chemical state of the ^{137}Ba in pollucite without opening the stainless steel capsules. To evaluate the extent to which high-energy EXAFS data can be interpreted, we analyzed a number of Cs and Ba standards in addition to barium-doped pollucite samples. The standards included a variety of structures from simple oxides and halides to titanates and silicates. Extremely weak EXAFS signals were obtained from the more complex silicates and titanates with distant first neighbor atoms. In addition, the amplitudes of the K-edge EXAFS for cesium are about half as intense as the corresponding values for barium. Several factors may have contributed to the apparent differences between the Cs and Ba data. Regardless of the specific origin, these factors reduce the extent to which the K-edge EXAFS data for cesium can be interpreted. We concluded that in materials with low atomic number backscatterers and low symmetry, such as pollucite, it is not possible to use the K-edge EXAFS for Cs and Ba to determine the effects of ^{137}Cs beta decay and transmutation on the pollucite structure. However, one can reasonably hope to identify the presence of metallic barium clusters or BaO, if either are the result of transmutation.

To overcome the shortcomings with the high-energy EXAFS, we have explored the use of NMR spectroscopy to examine the local structure of the cesium in some laboratory-prepared pollucite. Small quantities, typical of what we expect to recover from the sealed capsules, proved to be sufficient to obtain spectra with both magic-angle spinning and static NMR techniques. The chemical shift is expected to be sensitive to local structure and disorder. We expect to prepare a sample for NMR from the ^{137}Cs pollucite from an opened capsule. From this opened capsule, we will be able to prepare samples for L-edge EXAFS of Cs and Ba.

3. Microscopic Radiation Damage in Waste Forms

Amorphization has been commonly believed to be the most important effect of radiation damage in crystalline and ceramic materials. However, our study suggests that this may not be the case for ^{244}Cm-doped (1 wt%) phosphate crystals. The electron diffraction patterns of ^{244}Cm-doped $LuPO_4$ and YPO_4 samples showed little evidence for amorphization of the 18-year-old crystals. Transmission electron microscopic images consistently showed that the lattice of actinide-doped crystals remained largely intact in crystalline structure. Instead, numerous nanometer-sized (10-20 nm) bubbles were observed to have formed in the ^{244}Cm-doped samples.

We have further observed that, when the crystals were exposed to an electron beam, the embedded bubbles aggregated as a function of exposure time. This observation provides evidence that the aggregation of helium atoms created from α-decay of ^{244}Cm can produce bubbles in the crystals.

Fundamental understanding of the experimental results is being sought by theoretical modeling and computer simulation. Current accomplishments include (1) crystal field calculation for Cm^{3+} in disordered $LuPO_4$ and YPO_4 lattices and (2) Monte-Carlo simulation of α-decay events induced by atomic position displacements (amorphization). Simulation of structural disordering showed that, for most of the existing Cm^{3+} ions in samples of $^{244}Cm^{3+}$:YPO_4 and ^{244}Cm:$LuPO_4$, the average displacements of lattice ions that surround a Cm^{3+} ion amount to only about 0.2% of the unit cell dimension. This is consistent with AEM observation and laser-induced optical spectroscopic observation.[19]

Our studies show that, for α-emitting actinide ions in crystalline phosphates, amorphization is not a significant effect of radiation damage. Instead, formation of microscopic cavities (bubbles) is an important consequence of α-decay events. The amorphization-resistant property would then make orthophosphates a very attractive high-level nuclear waste form. However, aggregation and mobilization of cavities (bubbles) might increase the leach rate of radionuclides and influence the long-term stability of the waste forms. Further research is needed before we can draw a final conclusion on the long-term effects of radiation damage in orthophosphate waste forms.

4. Testing of Glass Waste Form for Low-Level Hanford Waste

Work is being conducted to provide technical support to the effort on privatization of the Hanford Tank Waste Remediation System. Tests were conducted with a reference glass (LD6Tc7) that had been doped with about 0.2 mass% technetium to study the release and disposition of this element as the glass corroded under a wide range of conditions. Tests were conducted at 40°C and S/V = 2000 m^{-1} with crushed samples to study the release of technetium from the glass as the solution approaches saturation. The results showed Tc, B, and Si to be released from the glass at similar rates, but sodium to be released faster. Sodium is released by an ion-exchange mechanism, while B and Si are released by hydrolysis reactions that control the matrix dissolution rate. An important result of these tests is that technetium is not released faster than the glass matrix dissolves. Long-term tests with crushed glass (~450 days) resulted in the formation of alteration phases and an increase in the dissolution rate, which was indicated by a rapid increase in the solution concentration of boron. The zeolites analcime and phillipsite were the predominant phases that formed.

Long-term PCT results are shown in Fig. II-17 in terms of normalized mass loss, which is the solution concentration of an element divided by the S/V ratio of the test and the mass fraction of the element in the glass. The solution concentrations of Na and Si did not increase to the same extent as the boron concentration because Na and Si were incorporated into the alteration phases.

[19] G. K. Liu, J. S. Luo, S. T. Li, C.-K. Loon, M. M. Abraham, J. V. Beitz, J. K. Bates, and L. A. Boatner, *Mater. Res. Soc. Proc.* **506**, 921 (1998).

The increase in the release of technetium was intermediate between that of Si and Na, indicating that much of the technetium released from the glass was being contained in alteration phases.

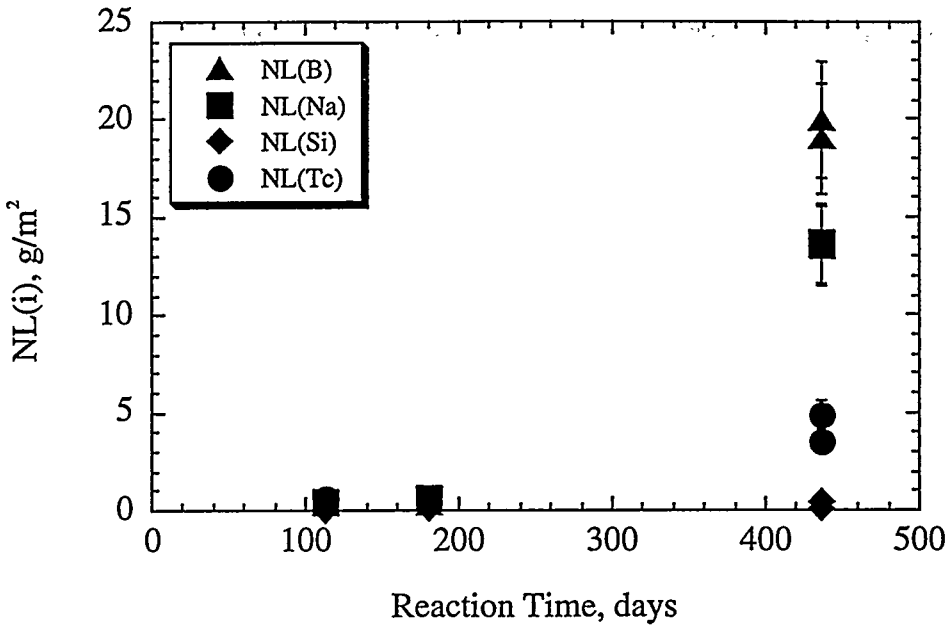

Fig. II-17. Normalized Mass Loss vs. Reaction Time for PCT with LD6Tc7 Glass in Demineralized Water at 90°C and S/V = 20,000 m^{-1}

Vapor hydration tests were conducted with LD6Tc7 glass to confirm that technetium was incorporated into alteration phases. Tests were conducted at 200°C to completely transform the glass into alteration phases. The reacted samples were submerged in demineralized water to allow soluble salts that formed when the test was completed to redissolve. This solution was then compositionally analyzed. The ratios of B:Na:Tc:Si measured in this solution were similar to those observed in the PCT (Fig. II-17). Portions of the altered glass were then dissolved in a mixture of nitric and hydrochloric acids and compositionally analyzed. These analyses showed that the technetium content of the alteration phases was almost the same as the technetium content of the glass. We did not isolate individual alteration phases to determine their technetium contents. This will be done in test to be conducted with British Nuclear Fuels Ltd. (BNFL) glasses that contain technetium.

Tests are also being conducted with low-activity waste glass to be produced by BNFL, which has the contract for Phase IB of the privatization effort. The objective is to provide information regarding the long-term corrosion behavior of the glass needed for performance assessment calculations.

H. Other Related Work

1. Technical Support for Hanford Privatization

We are providing technical consulting to the Regulatory Unit of the DOE Richland Operations Office in support of the ongoing effort to privatize treatment of the high-level radioactive waste currently stored in underground tanks at Hanford. This DOE office is responsible for regulation of the design, construction, operation, and decommissioning of the facilities that are to be built, owned, and operated by private companies for treatment and vitrification of the waste. Our technical support involves review and evaluation of the documentation that the private companies are required to submit to the Regulatory Unit in support of regulatory decisions.

During the past year, we participated in the review and evaluation of the "Initial Safety Analysis Reports" that were prepared by the two private organizations that participated in the first phase of the project: British Nuclear Fuels Ltd. and Lockheed Martin Advanced Environmental Systems. These evaluations provided input to the DOE decision to negotiate a contract with BNFL for a second phase. The objective of the second phase is to complete design, construction, licensing, and operation of the facilities needed to implement the waste treatment and vitrification processes identified in phase one. We are continuing to provide review and evaluation of the documentation supporting the decision regarding construction authorization that is to be made early in the second phase.

2. Procedure Writing

The CMT staff have been active in subcommittees of the American Society for Testing and Materials on test methods and on repository wastes for the nuclear fuel cycle. Recent activities have included the revision of three key procedures that address the testing of waste forms for disposal in a federal high-level waste repository:

- C1174, "Standard Practice for Prediction of the Long-Term Behavior of Waste Package Materials Including Waste Forms Used in the Geologic Disposal of High-Level Nuclear Waste"
- C1220, "Test Method for Static Leaching of Monolithic Waste Forms for Disposal of Radioactive Waste"
- C1285, "Standard Test Methods for Determining Chemical Durability of Nuclear Waste Glasses: The Product Consistency Test (PCT)"

These standards play important roles in nuclear waste management since, by law, standardized methods must be used when available for government projects. Most of the experimental testing programs discussed in this section utilize these standards. We are currently developing a method to measure the intrinsic dissolution rate of waste glasses, which is a value needed to model glass

dissolution in performance assessment calculations for disposal systems. The CMT staff are also active in the writing of new procedures on metal fuel pyrophoricity, degradation testing of aluminum, flow-through testing of spent nuclear fuel, and extension of dry storage of spent light water reactor fuel to 100 years.

3. Medical Isotopic Delivery for Treatment of Prostate Cancer

SourceTech Medical L.L.C. is an Illinois startup company seeking to develop radioactive sources for use as permanent implant devices for the medical treatment of prostate cancer. The company has entered into collaboration with ANL to develop an ^{125}I sealed source and will require sorption techniques and nondestructive methods to analyze various source designs. The deposition procedure is based on physical sorption of ^{125}I onto metallic substrates or chemical sorption onto a selective magnetic particle system. One magnetic particle system has shown extremely large iodine partition coefficients (10,600 mL/g at 25°C) for a 2000 ppm iodine solution at pH 12. The iodine loading capacity was 0.33 g of iodine per gram of particle. The sorption studies consistently produced 95-98% deposition of the total iodine at pH 2; this corresponds to 10 mCi of ^{125}I. The sorption studies are nearly complete, and ANL is awaiting the receipt of a titanium sealing process to evaluate and optimize the automated production of sealed ^{125}I sources.

4. Modeling of Flow Characteristics for Repository and Vadose Zone

Contaminant transport through water-containing (but unsaturated) pathways in engineered as well as geologic materials is an important issue in both mechanistic process-level modeling and larger scale performance assessments of waste behavior in the vadose zone (area between surface and water table). Diffusion is one of the important transport processes contributing to contaminant transport. Conca et al.[20] have gathered extensive data on ionic diffusivity in a wide range of unsaturated geologic and engineered materials and have found that water content is an important parameter. Significant but systematic changes in ionic diffusivity (by as much as four orders of magnitude) as the water content varies have been observed. Furthermore, the data did not show any percolation threshold, even for water content as low as 1% and below. This implies that water passageways with long-range interconnectivity exist even for water content that is far below the percolation threshold, as expected from conventional percolation theory. Fundamental quantitative understanding of these features of the data has been lacking.

We have developed a theoretical model of the ionic diffusivity in unsaturated engineered and geologic materials that mechanistically accounts for these observations. The model synthesizes two fundamental statistical mechanical approaches: renormalization group and effective medium theories. Model calculations indicated that it is important to take into account the correlation of the spatial distribution of the water content and its fluctuation from the average value. The model involves relatively straightforward computational process and yet rests on a

[20] J. L. Conca, M. Apted, and R. Arthur, *Mater. Res. Soc. Symp. Proc.* **294**, 395-402 (1993).

sophisticated basis. Detailed comparison of the results of the theory with the diffusivity data showed extensive agreement throughout the entire range of measured water content. The techniques that we have introduced in this study can be utilized to address other aspects of contaminant transport in the vadose zone, including flows and colloidal transport. They are particularly suited to address the scaling issue, which is concerned with the critical problem of having to address contaminant transport over a kilometer-size scale with attention being needed over details of transport at the level of centimeters or less.

5. Development of Rheology Control Aids

In recent years, state and federal agencies have been exerting considerable pressure to reduce volatile organic compounds in consumer products, such as paints, inks, and cosmetics. This has created a need for water-based rheological control agents with true thixotropic properties. We have examined the use of aqueous biphasic extraction (ABE) for preparing "organoclays" that have thixotropic properties and can be used to control the rheology of aqueous systems. The ABE system is used to produce a highly dispersed clay, free of mineral impurities. The dispersed clay has modified surface properties brought about by the adsorption of the water-soluble polymers used in generating the ABE system. The rheological properties of the organoclays produced with ABE make them useful as rheology control aids in a wide range of water-based products, including inks, paints, coatings, cosmetics, lubricants, caulks, pharmaceuticals, fertilizers, pesticides, oil drilling muds, lubricating greases, binders, and adhesives. In comparison tests conducted at the Coatings Institute of the University of Missouri-Rolla, the ANL materials exhibited true thixotropic behavior as opposed to the pseudoplastic behavior of commercially available products. The ANL materials were effective at controlling the rheology of latex paint at clay loading of 0.4 wt%. We are currently looking for industrial partners to commercialize the ANL process.

6. Development of Synchrotron X-ray Techniques for Protein Analysis

This project will provide fundamental proof-of-principle for an innovative means to prepare coherent monolayer films of proteins at the water/water interface of an aqueous biphase system. If successful, the approach will decrease the need to grow three-dimensional crystals. The present process is expensive and time-consuming and carries no guarantee that crystals can be grown. Further, even if crystals are obtained, there is no assurance that they will diffract well enough for detailed structural analysis. In addition, this approach will provide a means of determining the three-dimensional structure of fully hydrated proteins, thereby giving a more realistic view of biologically active structures. This approach is only now feasible because of the extraordinarily high degree of beam coherence at the APS.

During the past year, we established a collaboration with the University of Illinois at Chicago, and preliminary X-ray scattering experiments at the water/water interface were completed. Specifically, X-ray absorption and critical-angle measurements for a water/water interfacial system have been completed at the National Synchrotron Light Source. We found that X-ray absorption in polymer-water solutions was less than that in pure water. This finding

indicates that it is feasible to do crystallography in these systems. The critical angle at the water/water interface was about 2 milliradians. Grazing-angle X-ray diffraction requires an incident beam angle that is slightly less than the critical angle. Given the low critical angle at the water/water interface, the low vertical beam divergence (i.e., about 6 microradians) at the APS makes it possible to obtain usable scattering data.

III

Separation Science and Technology

The Division's R&D in separation science and technology is in two areas: (1) substitution of low-enriched uranium (LEU) for high-enriched uranium (HEU) in the production of ^{99}Mo and (2) treatment of radioactive, mixed, and hazardous waste.

The largest R&D effort presently being pursued is development of LEU targets and processing methods for production of ^{99}Mo to be used for medical applications. In this activity, we are working to convert all current processes, worldwide, from HEU to LEU. The program is international, with ongoing and new initiatives with partners in Indonesia, Canada, the United States, Korea, Australia, and Argentina.

The major activity in the waste treatment area involves R&D on solvent extraction processes for the cleanup of radioactive liquid waste. An alkaline-side cesium-extraction process for solvent extraction was pursued in cooperation with Oak Ridge National Laboratory, the Savannah River Technical Center, and the Savannah River Site. A significant effort is also underway to develop a magnetically assisted chemical separation process for several waste-treatment and environmental-cleanup applications, and a sol-gel technique is being developed for treating solids in radioactive alkaline waste.

A. Conversion of Targets for ^{99}Mo Production from Low-Enriched Uranium

The Reduced Enrichment for Research and Test Reactors (RERTR) program has been active for 21 years at ANL and many countries throughout the world. Researchers in CMT are part of the ANL team. Its major objective is to modify reactor and fuel designs so that reactors can switch from HEU to LEU with no or little loss in flux or cycle time. Many reactors have converted to LEU, and many more are in the process. While conversions of reactor fuel have proceeded, the amount of HEU being exported from the United States for use in ^{99}Mo production has become an ever more visible proliferation concern.

Technetium-99m ($t_{1/2}$ = 6.02 h), the daughter of ^{99}Mo ($t_{1/2}$ = 66.02 h), is the most commonly used medical radioisotope in the world. It is relied upon for over nine million medical procedures each year in the U.S. alone, comprising 70% of all nuclear-medicine procedures. Most ^{99}Mo is produced in research and test reactors by the irradiation of targets containing HEU. Because the worldwide effort to fuel research and test reactors with LEU instead of with HEU has been so successful, HEU is now used only for ^{99}Mo production in some countries. In addition, while there are only a few major producers of ^{99}Mo, many nations with developing nuclear programs are seeking to become producers of ^{99}Mo, both for domestic and foreign consumption. Therefore, one of the U.S. RERTR program's goals is the development of means to produce ^{99}Mo by using LEU. The two principal aspects of the work are (1) target development and (2) chemical process testing and modification.

Low-enriched uranium contains <20% ^{235}U. Currently, most of the world's supply of ^{99}Mo is produced by fissioning the ^{235}U in HEU targets—in most cases, enriched to 93% ^{235}U. Because of the lower isotopic fraction of ^{235}U in LEU, five times more uranium is required to produce the same yield of fission-product ^{99}Mo. Therefore, substituting LEU for HEU will require changes to both target design and chemical processing. Three major challenges have been identified with substituting LEU for HEU: (1) modifying the targets and purification processes as little as possible, (2) assuring continued high yield and purity of the ^{99}Mo product, and (3) limiting additional costs. Keeping the target geometry the same, thereby minimizing the effects of LEU substitution on target irradiation, necessitates modifying the form of uranium used. Changing the amount and form of the uranium in the target necessitates modifying at least one or, possibly, two target processing steps—dissolution and initial molybdenum recovery.

1. Progress in Target and Processing Development

The Cintichem process being used in Indonesia was developed in the United States and was licensed to Badan Tenaga Atom National (BATAN) by Medi-Physics, Inc. The U.S. DOE now owns this process and will be using it to produce ^{99}Mo at Sandia National Laboratories. Our program is examining the means to, and the ramifications of, switching to an LEU target for the production of ^{99}Mo by a modified Cintichem process. We are investigating a target composed of highly dense LEU metal foil as a replacement for HEU in both the acid-dissolution and basic-digestion steps. The irradiation and Cintichem processing of the LEU metal-foil targets are being demonstrated in cooperation with researchers at the Indonesian PUSPIPTEK facility.

The LEU target being used in these experiments is shown in Fig. III-1. In this target, a uranium foil is held between two concentric tubes. After irradiation, the ends of the tubes are cut off; the inner tube is pushed from the outer tube; and the uranium foil is recovered for subsequent processing. A slight taper in the tube facilitates disassembly. We identified three issues with this target design that needed to be addressed before the demonstration planned for Indonesia during August 1998 (see Sec. III.A.2).

The first issue was that fission-fragment recoils during the irradiation caused the uranium foil to bond to the inner and outer tubes, making it impossible to slide the tubes apart and recover

the uranium foil. Fission-fragment barriers needed to be attached to the uranium foil to prevent it from bonding to the tubes.[1] Fission-recoil barriers of Zn, Ni, and Al are being considered. Nickel and zinc can be dissolved by nitric acid; Zn and Al can be dissolved by sodium hydroxide. Therefore, the same type of target can be used for processes that begin by dissolving the irradiated uranium in acid or by digesting it in base. The barriers must be >7-μm thick for Ni and Zn, and >14-μm thick for aluminum. We have developed a method that will electrodeposit either Ni or Zn barriers onto the foil. Alternatively, the uranium foil can be wrapped in thin foils of Ni, Zn, or Al.

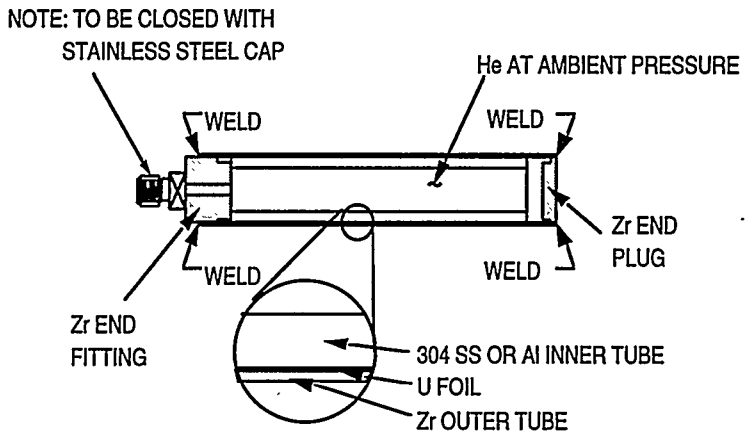

Fig. III-1. Schematic of LEU Foil Target

The second issue is the anisotropic grain growth of uranium during irradiation. This growth can tear the fission-fragment barriers, bond the uranium foil to the target tubes, and prevent its recovery. We have refined a method to β-quench these thin uranium foils and produce a fine, randomly oriented grain structure that prevents the tearing of the barriers.

The third issue is that the uranium foil could react with fission-fragment barriers as the irradiated target heats up during transport, compromising their effectiveness. We have, therefore, studied the reaction of the fission-fragment barriers with uranium under potential transport conditions.

The foils prepared at ANL for the demonstration in Indonesia were made of an "adjusted" uranium alloy containing 1000-ppm aluminum and 450-ppm iron. The last step in the fabrication of uranium foils is cold rolling to the final thickness (130 μm). This rolling induces preferred orientation of the crystal structure in the uranium foil. During 1998, we perfected a method for β-quenching these thin foils to produce a fine, randomly oriented grain structure. To produce fine-grained material, the piece is heated into the β region (T>668°C for pure uranium) and then

[1] G. L. Hofman, T. C. Wiencek, E. L. Wood, J. L. Snelgrove, A. Suripto, H. Nasution, D. Lufti-Amin, and A. Gogo, "Irradiation Tests of ^{99}Mo Isotope Production Targets Employing Uranium Metal Foils," Proc. of 19th Int. Meeting on Reduced Enrichment for Research and Test Reactors, Seoul, Korea, October 7-10, 1996, pp. 162-171 (1997).

rapidly cooled. Heat treatment was accomplished by immersing the material in molten lead at 720°C and then quenching with water. The uranium foils were individually sealed inside a can by beam-welding two pieces of 380-μm stainless-steel sheet with a uranium foil sandwiched between. Experiments showed that we could produce the desired crystal structure regardless of the amount of cold rolling by heat treating for 20 min in the molten lead, water quenching, heat treating for an additional 20 min, and finally water quenching. The foils used for the demonstration in Indonesia were heat-treated by this method.

After heat treatment, two of the foils for the demonstration had fission-recoil barriers electroplated onto them. Since uranium exposed to air or water always has a coating of the oxide, it is not possible to obtain a metal-to-metal bond by electroplating in aqueous solution. However, a mechanical bond can be obtained if most of the oxide is removed and the uranium surface is roughened by etching. Zinc and nickel have been successfully electroplated onto uranium foil in this way to obtain coatings 10-15 μm thick. The multistep procedure involves degreasing of the piece, followed by oxide removal by nitric acid, etching of the surface with hot ferric chloride solution, then reactivation of the surface with nitric acid. Water rinses are carried out between treatments. Figure III-2 is a microphotograph showing a successful zinc-plated uranium foil.

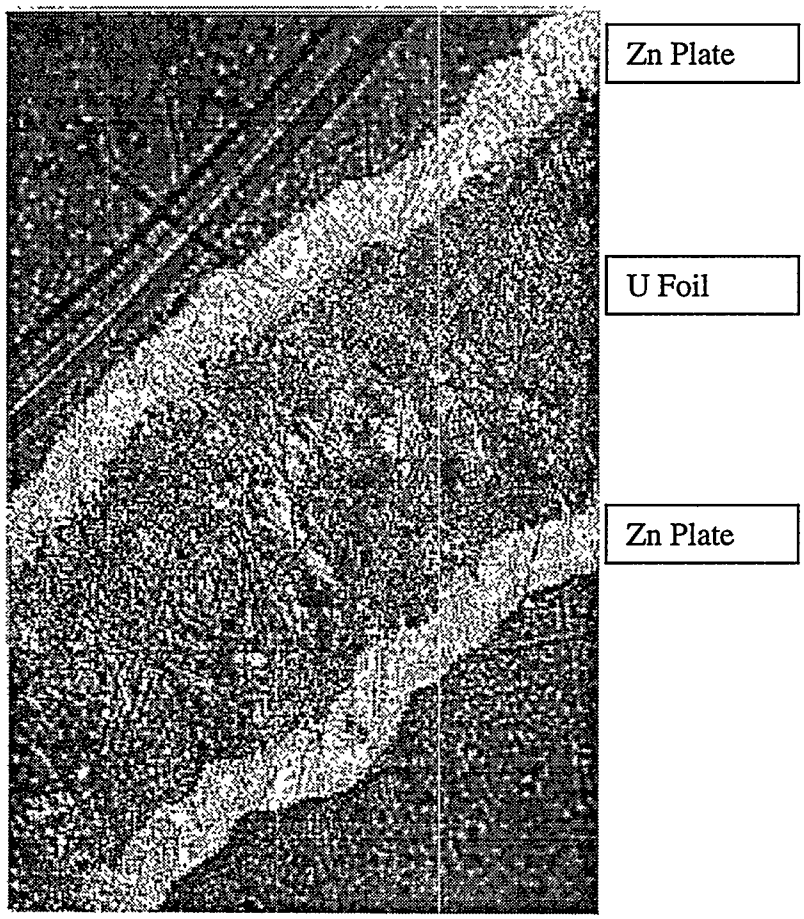

Fig. III-2. Section of Zinc-Electroplated Uranium Foil. Micrograph shows zinc plating, 10-15 μm thick, on uranium foil.

Rough calculations based on heat release due to radioactive decay of the fission products predicted that the target could reach a temperature as high as 375°C during transport. Several conclusions were reached. Nickel and aluminum do not react with uranium foil at temperatures up to 450°C. Zinc-uranium reactions at temperatures below 375°C are minimal. At a temperature of 400°C, the zinc and uranium begin to react. Uranium and zinc react extensively at temperatures near or above the melting point of zinc (419.6°C). Samples of the U/Zn reaction product were analyzed by inductively coupled plasma/atomic emission spectroscopy. The product typically contained 8-10 wt% uranium with the remainder zinc. The reaction products were analyzed by electron dispersive spectroscopy, which indicated that some previously unpublished phases might be formed. Overall, the reaction of the fission-fragment barriers with uranium should not be a problem under normal irradiation and transport conditions.

2. Demonstration of Cintichem Process

During August 1998, eight targets were irradiated in the Indonesian RSG-GAS reactor for either 112 or 120 h at 15 MW. Two targets were processed for ^{99}Mo recovery. The others will undergo metallographic examination. The targets are described in Table III-1.

Table III-1. Characteristics of LEU Metal-Foil Targets Irradiated in the RSG-GAS Reactor during August 1998

Target No.	Inner Wall[a]	Barrier		Inner Tube Extractable?	Foil Removed?
		Material	Thickness, μm		
1	304 SS	Zn foil	15	Yes	Yes
2	304 SS	Ni foil	15	Yes	Yes
3	304 SS	Zn plate	17[b]	Yes	Yes
4	304 SS	Ni plate	11	Yes	Yes
5	304 SS	Al foil	23	Yes	No
6	Al	Al foil	23	No	--
7	Zr	Ni foil	15	Yes	Yes
8	Zr	Zn foil	15	Yes	No

[a]All targets had an outer cylinder wall of zirconium.
[b]By weight, calipers gave a thickness of 21 μm. The plating density of zinc on the uranium foils has always been lower than theoretical.

After cooling for eight hours, the targets were disassembled. The results of disassembly are also presented in Table III-1. All inner tubes were extractable except for the target with an aluminum inner tube (No. 6), where the combination of high temperature from decay heat and the large thermal expansion coefficient for aluminum is believed to have resulted in a tight mechanical fit. The foils were easily removed from five of the seven targets that could be disassembled. The other two foils appeared to be stuck in the outer tubes. However, since all of

our experience has shown that foils with fission-fragment barriers do not bond to zirconium tubes, we believe these tubes may be only mechanically stuck. Further investigation is underway at the BATAN Radiometallurgy Installation.

Uranium foils with nickel fission barriers were springy and easily handled. Uranium foils with zinc barriers were brittle—especially the one with the electroplated zinc. The electroplated foil was so brittle that it cracked into pieces during handling. Since discovering this problem, we have been developing a new procedure for zinc plating to form higher-density zinc plates. We will test this new procedure in future irradiations to see if it decreases the brittleness of the zinc-plated uranium foils.

Following target disassembly, one target per week was shipped from Radiometallurgy Installation to the Radioisotope Production Centre for processing. Eventually, disassembly will also be performed in this facility. The foils were dissolved in 40 mL of 6 M nitric acid in a closed dissolver. The dissolver used was an improved design. Changes were made to reduce the dissolver weight (from 1.9 to 0.8 kg) so that it can be handled easily by remote manipulators in a shielded-cell facility. Dissolution of the metals generated NO gas. Figure III-3 shows the dissolution profile (pressure vs. time) for the irradiated uranium foil with the nickel-foil fission barrier. The profile for the Zn-plated uranium foil was nearly identical. The maximum pressure

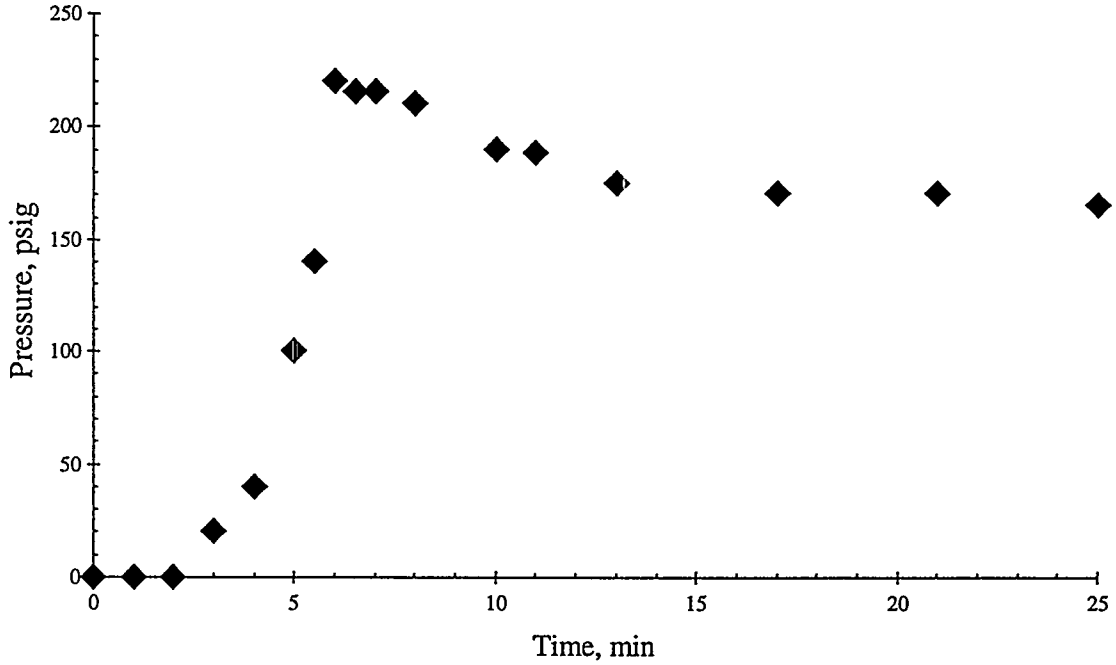

Fig. III-3. Pressure vs. Time for Dissolution of the Irradiated Uranium Foil with the Nickel-Foil Fission Barrier

was predictable from earlier work based on dissolving 9.1 g of uranium and 1 g of nickel.[1] The pressure peak is due to heat released in the reaction between the metals and nitric acid.

We concluded that the nickel fission barrier appears to be ideal for acid dissolution. Zinc fission barriers have the advantage that the target could be used for processes that begin by either acid dissolution or alkaline digestion of irradiated uranium. However, the problem of brittleness needs to be addressed. For a base-side barrier, zinc has the advantage over aluminum in that it (1) can be electroplated onto uranium and (2) can be used for both acid- and base-side processes. However, aluminum foil is inexpensive and readily available.

With one exception, the molybdenum recovery and purification process followed the typical behavior of HEU-target processing. The exception was that a liquid-nitrogen-cooled cold trap did not operate as expected in evacuating the dissolver. This problem is under investigation. With one exception, the solutions and solids were the same colors as those from processing HEU targets. The exception was the dissolver solution for the irradiated uranium foil with a nickel barrier; this solution was noticeably green, due to the presence of nickel, rather than yellow. All recovery and purification operations appeared to function as expected. Counting a fraction of the product solution in a proportional counter showed the ^{99}Mo yield to be what would be expected from a typical HEU target with the same ^{235}U content. However, problems with sampling and gamma analysis did not allow us to determine product purity. These problems will be addressed before the next LEU demonstration. Alpha-contamination analysis has not yet been completed. The alpha-analysis method developed will be used to measure alpha contamination of the ^{99}Mo as it proceeds through the modified Cintichem process.[2]

3. Future Plans

The uranium-foil target has moved from a conceptual design to a reliable prototype. The next step is to provide a design that will be economical to produce and have the flexibility to be manufactured in geometries applicable to a variety of irradiation requirements. Future targets will likely be fabricated with Zr or Al on both inner and outer walls. Doing so should aid in meeting the goals of economy and flexibility. Flexibility will also include creating an open-center target that allows both inner- and outer-wall cooling during irradiation. Target disassembly is still more awkward and time-consuming than necessary; improved methods for disassembly will also be designed into the next generation of targets.

The next in a series of LEU-processing demonstrations is scheduled to be run at PUSPIPTEK in the spring of 1999. Indonesian personnel are in the process of developing their skills in rolling and electroplating uranium foil. In the future, demonstrations will be run with targets prepared at PUSPIPTEK. A cooperative program is also scheduled to begin with the Argentine Comisión Nacional de Energía Atómica in January 1999 to convert their base-side

[2] C. Conner, M. Liberatore, A. Mutalib, J. Sedlet, D. Walker, and G. Vandegrift, "Progress in Developing Processes for Converting ^{99}Mo Production from High- to Low-Enriched Uranium—1998," Proc. of 21st Int. Meeting on Reduced Enrichment for Research and Test Reactors, October 18-23, 1998, Saul Paulo, Brazil, in press.

^{99}Mo production from HEU to LEU. We are also close to signing an agreement with the Australian Nuclear Science and Technology Organization on development of uranium-metal foil targets for application in their ^{99}Mo production.

B. Demonstration of Solvent Extraction Flowsheet

Over the past year, we continued our multi-year collaboration with Oak Ridge National Laboratory (ORNL) in the development of new solvent-extraction processes for separating Sr, Tc, and Cs from the alkaline supernatant in radioactive waste storage tanks. They would replace methods, such as use of ion-exchange columns and the in-tank precipitation (ITP) process at Savannah River Site (SRS), that are currently planned to carry out this operation. The two key advantages of solvent-extraction processes over other processes are that the elements are recovered (1) free of the other salts in the tank supernate and (2) without any added chemicals such as those required to strip Sr, Tc, and Cs from ion-exchange columns. These factors would greatly reduce the number of glass logs subsequently generated for waste disposal and, so, the overall cost of waste disposal.

As the need for an alternative to the ITP process at SRS became known, the effort at ANL and ORNL focused on the removal of cesium from salt-tank supernatants at SRS. The solvent-extraction techniques are referred to here as alkaline-side cesium extraction (CSEX). A key feature of CSEX processes is the use of a new extractant developed at ORNL, a calixarene crown called calix[4]arene-bis(*tert*-octylbenzo-crown-6) or, more simply, BoBCalixC6. The calixarene crown is used with a solvent modifier such as 1-(1,1,2,2-tetrafluoroethoxy),3-(4-*t*-octylphenoxy)-2-propanol (Cs-3), an alkyl aryl polyether. In every case, the diluent was Isopar®L. The work at ANL included data analysis, flowsheet development and testing, and flowsheet demonstration in a countercurrent, multistage minicontactor. Initial work evaluated different CSEX solvents for Cs and Tc removal from alkaline waste at the Hanford site by developing appropriate flowsheets based on solvent distribution ratios.

The CSEX process was evaluated in three multistage minicontactor tests. Additionally, single-stage minicontactor tests measured stage efficiency and hydraulic performance. We also performed hydraulic tests and measured ^{137}Cs distribution ratios under flowsheet conditions. The final flowsheet test, sketched in Fig. III-4, includes relative flow rates for the various aqueous phases that reflect the design needs at SRS. In the plant process, 30 to 40 contactor stages would be used. For the laboratory-scale tests, we used the 24 contactor stages available in our glovebox.

The first minicontactor test demonstrated that the alkaline-side CSEX process worked and identified a process problem that was not seen in batch tests. The second minicontactor test was identical to the third but had no solvent recycle. A comparison of these two tests allowed us to determine the effect of solvent recycle. Steady-state results for the third test (CS19), given in Fig. III-5, show reasonable agreement between the experimental results and model calculations. The combined results, along with a new correlation of stage efficiency with contactor operation and size that was developed as a part of this work, predict that a full-scale CSEX process plant would be able to meet the design objectives. These objectives are (1) a ^{137}Cs decontamination

factor of 42,000 in the aqueous raffinate and (2) the ability to concentrate ^{137}Cs in the waste by a factor of 12 in the feed to the glass plant. No further work in this area is planned.

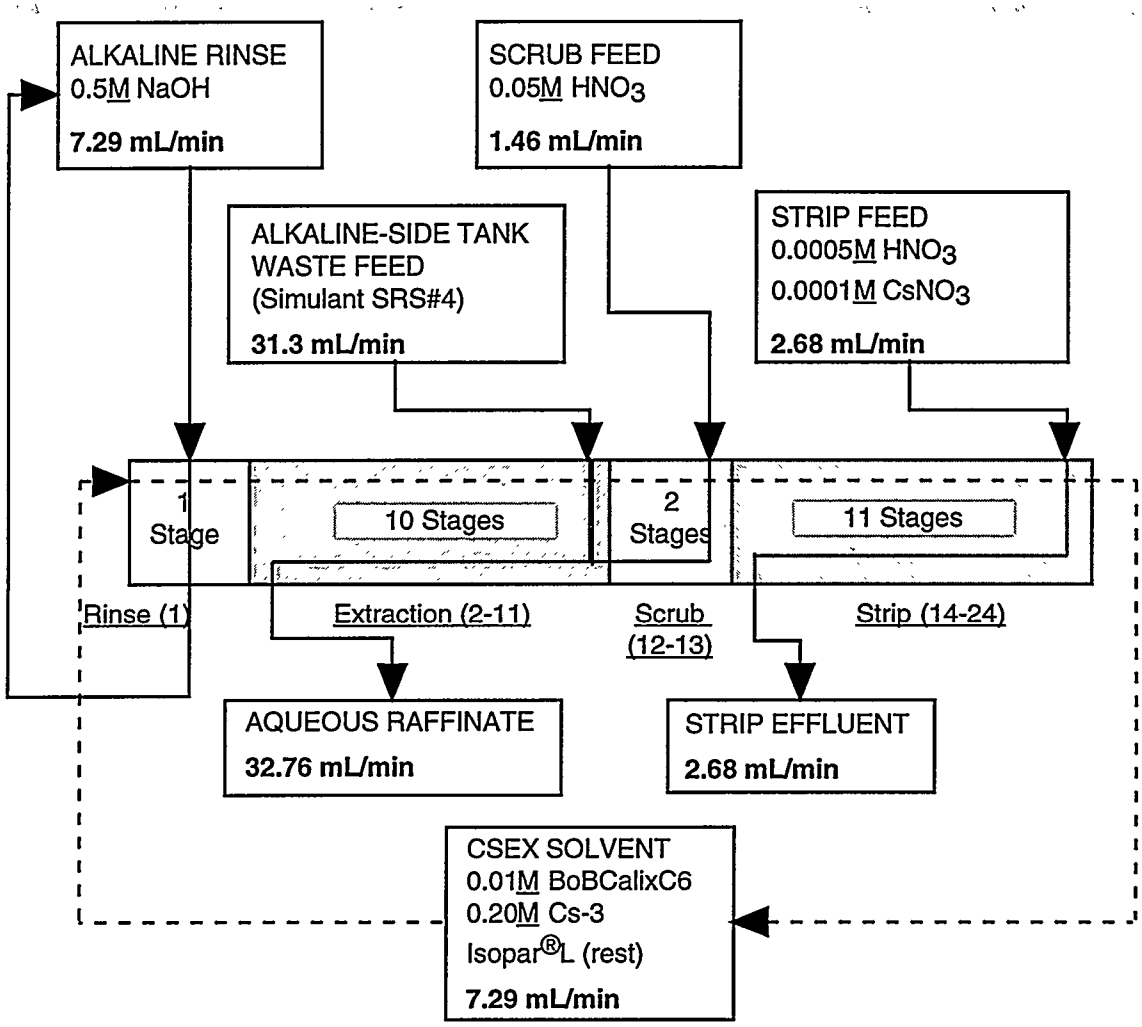

Fig. III-4. Flowsheet for Demonstration of the Alkaline-Side CSEX Process with Solvent Recycle (Test CS19)

C. Applications of Magnetically Assisted Chemical Separation

The magnetically assisted chemical separation (MACS) process developed in CMT provides an efficient and cost-effective way of removing radionuclides and hazardous components from nuclear, environmental, and industrial waste streams. For sites with waste streams containing low concentrations of transuranic or hazardous elements and large volumes

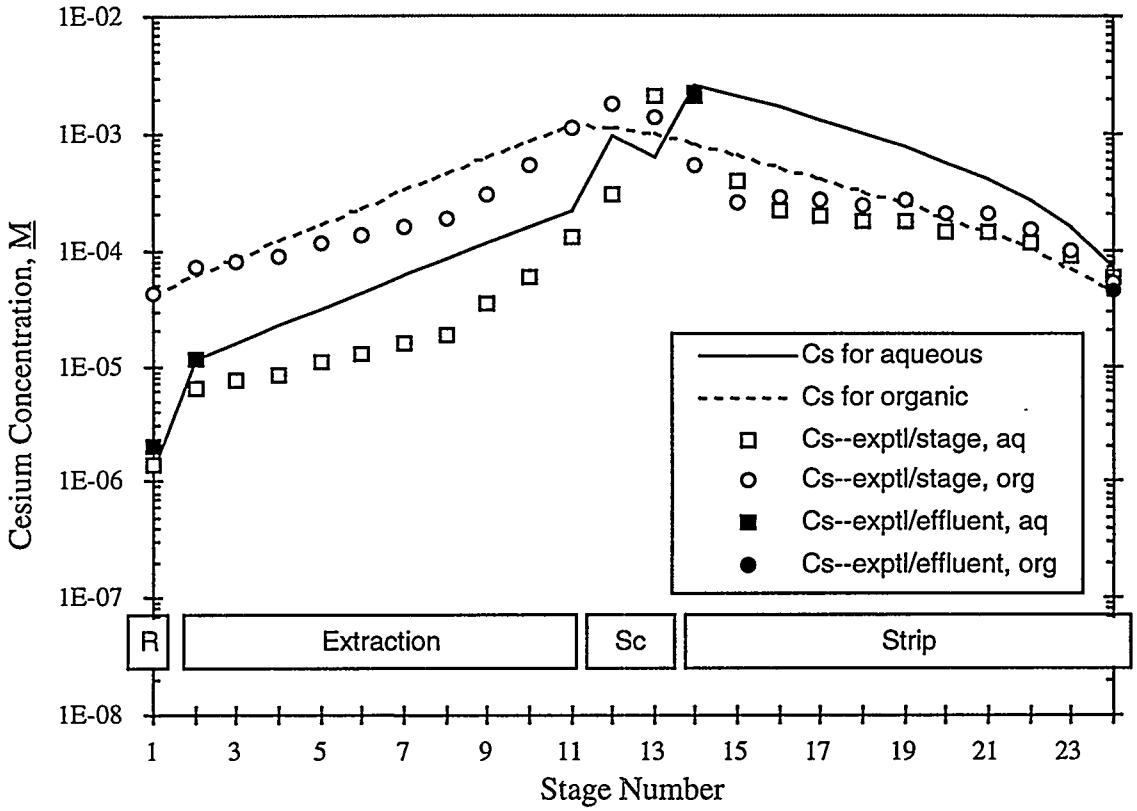

Fig. III-5. Stage-to-Stage Cesium Concentrations for Minicontactor Test CS19. Calculations based on the Generic TRUEX model developed earlier in CMT.[3] The abbreviations R = rinse, Sc = scrub, aq = aqueous phase, org = organic phase.

of water, decontamination of those waste streams to acceptable health and disposal levels process may offer significant improvement over traditional separation methods such as membrane filtration, ion exchange, and solvent extraction for the recovery of chemical species from dilute waste streams. Tiny, inexpensive superparamagnetic particles (30 nm to 25 μm), coated with selective chemical extractants, provide a simple way to remove these contaminants from solutions under a wide range of chemical conditions. The magnetic particles are coated with an extractant or ion exchange material, and, after sufficient mixing with the waste solution, magnetic fields are used to separate the particles from solution. The contaminant-laden coating is removed by using a small volume of stripping agent. The magnetic carriers are then regenerated. The concentrated solution containing the contaminant can either be disposed of or treated further to recover the radionuclides or hazardous metal. We have been working on several applications for the MACS particles, discussed below.

[3] J. J. Laidler et al., *Chemical Technology Division Annual Technical Report, 1994*, Argonne National Laboratory Report ANL-95/24, pp. 68-70 (1995).

1. Removal of ^{137}Cs from Milk

Following the Chernobyl accident, millions of acres of grazing land were contaminated with ^{137}Cs, and as a result, much of the milk produced in the Ukraine region of the former USSR is contaminated. In cooperation with the Energy System Division, we are studying the ability of the MACS process to remove the ^{137}Cs from the contaminated milk. One concern is the durability of MACS particles in the presence of microorganisms that can cause microbial-induced corrosion. We have completed a literature survey on common bacteria found in milk; typical structural effects that bacteria can have on the MACS particles can be identified by transmission and scanning electron microscopy. Common bacteria such as enterococci, micrococci, brevibacterium, and lactobaccilli can survive pasteurization and reduce the magnetic-particle shelf life by microbial-induced corrosion. We are developing, together with Cortex Biochem, Inc., silico-titanate magnetic particle composites. Sorption and radiation damage studies with contaminated milk surrogates and fouling (bacterial, radiolytic) conditions are planned.

2. Waste Minimization

The DOE Waste Minimization and Pollution Prevention program has funded CMT to determine the waste minimization potential of the MACS process for waste streams of concern to ANL Waste Management Operations (WMO), the organization responsible for on-site waste management. We thus evaluated the extension of the MACS concept to extractants other than the octyl(phenyl)–N_1N-diisobutylcarbamoylmethylphosphine oxide (CMPO) and tributyl phosphate (TBP) previously investigated.[4] The objective was to determine if other systems exhibit the synergism observed in the CMPO/TBP system. A MACS particle containing anion exchange material (Magacell Q™) and MACS particles coated with various neutral, basic, and acidic extractants were tested for extraction of actinides (U, Pu, and Am) and zinc from nitric acid solutions. The extractants included trioctylphosphine oxide (TOPO), trioctyl amine (Alamine 336), bis-2, 4, 4-trimethylpentyl phosphinic acid (Cyanex 272), and bis-2-ethylhexyl phosphoric acid (D_2EHPA). The results indicate that magnetic particles can be tailored with various extractants to remove actinide contaminants and exhibit large partitioning coefficients for the full range of expected acidity (see Table III-2). We will be continuing work with mixed waste systems and optimizing the MAC process for WMO waste streams.

3. Chrome Plating

Federal Machine, Inc. (West Fargo, ND) is a hard-chrome plating company interested in the use of the MACS process to cost effectively reduce Fe(III) and Cr(III) concentrations in their plating baths. Increases in dissolved iron in the bath increase the plating voltage and, therefore, costs. The iron separation system must have five elements: (1) high partitioning coefficients for target elements (K_d > 1000 mL/g), (2) sufficient loading capacity for target metals, (3) effective

[4] J. J. Laidler et al., *Chemical Technology Division Annual Technical Report, 1994*, Argonne National Laboratory Report ANL-95/24, pp. 74-77 (1995).

stripping of loaded metals, (4) the ability to recycle the particles, and (5) simple and compact equipment for near-tank use. In our preliminary experiments, Magacell Q™ and MACS particles coated with Cyanex 272/D_2EHPA were tested for Fe(III) removal from an actual spent plating bath (2.48 M H_2CrO_4) diluted by a factor of 100. The K_d values were determined to be low (<200 mL/g), and stripping was difficult.

Table III-2. Partition Coefficients for MACS Separation of Pu, U, and Am from Acidic Solutions

Coating	HNO_3 Conc., M	Partition Coefficients, mL/g		
		Pu	U	Am
0.25 M TOPO 0.5 M D_2EHPA	1	50,000	10,000	55
10% Alamine 336	4.9	340	--	52
1.2 M CMPO/TBP	0.01 1	150 23,000	300 9300	35 3000

Strong-acid cation exchange resins are known to be effective in removing Fe and Cr from chromic acid baths. Our experiments have produced high partitioning coefficients using these resins (K_d>6000 mL/g) in the diluted plating solution. Nearly total stripping (feed-to-strip volume ratio of 1:1) with 5 M H_2SO_4 has also been obtained. Future activities will be directed toward (1) determining the durability of the resins under repeated loading and stripping cycles, (2) producing MACS particles with these strong cation exchangers, (3) testing the tailored MACS particles, and (4) planning a pilot unit for Federal Machine.

4. Decontamination Systems for Components in the Nuclear Industry

In the nuclear power industry, radioactive decontamination techniques for stainless steel components have been unsatisfactory for many applications because of ineffective scale removal, lack of target specificity (i.e., damage to the metal substrate), and/or waste handling problems. Many chemical techniques are available to dissolve scales or films formed on ferrous metals, each with associated limitations. In cooperation with the Technology Development (TD) Division, we are developing a cradle-to-grave decontamination process based on the chemistry of 1-hydroxyethane-1,1-diphosphonic acid (HEDPA). After bulk treatment of the spent HEDPA liquor, a polishing step will be required prior to effluent discharge. We are investigating methods of bulk treatment of the spent liquor and the applicability of the MACS technology as a polishing step. A reducing agent, sodium formaldehyde sulfoxylate (SFS), is added to the decontaminating solution to increase the iron-oxide dissolution rate. Studies are addressing the proper concentration of SFS to produce acceptable decontamination rates and yet limit iron-phosphate precipitation that occurs at high iron and SFS concentrations. However, following use, precipitation may be an acceptable means to treat the spent solution. Treatment of this stream with anion exchange resin may also be an acceptable treatment.

Palisades Nuclear Plant (Covert, Michigan) is cooperating with CMT and TD in demonstrating the decontamination of stainless-steel piping by providing a small section of contaminated piping from their primary coolant system. The pipe will be shipped in sections for microscopic analysis, and a portion will be used to demonstrate the complete decontamination cycle. Decontamination will be evaluated, as well as the efficiency and economics of processing the spent HEDPA liquor.

D. Development of Sol-Gel System for Waste Disposal

A unique approach using sol-gel technology was developed for separating and recovering particulates and colloids from caustic waste slurries. The approach involves the addition of an alkali silicate and an organic gelling agent directly to the waste stream to immobilize particulates that range from macro sizes to submicron colloids. The particulates and colloids become trapped within a silica network that remains porous during the early stages of the sol-gel process. The freshly gelled monolith undergoes a process of syneresis, whereby the water and soluble salts are ejected from the monolith as it contracts. Initial laboratory tests have shown that it is possible to produce silica monoliths in 4 M hydroxide. Analysis of the mother liquor produced during syneresis indicated that recovery of particulates within the monolith was >99.999%. Salt recoveries from the mother liquor were in excess of 90%. A water wash (pH = 3) of the porous monoliths reduced the alkali metal concentrations to parts per million and produced a 40% aluminate recovery. Heating the washed monolith at 1400°C produced an extremely leach-resistant monolith, with the particulates encased in a fused silica matrix. Weight loss was not detectable during a standard leach test (MCC-1) at 90°C for 30 days.

IV

Electrometallurgical Treatment Technology

The CMT Division is developing an electrometallurgical process for treatment of spent nuclear fuels for disposal in a geological repository. It is capable of handling most types of spent fuel and is especially intended for fuels at risk of chemical reaction with the groundwater in the repository. These "at risk" spent fuels include metal fuels with various cladding and matrix materials, reactive compounds, and highly enriched fuels. The central feature of the electrometallurgical treatment is electrorefining of the spent fuel in a molten salt electrolyte at 500°C (773 K). The LiCl-KCl eutectic electrolyte is formulated to contain about 2 mol% UCl_3. When a potential is applied between the anode and cathode, uranium, active fission products, and transuranic (TRU) elements dissolve at the anode, while pure uranium product is deposited at the cathode. The fission products and TRU elements are left behind to accumulate, either in the anodic dissolution basket (more noble fission products) or in the molten salt electrolyte (active fission products and TRU elements). The TRU elements and more active fission products may be extracted by passing the molten salt through anhydrous zeolite or sorbing the salt into zeolite. The loaded zeolite is then combined with a suitable glass frit and hot pressed to make a stable waste form for repository disposal. Fuel cladding, assembly hardware, and the noble metal fission products left in the anodic dissolution basket are melted together to form a Zr-Fe-based metal waste form for repository disposal.

All the electrorefining process steps were developed in laboratory-scale experiments, and most have been demonstrated at the engineering scale (10- to 150-kg batch size). Past work also demonstrated the feasibility of using this process for treatment of N-Reactor fuel (Zircaloy-clad uranium), single-pass reactor fuel (aluminum-clad uranium), Experimental Breeder Reactor-II (EBR-II) fuel (steel-clad uranium alloy), aluminum-based fuel (an aluminum-alloy fuel), and fluoride salt fuel containing actinides and fission products. Select topics from the electrometallurgical programs in CMT are discussed below.

A. Electrorefining Development

Work continues on development of uranium electrorefining, the key step in electrometallurgical treatment of metallic spent nuclear fuel. The major focus during this reporting period was on determining the operating procedure and conditions that provide sustained operation of the high throughput electrorefiner (HTER), designated the Mark V anode-cathode module (ACM), that will be used to treat the EBR-II blanket fuel in the Fuel Conditioning Facility at ANL-West. Key design improvements for the ACM were based on testing of a 25-in. (0.6-m) dia HTER in CMT. Testing of this HTER was continued as needed to support the development of the ACM.

1. Advanced Electrorefiner

Effort has continued on development of an HTER having a throughput of >40 kg uranium per hour and maximum batch size of 150-kg uranium. This HTER contains 20 stainless steel anode baskets. The cathode consists of five concentric steel tubes that form four channels in which the anode baskets are positioned. Uranium scrapers are attached to the anode baskets. As the baskets rotate in the cathode channels, these scrapers remove the uranium electrodeposited on the cathode tubes. The uranium is then collected in a basket that is attached to the bottom of the outer cathode tube.

In earlier work,[1] tests of the 25 in. (0.6-m) dia HTER indicated a problem with uranium buildup caused by failure of the cathode scrapers. In the past year, an improved cathode scraper was designed and tested in this HTER. For this test, the improved scrapers were attached to the anode baskets in the inner and outer channels of the HTER. Segments of partially dissolved, unirradiated, Zircaloy-clad N-Reactor fuel (41.4 kg total, of which 36 kg was uranium) were loaded in the anode baskets. No fuel was loaded in two of the channels formed by the concentric cathode tubes.

Uranium was electrotransported from the anode baskets to the cathode tubes at a current density of 0.046 A/cm^2 (200 A). This is double the current density for sustained operation with the original cathode scrapers. The improved scrapers knocked the uranium off the cathode tubes in the space between the anode baskets. With the original scrapers, the uranium had been knocked off the cathode tubes in the narrow gap (0.6-cm wide gap) between the faces of the anode baskets and the cathode tubes, and uranium holdup between the electrodes had been a problem. After the improved scraper test, post-test examination of the fuel segments in the anode baskets showed that most of the 36-kg uranium had been anodically dissolved in the molten salt electrolyte.

The rotation speed of the anode drive in the improved scraper test was 40 rpm. This test employed no "stripping" (i.e., electrotransport of some of the uranium that was deposited on the cathode tubes back to the anode baskets). However, a molten salt wash cycle lasting 3 min was

[1] J. J. Laidler et al., *Chemical Technology Division Annual Technical Report, 1997,* Argonne National Laboratory Report ANL-98/13, pp. 98-100 (1998).

used every hour; during this time, the current was turned off while rotation of the anode drive was continued so that any uranium dendrites held up between the electrodes would fall into the collection basket. Post-test examinations showed no uranium holdup between the electrodes.

During this test, the electrorefiner voltage decreased from 0.35 to 0.15 V. Post-test examinations showed that this decrease was likely caused by the increased thickness of the dense uranium electrodeposited on the cathode tubes, which decreased the distance between the anode and cathode and decreased the resistance, as the number of ampere-hours increased. As a result, the electrorefiner resistance decreased from 1.8 to 1.0 mΩ. Stripping investigations are planned to develop an operating procedure that removes the dense uranium deposit from the cathode tubes.

The anode-drive power during the test is shown in Fig. IV-1. During the run, the anode-drive power increased from about 0.09 to 0.15 hp. This increase was caused by the increased thickness of the dense uranium deposit on the cathode tubes, which required more power to maintain the anode-drive rotation speed at 40 rpm. The spikes in the power profile are not an indication of impending stalling, as was the case with the original cathode scrapers. Instead, they indicate increased drag resistance as uranium is knocked off the cathode tubes and drops to the collection basket.

The above results show that the improved scraper design can prevent uranium holdup between the electrodes. Planned tests will continue to use the improved cathode scraper design, and an operating procedure will be developed to eliminate the dense uranium deposit on the cathode tubes. These tests are expected to lead to HTER designs and operating procedures that meet the different uranium throughput goals for the electrometallurgical treatment of various kinds of spent nuclear fuel.

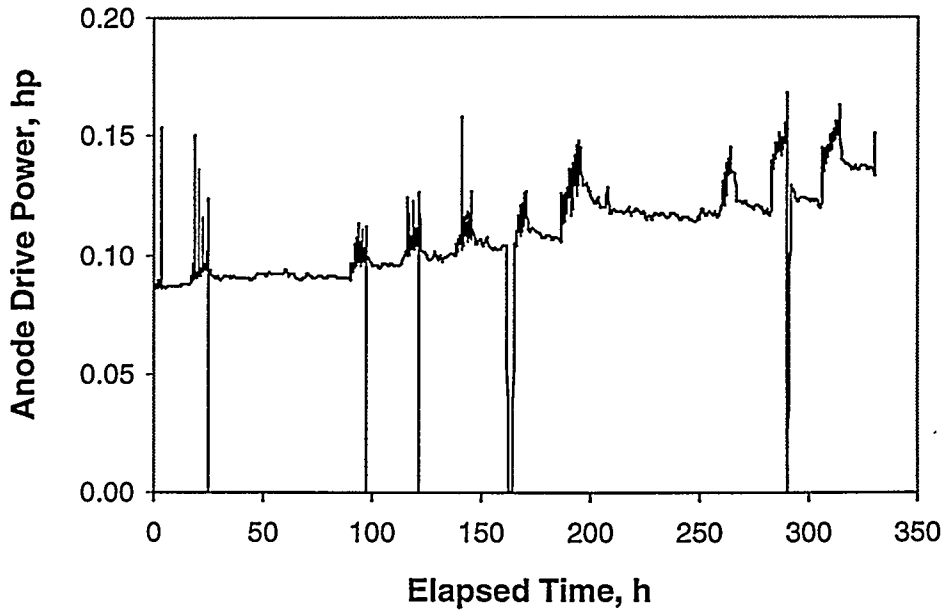

Fig. IV-1. Anode-Drive Power Profile for Experiment with High Throughput Electrorefiner

2. Development of Anode-Cathode Module for Mark V Electrorefiner

During the past year, the first Mark V ACM was tested with a 20-kg batch of unirradiated N-Reactor fuel. Figure IV-2 shows a top, cross-sectional view of the ACM, which has a 10-in. (25-cm) outer diameter. The following are key design features: two channels formed by three concentric cathode tubes and nine anode baskets (three baskets in the inner channel and six in the outer channel). The ACM is placed in a vessel filled with molten electrolyte. During operation, electrolyte is drawn from the bulk salt in this vessel and through the ACM, then discharged back into the bulk salt.

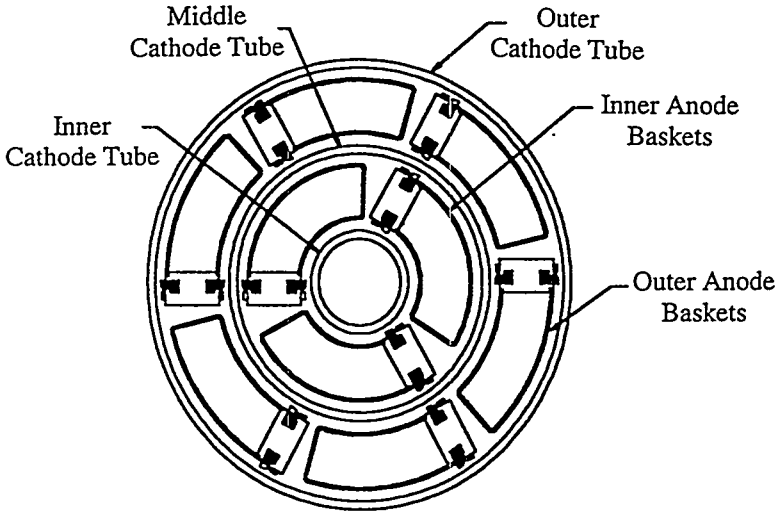

Fig. IV-2. Cross-Sectional View of Mark V Anode-Cathode Module

Based on the HTER tests (Sec. IV.A.1), the following conditions were included in the operating procedure that was used for the ACM test. The cutoff voltage was set at 0.45 V to separate uranium from the chopped N-Reactor fuel segments and to retain the Zircaloy cladding in the anode baskets. Each cathode channel had one empty anode basket. The operating temperature was 500°C, the uranium concentration in the molten salt was about 7 wt%, and the rotation speed of the anode drive was 40 rpm. Uranium was electrotransported from the anode baskets to the cathode tubes (electrodeposition) for 200 Ah. The initial electrodeposition current was 200 A, which was reduced as needed to maintain the ACM voltage below the 0.45 V cutoff. The current was turned off for about 4 min (molten-salt washing step) after the electrodeposition, the direction of rotation for the anode drive was reversed from that used during electrodeposition, and the anode drive was rotated at 40 rpm to remove uranium holdup from the cathode scrapers. The direction of rotation of the anode drive was reversed to pull the scrapers away from any uranium that may have been caught in the "L"-shaped union of the scrapers and the anode baskets.

After the first washing step, current was passed through the ACM (typically 20-70 Ah) to remove all the uranium from the cathode tubes (stripping). This step was needed to eliminate

buildup of the dense uranium deposit on the cathode tubes, which was observed in earlier HTER tests.[1] This dense uranium deposit had caused the anode drive to stall as a result of high drag forces that developed between the scrapers and the deposit. The stripping currents used in the ACM test were 400-600 A. Stripping was followed by a second washing step for 2 min. These operating steps were repeated until all of the uranium was electrotransported from the anode baskets to the cathode tubes. After stripping, an electrodeposition current of 600 A was applied for a short time.

During these operations, the ACM resistance varied between 0.6 and 6 mΩ. The lowest resistance was observed after stripping because the uranium that was deposited on the outside of the anode baskets resulted in a shorter effective spacing between the anode and cathode. As uranium was electrotransported from the anode baskets, the average electrodeposition current per cycle decreased as the number of cycles and resistance increased.

The total electrodeposition and gross current passed (electrodeposition plus stripping) for the present ACM test were 11,240 Ah and 15,750 Ah, respectively. The stripping ampere-hours (4510 Ah) was less than 30% of the total or gross ampere-hours. This result provides evidence that the empty basket in each channel reduces the amount of uranium stripped from the cathode tubes (relative to the amount of uranium that was electrotransported from the anode baskets). This is believed to occur by the formation of U^{4+} at the anode baskets from the U^{3+} in the salt. A major contribution to eliminating uranium holdup may be the U^{4+} dissolution of uranium buildup on the outside of the anode baskets. Another contribution may be intermittent short circuits between the anode baskets and cathode tubes. During these short-circuit periods, the U^{4+} can also dissolve some of the uranium on the cathode tubes. The dissolved uranium is likely to be deposited on the cathode tubes, where it would be knocked off the tubes by the cathode scrapers. Thus, uranium is recovered in the uranium collection basket, which is positioned away from the anode baskets and thus away from the vicinity where U^{4+} ions are generated.

The above test results demonstrate the sustained operation of the ACM and indicate that a 20 kg U batch of unirradiated N-Reactor fuel can be treated by the operating procedure summarized above. Post-test examination of the ACM showed no uranium holdup between the anode baskets and the cathode tubes. The cathode product in the collection basket after the initial ACM test is shown in Fig. IV-3.

The unconsolidated product was examined at the ANL Reactor Analysis Division to provide morphological and density data. The majority of the product consisted of irregularly shaped porous accumulations as large as 20 mm across, with a few granules as small as 1 mm in diameter. The density of the product was measured by liquid displacement in water after the product was washed to remove the salt. The measured density of the uranium product was 12.5 ± 0.5 g/cm^3. These data will be used to determine the operating conditions that provide a cathode product with the highest packing density in the cathode processor.

Figure IV-4 shows the Zircaloy cladding that was left in one of the anode baskets after all of the uranium was removed from the fuel segment. This fuel segment was cut from one end of the inner N-Reactor fuel element. No evidence of zirconium transport from the cladding could be detected.

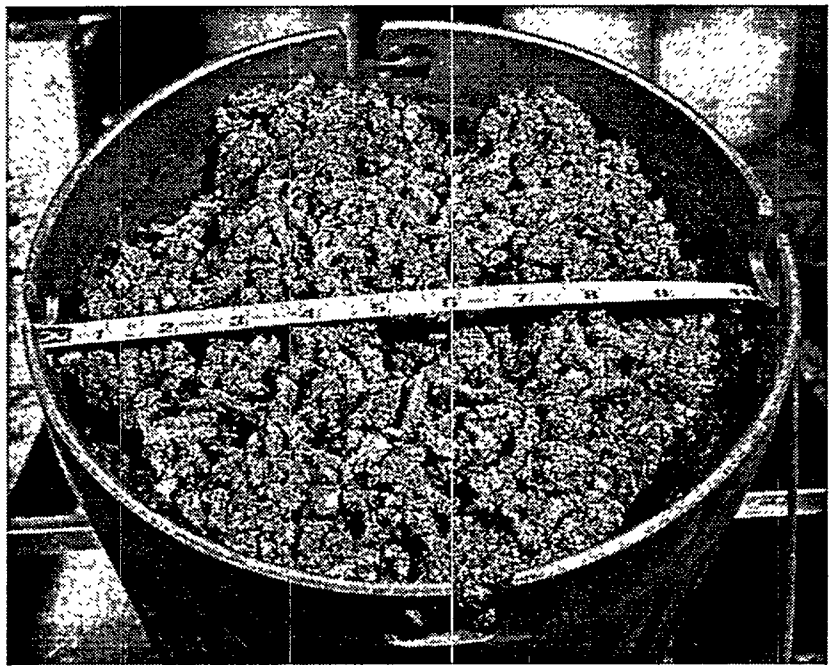

Fig. IV-3. Cathode Product from the Initial Mark V Test

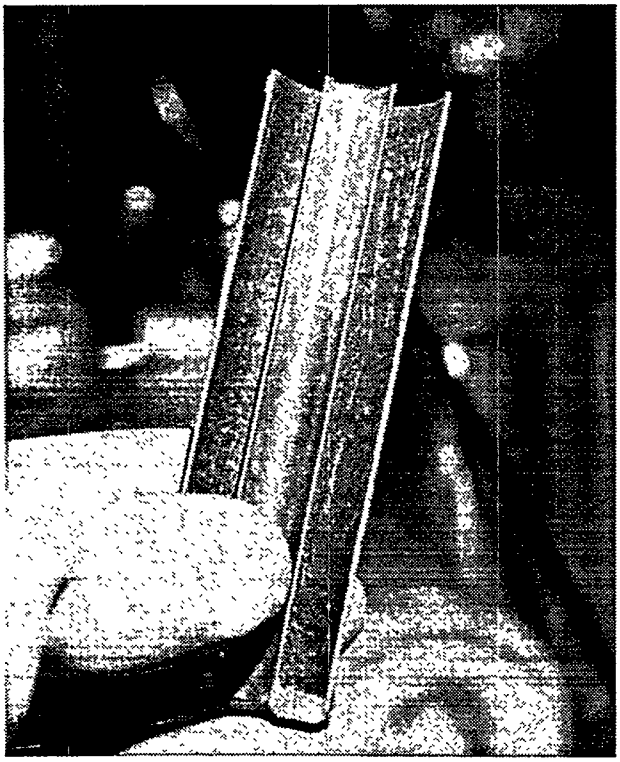

Fig. IV-4.

Zircaloy Cladding from Anode Basket after Initial Mark V Test

A uranium mass balance has been completed for the above experiment in which 20 kg of cathode product (about 16 kg of uranium) was collected. The amount of uranium that was electrotransported from the anode baskets was calculated from the weight of the anode baskets and fuel at the start of the experiment minus the weight of the anode baskets and remaining fuel after the experiment. The calculated value is 18.7 kg uranium, which is 2.7 kg (14.3 wt%) more than the 16 kg in the cathode product. This difference between (1) the weight of uranium that was electrotransported from the anode baskets and (2) the weight of uranium that was collected on the cathode tubes and in the cathode product collection basket is attributed to the fines that were swept out of the ACM as molten salt was drawn into the bottom of the ACM from the bulk salt and discharged back into the bulk salt.

A likely path of escape for uranium from the ACM is through the 80-mesh screen that covers the openings in the cathode-product collection basket and permits salt flow. Another possible path is through the gap between the top of the collection basket and the bottom of the outer cathode tube. The collection basket is supported with two pins that are welded to the outer cathode tube. Plans are to test improved collection basket designs that will reduce the loss of fines from the ACM. Tests are also planned with simulated EBR-II blanket fuel segments in the ACM. Operating procedures will be developed with this fuel.

3. Aluminum-Based Spent Fuel

Development work has continued on an electrometallurgical process for treating spent aluminum-based fuels. This fuel is predominantly used in foreign and domestic research reactors. Over the next four years, 128 metric tons of spent aluminum-based fuel will be shipped to the Savannah River Site from U.S. and foreign research reactors. When originally fabricated, the fuel contained over 55 metric tons of uranium at an average enrichment of approximately 20%. The primary options at present are processing the spent fuel in existing PUREX facilities at the DOE Savannah River site and direct disposal of the fuel in a geological repository. Along with simply melting of the fuel and addition of depleted uranium, electrometallurgical treatment of the fuel is considered a backup option. Because electrometallurgical treatment separates the aluminum from the spent fuel for disposal as low-level waste, the high-level waste volume is reduced by better than 80%. The process is well suited for operation after 2005 when the rate of spent fuel shipments begins to decline. Additionally, the existing PUREX facilities at Savannah River are scheduled to be decommissioned around 2005.

Electrometallurgical treatment is also well-suited to the wide variety of aluminum-based fuels that will ultimately end up at the Savannah River Site. Alloys such as UAl_x-Al, U_3Si-Al, and U_3O_8-Al are all compatible with this technology. In addition to treating spent aluminum-based fuel, this technology can be applied to recovering uranium from scrap generated by fuel fabrication. The recovered uranium can then be recycled into subsequent batches of fresh aluminum-based fuel.

The overall process flowsheet (Fig. IV-5) has changed very little from the one described in last year's report.[2] In the process, the spent fuel is melted under a salt flux, and silicon is added to the molten fuel. Rare earth and active metal fission products are extracted from the fuel into the salt flux. The remaining metal (aluminum, actinides, and noble metal fission products) is then cast into anode ingots and loaded into a high-throughput electrorefiner. In this electrorefiner, aluminum is removed from the remaining metal by electrotransport. After all the aluminum has been removed, the anode baskets contain only the actinides and noble metal fission products. These baskets are then transferred to a second electrorefiner, where uranium is removed by electrotransport. The noble metal fission products remain in the anode and are incorporated into a Fe-Zr alloy waste form. Transuranics such as plutonium remain in the molten salt of this second electrorefiner. The fission products and transuranics must then be chemically stripped from the fluxing salt and the uranium electrorefiner salts, respectively. These high-level waste products are then oxidized and incorporated into a glass waste form.

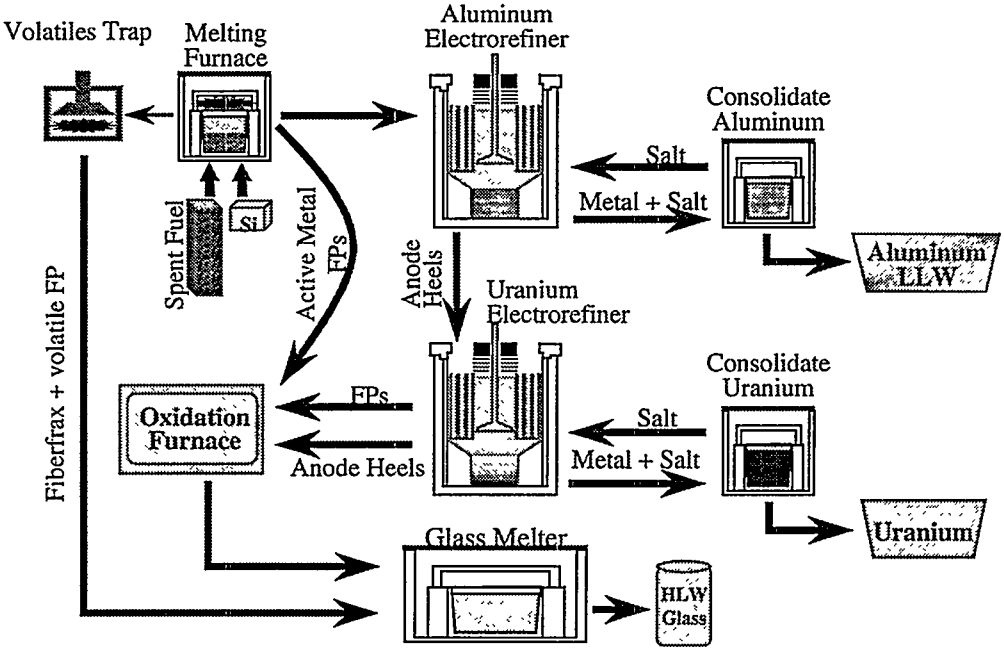

Fig. IV-5. Flowsheet for Electrometallurgical Treatment of Aluminum-Based Fuel. (FP = fission product, LLW = low-level waste, and HLW = high-level waste.)

Many of the steps in the flowsheet shown in Fig. IV-5 have been demonstrated in other programs. Electrorefining uranium, for instance, has been demonstrated in the treatment of spent EBR-II fuel. In 1997, we demonstrated electrorefining of pure aluminum and of aluminum from a U-Al-Si alloy.[2] Under near-optimum conditions, the electrorefined aluminum product contained only 500 ppm uranium.

[2] J. J. Laidler et al., *Chemical Technology Division Annual Technical Report, 1997,* Argonne National Laboratory Report ANL-98/13, pp. 106-108 (1998).

Much of the work this past year has focused on the extraction of rare earth and active metal fission products in the initial melting/fluxing step. Several tests were conducted in which a U-Al-Si alloy containing representative alkali, alkaline earth, and rare earth metals was electrorefined in a potassium cryolite-based salt. As expected, the alkali and alkaline earth metals were extracted into the molten salt and remained there. We were surprised, however, to find that the rare earth metals were also extracted into the molten salt. Our initial thermodynamic calculations predicted that the rare earth metals would not be extracted. However, additional and more-refined calculations confirmed what had been observed experimentally—namely, the extraction of rare earth metals into the potassium cryolite-based salt. Measurements of the exchange equilibria of representative rare earth metals between molten aluminum and the potassium cryolite-based salt are in progress.

B. Synthesis of UCl_3 for the Mark V Demonstration

In the previous annual report,[3] we reported on progress made to prepare UCl_3 needed for continued operation of the Mark V electrorefiner being used to treat spent EBR-II fuel at ANL-West. In addition, we reported that we had prepared one batch of 46 mol% LiCl-24 mol% KCl-30 mol% UCl_3, which contained 14.5 kg UCl_3. This product was prepared by the reaction of $CdCl_2$ with uranium in a LiCl-KCl electrolyte at 500°C. The total amount needed for the initial phase was 110 kg UCl_3, while future needs require one metric ton.

During the past year, we prepared seven more 20-kg batches of the salt containing 14.5 kg UCl_3. We also completed an economic assessment of the best synthetic route for preparing one metric ton of UCl_3. The seven additional batches of UCl_3 were prepared over a several month period, with each batch requiring approximately one week for completion. The experimental procedure consisted of additions of $CdCl_2$ to a LiCl-KCl salt, which was contained in a thin wall crucible of mild steel. A basket containing uranium in excess of the amount needed to react with $CdCl_2$ was also placed in the crucible prior to the start of $CdCl_2$ addition. The $CdCl_2$ was added in increments of 400-800 g. A wait period of 20-30 min allowed dissipation of the heat generated in the reactor. After the $CdCl_2$ was added, the contents were mixed for an additional time and then heating stopped. When the crucible contents were cooled, the product salt was recovered and sampled.

The product from each UCl_3 preparation was analyzed for the major metallic components (Li, K, and U), as well as the expected impurity elements (Cd, Fe, Cr, and Ni). The presence of Ni, Cr, and Fe was possible because the basket used to contain the uranium was made from stainless steel. The product was also analyzed by X-ray diffraction to establish the uranium phase(s) present. The elemental analysis indicated a slight variation for the major elements from batch to batch. The impurity elements were generally near detection limits (~0.001 wt%) with the exception of cadmium, which in some cases was higher.

[3] J. J. Laidler et al., *Chemical Technology Division Annual Technical Report, 1997,* Argonne National Laboratory Report ANL-98/13, pp. 101-102 (1998).

The X-ray diffraction results indicated that the uranium was in the form of $KU_{1.67}Cl_6$. There was no indication of UO_2 present. The X-ray results and the elemental analysis indicated that we had produced a high-purity product which was acceptable for use at ANL-West.

The economic study was based upon the lowest cost method for preparing one metric ton of UCl_3. This study began with a thorough review of the published synthetic routes for preparing UCl_3. For convenience, the synthetic routes were broken down to three methods:

I. Prepare UCl_4 and reduce UCl_3
II. Form UH_3 and react with HCl
III. React uranium with suitable metal chloride

As part of this review, we examined the factors that would ultimately affect our choice on which of these three methods was the best for preparing UCl_3. The factors considered were product purity, safety, heat generation and rejection, reaction complexity, conduction materials, reaction completeness, and availability and cost of high-purity reagents.

This analysis indicated that method I was unacceptable because it required multiple steps involving the probable use of Cl_2 in addition to a strong reducing agent. This approach was tried by a commercial vendor at our request, and the results were that the product was not high purity but a mixture of phases. Method III was given considerable attention and was successfully used to prepare 110 kg UCl_3. However, our analysis indicated that the cost of high-purity $CdCl_2$ made this approach somewhat more expensive than method II. We concluded that the most economic approach was method II, but with a slight variant: the initial hydriding step would be eliminated because of problems associated with handling large quantities of pyrophoric hydride, and the uranium would be treated directly with HCl using a LiCl-KCl electrolyte. The resulting product would have the same composition as described in the preparation of the seven additional batches of UCl_3. Laboratory-scale experiments are planned to evaluate the optimal conditions needed for this method.

C. Reduction of UO_2 by Zirconium in Liquid Bismuth

The DOE has a significant amount of Zircaloy-clad nuclear fuel in its waste inventory. Leaving the fuel in its current condition has been considered, but this is not a desirable option. An option being considered is to treat this fuel by removing and disposing of the fission products and recovering the uranium for reuse. A considerable amount of experimental work has been conducted for treatment options that involve the use of either Ca or Li. With these reductants, the oxide fuel is converted to uranium metal and either CaO or Li_2O. Regardless of whether Li or Ca is used, a number of problems have not yet been resolved, including (1) the length of time to obtain complete reduction is often a major concern, (2) incomplete reduction often occurs when Zircaloy clad pellets are reduced because the chemical reductant is unable to penetrate the massive pellets in a reasonable time, and (3) the use of either one or both reductants requires the electrochemical decomposition of the Li_2O or CaO which is dissolved in a molten salt. We are thus investigating a treatment option that would not require an electrochemical decomposition step and would achieve complete reduction when Zircaloy cladding was used.

The treatment option involves reduction of the UO_2 by reaction of the zirconium from the Zircaloy cladding and a molten metal solvent, bismuth. Analysis of the available thermodynamic data for UO_2, Zr, and U in bismuth led us to the conclusion that the reduction of UO_2 by zirconium using liquid bismuth is possible. The overall reaction is $UO_2 + Zr_{(Bi)} \rightarrow ZrO_2 + U_{(Bi)}$. However, there is some doubt that this reaction will occur because the activity coefficient of zirconium in bismuth used in our analysis is based on limited experimental data. As a result, we conducted an experimental study to determine if this reaction occurs and, if so, what the rate is. Nine experiments were conducted using a modification of equipment employed for work related to treatment of waste salt from the Molten Salt Reactor Experiment.[4] The major modification of the equipment was the use of carbon steel baskets, which served both as an electrorefiner stirrer and a container for UO_2 and Zr. The bismuth was contained initially in an AlN crucible, and the basket was located in this crucible. The basket was attached to a shaft in the cathode position of the electrorefining cell.

The experimental procedure consisted of placing one piece of zirconium weighing 18.33 g and four pellets of UO_2 weighing 11.81 g into the basket, and placing this basket so that it was ~0.6 cm from the bottom of the AlN crucible. Next, 0.6 kg bismuth was added to the AlN crucible, and the contents slowly lowered into a furnace well. When the contents were at the operating temperature (~200°C), the basket was rotated at 16 rpm for the first experiment; at 16 to 27 rpm for the second experiment; and 27 to 48 rpm for the third experiment. All subsequent experiments were conducted with the basket rotating at 48 rpm. At the end of the desired heating period, the basket was removed, and the bismuth phase within the AlN crucible was sampled and analyzed by inductively coupled plasma/atomic emission spectroscopy. This procedure was repeated for the balance of the experiments. The test duration was varied from 5.9 to 258.4 h. No additional reagents were added after the initial loading.

The analytical results for U and Zr are shown in Fig. IV-6. The time interval between data points corresponds to the duration for that experiment. The results indicate an initial barrier to the reaction which extends to ~100 h. After this period, the reduction reaction occurs in a steady fashion, albeit slowly, with the average concentration increase being ~3 x 10^{-4} wt% uranium per hour. The uranium results suggest that the solubility limit of U in Bi had not been reached. However, the zirconium values indicate that the solubility limit for this element had been reached. The analytical results for the expected impurity elements, such as Al, Fe, Cr, and Ni (these were all <0.01 wt%), indicate that the sampling procedure and the subsequent wet chemical dissolution step did not dissolve the stainless steel buckets used for sampling. The low aluminum results are consistent with our visual findings that there was no attack of the AlN crucible.

Visible examination at the end of each experiment indicated no attack of the UO_2 pellets after the first two experiments, and wetting of two of the four pellets by the bismuth phase after the third experiment. The remaining two UO_2 pellets appeared to be wet by the bismuth phase only in the last two experiments. We concluded that the attack of UO_2 by zirconium did not

[4] J. J. Laidler et al., *Chemical Technology Division Annual Technical Report, 1997,* Argonne National Laboratory Report ANL-98/13, pp. 103-106 (1998).

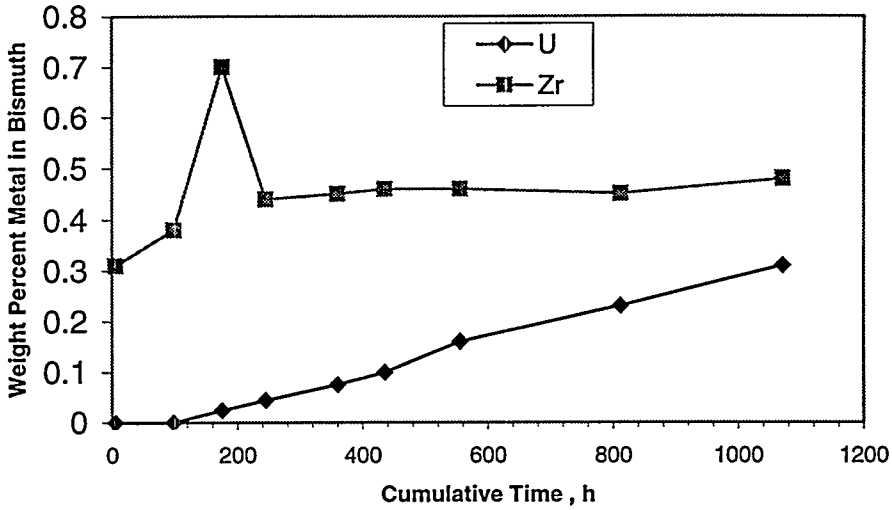

Fig. IV-6. Uranium and Zirconium Content in Bismuth after Reduction Experiments at 200°C

destroy the physical integrity of the pellets, indicating that the reaction occurred on the surface and was progressing slowly inward.

After the initial tests, some mossy material was found adhering to the outside of the baskets containing UO_2 and zirconium at a level corresponding to the height of the bismuth phase. The amount of this material increased in subsequent tests. Chemical analysis of this material indicated that it contained ~5 wt% zirconium but essentially no uranium.

These experiments demonstrate that UO_2 can be reduced by zirconium dissolved in liquid bismuth. There appears to be some initial barrier to the reduction, but after this period, the reaction occurs at a low but steady rate. Since the effects of temperature, mixing speed, basket design, and UO_2 particle size have not yet been studied, it is possible that higher reduction rates could be obtained. Furthermore, if the uranium that was found during reduction was electrochemically removed from the bismuth phase, reduction rates could be improved.

D. Waste Form Development

The electrometallurgical treatment process generates two high-level waste streams. One is a metal waste stream composed of cladding remnants, noble alloying fuel constituents (such as zirconium), noble-metal fission products, and small amounts of actinides that may not have been electrotransported. These metals are blended with additional zirconium, if required, and melted to make a compact and durable waste form. Development of the metal waste form is mostly complete, and our present major emphasis is on the qualification of the waste form for geologic disposition. Some work is also being done in support of other aspects of the electrometallurgical treatment process, including development of crucible materials for fabrication of the metal waste form and for the uranium melting step in the electrometallurgical process.

The process salt must be disposed of from time to time for any of several reasons, including buildup of radionuclides; this generates a second waste stream. This salt is incorporated into the lattice of zeolite A, and the resulting "salt-loaded zeolite" is blended with glass and hot-compacted to make a durable ceramic waste form. Again, a reference composition and process method have been chosen for scaleup and demonstration. However, we are working on several improvements.

Overall, our efforts have been focused on four basic areas: characterization of the waste forms, support for the effort to demonstrate and qualify electrometallurgical treatment with spent EBR-II fuel, and two improvements to the process that have large potential payoffs—development of advanced fabrication methods for the ceramic waste and development of a molten salt ion-exchange column that will concentrate radionuclides in the zeolite and allow indefinite reuse of the process salt.

1. Development of Metal Waste Form

Stainless steel-zirconium (SS-Zr) waste forms have been developed for the disposition of metallic waste generated during the electrometallurgical treatment of spent nuclear fuel. The waste forms contain spent fuel cladding, noble metal fission products, actinide elements, and in some cases, zirconium from the alloy fuel. (The designation "noble metal" means a metallic element that is inert, that is, electrochemically noble, in the electrorefiner system.) The baseline waste form for spent fuel from EBR-II is the stainless steel-15 wt% zirconium (SS-15Zr) alloy. In practice, the zirconium content of the waste form may vary from 5 to 20 wt% zirconium, depending on the fuel (driver or blanket) being treated. Also, the waste forms may contain up to 4 wt% noble metals and up to 10 wt% actinides (mainly uranium).

The research emphasis for the past year has been the testing of waste form alloys. The standard practice ASTM C 1174-91[5] was used in designing a test matrix for the metal waste form. The matrix is intended to provide a qualification-relevant data base for future repository acceptance of the metal waste form. Large-scale (~3 kg) alloy ingots containing 0 to 20 wt% zirconium and 0 to 5 wt% noble metal elements were generated in an induction furnace and sectioned to obtain specimens required for the various tests.

Typical microstructures from an SS-5Zr and SS-15Zr alloy are shown in Fig. IV-7. The SS-5Zr alloy shows a three-phase microstructure containing two iron solid solutions, ferrite (α) and austenite (γ), and a $ZrFe_2$-type Laves intermetallic, designated as $Zr(Fe,Cr,Ni)_{2+x}$. The SS-15Zr alloy displays a eutectic microstructure containing ferrite and $Zr(Fe,Cr,Ni)_{2+x}$. Small amounts of austenite and a $Fe_{23}Zr_6$-type intermetallic, designated $(Fe,Cr,Ni)_{23}Zr_6$, are also present in the SS-15Zr alloy.

[5] American Society for Testing and Materials, *Annual Book of ASTM Standards,* ASTM C 1174-91, Vol. 12.01, Philadelphia, PA, pp. 598-611 (1997).

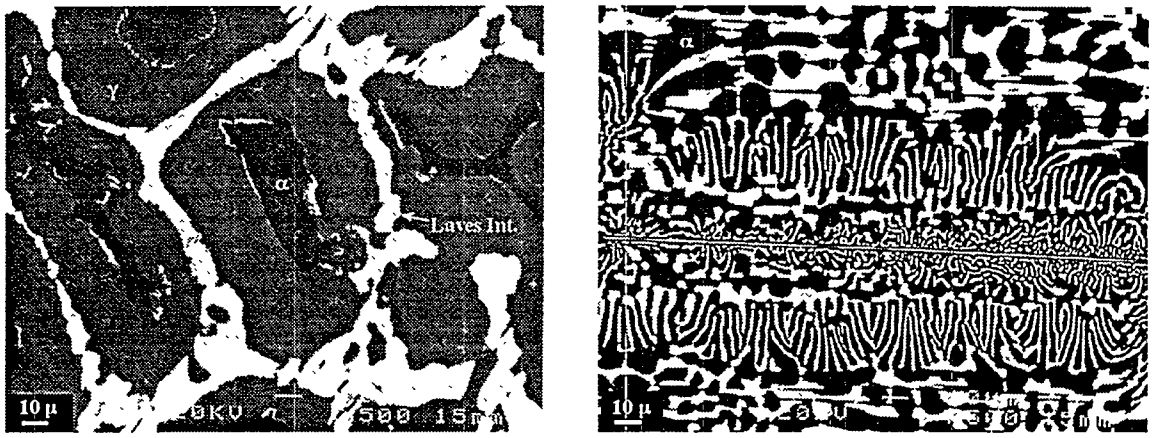

(a) (b)

Fig. IV-7. Typical Microstructures of (a) Stainless Steel-5 wt% Zirconium Alloy and (b) Stainless Steel-15 wt% Zirconium Alloy. The SS-5Zr microstructure contains the iron solid solutions ferrite (dark) and austenite (gray), and the $Zr(Fe,Cr,Ni)_{2+x}$ intermetallic (bright). The SS-15Zr microstructure shows only ferrite and $Zr(Fe,Cr,Ni)_{2+x}$.

Zirconium plays a crucial role in the incorporation of fission products and actinides in the SS-15Zr waste forms. The $Zr(Fe,Cr,Ni)_{2+x}$ intermetallics are the preferred site for several noble metals (such as Ag, Nb, Pd, Ru, Sn, and Ta) and actinide elements (such as U, Pu, and Np). Fission product and actinide incorporation in alloy phases is strongly influenced by the volume fraction of $Zr(Fe,Cr,Ni)_{2+x}$, which is, in turn, influenced by the zirconium content of the alloy. The noble metal distribution was investigated for alloys containing from 0 to 20 wt% zirconium. The noble metals were incorporated in alloys containing 15 and 20 wt% zirconium, but noble metal-rich phases were observed in 5 wt% zirconium alloys when the total noble metal content increased above ~1 wt%. Noble metal-rich phases appeared only when the $Zr(Fe,Cr,Ni)_{2+x}$ intermetallics were saturated with these elements. In stainless steel alloys with no zirconium, fission products such as Nb, Pd, Ag, and Sn always precipitated to form noble metal-rich phases.

The long-term (>1000 yr) radioactivity of nuclear waste forms is dominated by the long-lived fission product isotopes, such as technetium, and the actinide elements. The distribution of Tc and U in phases of the SS-15Zr alloy was studied by neutron diffraction. The lattice parameters and volume fractions presented in Table IV-1 are from Reitveld refinements of neutron diffraction data collected at Argonne's Intense Pulsed Neutron Source (IPNS). Phases rich in technetium were not observed in neutron diffraction patterns obtained from the SS-15Zr-2Tc alloy, although this element is incorporated into all phases of the alloy. Uranium is present only in the intermetallic phases of the SS-15Zr-5U alloy; phases rich in uranium were not observed in this alloy.

The principal conclusion from these results is that SS-15Zr waste forms can readily accommodate the noble metal fission products and actinide elements from the EBR-II fuel being treated at ANL-West. Fission product-rich phases (and potentially actinide-rich phases), however, may be present in alloys containing ≤5 wt% zirconium.

Table IV-1. Lattice Parameters and Volume Content of Phases in SS-15Zr, SS-15Zr-2Tc, and SS-15Zr-5U Alloy

	Lattice Parameters, nm			Content, vol%		
	SS-15Zr	SS-15Zr-2Tc	SS-15Zr-5U	SS-15Zr	SS-15Zr-2Tc	SS-15Zr-5U
Ferrite	a=0.2876	a= 0.2879	a= 0.2876	40 ± 6	44 ± 5	45 ± 4
Austenite	a=0.3596	a= 0.3598	a= 0.3595	9 ± 1	7 ± 1	5 ± 2
Laves C36	a=0.4908 c=1.6016	a= 0.4904 c= 1.5989	a= 0.4923 c= 1.6016	33 ± 5	19 ± 5	13 ± 4
Laves C15	a=0.6938	a= 0.6931	a= 0.6959	16 ± 2	22 ± 7	21 ± 4
$Fe_{23}Zr_6$ –type	a=1.1690	a= 1.1660	a= 1.1669	2 ± 1	8 ± 1	17 ± 2

To be acceptable in a geologic repository, waste forms must be shown to have suitable physical characteristics and chemical durability. The waste forms must be tested to establish their corrosion behavior and to allow a "repository-relevant" performance assessment. To address these issues, a qualification test matrix was established to systematically generate data for the SS-15Zr waste forms. In addition to providing information on material properties, the test plan has been designed to examine the effect of zirconium and noble metal contents on the corrosion behavior of the alloy waste forms.

The implementation of the test plan is well underway. The microstructure of waste form alloys has been studied by microscopy, diffraction, and spectroscopy. The microstructures confirm the role of zirconium in the incorporation of fission products. Mechanical properties of alloys were measured by tensile, impact, and compression testing. Thermophysical properties were determined by measurements of density, specific heat, thermal expansion, and thermal conductivity. The results to date show that mechanical and thermal fractures are unlikely to occur during processing and storage of the metal waste form.

A significant number of electrochemical corrosion tests, immersion corrosion tests, and vapor hydration tests have been conducted on the waste forms. The electrochemical tests were conducted by the linear polarization method in test solutions that ranged in pH from 2 to 10. Corrosion rates of waste form alloys are compared with those of candidate materials for nuclear waste canisters in Fig. IV-8. The corrosion rates of the waste form alloys are comparable in magnitude to those for Alloy C-22 (57Ni-21Cr-13Mo), which is the current choice for the "corrosion resistant" lining of the nuclear waste canisters, and two to three orders of magnitude lower than the rate for mild steel, which is the "corrosion allowance" material in the canister.

Immersion corrosion tests provide information on the selective leaching of elements into representative test solutions. Immersion tests in tuff-equilibrated groundwater (simulated J-13

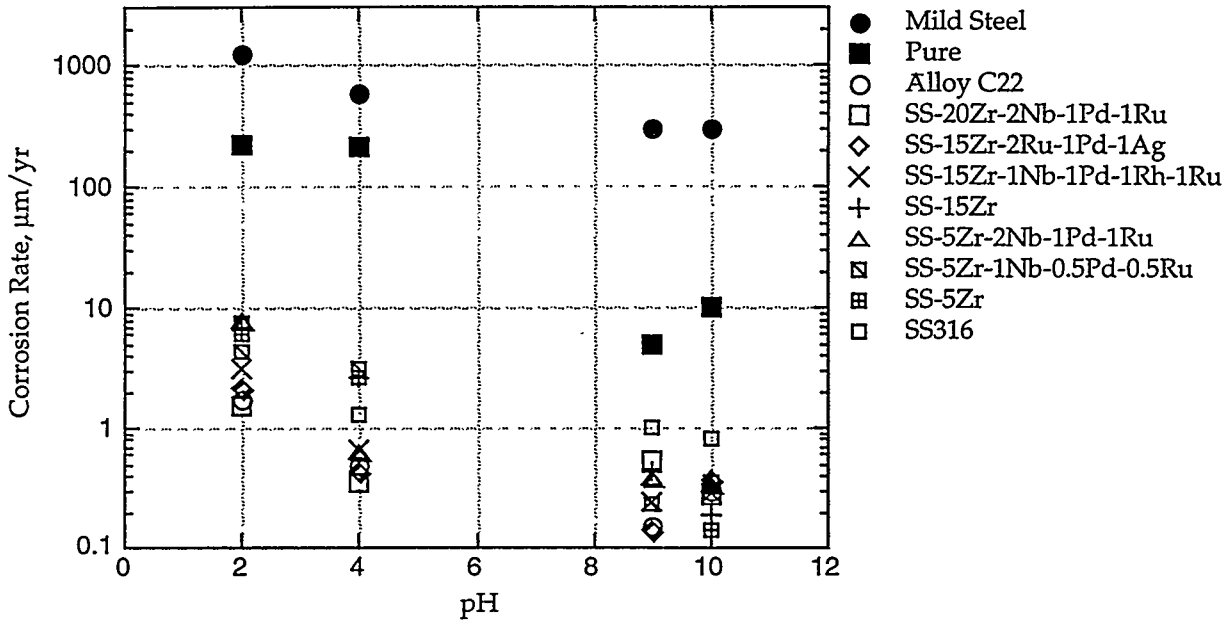

Fig. IV-8. Corrosion Rates for Candidate Metal Waste Forms and Other Alloys

solution representative of the well water at Yucca Mountain) at 90°C were conducted on waste form alloys. Minimal surface corrosion was observed on the specimens after 90 days; most samples retained their as-polished surfaces. Negligible quantities of alloy constituents were present in solution, indicating that the waste form alloys are very resistant to corrosion under the test conditions. The waste form alloys showed excellent retention of fission product elements even in immersion tests designed to accelerate alloy corrosion (200°C, 28 days, deionized water).

The corrosion behavior of the waste form alloys in steam was studied by the vapor hydration test. Monolithic specimens were suspended in a sealed stainless steel vessel containing a small quantity of deionized water and heating to 200°C; the water was vaporized and created a saturated steam environment. After 182 days, oxide layers formed on the waste form alloys, averaging ~1 µm in thickness. In contrast, pure iron specimens showed a 10-60 µm oxide layer after only 7 days. Some borosilicate glasses and ceramic-based waste forms show alteration layers that are up to 300-µm thick after 56 days. The relatively small oxide layers that form on SS-Zr alloys demonstrate the excellent durability of these waste forms. These protective oxide layers apparently impede oxygen diffusion and retard further oxide growth (passivation behavior). Efforts are underway to characterize the oxide layers and determine the corrosion mechanisms for the waste alloys.

2. *Development of Crucible Materials*

The electrometallurgical treatment of spent nuclear fuel involves two key steps that require the melt consolidation of reactive metals. First, the uranium metal product from the electrorefiner is consolidated at 1200°C in a cathode processor. Second, the metal wastes (i.e., stainless steel cladding, zirconium, and fission product metals) are melted at 1600°C in a waste-form casting furnace to create the SS-Zr alloy. In both steps, the process metals are initially

coated with remnant LiCl-KCl-UCl_3 salt from the electrorefiner, which contains 2 to 5 wt% uranium.

Our mission for this portion of the project is to develop crucibles that have high-temperature chemical resistance to the molten metals and salts and may be used more than once without handling. The existing crucibles employ graphite with a loose ZrO_2 "wash" coating for uranium melting and dense Y_2O_3 crucibles for the SS-15Zr alloy. Both of these crucibles are single use. The ZrO_2 wash coating must be re-applied after each uranium melt, and the Y_2O_3 crucibles consistently fracture into multiple pieces as the SS-15Zr alloy cools.

There are two aspects to our approach. First, fundamental thermodynamic studies and small-scale screening experiments are used to evaluate a wide range of stable ceramic materials. Second, materials with demonstrated potential are refined and tested through high-temperature interaction experiments and fabricated into prototype test crucibles. Integrated Thermal Sciences, Inc. (ITS) was contracted to carry out some interaction experiments and prototype fabrication.

We evaluated the resistance of numerous ceramic materials to molten metals at high temperature. Small metal samples of Zr, SS-15Zr, Zr-8SS, and U were placed on flat ceramic substrates and heated in vacuum to temperatures up to ~2100°C. The first set of test substrate materials included approximately 20 stable oxide, carbide, nitride, boride, and surface-protected metals. The data from these screening experiments led us to eliminate many materials from consideration, including the carbides, borides, and surface-protected metals, as well as some of the oxides and nitrides. A number of mixed oxide and nitride ceramics were selected for further study.

Oxide ceramics such as CaO and HfO_2 mixed separately with ZrO_2 or rare earth oxides, as well as CaO mixed with HfO_2, were evaluated in a second set of interaction experiments. Solid-solution, single-phase material of HfO_2-15 wt% Y_2O_3 was found to be the most resistant to molten zirconium alloys and uranium. Sessile drop experiments with this material showed liquid metal-ceramic contact angles of nearly 180°, or nearly complete non-wetting. In addition, a specialty nitride ceramic crucible with a composition proprietary to ITS has been developed.

In addition to the metal interaction studies, we conducted salt interaction experiments using differential scanning calorimetry (DSC). These salt interaction experiments were used to evaluate the resistance of the oxide and nitride crucible materials to the LiCl-KCl-UCl_3 salt. Thermodynamic calculations had indicated that UCl_3 is the most likely to react with the crucible materials. In these experiments, small mixtures of salt and ceramic powder in sealed pans were heated to 550°C over four thermal cycles to monitor changes in the salt behavior and the enthalpy of salt-ceramic reactions. In distillation experiments, small test crucibles with salt were heated to 1200°C for ~1 h under a rough vacuum to distill the salt away (simulating the cathode processor). In sum, the salt interaction test results demonstrated that both the HfO_2-15 wt% Y_2O_3 and the nitride crucible materials are very resistant to interactions with the LiCl-KCl-UCl_3 salt. These materials should, therefore, be resistant to salt interactions during the distillation. Confirmation tests at ~1200°C are scheduled to demonstrate this resistance.

Both small-scale (5-cm dia by 10-cm height) and large-scale (10-cm dia by 15-cm height) prototype crucibles were fabricated by ITS for demonstration testing. All nitride crucibles were fabricated as coatings on a refractory metal base, whereas the oxide crucibles were fabricated as slip-cast, monolithic materials. A single small-scale nitride crucible was used for a salt distillation test and for four melts of ~40 g uranium metal at temperatures up to 1500°C; the crucible was darkened, but it remained usable for further testing. Two large-scale nitride crucibles were tested in three melts and pours of SS-15Zr; the crucibles failed due to fabrication flaws. Small and large-scale HfO_2-15 wt% Y_2O_3 crucibles were used to successfully melt zirconium alloys, but they were too fragile to be used as monolithic ceramics. Fabrication methods are being improved, and all new oxide crucibles are being fabricated as coatings on refractory metals. In summary, the nitride material looks most promising for uranium melting, while HfO_2-15 wt% Y_2O_3 looks most promising for SS-15Zr melting, but use of the nitride for SS-15Zr or HfO_2-15 wt% Y_2O_3 for uranium may also prove acceptable. Future work will focus on improving crucible fabrication methods to enable production of full-scale crucibles (up to ~40-cm dia), performing melting experiments to demonstrate the crucible durability and chemical resistance, and conducting analytical experiments to quantify the structure and composition of the ceramic coating.

3. *Development of Ceramic Waste Form*

Several activities were undertaken in our efforts to develop the ceramic waste form: improvements of the current fabrication process, support of process demonstration and waste form qualification, advanced characterization, and development of advanced techniques for isolation of radionuclides and fabrication of the ceramic waste form.

a. Support of Demonstration Process

Before this year, most development work had been done with powders whose average particle size was less than 10 μm because pure zeolite A is only available in this form. Granular zeolite A contains proprietary binders, thought to be primarily clays, which make up 5 to 20 wt% of the material. Binders add another component to the waste form and introduce uncertainty into the interpretation of waste form behavior. Fine powders allow for more intimate contact between the zeolite and salt during blending, but granular materials flow much more readily than powders, making them more suitable for remote operations and increasing green density for hot isostatic pressing (HIP). We also looked for changes in the leach resistance and physical integrity of the waste form composite caused by the binder. Initial results with granules up to ~840 μm were quite promising. Further characterization of the behavior of these materials is being undertaken with waste form samples produced by HIP of several combinations of granulated zeolites and Pemco P-5D95-PS glass frit with particle sizes from 60 to 325 mesh (250 to 45 μm). These waste forms are being leach tested.

The amount of glass needed as a binder is a key property of the ceramic waste form. Too little glass results in a waste form which will not perform well; too much glass increases its mass and volume unnecessarily. A series of waste forms was prepared using UOP-7 zeolite mixed with a simulated waste salt to a total loading of 3.8 chlorides per unit cell. The salt

had the elemental composition expected after processing 300 driver fuel subassemblies. The blended zeolite was mixed with Glass 57 to an overall proportion of 25 wt% glass. The resultant mixture was converted to a ceramic waste form using our standard HIP profile of a one hour soak at 900°C and 170 MPa. Thirty waste forms were produced at glass loadings of 0-40 wt% in 5 wt% increments. Cesium loss during a standard leach test (MCC-1) of 3 days was used as a measure of performance; it increased significantly at and below 20 wt% glass, as shown in Fig. IV-9. Because of the need for some margin of error during normal processing, a glass content of 25 wt% was adopted.

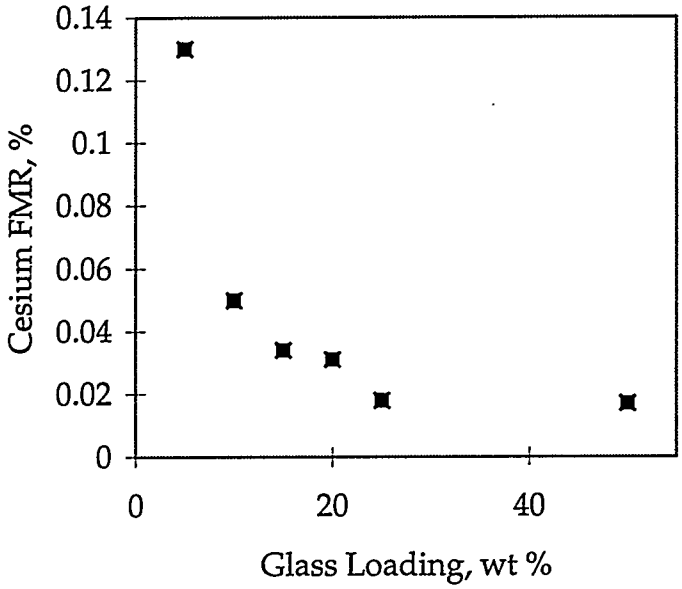

Fig. IV-9.

Cesium Fractional Mass Release (FMR) vs. Glass Content in Ceramic Waste Form

b. Support of Waste Form Qualification

Three kinds of specimens were provided to support the waste form qualification at CMT. Fifty specimens of our reference sodalite-glass composites were fabricated using the standard HIP method. Two additional specimens containing uranium were also prepared by the HIP method. Finally, 30 plutonium-bearing samples were fabricated with a hot uniaxial press (HUP) because our HIP laboratory is not approved for plutonium work, but the HUP can be used in our plutonium glovebox.

c. Advanced Characterization of the Ceramic Waste Form

To investigate the effects of storage of the reference ceramic waste form at elevated temperatures, we made a set of samples to our reference specification and held them at 600°C in air for three months. (Another set is being similarly exposed; they will be removed after one year.) After the test period, the waste forms were characterized by leach testing and density and porosity measurements. Optical analyses included X-ray diffraction (XRD), scanning electron microscopy (SEM), and electron dispersive spectroscopy (EDS). Examination of the three-month samples indicated that the extended heat soaking/storage affected the waste forms in

two relatively minor ways. First, chloride ion loss during MCC-1 leach testing over 3 days was found to be higher than reference specimens without heat soaking. This difference was not as apparent in a 28-day MCC-1 test. Second, SEM/EDS results indicated an increased number of salt rings/pores and NaCl crystals on the surface of the heat-soaked samples. These differences aside, porosity, loss of ions other than chloride in the leach tests, and overall integrity were identical to reference samples that had not been heat-soaked. A one-year test is in progress to increase our understanding of storage effects and provide a longer term baseline for assessing waste form performance.

In the direct disposal of process salt, up to 2 mol % of $PuCl_3$ or UCl_3 will appear in the multi-component waste salt. This salt will be blended with "anhydrous" zeolite (which contains water in amounts up to 1 wt%) at 500°C. Thermodynamic equilibrium calculations indicated that both zeolite and water should react with UCl_3 in a spontaneous exothermic reaction leading to UO_2. The situation with $PuCl_3$ is less clear.

Experiments were conducted to evaluate the interactions of plutonium and its aluminosilicate host. Analysis is not complete, but results to date show that plutonium does not interact destructively with the zeolite lattice. In these experiments, varying amounts of $PuCl_3$ were blended with zeolite 4A and the water content of the zeolite held constant. When less $PuCl_3$ was used than would have been stoichiometrically required to react with the water, PuO_2 formed. A substantial excess of $PuCl_3$ (over water) formed plutonium oxychloride. In neither case was any zeolite decomposition product detected. Since the zeolite is always expected to contain more water than required to react with Pu and U, PuO_2 is the expected species in the ceramic waste form.

In MCC-1 leach testing of 3 and 28 days, sodalite-glass composite waste forms loaded with plutonium performed as well as the reference composites. The plutonium concentration in the leachate was lower than that of the other leachable components by an order of magnitude. The plutonium-bearing samples are at least comparable to other nonradioactive samples produced to date; we believe that the ceramic waste form will retain plutonium very well.

Differential scanning calorimetry was used to follow the thermal processes in powdered mixtures of uranium-bearing salt and zeolite. Samples, typically weighing 10 mg, were contained in covered graphite crucibles in a differential scanning calorimeter. The salt, $(K,Li)_3U_5Cl_{18}$, containing 52 wt% uranium, made up 10, 20, or 30 wt% of the sample in the several tests. The zeolite 4A powder contained 0.12-0.13 wt% H_2O. Scans comprised a 1-min initial isotherm at 25°C, temperature increase at 20°C/min, and a 10-min final isotherm at 725°C. The salt was found to melt congruently at 412°C. The overall process taking place in the zeolite-salt mixture was exothermic between 25°C and about 425°C. The process then became endothermic between about 425°C and 725°C. A sharp feature observed at 21 min coincided with the salt melting point at 412°C. The endothermic part of this feature was associated with the salt melting, while the exothermic part was probably due to the salt absorption into the zeolite matrix.

Supplemental information on phase composition was obtained by powder XRD of uranium-bearing salt and zeolite. Samples were heated to temperatures between 25 and 725°C at 20°C/min in the differential scanning calorimeter, then quenched *in situ* at 320°C/min, placed in a specially designed hermetic holder, and analyzed. In a typical sequence of XRD patterns from samples quenched from 200, 375, 550, and 725°C, little change was seen between 25 and 200°C. The first signs of UO_2 appeared at 375°C, along with a slight decrease of the $(K,Li)_3U_5Cl_{18}$ peak intensities. The diffraction peaks of UO_2 increased in intensity at 550 and 725°C, while those of $(K,Li)_3U_5Cl_{18}$ disappeared completely. The intensities of the diffraction peaks associated with zeolite 4A were not affected at any temperature. Their position at 725°C was shifted toward higher values compared to their original position at 25°C. This is consistent with the expansion of the zeolite structure upon salt absorption. Powder diffraction patterns of zeolite 4A mixtures containing 20 and 30 wt% $(K,Li)_3U_5Cl_{18}$ exhibited these same features, but also showed a marked decrease in zeolite 4A peak intensities when heated to 725°C.

Application of a novel technique, simultaneous DSC/synchrotron XRD at a beamline of the Advanced Photon Source, led to significant new results. A complete diffraction pattern was obtained every 10°C while powdered mixtures of zeolite 4A and 30 wt% $(K,Li)_3U_5Cl_{18}$ were heated in a special sample holder at 10°C/min from 25 to 600°C. The results confirmed that $(K,Li)_3U_5Cl_{18}$ reacts with zeolite 4A and forms UO_2. The reaction onset temperature was pinpointed at 350°C, and we were able to identify two previously unseen intermediates: USi_2 and $(K,Li)_2UCl_5$. Correlation of the scanning calorimetry, powder X-ray diffraction, and synchrotron data indicated that the endothermic process observed in the mixtures of zeolite 4A + $(K,Li)_3U_5Cl_{18}$ is a reaction of UCl_3 with H_2O and zeolite 4A, leading to the formation of UO_2. It appears to start as a solid-state process at 347°C, i.e., 65°C below the salt melting point, and to continue after the salt melting and absorption by the zeolite matrix. The reaction is complete at 725°C. The absence of a large salt-melting endotherm is explained by the reduced amount of solid salt present when the temperature reaches the melting point (412°C), and, probably more importantly, by the simultaneous exothermic absorption of the liquid salt into the zeolite matrix. The processes taking place in the zeolite 4A + $(K,Li)_3U_5Cl_{18}$ mixture upon heating can be summarized as follows:

$$\frac{8}{7}(K,Li)_3U_5Cl_{18} \leftrightarrow \frac{12}{7}(K,Li)_2UCl_5 + 4UCl_3 \quad (1)$$

$$4\,UCl_3 + 8\,H_2O \leftrightarrow 4\,UO_2 + 12\,HCl + 2\,H_2 \quad (2)$$

$$4\,UCl_3 + 12\,NaAlSiO_4 \leftrightarrow \frac{11}{3}\,UO_2 + \frac{1}{3}\,USi_2 + \frac{34}{3}\,SiO_2 + 12\,NaCl + 6\,Al_2O_3 \quad (3)$$

Reaction of UCl_3 with water (Eq. 2) seems to be kinetically favored compared with the reaction of UCl_3 with zeolite 4A (Eq. 3) so that, at normal uranium and water levels, essentially no zeolite 4A attack occurs. Equation 2 might become more important during column operation, where the uranium-to-water ratio is higher.

The leach resistance of glass-bonded zeolite samples loaded with uranium was evaluated in 3- and 28-day MCC-1 tests. The presence of uranium in these waste forms did not have a detrimental effect on their leach behavior compared with non-uranium waste forms. There was no observable difference between the rates of release of those cations that were present in both types of waste forms, for example, Al^{3+}, Si^{4+}, Cs^{+}, and Sr^{2+}. Uranium release rates were comparable to those of Nd and Ce from both types of waste forms.

d. Radionuclide Concentration in Zeolite

Batch ion-exchange experiments suggested that a zeolite bed that has been preloaded with LiCl-KCl will remove the waste radionuclides from electrometallurgical process salt that has reached its maximum allowable concentration of transuranic and fission-product radionuclides. This will allow the zeolite to be reused in the treatment of additional fuel, rather than discarded. The overall waste volume should thus be substantially reduced compared with direct disposal of the process salt.

Partition of cations between salt and zeolite was determined by batch equilibration at 500°C in a simple stirred salt bath. Five salt compositions were examined. One composition was representative of the fission product concentration that would result from processing a modest amount of EBR-II fuel; a second composition, used to study concentration effects on partition, contained only one-tenth that amount of fission products; and three compositions contained only Li, K, and one other fission product cation (Cs, Sr, or La). After equilibration, zeolite and salt were separated, and excess salt was washed from the zeolite. Both zeolite and salt were analyzed, then exchange factors were calculated according to

$$nX_nCl(s) + mY_m(z) \leftrightarrow mYCl(s) + nX_n(z) \tag{4}$$

$$\text{Exchange Factor} = \left(\frac{x_z}{x_s}\right)^n \left(\frac{y_s}{y_z}\right)^m \tag{5}$$

where x_i and y_i are the mole fractions of ions X and Y in the zeolite (z) or salt (s). We determined ion exchange as a function of immersion time to obtain information on the kinetics of the process and on the equilibrium compositions. After immersion for 24 hours, the salt and zeolite compositions approached equilibrium. The values of the exchange factors are summarized in Table IV-2. These values are being employed in developing a computer model of the behavior of an ion exchange column. The finding that the exchange factors for all the cations of interest are generally larger than those of Li and K suggests that a column preloaded with Li and K should efficiently remove the cations from the waste salt.

After ion exchange with the waste salt, XRD showed that the zeolite crystal structure undergoes some reduction in crystal symmetry. This gives rise to new peaks in the diffraction patterns, which are consistent with a face-centered cubic structure. These new features were observed after exchange with Sr and Ce, but not Cs. This suggests that Sr and Ce

Table IV-2. Exchange Factors between Salt and Zeolite for Five Salt Compositions

	Normal	Dilute	Cs Only	Sr Only	La Only
Li	1.33	2.17	2.28	2.96	1.47
K	1.00	1.00	1.00	1.00	1.00
Na	1.01	1.70	-	-	-
Cs	5.94	9.50	3.2	-	-
Sr	0.83	3.67	-	4.0	-
Ba	1.04	11.1	-	-	-
Y	1.98	2.05	-	-	-
La	5.34	6.50	-	-	2.8
Ce	4.54	5.99	-	-	-
Pr	3.75	5.67	-	-	-
Nd	3.67	5.60	-	-	-

reside at similar sites within the crystal lattice. This is also consistent with the competitive exchange between the alkaline earth and rare earth elements observed in the immersion tests with the simulated process salts.

We are attempting to identify the factors that will allow us to remove waste radionuclides from the electrometallurgical treatment process salt as effectively as batch equilibrium experiments indicate to be possible. To this end, we are running tests with a laboratory-scale ion exchange column (30-cm long) at temperatures of 500-600°C and flow rates of 3.4-60 g/min. Tests to date indicate that the column is very effective in removing rare earth elements but is much less effective for Cs, Ba, and Sr. We found that breakthrough of the rare earths occurs after passing approximately five bed volumes of process salt. (We define "breakthrough" as that point when concentration of any waste ion reaches 20% of its influent concentration.) The least strongly sorbed radionuclides break through shortly after the salt originally present in the column from preloading is displaced, even at the lowest flow rates tested so far. Approximately one bed volume of salt is treated before Cs, Ba, and Sr breakthrough, far less than would be anticipated. Even at one bed volume of salt treated per column, however, there is some reduction in waste form volume compared with direct disposal of the process salt.

In plots of the effluent concentration versus the salt volume treated, the breakthrough curves are broad, indicative of significant axial dispersion. At very low flow rates as is the case here, diffusion of the cations within the salt phase might become significant, although scoping calculations indicate that it should not be a problem. Other factors such as channeling and slow exchange kinetics contribute strongly to effluent concentration. We see some differences in the location of the breakthrough in the effluent curves as the test temperature and the salt flow rate are varied, consistent with these factors.

In batch ion exchange tests with the laboratory-scale column, the kinetics of exchange for the rare earths was found to be slower than that observed for Cs and Sr. This should result in more rapid breakthrough for the rare earths when sorption rates are low compared with the salt flow rate. In fact, just the reverse is the case, as would be expected from the exchange equilibria. The column has done a good job of removing rare earths from the salt. This observation suggests that the rare earths may not be incorporated into the zeolite by a simple ion exchange, but they may be reacting with some component of the zeolite beads, such as the binder or zeolithic water, to form oxides or oxychlorides.

For some fuels, such as N-Reactor fuel, transuranics are the only species that actually need to be removed from the salt for operational reasons. The effectiveness of the column for rare earth sorption suggests that the column would also be effective in removing transuranics from the salt. We are currently measuring the partition of plutonium relative to other salt constituents.

e. Development of an Advanced Fabrication Method

We are developing a manufacturing method ("pressureless" consolidation) that simplifies fabrication, increases throughput, and decreases the space and handling requirements for the ceramic waste form. This method uses the same zeolite-glass mixture that is employed in the HIP fabrication. However, the zeolite-glass mixture does not have to be put through a complex set of operations to load, densify, evacuate, and weld a few cans for a lengthy batch cycle in HIP. Rather, the powders are poured into a train of reusable setters that are passed through a tunnel furnace. Consolidation occurs in the furnace near 850°C when the glass phase becomes a viscous liquid; the setters are simply inverted at the end of the furnace for reuse, and the finished waste forms then recovered.

Our initial work used fine-grained glass and zeolite with average particle sizes of less than 20 μm. Although fine powders have excellent kinetics of consolidation, their inherently poor flow characteristics pose a problem for remote handling. Initial studies indicated that particle size distributions ranging from 44 to 125 μm for both the glass and the zeolite are best suited for densification using pressureless consolidation.

Scaleup of the pressureless consolidation process for ceramic waste forms was successfully demonstrated by the production of six 100-g and two 840-g samples of ceramic waste form. As shown in Fig. IV-10, the corrosion resistance of the waste forms produced by pressureless consolidation is generally comparable to that of HIP-fabricated waste forms of the same composition.

We continue to refine our understanding of fundamental scaleup issues, to develop larger scale prototypes fabricated by pressureless consolidation, and to identify preferred production equipment. The results of both empirical and basic investigations will be incorporated in an analytical model that will be used as an aid to scaleup and process optimization.

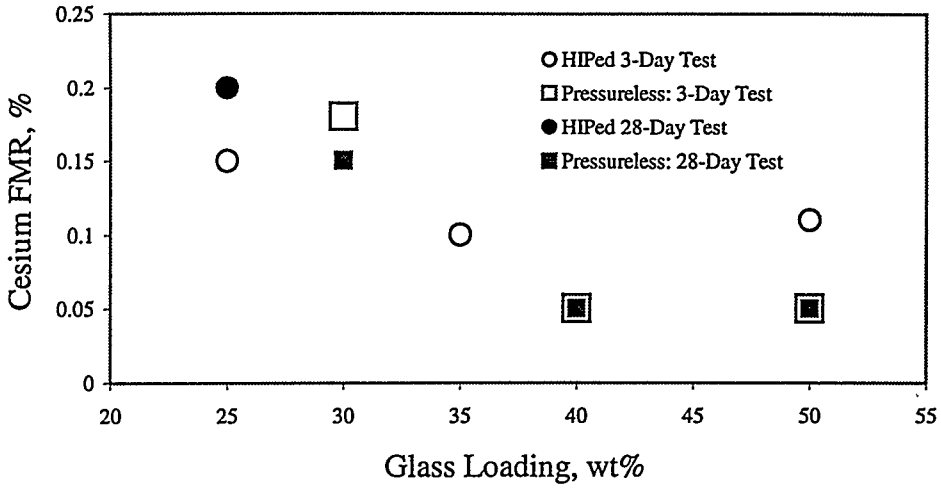

Fig. IV-10. Fractional Mass Release (FMR) of Cesium from HIP and Pressureless Consolidated Waste Forms

V

Pyrochemical Process Applications

The U.S. Department of Energy inventory of spent nuclear fuel consists of ~2700 metric tons of heavy metal and over 100 fuel types. Concerns about the enrichment, chemical stability, and physical condition of many of these fuel types complicate the task of preparing and qualifying them for repository disposal. The electrometallurgical treatment technique (see Sec. IV) can convert many of these spent fuel types into a uniform set of well-characterized, stable product streams, and this would greatly simplify the process of preparing and qualifying these fuels for storage or disposal.

The chemical composition of the fuel matrix and cladding determines whether a particular fuel can be directly treated using the electrometallurgical process, or if a pretreatment step is required. For example, oxide fuel types require a pretreatment step that will reduce the actinide oxides to the metallic form prior to electrorefining. The CMT Division has been developing a pretreatment process that uses lithium at 650°C in the presence of molten LiCl to reduce the actinide oxides to the corresponding metals and Li_2O. The Li_2O, which is soluble in LiCl, is then electrolytically decomposed at 650°C in a salt-recovery step. The resulting salt, which is low in Li_2O concentration, and the lithium metal are recycled for subsequent fuel reductions.

During the past year, work continued on developing both the reduction and salt-recovery portions of the lithium reduction process, with an emphasis on process scaleup. Corrosion tests were also conducted to identify candidate construction materials for a pilot-scale oxide reduction facility planned at ANL-West.

A. Development of Lithium Reduction Process

During the past year, laboratory-scale experiments were performed to identify and quantify the key parameters controlling the reduction rate. The results of these experiments were then used to specify the design and operating conditions for engineering-scale reduction

experiments (Sec. V.B). In addition, experiments were conducted to test prototypes of equipment designed for the engineering-scale experiments.

1. Reduction Step

In the lithium reduction process, the actinide oxides are reduced by lithium dissolved in LiCl. As lithium is consumed during the reduction, it must be continually replaced in the reduction salt. This is accomplished by keeping the reduction salt in contact with molten lithium. Ideally, the reduction system is designed such that the salt is kept saturated in lithium at all times. It was postulated that the area of contact between the reduction salt and molten lithium is an important factor in achieving this saturation.

Lithium is supplied to the reduction salt in the form of porous metal disks saturated with molten lithium. A series of experiments was performed to investigate the effect that changing the surface area of these disks had on the reduction rate. To allow this information to be used in scaling up the process, the key variable was the projected surface area of the lithium-saturated, porous metal disks divided by the total volume of the reduction salt (S/V). Figure V-1 presents the results of experiments with S/V ratios of 0.05 and 0.1 cm^{-1}. The fuel loading and fuel basket design were the same in the two experiments. Reductions were carried out with 200 g of crushed UO_2 contained in a 325-mesh stainless steel screen pouch.

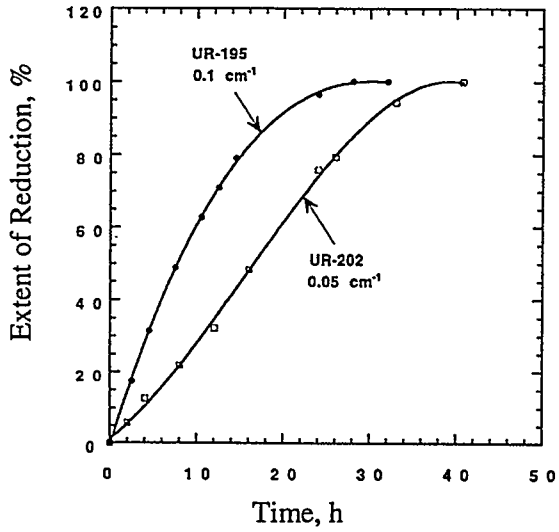

Fig. V-1.

Effect of Ratio of Lithium Source Surface Area to Salt Volume on the Reduction Kinetics

As seen in Fig. V-1, the reduction was complete in about 28 h for the higher ratio, while it took about 40 h for the lower ratio. Also, the reduction rate was found to be directly proportional to the S/V ratio, at least in this range. Ratios greater than 0.1 cm^{-1} were not tested as it would not be feasible to duplicate them in the engineering-scale facility.

During experiments testing a fuel basket prototype, it was discovered that the Li_2O concentration in the reduction salt also had an effect on the reduction kinetics. Figure V-2 shows the results of UO_2 reductions performed over three Li_2O concentration ranges. These experiments

were performed under identical conditions with an S/V ratio of 0.05 cm^{-1}. It only took about 20 h for complete reduction in the 0 to 0.9 wt% Li_2O concentration range, while it took about 28 and 40 h for the other two experiments with higher Li_2O concentrations in the salt. Thus, the Li_2O loading of the salt does have a significant impact on the reduction kinetics, but it is not yet clear why this is so. Future experiments will address this issue.

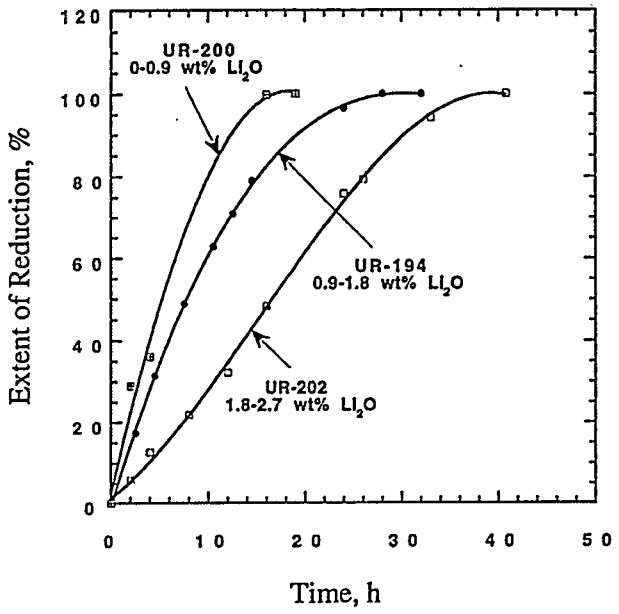

Fig. V-2.

Effect of Li_2O Concentration of Reduction Salt on Reduction Kinetics

2. *Salt-Recovery Step*

Work on the salt-recovery step focused on preparations for an engineering-scale test, ES-8 (see Sec. V.B.4), and preliminary experiments to determine if SnO_2 could be used to replace the costly platinum now used as the anode material. Laboratory-scale and intermediate-scale electrochemical cells were constructed to study these issues. The laboratory-scale cell (0.5 L volume) has a porous stainless steel cathode to collect liquid lithium, an anode made of the material under study, and a liquid-lithium reference electrode. Provision was made for continuously measuring the oxygen concentration of the gas evolved at the anode compartment. The intermediate-scale cell (2 L volume) incorporated all the design features of the engineering-scale cell. It used a stainless steel crucible, a platinum anode, and a porous stainless steel cathode.

Experiments in preparation for ES-8 were designed to determine the safe operating conditions and procedures for electrowinning lithium in a Li-LiCl-Li_2O system using a platinum anode. Three considerations guided the design of the experiments: (1) the cell must operate at a high enough current density and efficiency to produce lithium at a useful rate, (2) the cell must be designed and operated to avoid attack of the platinum anode by metallic lithium, and (3) the cell must be operated to avoid decomposition of the electrolyte, because the platinum anode is subject to rapid attack by chlorine. These considerations were addressed by careful design of the cathode and selection of the operating procedures.

A number of intermediate-scale cells were tested to model the operation of the engineering-scale cell and to test the planned operating procedures. These cells were approximately one-half to one-third the linear dimensions of engineering-scale cells. The platinum anode was about one-fourth the diameter of the engineering-scale anode. The cells ran reliably at applied potentials in the range of 3.5-3.8 V, with anode current densities on the order of 2-3 A/cm^2 and current efficiencies of 70-90%.

Experiments were also performed to evaluate SnO_2 as a replacement anode for platinum. Potential replacement materials for the anode (magnetite, nickel oxide, and tin oxide) had been previously identified.[1] Preliminary tests of specific properties indicated that all these materials should be adequate, but none was fully demonstrated. Of these materials, SnO_2 was chosen for detailed testing because it is readily available commercially. (Stannex® electrodes are a family of tin oxide electrodes made for the glass industry.) The present experiments were directed to investigate the possible side reactions on the SnO_2 anode at high cell voltage and identify the conditions required to run the lithium oxide electrolysis safely at high current efficiency.

The key properties for the anode material are chemical stability, catalytic activity, and electronic conductivity. These experiments showed Stannex® to be stable in the cell environment, catalytically active at the cell conditions, and a relatively good electronic conductor. It is significantly less conductive than metals, however, and this property must be considered in cell design and operation. Lithium has been produced in the laboratory-scale cells with both SnO_2 and Stannex®. The standard-grade Stannex® anode exhibited no visible attack after a test in which the lithia content of a cell was reduced from about 2 to 1 wt% at a current efficiency of 70-80%. Future testing includes building an intermediate-scale electrowinning cell with the Stannex® anode and improving the method used to connect the anode to the current lead.

3. Electrorefining Step

One of the principal design goals for the lithium reduction process is that the number and duration of its component steps be kept to a minimum. In keeping with this goal, the present system design has no intermediate steps between the reduction and electrorefining; the fuel will be transferred to the electrorefiner directly after the reduction.

In the past year, experiments were conducted to determine if the morphology of the reduced fuel (crushed or clad pellet) has any effect on the electrorefining step. For these experiments, a laboratory-scale electrorefining cell was constructed with an outer stainless steel crucible, a stainless steel rod as cathode, and a fuel basket as anode. Ceramic sleeves around the anode and cathode ensured that they were electrically isolated from each other as well as the rest of the cell. A catch basket was also provided at the bottom of the cell to recover any uranium dendrites that may break away from the cathode deposit.

---

[1] J. J. Laidler et al., *Chemical Technology Division Annual Technical Report, 1997,* Argonne National Laboratory Report ANL-98/13, p. 127 (1998).

Two significant electrorefining experiments were performed this past year. In the first, crushed UO_2 was reduced and then transferred directly to the electrorefining cell. The second experiment was essentially the same, except clad UO_2 pellets were used. In the electrorefining of the reduced UO_2, only uranium metal was transported to the cathode. Unreduced UO_2 and cladding hulls (in the case of reduced clad fuel pellets) remained in the anode basket. Most of the reduced product was recovered as uranium dendrites on the cathode. Figure V-3 shows the uranium dendrites and empty cladding hulls recovered from the electrorefining of the reduced pellets. The electrorefining experiments confirmed that reduced product, in crushed or clad pellet form, can be easily electrorefined. The test results also validated the analytical techniques used to determine when the reduction was complete. Future work includes an engineering-scale electrorefining test that uses the product from a future reduction experiment.

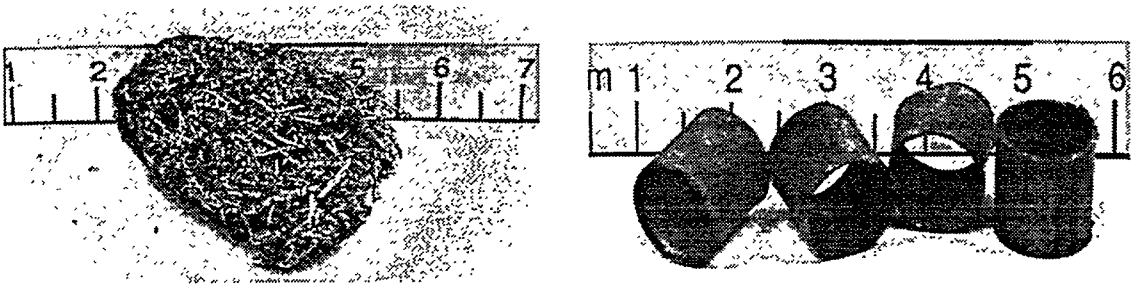

Fig. V-3. Uranium Dendrites (left) and Cladding Hulls (right) Recovered from Electrorefining of Reduced Clad Fuel Pellets

B. Engineering-Scale Experiments

The purpose of the engineering-scale experiments is to obtain design information and operating experience needed for scaling up the reduction and electrowinning processes to equipment sizes required for processing DOE spent oxide fuels at ANL-West and elsewhere. To meet this objective, the facility used for these experiments was designed to support the reduction of kilogram quantities of fuel. The engineering-scale facility consists of three major components: the reduction vessel, the electrochemical vessel, and the casting station. The reduction vessel holds the salt, fuel, and lithium during the reduction step; the electrochemical vessel holds the molten salt during the salt-recovery step; and the casting station provides a means to cast the regenerated salt into ingots for storage between process steps. During the past year, four engineering-scale experiments with kilogram quantities of UO_2 have been completed: three reduction experiments (ES-5, -6, and -9) and a scaleup test (ES-8) of the salt-recovery process.

1. Reduction Test ES-5

The results of two engineering-scale experiments completed in earlier years indicated that the engineering-scale experiments had much lower reduction rates than obtained in laboratory-

scale experiments.[2] This was thought to result from differences in the method used to introduce lithium into the reduction salt between the two experimental conditions. Potentially, the most significant of these differences was that the relative surface area of the lithium exposed to the salt in the laboratory-scale experiments was higher than that in the engineering-scale experiments. A contributing factor may have been the design of the engineering-scale fuel baskets. Because these were not as rigid as those in the laboratory-scale tests, they tended to bow outward as the loaded fuel settled during the course of the experiment. This increased their effective thickness and possibly restricted the access of the dissolved lithium to the fuel.

These explanations were tested in an engineering-scale experiment, designated ES-5. The fuel basket design was similar to that used in the previous engineering-scale experiment except that it was made more rigid. The fuel basket consisted of two separate compartments bolted to a single steel plate at the bottom. The compartments were separated by a 1-cm gap to allow free access of salt to all faces of the fuel basket. The compartments were made of a thick-gauge (10 mesh) stainless steel screening with a 325-mesh stainless steel screen lining on the inside. Each basket compartment was 1.5-cm thick, 8.9-cm wide, and 38-cm long. A photograph of the basket is provided in Fig. V-4.

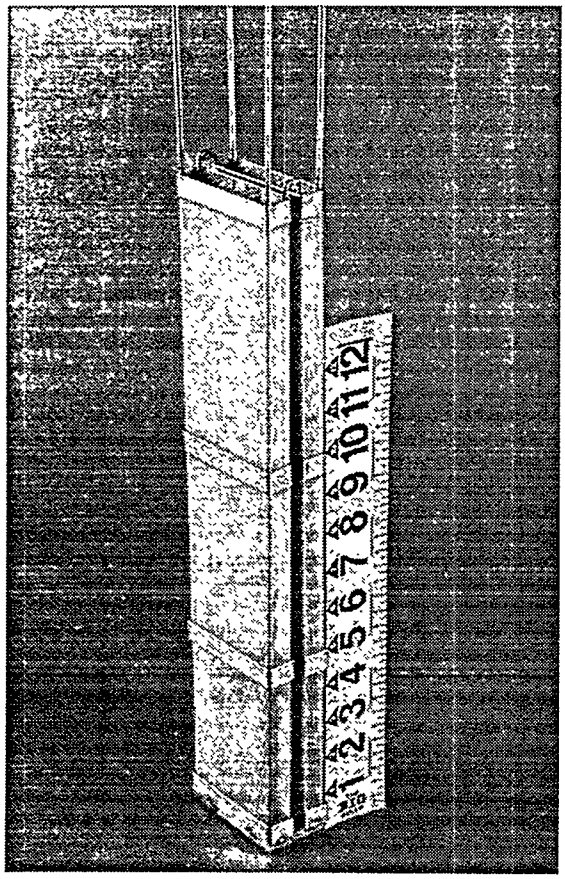

Fig. V-4.

Fuel Basket Used in ES-5 Experiment

[2] J. J. Laidler et al., *Chemical Technology Division Annual Technical Report, 1997,* Argonne National Laboratory Report ANL-98/13, pp. 127-129 (1998).

A new method was developed for introducing lithium into the reduction salt. Prior to experiment ES-5, lithium was supplied to the reduction salt by molten lithium metal floating on the surface of the salt. In the new lithium containment concept, the lithium was held submerged in the salt in a porous stainless steel foam. This arrangement served to protect the lithium from interacting with the glovebox atmosphere and to provide a sufficient lithium-salt contact area for saturation of the salt with lithium (see Sec. V.A.1). The lithium source for ES-5 was designed to provide an S/V ratio of 0.1 cm^{-1}.

The results of ES-5 were very encouraging. The reduction rate, determined from the Li_2O concentration in the salt samples, was found to be similar to that obtained in the laboratory-scale experiments. The reduction was essentially complete in 12-20 h; this is the fastest reduction to date in the engineering-scale system. The product showed no evidence of unreduced UO_2 either by visual examination or by X-ray diffraction. Also, the modifications to the fuel basket eliminated the problems of basket deformation (bowing) observed in previous engineering-scale experiments.

2. Reduction Test ES-6

One of the design criteria for the pilot-scale oxide reduction facility planned for construction at ANL-West is that it be compatible with the Mark-V electrorefiner, which is being used for the electrometallurgical treatment of spent EBR-II fuel (Sec. IV). This requires that the oxide fuel be reduced in the Mark V basket assembly, which is then transferred to the electrorefiner. The Mark V basket is, however, thicker than the fuel basket tested in ES-5 and thus required an independent test. The Mark V basket consists of a perforated-sheet metal shell with a single insert made of 325-mesh stainless steel screening. The insert is about 2.7-cm thick. Figure V-5 shows the outer shell and the insert in a Mark V basket. This basket is different in two aspects from the ES-5 basket: (1) it is about twice as thick and (2) its exterior is made of perforated sheet metal instead of 10-mesh screening. While the basket thickness is likely to affect the reduction kinetics, the second factor may affect the extent of salt access in the basket area.

The reduction rate in ES-6 was significantly lower than that measured in ES-5. The ES-6 reduction was stopped after about 78 h when it was apparent that the Li_2O concentration of the reduction salt would not increase further. However, the estimated extent of reduction, based on Li_2O concentration, was only 80-85%. Visual examination of the product at the end of the experiment showed no evidence of unreduced UO_2. It was not clear from measured titration data when the reduction was complete because of the scatter in the data. The bulk of the reduction appears to have been completed in about 50-60 h.

3. Reduction Test ES-9

The results of ES-6 indicated that the thickness of the insert for the Mark V fuel basket leads to excessively long (>60 h) reduction times. A modification to that insert was devised to improve access of salt to the fuel; in effect, this increased the surface area of the fuel exposed to

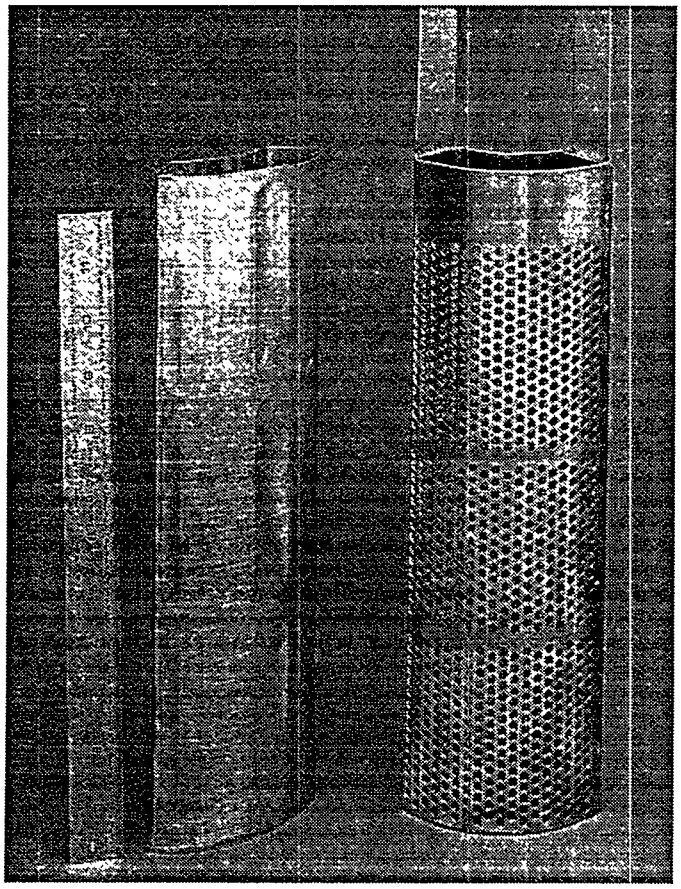

Fig. V-5.

Mark V Outer Basket and Insert Used in Experiment ES-6

the salt. In general, the idea was to combine aspects of the successful ES-5 fuel basket design with the Mark V outer basket. This was done by replacing the single insert in the existing Mark V design by an insert consisting of four pouches with a 0.4-cm separation between the individual pouches. This modified insert is designed such that it fits inside the existing Mark V fuel basket. Figure V-6 shows the Mark V fuel basket and modified insert.

The performance of the modified insert can be compared to that of the existing insert on the basis of throughput. This measure of performance is required because the modification reduced the capacity of the insert from 3.7 to 2.8 kg; thus, any increase in reduction rate has to, at least, offset the loading reduction.

Figure V-7 gives the reduction results of ES-9 along with ES-6. The results of ES-9 indicate that significantly faster reductions were obtained with the modified insert design. The extent of reduction was determined by measuring the Li_2O concentration in the salt, visually examining the product, and conducting X-ray diffraction of the product. By use of the modified insert, the reduction was completed in about 25-30 h, while it took 60-80 h in ES-6. The estimated extent of reduction in ES-9 (90-95%) also appears to be better than that in ES-6 (80-85%). This was attributed to the larger thickness of the Mark V fuel basket insert used in experiment ES-9. The new insert design improved the reduction rate significantly. On the basis of product throughput (kilograms of UO_2 reduced per hour), the modified insert design is estimated to be better by about 60%. Since the Mark V outer basket is unchanged, the new insert

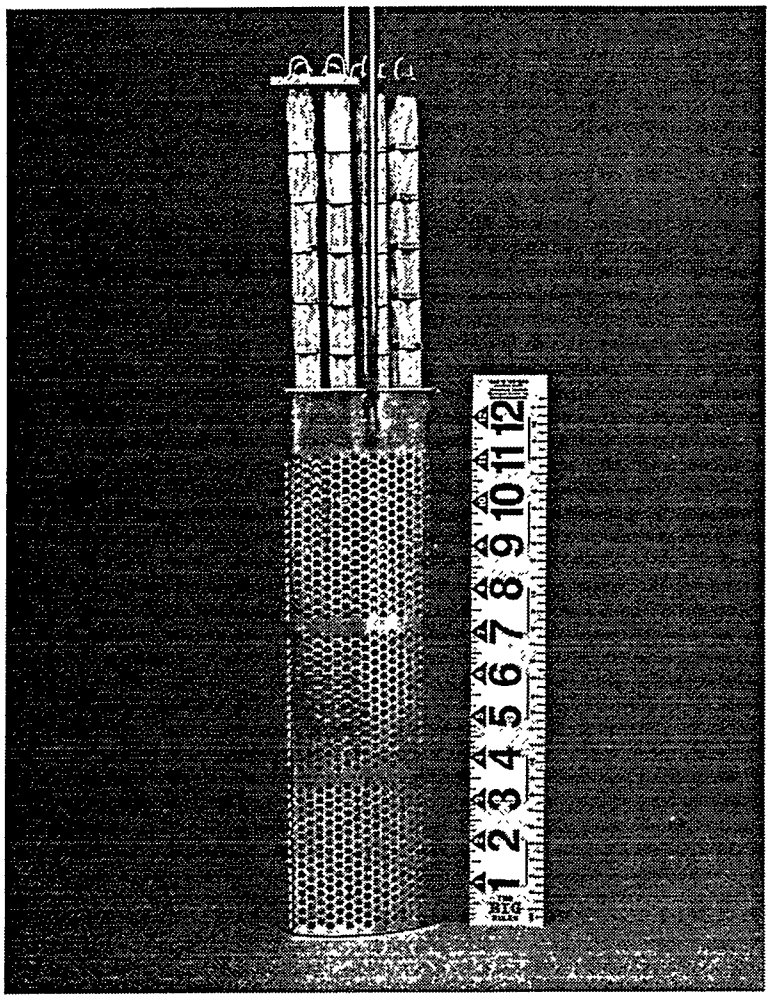

Fig. V-6.

Basket Assembly and Insert with Four Fuel Pouches for Experiment ES-9

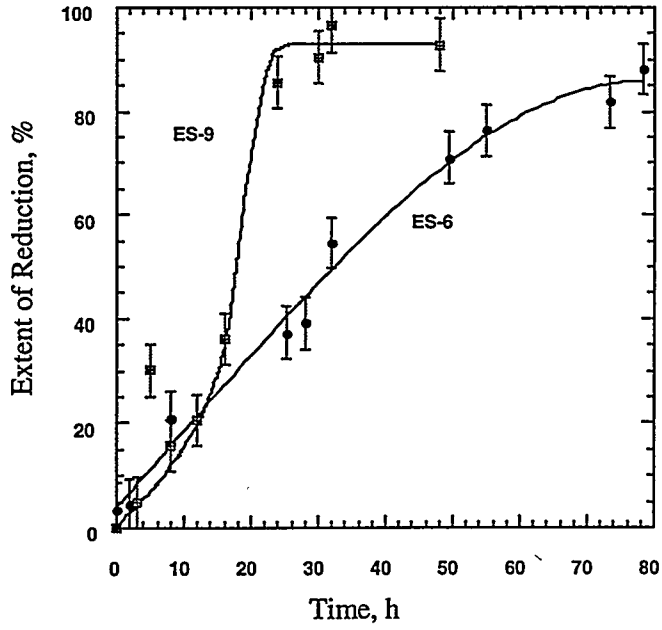

Fig. V-7.

Extent of Reduction as a Function of Time in Experiments ES-6 and ES-9

design is expected to have no impact on the electrorefining process, and thus, it should be possible to use the same basket in the two process steps. Another engineering-scale reduction experiment is planned to test the fuel-basket design concept for holding fine particles (<45 μm) of fuel.

4. Salt-Recovery Test ES-8

The major goals of experiment ES-8 were to demonstrate the salt-recovery step at the engineering scale and test its compatibility with the reduction step. The electrochemical cell used in ES-8 was a scaled-up version of a design repeatedly demonstrated in intermediate laboratory-scale cells (see Sec. V.A.2). A porous metal cathode was used to contain the lithium and keep it below the salt surface to minimize the risk of it recombining with oxygen in the cover gas. To further test compatibility between the reduction and salt-recovery steps, the cathode material was identical to that used as the lithium sources for the engineering-scale reduction experiments ES-5, -6, and -9. The anode was a Pt-Rh plate formed into a cylinder, 5.7 cm in diameter, and was positioned close to the salt surface and away from the cathode such that the oxygen produced had only a short distance to diffuse to reach the cover gas. In addition, the gas space above the salt was continually purged with argon to keep the oxygen concentration in the vessel at a minimum. The cell was operated at a constant voltage of 3.7 V. Figure V-8 provides a cut-away view of the engineering-scale cell.

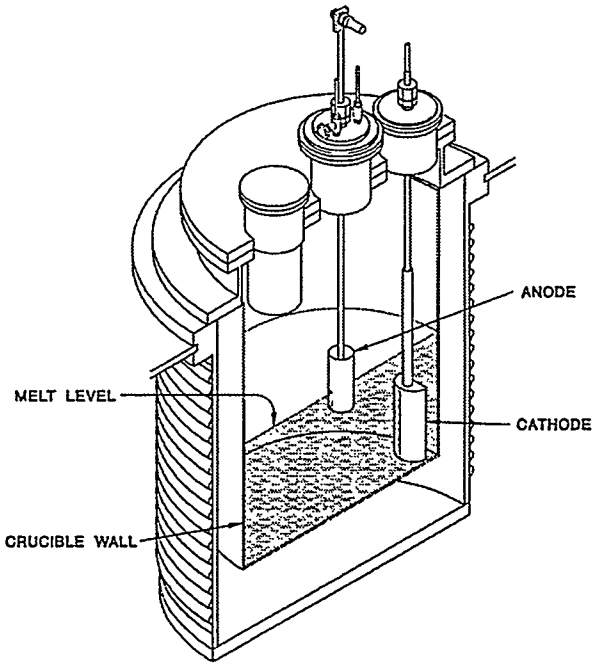

Fig. V-8.

Cross-Sectional Schematic of Engineering-Scale Cell Used in Experiment ES-8

The salt used in ES-8 was that remaining from the previous engineering-scale reduction experiment, ES-6. In ES-6 the starting concentration of Li_2O was 2 wt%, and the final concentration at the end of the reduction was 3 wt%. The goal of ES-8 was to show that this salt could be recovered by reducing the Li_2O concentration back to the starting value of 2 wt%, thus

demonstrating a reduction-electrowinning cycle. As shown in Fig. V-9, the actual Li_2O concentration was driven slightly below 2 wt%, to 1.8 wt%. The total time required for this was approximately 45 h, with approximately 4400 Ah of charge passed.

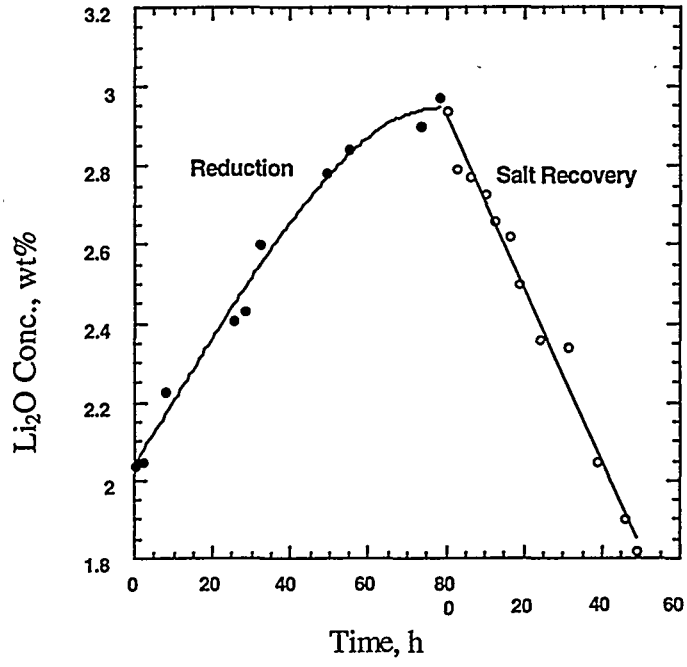

Fig. V-9. Variation of Li_2O Concentration in Bulk Salt as Function of Time for Reduction (ES-6) and Salt-Recovery (ES-8) Experiments. The concentration of Li_2O in the bulk salt is a direct measure of the progress of each of the respective process steps.

On the whole, ES-8 successfully demonstrated that the reduction and electrowinning steps are compatible. The cell ran in a stable and trouble-free manner. The lithium was recovered in a form suitable for use as a lithium source in future reductions. And even though the cell design was not optimized, the time required for the electrowinning was on the same order as the reduction times. Analysis of the ES-8 results indicated some differences between the engineering- and the laboratory-scale cells. Typically, in the laboratory-scale cell, the anode current density would be in the range of 2-3 A/cm^2. In the engineering-scale cell, the anode current density was estimated to be on the order of 600 mA/cm^2, and the total current was not proportional to the depth of the anode in the melt. The calculated 30% current efficiency was also significantly lower than the 50-80% current efficiencies obtained in the laboratory-scale cells. Apparently the larger scale cell resulted in larger dissipative losses. Possible sources of these losses include the bulk resistance of the salt and the hardware that feeds current to the anode and cathode, and possible recombination of lithium and oxygen. Future engineering-scale experiments with salt recovery will be directed toward evaluating the suitability of the SnO_2 anode.

C. Materials Evaluation for Pilot-Scale Facility

In support of design work being performed on the pilot-scale oxide reduction facility planned for construction at ANL-West, a series of tests was performed to evaluate candidate materials for vessel construction. Materials studies have focused on two distinct environments that will be encountered in the pilot-scale facility. For the oxide reduction step, the significant aspects of the environment are (1) the salt, consisting of LiCl with Li_2O, Li metal, and possible Li_3N, (2) the cover gas, consisting of argon with nitrogen contamination, and (3) the temperature, which is nominally 650°C. For the salt-recovery step, the significant features of the environment are (1) the salt, consisting of LiCl and Li_2O, (2) the cover gas, which will be predominantly argon with oxygen and possible nitrogen contamination, and (3) the temperature, which is also 650°C.

The initial test in simulated reduction-vessel conditions was run for 30 days. To accelerate possible corrosion the test was run at 725°C. The gas (argon) was supplied to the test by bubbling it through the molten salt pool. The salt consisted of LiCl with 3.5 wt% Li_2O and 1 wt% Li_3N. Saturation of the salt with lithium metal was assured by porous stainless steel (SS) cylinders filled with lithium, which were submerged in the salt. The Li_3N was included to simulate the possible reaction with the nitrogen in the hot-cell environment. Eleven coupons were tested with nominal dimensions of 7.6-cm long, 0.3-cm thick, and 2.5-cm wide. All had an autogeneous weld centrally located along one side of the length. Materials included 316L SS (annealed, as-welded, and welded and aluminized), 2.25Cr/1Mo (annealed and as-welded), 422 SS (annealed and as-welded), 430 SS (annealed and as-welded), and tantalum (annealed and as-welded). The result of this corrosion test was that essentially no material loss was observed for any materials except tantalum. The tantalum samples each lost approximately 1 wt% during the 30-day accelerated test.

A companion test to the above was done in a gas consisting of 90% Ar/10% O_2 to simulate the conditions of the lithium electrowinning vessel. Conditions were the same except that the lithium-filled cylinders were not used because any dissolved lithium would have been converted to Li_2O by the oxygen. In this case, the materials tested included 316L, 422, 430, and 2.25Cr/1Mo (each in as-welded; welded and annealed; welded and aluminized; and welded aluminized, and annealed conditions). The samples were identical in configuration to those for the reduction vessel test. The result of this test was that all samples were completely destroyed by corrosion within 30 days.

A less severe test in simulated electrowinning conditions was run with select materials in order to aid in understanding the corrosion mechanisms and to rank materials for corrosion resistance. This test was identical in configuration but was run for 6 days at 650°C. It also used gas of 90% Ar/10% O_2; Li_3N was not included in this test because it should be converted to Li_2O during the test. Sample materials were 304 SS, 316L SS (welded), 316L SS (welded and aluminized), Inconel 600, and Inconel 625. The results of this test indicated that Inconel 600 (2.2 wt% loss) was by far the most corrosion resistant of the materials tested.

A followup test was run to better assess nickel-based alloys for corrosion resistance in this environment. This test was identical to the above test, except that the materials tested were

Inconel 600, Inconel 625, Haynes 242, and Krupp Alloys 31, 33, 59, 602CA and 45TM. Again the Inconel 600 underwent the least severe corrosion. A third 6-day test was run to examine the effect of lowering the oxygen pressure (cover gas was 95% Ar/5% O_2) over ferrous alloys. The results of this test have not been fully analyzed, but it appears that the reduced oxygen partial pressure resulted in significantly less corrosion. Future work will include a 90-day test of the reduction vessel materials to verify their performance.

VI

Basic Chemistry Research

Basic chemistry research is being pursued on fundamental issues that relate to homogeneous and heterogeneous catalysis, ion transport mechanisms in electrochemical devices, high-critical-temperature superconductivity, and the decontamination of radioisotope-impregnated materials.

A. Physical Organometallic Chemistry

This program employs *in situ* spectroscopic and mechanistic techniques to examine the reaction chemistry of processes that are used in the chemical industry or are under development. Recent catalysis research encompasses (1) the first *in situ* nuclear magnetic resonance (NMR) investigations of carbon monoxide hydrogenation and olefin hydroformylation processes in supercritical fluids at high temperatures and pressures and (2) the study of extremely robust polyfluorophthalocyanine catalysts for hydrocarbon activation processes. Also, in a program associated with the development of the lithium-polymer battery (Sec. I.A), toroid cavity imaging techniques are being developed for the *in situ* examination of lithium-ion transport.

1. Catalytic Chemistry in Supercritical Fluids

Supercritical fluids (CO_2 or water) offer environmentally benign alternatives to toxic organic solvents frequently used in homogeneous catalysis. An additional advantage is the elimination of energy-intensive distillations necessary for product separations and catalysis recovery from organic solvents. Our previous work focused on the hydroformylation of olefins catalyzed by cobalt carbonyl hydride in supercritical carbon dioxide.[1,2] We found that the selectivity for the desired straight-chain aldehyde product was improved by a factor of two in the

---

[1] K. W. Kramarz, R. J. Klingler, and J. W. Rathke, "Nuclear Magnetic Resonance (NMR) Spectroscopy in High-Pressure/High-Temperature Catalysis," Presented at the 215th Am. Chem. Soc. National Meeting, Dallas, TX, March 29-April 2, 1998.

[2] J. W. Rathke, R. J. Klingler, R. E. Gerald, K. W. Kramarz, and K. Woelk, *Prog. Nucl. Magn. Reson. Spectrosc.* 30, 209-253 (1997).

low-viscosity supercritical fluid.[3,4] Furthermore, this selectivity enhancement was not obtained at the expense of the overall rate of aldehyde production. These results demonstrated that supercritical fluids can offer true process advantages in addition to environmental ones. In order to extend the scope of supercritical carbon dioxide as a catalytic reaction medium, we decided to examine the $HCo(CO)_4$-catalyzed hydrogenation of carbon monoxide. The hydrogenation of carbon monoxide was followed over the temperature range of 180-210°C in a mixture of $CO/H_2/N_2$. Methanol and methyl formate were the first observable products, consistent with the observations for this reaction in various organic solvents.[5] The reaction sequence is

$$CO + 2H_2 \rightarrow CH_3OH \quad (1)$$

$$2CO + 2H_2 \rightarrow HC(O)OCH_3 \quad (2)$$

One difference from the liquid phase is that proton transfer is slow in the gas phase. Thus, the water resonance remained distinct from the methanol resonance up to 210°C. The reaction kinetics was not investigated in detail. However, one goal was to measure the activation energy in the supercritical fluid for comparison to the value previously determined in dioxane. Methanol and methyl formate were found to increase as a linear function of time. Nonlinear behavior is not expected at low percent conversions of the CO/H_2 reactants, as long as the $HCo(CO)_4$ catalyst is stable. Consistent with our previous experience, the hydride was found to be stable over the 180-210°C temperature range. In contrast, the water concentration gradually decreased due to the water-gas shift reaction, which is also catalyzed by $HCo(CO)_4$. For comparison to the solution-phase data,[5] the initial rates of methanol production were divided by the average hydride concentration to yield an effective first-order rate constant (k). Table VI-1 lists k values for several reaction media. The gas-phase rate constant is quite similar to that for heptane, although the hydrogen partial pressure was somewhat lower in the gas-phase experiment. Qualitatively, this is similar to the behavior that we have previously found for the $HCo(CO)_4$-catalyzed hydroformylation of olefins.[1-5] In that case, supercritical carbon dioxide was comparable in solvation properties to heptane or methyl cyclohexane.

Significantly, additional products became evident in the ^1H NMR spectra at 200-210°C. These resonances are consistent with the formation of higher alcohols, as depicted in Fig. VI-1. These assignments were confirmed by extracting the crude reaction product with CD_3CN and obtaining high-resolution ^1H NMR spectra for comparison to authentic standards. The high-resolution spectra indicated the presence of ethanol, propanol, and ethyl formate. All of the individual resonances, including the correct multiplicity due to proton coupling, were resolved in the high-resolution spectra of the end reaction product. The limited spectral resolution of the high-pressure probe (approximately 30 Hz) did not allow such a definitive assignment under *in situ* reaction conditions. For example, it was not possible to resolve any proton coupling in the

---

[3] J. W. Rathke and R. J. Klingler, "Cobalt Carbonyl Catalyzed Olefin Hydroformylation in Supercritical Carbon Dioxide," Patent No. 5,198,589 (March 30, 1993).

[4] J. W. Rathke, R. J. Klingler, and T. R. Krause, *Organomet.* **10**(5), 1350-1355 (1991).

[5] R. J. Klingler and J. W. Rathke, "Homogeneous Catalytic Hydrogenation of Carbon Monoxide," *Prog. Inorg. Chem.* **39**, 113-180 (1991).

Table VI-1. Comparative Rate Data for CO Hydrogenation Catalyzed by $HCo(CO)_4$

Solvent	Temp., °C	Partial Pressure, atm		Rate Constant, s^{-1}
		H_2	CO	
Heptane	200	145	145	5×10^{-6}
Benzene	200	145	145	2×10^{-5}
Dioxane	196	148	148	4×10^{-5}
CF_3CH_2OH	200	153	153	1×10^{-4}
Gas Phase	200	109	164	8×10^{-6}

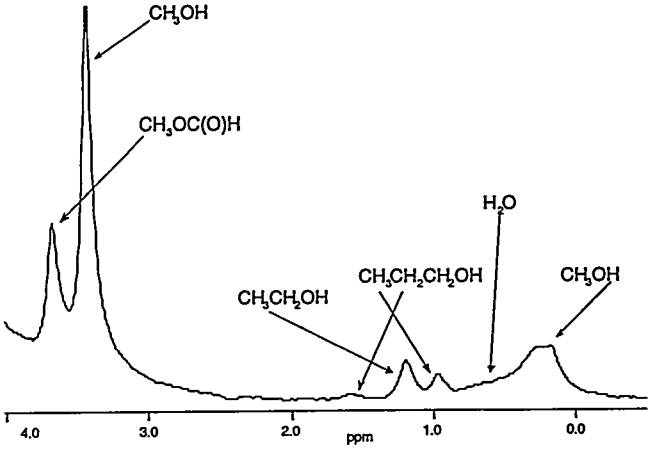

Fig. VI-1. *In Situ* ^1H NMR Spectrum Showing Higher Alcohol Production for $HCo(CO)_4$-Catalyzed Hydrogenation at 210°C

high-pressure spectra. In addition, with limited resolution, some of the methylene resonances for the higher alcohols lie under the intense methyl resonances of the methanol and methyl formate. Consequently, we could not directly resolve all the methylene resonances for the higher alcohols. Fortunately, all of the end methyl groups have distinctive chemical shifts and can be used to follow the production of the higher alcohols under *in situ* reaction conditions. Again, these observations are consistent with the previous work in organic solvents, where the higher alcohols were determined to be secondary products produced from alcohol homologation.[5] However, it is somewhat surprising that alcohol homologation would occur in the gas phase because a key step in the standard mechanism for $HCo(CO)_4$-catalyzed alcohol homologation involves proton transfer:

$$ROH + HCo(CO)_4 \rightarrow ROH_2^+ + Co(CO)_4 \qquad (3)$$

Furthermore, the poor selectivity of $HCo(CO)_4$-catalyzed alcohol homologation is generally attributed to this step because the alkylating properties of the resultant ROH_2^+ cations are driven by the leaving ability of water and are very insensitive to the length of the alkyl chain. Therefore, the gas-phase systems show promise of achieving enhanced selectivity if these proton transfer steps can be eliminated or better controlled.

Future effort will be directed toward determining the kinetics of supercritical fluid-phase alcohol homologation for comparison to solution-phase systems. In addition, a range of carbonylation reactions is under investigation using a $HCo(CO)_4$ catalyst. Reactions of this type are important steps in the production of fine chemicals and pharmaceuticals.

2. Hydrocarbon Activation Chemistry

Metallophthalocyanines (MPc's) have been used as catalysts in our studies because of their high-temperature stability and their similarity in structure to porphyrins, which are the prosthetic groups of heme enzymes that catalyze the aerobic oxidation of hydrocarbons in biological systems.[6] We have previously investigated the catalytic activation of carbon-hydrogen bonds by MPc's under both reduction[7,8] and oxidation conditions.[9] Metallophthalocyanines have such high versatility because many of them undergo multiple oxidation and reduction reactions to form stable products.[10] Therefore, studies of the redox reactions of MPc's are important for MPc-catalyzed reactions. An important question is whether the redox reaction occurs on the metal or on the MPc ring. We have found that in the highly fluorinated (FPc)(Me)Rh(III) and (FPc)(PMe_3)(Me)Rh(III) [where FPc^{2-} = dianion of 1,4,8,11,15,18,22,25-octakis(trifluoromethyl)phthalocyanine], the one- and two-electron reductions are ring-reduction reactions, leading to the formation of Rh(III) complexes of $FPc^{\bullet 3-}$ and FPc^{4-}. Figure VI-2 shows the $FPcH_2$ structure.

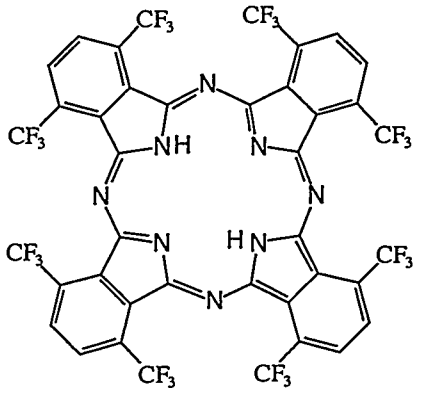

Fig. VI-2. Structure of $FPcH_2$

When (FPc)(PMe_3)(Me)Rh(III) was reacted with $NaBH_4$ in methanol-d_4, a paramagnetic complex and an antiaromatic complex were successively produced. On the basis of ^1H NMR and electrochemical studies, these two products were assigned to ($FPc^{\bullet 3-}$)(PMe_3)(Me)Rh(III)$^-$ and ($FPcD^{3-}$)(PMe_3)(Me)Rh(III)$^-$, respectively. The spectral changes accompanying the reaction are presented in Fig. VI-3, which shows that all the resonances of ($FPc^{\bullet 3-}$)(PMe_3)(Me)Rh(III)$^-$ are broad, as expected of a paramagnetic complex. The assignment of the odd electron to the FPc

---

[6] B. Meunier, *Chem. Rev.* **92**, 1411 (1992).

[7] M. J. Chen and J. W. Rathke, *Organometallics* **13**, 4875 (1994).

[8] M. J. Chen, L. Nuñez, J. W. Rathke, and R. D. Rogers, *Organometallics* **15**, 2338 (1996).

[9] M. J. Chen, D. E. Fremgen, and J. W. Rathke, *J. Porphyrins Phthalocyanines* **2**, 473 (1998).

[10] A. B. P. Lever, E. R. Milaeva, and G. Speier, in *Phthalocyanines: Properties and Applications*, Eds., C. C. Leznoff and A. B. P. Lever, Vol. 3,Wiley-VCH, New York, pp. 1-70 (1993).

ligand is supported by several findings. First, assignment of the odd electron to Rh would create $(FPc)(PMe_3)(Me)Rh(II)^-$, which belongs to the class of very unstable, 19-electron complexes. This is not consistent with the stable product observed. Second, the ^1H NMR spectrum of $(FPc^{\bullet 3-})(PMe_3)(Me)Rh(III)^-$ is very similar to that of $(FPc^{\bullet 3-})(PMe_3)_2Rh(III)$, which has been fully characterized as a ligand-centered radical complex.[11] Finally, the first and second reduction potentials of $(FPc)(PMe_3)(Me)Rh(III)$ (-0.416 and -1.083 V vs. standard calomel electrode) are not significantly different from those of the five-coordinated (FPc)(Me)Rh(III) (-0.428 and -1.079 V vs. standard calomel electrode). These results are more in line with ligand reduction processes, since the presence of PMe_3 should greatly reduce the reduction potentials of $(FPc)(PMe_3)(Me)Rh(III)$ if the reaction occurs on the metal ion.

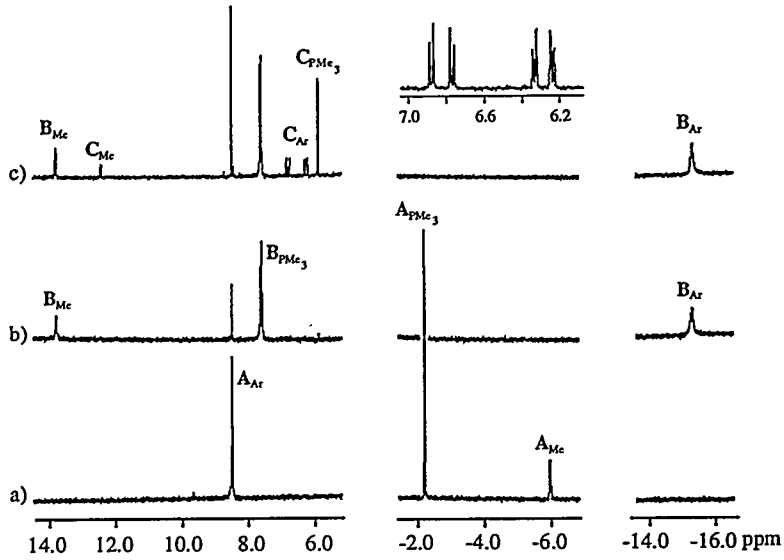

a) $(FPc)(PMe_3)(Me)Rh(III)$
b) $(FPc^{\bullet 3-})(PMe_3)(Me)Rh(III)^-$
c) $(FPc^{3-})(PMe_3)(Me)Rh(III)^-$

Fig. VI-3. *In Situ* ^1H NMR Spectral Changes Accompanying the Reduction of $(FPc)(PMe_3)(Me)Rh$ with $NaBH_4$ in Methanol-d_4

The ^1H NMR spectrum of the second product in Fig. VI-3c clearly indicates that it is an antiaromatic compound, since its ring protons appear in the region of δ = 6.2-6.9 ppm. Therefore, the two electrons are added to the FPc ligand to form the antiaromatic, 20-electron FPc^{4-} ligand. Furthermore, the fact that these aromatic resonances appear as two AB quartets (inset) suggests that one of its meso nitrogens is deuteronated, and that the second product is best formulated as $(FPcD^{3-})(PMe_3)(Me)Rh(III)^-$.

We have shown in this study that, in the one- and two-electron reductions of $(FPc)(Me)Rh(III)$ and $(FPc)(PMe_3)(Me)Rh(III)$, the electrons are added to the ligand-based

[11] M. J. Chen, L. M. Utschig, and J. W. Rathke, *Inorg. Chem.* **37**, 5786 (1998).

orbitals to produce a paramagnetic and an antiaromatic complex. Although $(FPc^{\bullet 3-})(Me)Rh(III)^-$ and $(FPc^{\bullet 3-})(PMe_3)(Me)Rh(III)^-$ are very stable under inert atmosphere, both $(FPcD^{3-})(Me)Rh(III)^-$ and $(FPcD^{3-})(PMe_3)(Me)Rh(III)^-$ slowly eliminate a meso nitrogen to give the ring-contracted α,β,γ-triazatetrabenzocorrole complexes. Future work will be devoted to studying the stability and the catalytic activities of selected MPc catalysts under oxidation conditions, with the aim of finding more stable and more active MPc catalysts for hydrocarbon oxidations.

3. Ion Transport Mechanisms

Basic studies are in progress on the structure, mobility, redox chemistry, and spatial disposition of the ions, polymer host, and electrolytic products in a variety of electrochemical devices, including rechargeable lithium batteries. In this research, we utilize a device called the "near-electrode imager," which was invented and developed at Argonne to perform *in situ* NMR spectroscopy and magnetic resonance imaging (MRI) of electrochemical systems. While this device can be used in the traditional manner of an NMR probe for recording high-resolution and wide-line NMR spectra, it also has the capability to correlate NMR parameters such as chemical shift, indirect spin-spin coupling, and spin-lattice relaxation with a spatial dimension, namely, the dimension directed radially from the central conductor/electrode.

We have demonstrated the first MRI images of the radial concentration profile for the anions in a polyethylene-oxide (PEO) polymer electrolyte in the region adjacent to the working electrode at different stages of cell polarization.[12] The localized formation of redox chemistry byproducts (e.g., HF and dendritic Li) and different microscopic environments containing solvated Li^+ were also observed at electrode surfaces in different electrochemical systems.[13] In these and similar systems, the chemical shift is the key NMR parameter that allows us to assign the spatial distribution (radial concentration profile) of the different resonances detected in the one-dimensional NMR spectrum to unique chemical species.

One of our most recent investigations focuses on the interaction of ^7Li nuclei with electric field gradients, known as the "quadrupole interaction." In a polymer electrolyte consisting of $LiN(SO_2CF_3)_2$ dissolved in PEO, the ^7Li NMR chemical-shift dimension recorded by the near-electrode imager was extended to measure this interaction. Although the quadrupole interaction also manifests itself along the chemical shift dimension, the spectral features that are produced by this interaction are distinct from those produced by chemical shielding and provide unique information about the local electrostatic environment of the ^7Li nuclei. The ability of the near-electrode imager to detect a broad pattern of resonances due to the quadrupole interaction makes it possible to investigate the spatial distribution in an electrochemical cell of lithium ions that are contained in crystalline phases.

---

[12] R. E. Gerald II, R. J. Klingler, J. W. Rathke, G. Sandí, and K. Woelk, "*In Situ* Imaging of Charge Carriers in an Electrochemical Cell," *Spatially Resolved Magnetic Resonance*, Eds., P. Blümler, B. Blümich, R. Botto, and E. Fukushima, Wiley-VCH, Weinheim, pp. 111-119 (1998).

[13] G. Sandí, R. E. Gerald II, R. J. Klingler, J. W. Rathke, K. A. Carrado, and R. E. Winans, "Studies of Electrolyte Penetration in Carbon Anodes by NMR Techniques," Proc. of 194th Meeting of Electrochem. Soc., Lithium Battery Symp., November 1-6, Boston, MA (1998).

The phase diagrams of many polymer electrolytes indicate regions that are composed of amorphous and crystalline solids. In $LiN(SO_2CF_3)_2$/PEO, the crystalline phase is a helical structure with the stoichiometry PEO_3 $LiN(SO_2CF_3)_2$.[14] This phase does not contribute to ionic conductivity and, therefore, can be considered a chemical-phase bystander. Since this crystalline phase can coexist in (metastable) equilibrium with the ion-conducting amorphous phase, it is desirable to understand what role this phase has in performance characteristics of the polymer electrolyte. For example, will the crystalline phase rapidly dissolve in response to a change in lithium-ion concentration in the amorphous phase brought about by cell polarization? Does the crystalline phase impede ion mobility in the surrounding amorphous phase? Does the ratio of crystalline to amorphous phases change in the regions adjacent to the electrodes due to changes in the chemical potential at the electrode-electrolyte interface? These questions can be answered by recording and analyzing spatial maps of the crystalline and amorphous phases of a polymer electrolyte throughout a charge/discharge cycle in an electrochemical cell.

The radial concentration profile of ^7Li (Fig. VI-4) was obtained for the crystalline phase of a $LiN(SO_2CF_3)_2$/PEO electrolyte within an electrochemical cell contained in the near-electrode imager. The ^7Li quadrupole powder pattern is over 80-kHz wide in the chemical-shift dimension. A quadrupole coupling constant of 5 kHz was calculated from the data and indicated that these lithium ions were located at a site with axial symmetry and a low electric field gradient, were immobile on the microsecond time scale, and were randomly distributed in a crystalline phase. The lithium ions in the amorphous phase were represented by a narrow and intense resonance superimposed onto the powder pattern at the center of the spectrum. The spatial dimension revealed that the characteristic powder pattern was found at each radial position in the battery. This indicated that lithium in the crystalline phase was uniformly distributed in the polymer electrolyte. A variable temperature study showed that the crystalline phase rapidly and uniformly disappeared throughout the cell when it was heated to 50°C. Subsequently, the crystalline phase required several weeks to reform at 22°C. The image in Fig. VI-4 demonstrated that the ^7Li quadrupole powder pattern can be used to map the spatial distribution of immobile lithium ions in a lithium battery. To our knowledge, this was the first and only demonstration of the spatial distribution of immobile lithium ions in a battery, recorded *in situ* under operational conditions.

In future studies using the near-electrode imager, we will record the radial concentration profiles of the lithium ions in the amorphous and crystalline phases, before and after cell polarization. The resulting images should reveal the distinct functions of the mobile and immobile lithium ions in a lithium-ion battery. In addition, we are modifying our electrochemical device so that it can be placed in a beam line of the Advanced Photon Source at ANL. The diffraction data will reveal the size of the PEO_3 $LiN(SO_2CF_3)_2$ crystallites at a specified radial position. The MRI data will map the radial distribution of the crystallites. Thus, simultaneous diffraction and MRI images will correlate the average crystallite size with the spatial distribution of the crystallites at different stages in a charge/discharge cycle of a lithium-ion battery.

[14] Y. G. Andreev, P. Lightfoot, and P. G. Bruce, *J. Chem. Soc., Chem. Commun.*, p. 2169 (1996).

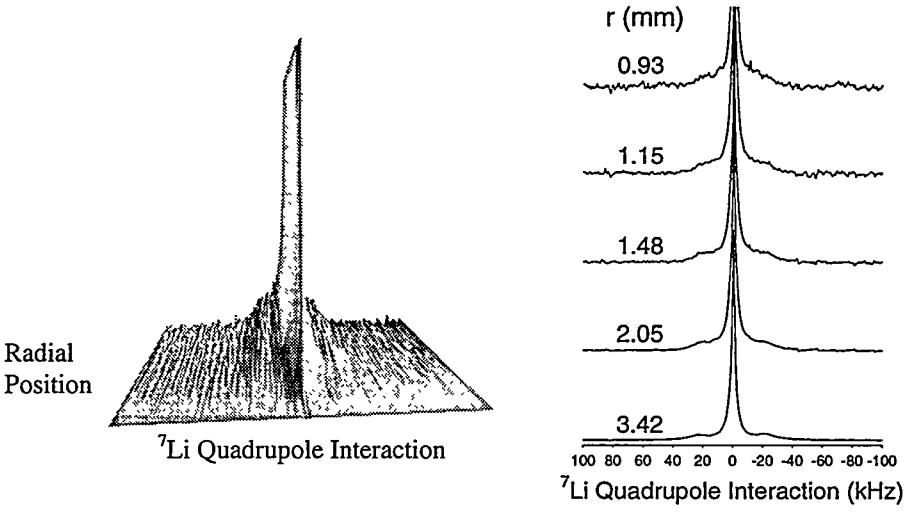

Figure VI-4. Magnetic Resonance Image (left) and Image Cross Sections (right) of $^7Li^+$ Ions in the Polymer Electrolyte $LiN(SO_2CF_3)_2$/PEO Recorded with the Near-Electrode Imager at 22°C. The radial dimension of the image extends from the working electrode/electrolyte interface located at 0.63 mm and the counter electrode located at 4.93 mm.

B. Heterogeneous Catalysis

A new program within CMT has been initiated with the objective of developing heterogeneous catalysts for the hydrodesulfurization of diesel fuel and the etherification of synfuel-derived phenolics. In previous years, this program has been carried out in the ANL Chemistry Division.

1. Selective Desulfurization of Diesel Fuel

Because the sulfur content of crude oil is rising as oil quality declines, refiners need more robust, higher-activity catalysts for hydrodesulfurization (HDS). Past work (at Argonne and elsewhere) in HDS catalysis has concentrated on single aspects, such as activity or selectivity. Current CMT projects seek to optimize all aspects of the catalyst, including active-phase type and synthesis, support porosity, and so on, while also gaining a fundamental understanding of the oil to be processed.

Working under a cooperative R&D agreement with UOP (Des Plaines, Illinois), we are focusing on three areas: development of processing techniques to reduce particle size, identification of the "bad actors" in the feed and products, and development of improved catalyst supports. The work is still in an early stage of development.

Formerly, researchers felt that reducing the size of metal clusters in catalysts to fewer than 50 atoms per particle would increase catalyst activity (per metal atom) by one to two orders of magnitude. In the current work, high-activity particles are being made by using new active metal phases (carbides and nitrides) in conjunction with advanced metal impregnation techniques (metal atom vapor deposition and microwave decomposition of cluster complexes). The active phases are being placed on a variety of high-surface-area supports such as alumina and molecular sieves. This work has shown that small particles alone are insufficient to boost catalyst activity. Greater dispersion of the metal must be used in conjunction with an optimized support to gain the full benefits of the small metal clusters. In the future, X-rays from Argonne's Advanced Photon Source will permit full characterization of these metal particles, which would be far too small to be seen by other X-ray sources.

To gain a clearer understanding of individual components in the feed and products, we are using high-resolution mass spectrometry and neutron scattering techniques. This work has revealed the nature of the "bad actors" in the heavy fraction of crude oils, those molecules that limit HDS conversion. Data collected thus far on the size of asphaltene molecules and the feed molecules have called current literature values into question (see, for example, Speight et al.[15]). The results imply that the oxide supports currently used in commercial HDS operations may have pore diameters that are overly large, wasting valuable catalyst surface area.

The pore size of the catalyst is being investigated by two different approaches, each involving unique support materials. In the first, mesoporous clays are custom-synthesized with pores that more closely match the molecular diameters of the feed molecules as determined via neutron scattering. Catalysts containing pores approximately 50% larger than the feed molecules have been shown to have improved catalyst performance when compared to catalysts with pores that are either significantly larger or smaller. The focus of future work will be on optimizing these pore geometries.

The second approach involves combining the active phase and support in one structure. Cobalt clusters, one of the known active phases in HDS catalysis, have been tried as pillars in a structure of molybdenum sulfide (MoS_2), a material with both catalytic and support roles in commercial catalysts (Fig. VI-5). The advantage of this type of catalyst is that the active phase (Co_6S_8) is in intimate contact with the support phase (MoS_2). The support anchors the feed molecules at the site of the catalysis, optimizing the interaction between the three necessary phases (active phase, support, and feed). The cobalt-pillared MoS_2 materials have activities comparable with those of commercial catalysts (e.g., Crosfield 465 and 504), but with better selectivities for the most desirable products. The next year's work will concentrate on using these optimized catalysts under processing conditions where the asphaltene molecular sizes match the catalyst pores.

[15] J. G. Speight et al., *Rev. Instr. Fr. Petro.* 40(1), 51-61 (1985).

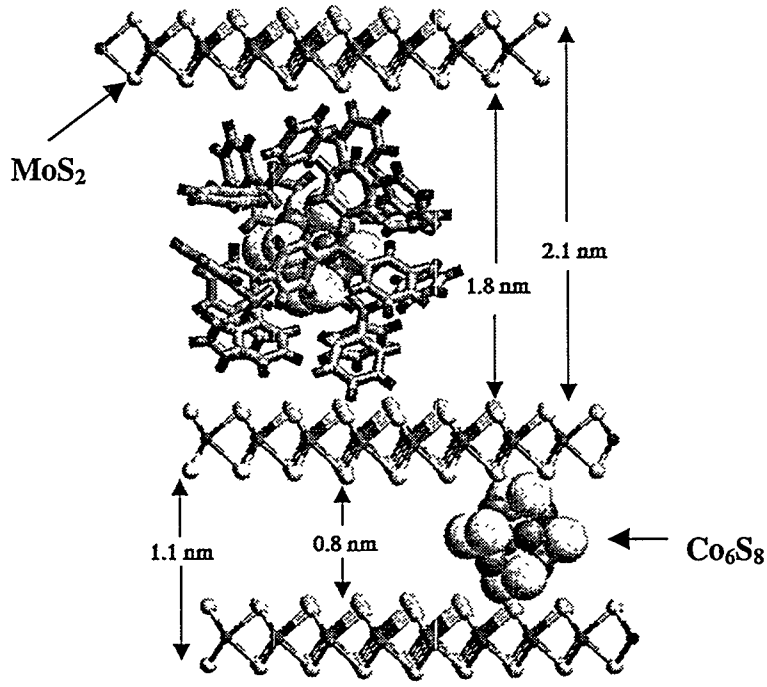

Fig. VI-5. Active HDS Catalysts Formed by Pillaring of MoS_2 with Co_6S_8

2. *Etherification of Coal Liquids*

A research program is underway to create heterogeneous catalysts to promote the etherification of synfuel-derived phenolics, thereby generating useful aryl alkyl ethers. The resulting low boiling fractions can be blended as octane improvers and oxygenates for gasolines, and the middle boiling fractions can be blended into diesel fuels. As additional justification the following is noted:

1. The middle distillate fractions derived from synfuel sources, such as the liquefaction or pyrolysis of low rank coal, contain high levels of phenolics.

2. The removal of phenolics by existing routes, such as hydrotreating, consumes large quantities of hydrogen.

3. The presence of these phenolics often accelerates catalyst aging during processing.

4. These phenolics are relatively unstable when present in fuels, leading to the formation of gums and heavy cross-linked products.

This effort is being directed toward formulating, evaluating, and establishing catalytic solids that promote the etherification reaction of alkyl hydroxyl groups with alcohols. At the

same time, it is necessary to minimize alkylation reactions that result in attachment of methyl or ethyl groups to the phenolics that yet retain their phenolic functionality.

Experiments are being carried out with model reactants (methanol and ethanol with phenol and cresol) in a continuous flow unit at reaction temperatures of 150-300°C and pressures of ambient to 10 atm (about 0.1 MPa). Initial results have confirmed the value of acid catalysts for the above model systems. Both commercially available and internally formulated catalysts have been evaluated. The latter are best at this time. As the catalyst technology improves, evaluation will be undertaken with samples of coal-derived pyrolysis product, which have been obtained from the TEK-KOL Partnership (ENCOAL Corp. and SGI International). The goal is to make catalysts that have both a reasonable life with coal-derived feedstocks and yet can be regenerated. It has been proposed that Argonne interact with the DOE Federal Energy Technology Center (FETC) for selected product analyses. In addition, both FETC and TEK-KOL will be informed of our ongoing progress so that their feedback can be obtained.

C. Energy and Environmental Research

This program involves fundamental studies that are relevant to new electric power technologies and decommissioning/decontamination strategies for nuclear facilities—two subjects of forefront interest to DOE. The specific research topics relate to improvements in the performance of high-temperature ceramic superconductors and the detailed characterization of surfaces contaminated with radionuclides.

1. *High Temperature Superconductivity*

The research program on high-critical-temperature superconductivity (HTS) is directed primarily at the study of phase evolution and microstructure development in silver-sheathed $(Bi,Pb)_2Sr_2Ca_2Cu_3O_x$ (Ag/Bi-2223) composite conductors. This research activity is carried out in close collaboration with American Superconductor (ASC)—a leading manufacturer of HTS products. During the past year we have made significant progress in three areas: optimizing heat treatment conditions, exploring microstructural transformations *in situ*, and identifying phases that form during heat treatment.

One recently completed study focused on phase evolution and microstructure development in Ag/ Bi-2223 composite conductors as a function of filament count (1, 19, 85, and 361), precursor powder type (metallic powder or oxide powder), oxygen partial pressure ($<10^{-3}$ to 0.13 atm), temperature (790 to 855°C), and time (0 to 6000 min). Favorable conditions for rapid Bi-2223 phase formation and stability were achieved with an oxygen partial pressure around 0.08 atm, regardless of precursor type or filament count. In general, the rate of the Bi-2223 formation reaction increased and the width of the temperature window for rapid kinetics became broader as the filament count increased. The most rapid kinetics and the broadest heat treatment window were observed for the metallic powder composite containing 361 filaments. These trends in Bi-2223 formation rate and stability were found to be associated with the increased proximity of powder to silver as the filament count increases and the filament transverse dimensions become smaller. Each conductor type (in terms of precursor form and

filament type) had an optimum processing temperature at an O_2 partial pressure of 0.08 atm that produced a microstructure consisting of well-developed Bi-2223 grain colonies with the least amount of second phase. This optimum temperature was near the peak of the reaction-rate-versus-temperature profile for each conductor type. These findings have been factored into ASC's processing practices and have contributed to improvements in the performance of their Ag/Bi-2223 multifilament conductor.

Figure VI-6 shows SEM images for three 85-filament specimens processed in 0.08 atm O_2 at 810, 820, and 830°C. Although the percent conversion of $(Bi,Pb)_2Sr_2CaCu_2O_x$ (Bi-2212) to Bi-2223 was >85% for all three specimens, the microstructures display considerable differences. The Bi-2223 grain structure in the specimen heat treated at 810°C (Fig. VI-6a) is poorly developed, second phases are prevalent but relatively small, and there are no platy growths into the silver sheath. The 820°C specimen (Fig. VI-6b) has the best microstructure in terms of the relative amount of second phase, the number of platy growths into the silver sheath, and Bi-2223 grain colony development. The specimen heat treated at 830°C (Fig. VI-6c) has a well developed Bi-2223 grain structure, but contains domains of appreciable second-phase growth (dark regions) and also exhibits numerous platy protrusions of Bi-2223 grains into the silver sheath. Our collective experience with Ag/Bi-2223 composites having the same powder stoichiometry as these samples and processed in 0.08 atm O_2 has shown that a heat-treatment temperature of 825°C produces the highest critical current densities.

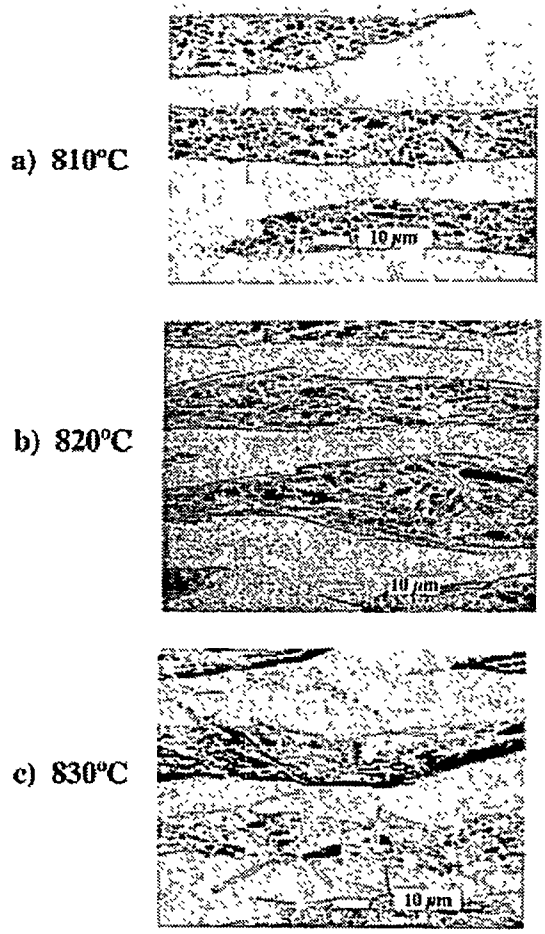

Fig. VI-6.

Scanning Electron Micrographs (transverse view) of 85-Filament Specimens Processed at (a) 810°C, (b) 820°C, and (c) 830°C in 0.08 atm O_2 for Sufficient Times to Achieve >85% Bi-2223

Recently completed analyses involving environmental scanning electron microscopy (ESEM) of multifilament Ag/Bi-2223 composite wires present a graphic visualization of the morphological and chemical changes that take place when a Bi-2223 precursor powder (consisting of Bi-2212 and a Pb-Ca-Cu-O second phase) reacts in a silver sheath to form Bi-2223. When viewed sequentially with increasing temperature, the ESEM images of the silver sheath and the ceramic powder cores embedded in the sheath reveal a variety of transformations. These results include (1) coarsening/agglomeration of the precursor powder, (2) the opening and eventually the filling in of gaps in the powder that run in both the longitudinal and transverse directions, (3) recrystallization of the silver sheath and the appearance of what looks like second-phase crystallites on the silver surfaces, (4) growth of layered Bi-Sr-Ca-Cu-O phase grains (presumably Bi-2212 and Bi-2223), (5) turning of layered phase grains to favor being parallel to the longitudinal (rolling) direction, (6) Ostwald ripening (small grains dissipating as large grains continue to grow), and finally (7) partial melting at the highest temperatures. These ESEM measurements have provided visual evidence of important process-relevant phenomena for which only indirect speculative evidence had heretofore been presented.

Raman microspectroscopy and imaging Raman microscopy methods implemented in our laboratory have proven to be powerful tools for studying the evolution and spatial distribution of chemical phases in bismuth-based HTS ceramics. These techniques have been applied to compressed/sintered powders and silver-clad composite conductors in conjunction with scanning electron microscopy and energy dispersive X-ray spectroscopy. Many important insights have been gained about the identity, size, shape, orientation, and spatial distribution of the various nonsuperconducting secondary phases (NSPs) that form and dissipate during heat treatment of bismuth-based, silver-clad composite tapes. The results have allowed us to determine key mechanistic features that influence the formation of the superconducting phases as heat treatment progresses, including the location of lead-rich NSPs and the identification of the constituent phases in certain NSP agglomerations that tend to persist as HTS phase formation proceeds to completion. Armed with this new knowledge, we are in the process of developing methods to dissipate these agglomerations based on the manipulation of oxygen pressure and temperature.

Future work in this program will emphasize the reduction/dissipation of nonsuperconducting second phases in Ag/Bi-2223 composite wire and novel practical methods for improving flux pinning and critical current density in bismuth-based HTS composites. Progress in these areas is needed to boost the performance of HTS conductors in electric power equipment, such as motors, generators, transformers, fault current limiters, and transmission cables.

2. *Environmental Management Science*

The aim of this program is to develop a detailed understanding of the mechanism by which radionuclides and heavy metal ion contaminants are incorporated into the surface films on metals and alloys. Knowledge gained from these studies is of importance in developing technologies for the decontamination of piping systems, storage tanks, buildings, and equipment that have been used in nuclear research and development and in fuel processing facilities. Radioactive contamination resides in the corrosion scales of the metals and alloys. We have simulated their formation by electrochemical deposition processes and have investigated the

structure and composition of the surface films *in situ* by synchrotron X-ray absorption spectroscopy, as well as infrared and laser Raman scattering techniques.

It is widely accepted that the corrosion film on Ni contains $Ni(OH)_2$ in the passive region. Nickel oxides are also particularly interesting as a model system because of the variety of sites into which a heavy metal can be incorporated. We have therefore prepared thin films to simulate this corrosion product and studied the incorporation of Cr and U in them. Chromium is of great interest from the environmental standpoint because industrial processes, such as tanning and plating, have resulted in widespread contamination of soil by soluble Cr^{6+} compounds that are highly toxic. Its remediation is therefore of high priority in environmental cleanup operations that are mandated by stricter laws and regulations. Synchrotron-based investigations by X-ray absorption near edge structure (XANES) and extended X-ray absorption fine structure (EXAFS) techniques have been used to elucidate the site occupancy and local structure of Cr^{3+} and Cr^{6+} incorporated into electrodeposited $Ni(OH)_2$ films. The films were prepared by co-deposition at constant current from aqueous solutions of nickel nitrate, chromium nitrate, and potassium chromate. The EXAFS measurements show that in films produced from Ni^{2+} and Cr^{3+} solution, Cr^{3+} is incorporated into Ni lattice sites in $Ni(OH)_2$. On the other hand, codeposition of Cr^{6+} with $Ni(OH)_2$ results in CrO_4^{2-} occupying the interlamellar sites of the brucite structure. These results are also relevant to other technological areas (e.g., corrosion protection) and have been submitted for publication.[16,17]

Cathodic codeposition of $Ni(OH)_2$ and uranium from uranyl nitrate solution resulted in a phase that is very similar to uranyl hydroxide, $UO_2(OH)_2$. Figure VI-7 shows the uranium L_3 XANES spectrum of the co-deposited material compared to that of the starting solution of uranyl nitrate. Figure VI-8 shows the Fourier transform of the EXAFS data and the theoretical fit used to derive various structural parameters. Analysis of these data showed the axial U-O distances to be equal to 1.824 Å. In addition, we found six equatorial U-O bonds, which consist of three bonds with a U-O distance of 2.30 Å, and another three with a U-O distance of 2.47 Å. These distances are close to those found for $UO_2(OH)_2$ by others.[18] Further work on this system is in progress.

We are also developing the technique of synchrotron far infrared reflection spectroscopy for the *in situ* surface analysis of contaminant adsorption and film formation on metals.[19] In addition to the study of ultra-thin oxide films, the technique holds much promise for the detection of hazardous inorganic ions, for example, CN^- and organic energetic materials at monolayer and sub-monolayer levels.

---

[16] M. Balasubramanian and C. A. Melendres, "An X-ray Absorption Near-Edge Spectroscopy Study of the Oxidation State of Chromium in Electrodeposited Oxide Films," to be published in *Electrochimica Acta.*

[17] M. Balasubramanian and C. A. Melendres, "Local Structure of Chromium Incorporated into Electrodeposited Nickel Hydroxide Films," to be published in the *Journal of Synchrotron Radiation.*

[18] P. G. Allen, D. K. Shuh, J. J. Bucher, N. M. Edelstein, et al., *Radiochim. Acta* **75**, 47 (1996).

[19] C. A.Melendres, *Synch. Rad. News* **11**, 39 (1998).

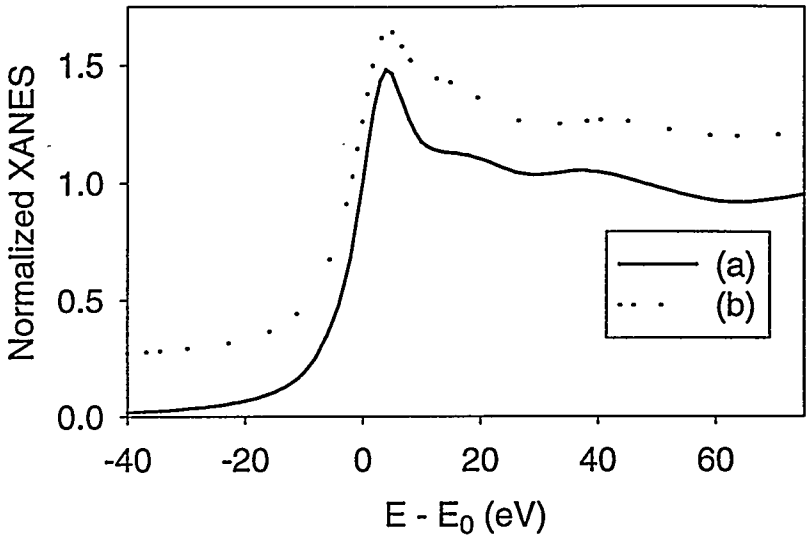

Fig. VI-7. Uranium L_3 XANES Spectra of 1 M Uranyl Nitrate Solution (curve a) and Uranium Codeposited with $Ni(OH)_2$ (curve b)

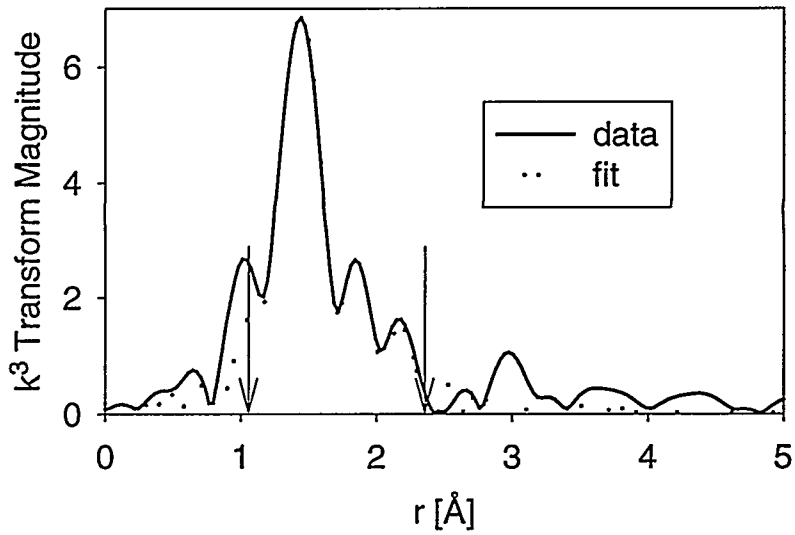

Fig. VI-8. Fourier Transform of Fig. VI-7 for Uranium Codeposited with $Ni(OH)_2$. Vertical arrows indicate the spectral region fitted. (Symbols: k = momentum and r = bond length.)

VII

Analytical Chemistry Laboratory

A. Introduction

The Analytical Chemistry Laboratory (ACL) operates in the Argonne system as a full-cost-recovery service center, but it has a mission that includes a complementary research and development component in analytical chemistry and its applications. Because of the diversity of research and development work at ANL, the ACL handles a wide range of analytical problems in its technical support role. Some routine or standard analyses are done, but the ACL usually works with commercial laboratories if high-volume, production analyses are required by its clients. It is common for the Argonne R&D programs to generate unique problems that require significant development of methods and adaption of techniques to obtain useful analytical data. Thus, much of the support work done by the ACL is very similar to applied research in analytical chemistry.

The ACL is administratively within CMT, its principal ANL client, but it provides technical support for many of the other technical divisions and programs at ANL. The ACL has three groups—Chemical Analysis, Instrumental Analysis, and Organic Analysis, which together include about 25 staff members. Talents and interests of staff members cross group lines, as do many projects within the ACL. The ACL receives about 1600 jobs annually, many of which involve several samples.

The Chemical Analysis Group uses wet-chemical and instrumental methods for elemental, compositional, and isotopic determinations in solid, liquid, and gaseous samples and provides specialized analytical services. The Instrumental Analysis Group uses nuclear counting techniques to determine the radiochemical constituents in a wide range of sample types, from environmental samples with low radioactivity to samples with high radioactivity that require containment. The Organic Analysis Group uses a number of complementary techniques to separate organic compounds and measure them at trace levels and has performed development work in sensors, chemometrics, and detectors.

The ACL continues to upgrade its analytical instruments. A carbon/sulfur determinator and a oxygen/nitrogen determinator were installed in 1998. An ion chromatograph replacement was procured and installed for use with radioactive samples. Both a low-level α/β proportional counter system and an accelerated solvent extractor for organic materials were procured in 1998 and will be installed in early 1999.

B. Technical Highlights

The ACL provides analytical chemistry support to CMT, other ANL divisions and programs, other DOE sites, DOE's Chicago Operations Office, and DOE Headquarters. In addition, ACL conducts research and development programs funded by DOE and other sponsors. Selected accomplishments for 1998 are summarized here. In addition, the ACL did analytical work on many other projects, which are described in more detail elsewhere.[1]

1. Support for Nuclear Technology Programs

The ACL analyzed samples from experiments conducted by several projects in CMT's Nuclear Technology Department. Results from analysis of these samples supported efforts that included development of a zeolite waste form, treatment of spent oxide and metallic fuels, and investigation into the use of a metal other than lithium for reducing uranium oxide in liquid bismuth. The samples varied in the dissolution techniques required before measurement of the requested analytes. Several analytical methods were applied to obtain elemental, isotopic, and compound information, including inductively coupled plasma/atomic emission spectrometry (ICP/AES), inductively coupled plasma/mass spectrometry (ICP/MS), X-ray diffraction (XRD) spectrometry, and thermal ionization mass spectrometry (TIMS). Many of the submitted samples contained radioactive materials, such as plutonium. These types of samples were analyzed with instruments, such as the ICP/AES system, that had been modified for use with the radioactive samples. Some of the analytical results appear in Secs. IV and V.

2. Application of X-ray Diffraction to Waste Form Development

One application of X-ray diffraction (XRD) was in CMT's Nuclear Technology Department. The Waste Form Development Group in this department used XRD to examine zeolite and sodalite waste forms that may contain compounds such as PuO_2 or UO_2. A ceramic waste form will be prepared from zeolite that has been contacted with electrorefiner salt, which contains uranium, plutonium, and various other fission products. Theoretical calculations indicated that the plutonium present in this waste form will cause no harmful interactions. To verify this expectation, the Waste Form Development Group prepared ceramic waste forms for testing by mechanically blending a mixture of zeolite 4A and salt containing ^{239}Pu. The blended zeolite was mixed with a glass binder, and the resulting mixture was pressed by a hot uniaxial

[1] D. W. Green et al., *Analytical Chemistry Laboratory Progress Report for FY 1998*, Argonne National Laboratory Report ANL/ACL-98/2 (December 1998).

press. Under these conditions, zeolite converted to sodalite. An important part of these studies was the determination of the structure of materials used, and the waste forms produced. Capillary XRD studies were performed to make these determinations.

Although rotating anode XRD would yield higher resolution, radiological constraints dictate the use of sealed capillaries. The XRD results helped determine the chemical form of the plutonium-loaded salt to manufacture the ceramic waste forms, verify the quality of the zeolite used, and confirm that the zeolite/glass/salt mixture did, in fact, convert to sodalite as expected. Indications were also seen in the XRD data that various thermodynamic factors in the zeolite/salt exchange process affected the fate of the plutonium in the waste form.

3. Chemical Analysis of Nuclear Fuel Residues in Cladding Segments

The ACL analyzed a challenging set of samples related to a test carried out by engineers in CMT to evaluate how well their high throughput electrorefiner (HTER) will retain noble metals in the anode baskets when uranium is electrotransported from chopped metallic fuel (see also Sec. IV.A). In this test, two baskets in the inner channel of the HTER were loaded with segments of unirradiated uranium/zirconium/fissium metal alloy clad in stainless steel. The HTER was operated to achieve anodic dissolution and separation of the uranium in the segments, and then segments were taken from top to bottom of each basket. These segments were submitted to the ACL for chemical analysis of the residue in the cladding. The remaining segments were subsequently processed again in the HTER to increase the fraction of uranium removed from them, and a second set of segment samples was also submitted for analysis.

The ACL analysts first weighed each segment and then treated each one with a mixture of acids to dissolve the fuel residue while only slightly attacking the stainless steel cladding hull. After the fuel was dissolved, each cladding hull was washed, dried, and individually weighed. Solutions containing the dissolved residue from each segment were analyzed by ICP/AES to determine U, Zr, the fissium elements (Mo, Ru, Pd, and Rh), and electrorefiner salt constituents (Li, K, and Cd). The ICP/AES analysts also reported values for dissolved components of the stainless steel cladding (Fe, Ni, Cr, and Mn).

By measuring all these components, the analysts were able to compile the data in a way that allowed the mass of each element to be calculated relative to the mass of cladding in each segment. This, in turn, permitted an evaluation of the extent to which each fuel component had moved out of the cladding hull. In the end, a combination of thorough chemical analysis and creative presentation of the analysis results helped the CMT engineers obtain the information they required from their tests.

4. Analysis of Complicated Oxides for Melt Attack and Coolability Experiments

The Reactor Engineering Division at ANL is conducting Melt Attack and Coolability Experiments (MACEs) to investigate the interactions that will occur between molten core

components and concrete when the fuel debris from a severe reactor accident comes in contact with the basement of the reactor containment building under overlying water. The ACL has assisted these studies by providing comprehensive chemical analysis of samples retrieved from test assemblies, where prototypic corium is heated to the molten state and allowed to contact a concrete base with a water overlayer. The ACL analyzed a set of about 50 oxide samples that included portions of debris, solidified melts, crusts, and corium from MACEs and earlier advanced containment experiments.

The lithium tetraborate fusion procedure used for these analyses left only minor residues undissolved in most cases. The undissolved material was isolated and dissolved with a sealed-tube (Carius tube) procedure and analyzed separately for inclusion in the sample composition. Solutions obtained for each sample were analyzed by ICP/AES to provide information on 19 component elements. Completeness of each analysis was evaluated by calculating a sum-of-oxides mass balance; results ranged from 88 to 107%, with an average near 100%. Selected samples were also examined by XRD to identify major chemical phases present in them. The data from all the samples are being used by the MACE program to help interpret information recorded when individual frozen debris regions were formed during the tests. The data are also being used to develop and validate phase-segregation models employed in interpreting the MACE results.

5. Characterization of Phosphate-Ceramic-Stabilized Hazardous Waste

Researchers in the ANL Energy Technology Division (ET) are developing a stabilization process that converts solid waste materials into chemically bonded phosphate ceramics. These ceramics have physical properties that make them good candidates for use as structural products. During 1998, ACL staff assisted this development by performing tests to determine the leach resistance of both simulated and actual wastes at several stages in the stabilization process. In this work, we applied the Toxicity Characteristic Leaching Procedure (TCLP), as described in U.S. EPA Method 1311, and other standard leaching tests.

In applying the TCLP, we extracted waste samples with an acetic acid buffer solution to simulate leaching that might occur under landfill conditions. The leachates were analyzed by ICP/AES, ICP/MS, and cold vapor atomic absorption to determine the concentrations of Pb, Cd, Cr, Ni, As, Ba, Se, Ag, Mo, Fe, Cs, Ru, Sr, La, Nd, Y, Hg, and other elements. In addition, concentrations of the radioactive isotopes ^{137}Cs, ^{238}U, ^{235}U, ^{241}Am, ^{99}Tc, and ^{90}Sr were determined in waste samples by gamma spectrometry or radiochemical separation followed by alpha or beta counting methods. Ion chromatography was used to determine the concentrations of phosphate, nitrate, sulfate, and chloride leached from the ceramic matrix.

This year, TCLP tests were performed on (1) samples from ceramic stabilization of hazardous metals in solid and liquid radioactive wastes from experimental processes and (2) simulated waste forms that contained hard-to-stabilize chemical species such as anionic forms of hazardous metals like chromate, antimonate, selenate, and arsenate ions. Some TCLP test results evaluated the effectiveness of chemical treatment (e.g., with reducing agents) in helping stabilize such anionic species. With this information, the ET researchers are developing

treatment alternatives and strategies that permit their process to handle a wide variety of waste compositions.

6. Chemical Analysis of Lithium Aluminate for the Tritium Target Qualification Project

In its Tritium Target Qualification Project (TTQP), Battelle's Pacific Northwest National Laboratory is coordinating manufacture of ^{6}Li-enriched lithium aluminate ceramic pellets for use as tritium-production targets for DOE. The ceramic pellets are made by sintering lithium aluminate powders prepared with a specified lithium isotopic composition and lithium-to-aluminum stoichiometry. The ACL became involved in the TTQP during 1997, when we were asked to provide chemical analysis of developmental batches of the powder and pellet materials and to perform certification analysis of two production lots of pellets incorporated into a pilot-scale assembly that was fabricated for demonstration testing of the tritium-producing technology. We used a special sealed-tube procedure for dissolving the refractory samples in hydrochloric acid at 300°C. The solutions were then analyzed by thermal-ionization mass spectrometry to determine lithium isotope ratios, specialized assays to determine lithium (using isotope dilution) and aluminum (by 8-hydroxyquinolate gravimetry), and an acid-reaction/gas-evolution procedure to measure carbonate impurity.

During 1998, the TTQP pursued efforts with private-sector commercial vendors to develop production-scale processes for manufacturing the lithium aluminate powders and pellets needed for tritium production in coming years. In support of these efforts, the ACL provided chemical analysis of several developmental powder and pellet batches using our qualified procedures. Results of our measurements helped to evaluate alternative production methods and processes and to identify products that met program specifications.

7. Alternative Methods for Analysis of Lithium Aluminate Ceramics

The ACL has been providing data from chemical analysis of lithium aluminate ceramic materials to the Tritium Target Qualification Project (TTQP). This project has been administered by Pacific Northwest National Laboratory (PNNL) for nearly two years, during which the program has worked to establish capabilities comparable to the private sector. Some of the procedures that we use in the ACL for specific analyses were developed years ago and are required for the current work because they are established and qualified, even though alternatives exist that might be more attractive in a situation involving higher volume production. Recently, PNNL asked analysts in the ACL to investigate two alternative methods that appeared to offer particular advantages.

One study looked at an instrumental combustion method for total carbon to replace the acid-reaction/carbon-dioxide-evolution method currently used to measure carbonate impurity in lithium aluminate. The total carbon determination is fast and efficient. The total carbon in specimens we tested correlated strongly with carbonate content but showed that the ceramics also contained carbon in forms other than carbonate. Based on these results, the TTQP is reviewing the lithium aluminate specifications and expects to replace the carbonate limit with a

limit on total carbon. This change will better address the basis for the carbonate limit and, at the same time, permit use of the more efficient instrumental method by laboratories that test the ceramic materials.

The other alternative method involves replacement of the current sealed-tube (Carius tube) method we have used for dissolving dense gamma-phase lithium aluminate for subsequent analysis operations. The alternative dissolution uses a newly available microwave apparatus for sample heating and digestion. The microwave apparatus has performance specifications that allow heating the Teflon digestion vessels holding the samples to temperatures approaching the 300°C for the Carius tube method. Work completed so far has demonstrated that the microwave system is capable of achieving complete dissolution. However, we have found that performance is not uniform when multiple Teflon vessels are heated at the same time. Because the microwave system promises convenient operation, enhanced efficiency, and ready transfer of operations to commercial laboratories, we plan to pursue resolution of this shortcoming in the next year.

8. The Department of Energy's Integrated Performance Evaluation Program

The ACL is developing and implementing a comprehensive Integrated Performance Evaluation Program (IPEP) for DOE's Office of Environmental Management as part of its National Analytical Management Program. The IPEP is designed to provide information on the quality of radiological and nonradiological analysis data generated by all analytical chemistry laboratories that provide DOE and its contractors with data on environmental restoration and waste management samples. The ACL has been assisting in developing program requirements and in implementing the program. The staff of CMT's Computer Applications, Network, and Security Group has assisted the ACL in developing strategies and systems for handling large data sets and in compiling and analyzing data from performance evaluation program studies.

We redesigned and updated the IPEP World Wide Web server (http://www.cmt.anl.gov/ipep/ipep.html). The web site contains general information about the IPEP, including contact names, distribution schedules for performance evaluation program studies, and hyperlinks to other servers of interest.

9. Performance Demonstration Programs for the WIPP

The Waste Isolation Pilot Plant (WIPP) is a DOE installation in Carlsbad, NM, designed to dispose of transuranic (TRU) waste left from the research and production of nuclear weapons. The ACL was also involved with the preparation and distribution of performance demonstration samples that simulate the headspace in WIPP waste canisters. The ACL acquired relevant gases from a specialty gas vendor and used them to prepare standard gas mixtures containing known concentrations of various volatile organic compounds (VOCs), hydrogen, and methane. These standard gas mixtures were metered through a heated, multiport manifold (constructed by ACL) into several SUMMA canisters simultaneously, which provided uniform samples in each canister. The canisters were labeled, packaged, and shipped to laboratories that the WIPP Carlsbad Area Office wants to qualify for headspace gas analysis. The ACL performed a

confirmation analysis on an aliquot of each of the gas mixtures for VOCs, methane, and hydrogen.

10. Multiagency Radiochemistry Laboratory Analytical Procedures

The *Multiagency Radiochemistry Laboratory Analytical Procedures Manual* is being drafted to provide guidance in all relevant areas of radioanalytical work for laboratory personnel and project managers. Agencies contributing to this document include DOE, the Environmental Protection Agency, the Department of Defense, and the Nuclear Regulatory Commission. The manual discusses the theory and background of various analytical techniques as applied to samples containing radiological analytes. It is designed to be of use to developers of standard operating procedures for radiological analyses, so they can understand various options and choose the best analytical approach for a given situation.

Because of our radiological expertise, the ACL was asked to provide technical support to the manual. Members of the ACL wrote chapters on "Sample Dissolution, Separation Techniques, and Evaluation of Radiological Laboratories" and also provided technical comments on a chapter about "Sample Preparation."

11. Analytical Services for Site Remediation

The ACL, in cooperation with the Energy Systems Division, set up an analytical system in a mobile laboratory for ANL's Environmental Management Operations (EMO). The mobile laboratory was designed to remediate soil contaminated with VOCs at a hazardous site within the ANL-East boundaries. The system comprised a static headspace sampler followed by gas chromatography/mass spectrometry (GC/MS) analysis. It was used to quantitate the levels of a wide range of VOCs in the experimentally treated soil. An analytical method was developed that allowed fast screening of samples that may be contaminated at a level from 10 ppb to 500 ppm. Several hundred samples were analyzed, with very fast turnaround time. Having data on hand helped EMO to quickly address remediation needs instead of having to wait weeks to get results back from contract laboratories. The data that we were able to provide with quick turnaround time were compared to the full RCRA (Resource Conservation and Recovery Act) analysis of the same soils and showed good agreement. Since the work was done in a mobile on-site laboratory, shipping and other sample handling costs were greatly reduced.

12. Support for Development of High-Temperature Superconductors

The researchers in the Chemistry and Materials Science Divisions have been developing methods for depositing thin films of high-temperature superconducting compounds on semiconductor substrates such as silicon. For these development efforts, ACL characterized impurities in the films and determined the elemental stoichiometry of the major constituents. For this work, ACL analysts also devised ways to effectively dissolve the thin film coatings without attacking the underlying substrates. The solutions obtained have been analyzed by ICP/AES and ICP/MS to measure the very small amounts of individual elements present in the films. These efforts have permitted characterization of microgram quantities of material contained in films

that are only a thousand angstroms thick. Through these and related activities, the teamwork among chemists, ceramists, and analysts is helping to move the technology of superconducting ceramics toward practical applications.

13. Characterization of Silo Waste for Fluor Daniel Fernald

Fluor Daniel Fernald is evaluating options for the remediation of material stored in Silos 1 and 2 of Operable Unit 4 at the Fernald site in Ohio. The material in these silos consists predominantly of residues from pitchblende ore processed to extract uranium. To aid in selecting among available treatment options for remediating the silo contents, Fluor Daniel Fernald requested that the ACL analyze material from each of the two silos to identify the primary chemical compounds present.

In this effort, we determined the elemental composition of three subportions of each silo material and examined corresponding subsamples by XRD to provide information on specific compounds present. For the elemental analysis, each subsample was analyzed to determine 33 elements, including carbon, sulfur, phosphorus, and an assortment of metals. Of these, 31 elements were determined by ICP/AES after total dissolution of each sample using a lithium tetraborate fusion. Carbon and sulfur were measured with commercial combustion analyzers. We also determined the distribution of carbon between organic and inorganic (carbonate) forms in selected samples. Ultimately, information from the elemental determinations and XRD patterns was combined and interpreted to allow assignment of the major components in each material to specific compounds. This analysis resulted in our assigning approximately 86% of the Silo 1 material's mass to the specific compounds. In the Silo 2 material, an average of 81% of the material's mass was assigned to specific compounds. Fluor Daniel Fernald is evaluating these results with regard to potential implications for various processes to stabilize the silo materials for disposal.

14. Chemometrics: Sensor Algorithms and Medical Image Analysis

Progress was made on two ongoing chemometric projects this year. The first project involves the development of algorithms and a data analysis system for multivariate sensor data. Advanced sensors of any type (optical, chemical, electrochemical, nuclear, etc.) provide voluminous quantities of data that must be extracted in near real-time and converted into a form useful for decision makers. Goals are the following: (1) extract information from sensor data, including hyperspectral imagers, (2) use quantitative/qualitative algorithms to model the extracted information, (3) conduct all operations in near real-time, and (4) provide estimates of the reliability of the final answers.

Algorithms in C/C++, Fortran, and Matlab have been developed to perform data preprocessing, linear discriminate analysis, digital signal processing, and neural network modeling. A multivariate calibrations module has been developed, which includes a partial least squares (PLS) algorithm and an improved principal component regression (IPCR) algorithm. The latter provides statistical estimates of the reliability of the model answers. A graphical user interface in Matlab was completed to enable easy application of the preprocessing, pattern

recognition, and multivariate calibration modules. The data analysis package is now available for Win95/WinNT, as well as UNIX operating systems.

The second chemometric project is a collaborative effort with the Theumatology Clinic at the University of Chicago Center for Advanced Medicine. We are investigating the efficacy of thermal imaging for monitoring the extremities of rheumatoid arthritis patients. Rheumatoid arthritis randomly attacks the joints, causing pain, inflammation, and deformity. This clinical study has monitored over 30 rheumatoid arthritis patients during a four-month period. An infrared camera was used to acquire thermal images of the hands, feet, and knees of the patients. Blood tests and physical examinations were also conducted. Multivariate statistical analysis is being used to determine the correlation between the information provided by the thermal images and the traditional medical measurements.

15. Preparation of Osmium-189 Targets for Photon Excitation Studies

In collaboration with researchers in the Physics Division, the ACL prepared an osmium target for photon excitation studies by electroplating osmium metal into a copper planchet. The resulting target was used for photon excitation studies in which the high flux of protons from the Advanced Photon Source (APS) would excite osmium nuclei by a process called "nuclear excitation by electron transition." The initial preparation of osmium targets was very successful; the starting point was dissolution of osmium tetraoxide in a plating solution containing sodium hydroxide, sodium monohydrogen phosphate, sulfamic acid, and potassium hydroxide.

Subsequent to this initial work, the team of physicists wanted to produce ^{189}Os isotope targets by starting with metallic osmium rather than osmium oxide. Only 100 mg of metallic ^{189}Os powder was available. To ensure the conversion of ^{189}Os metal into osmium tetraoxide, a separate experiment was carried out successfully with isotopically "natural" metallic osmium. To convert metallic osmium into osmium tetraoxide, the metal must be heated in the presence of oxygen, which produces gaseous osmium tetraoxide. A special apparatus was assembled to efficiently trap all of the gas generated, which was then dissolved in a plating solution. The ^{189}Os electroplated targets were used in APS and generated very useful data.

16. Effect of Spectral Resolution on Pattern Recognition Analysis Using Passive Fourier Transform Infrared Sensor Data

Previous work in ACL resulted in the development of an automated pattern recognition methodology for use with sensor data.[2] In collaboration with Ohio University, the Fourier transform infrared (FTIR) spectral data of two nerve agent simulants, diisopropyl methyl phosphonate (DIMP) and dimethyl methyl phosphonate (DMMP), were used as test cases to

[2] J. J. Laidler et al., *Chemical Technology Division Annual Technical Report, 1997,* Argonne National Laboratory Report ANL-98/13, pp. 162-163 (1998).

determine the spectral resolution that gives optimal pattern recognition. The DIMP simulant was used as the target analyte for detection, while DMMP was used to test the ability of the pattern recognition methodology to detect the analyte selectively. A passive FTIR sensor was used to collect interferogram data. The methodology was based on the application of pattern recognition techniques to short segments of single-beam spectra obtained by Fourier processing the collected interferogram data.

This work examined the effect of varying spectral resolution on the quality of pattern recognition results. The objective was to determine the optimal spectral resolution to be used for data collection. The results of this study indicated that the data with a nominal spectral resolution of 8 cm^{-1} provide sufficient selectivity to give pattern recognition results comparable to those obtained by using higher resolution data. We found that, while higher resolution did not increase selectivity sufficiently to provide better pattern recognition results, lower resolution decreased selectivity and degraded the pattern recognition results. These results can be used as guidelines to maximize detection sensitivity, minimize the time needed for data collection, and reduce data storage requirements.

17. Radiological Analysis Support for Sampling Sites of U.S. EPA Region V

In 1994, Environmental Protection Agency (EPA) Region V and the ACL established an interagency agreement so that the ACL could provide special analytical services (SAS) for samples collected within Region V. This agreement requires that, to the extent possible, SAS samples be analyzed by methods found in the EPA compendium *Test Methods for Evaluating Solid Waste, Physical/Chemical Methods* (SW-846). Alternative methods may be used with prior EPA approval. In 1998, a large number of samples were received for the determination of specific radionuclides. The samples were submitted as part of three major programs for site remediation.

One site in Ottawa was used in the past by a company that applied luminescent paint containing ^{226}Ra to clock dials. As a part of a followup to determine the integrity of landfills used to hold waste removed from this site after its demolition, two separate sampling phases resulted in 410 soil and water radiological samples being taken from a landfill, the area around an original company building foundation, and the surrounding grounds. The samples were submitted to the ACL for the determination of ^{226}Ra by gamma spectroscopy and $^{235/238}U$ and ^{232}Th by alpha spectroscopy. Analytical results for all samples were reported in 18 data packages, which contained all analytical results, quality control data, instrument output, and other documentation associated with the samples (notebook entries, chain-of-custody forms, etc.).

Two sites in Michigan, the Belding Warehouse (Belding, MI) and the Benton Harbor Warehouse (Benton Harbor, MI), were privately owned facilities. Each site was used to store hundreds of World War II artifacts, including airplane instrument panel gauges, switches, and compasses that were marked with luminescent paint containing ^{226}Ra. Material stored at both facilities was later found to be contaminated with radium dust from deteriorating gauges. Shredded material (180 samples) was packed and shipped to the ACL in one-gallon metal paint

cans to be analyzed by gamma counting. Because the ACL uses a high purity germanium detector and the contractor a NaI detector, a self-absorption curve unique to the sample and the sample geometry was developed by ACL analysts for the germanium detector. Analytical results for all samples were reported in eight data packages, which contained all analytical results, quality control data, instrument output, chain-of-custody records, notebook entries, and other related documentation.

18. Characterization of Particulate Debris from a Commercial Nuclear Reactor

The ACL helped provide base composition information on several samples of particulate debris that were obtained during scheduled maintenance operations on the cooling systems of a commercial nuclear reactor, the Point Beach Nuclear Power Plant in Two Rivers, WI. The samples included particulate matter removed from a primary coolant pump seal, material obtained from a wipedown cleaning of a filter assembly, and material collected from a blowdown flow-throttle valve in the steam generator. Many of the samples were slightly radioactive.

The ACL's approach to characterizing each particulate composition included examining the debris samples by XRD and determining their elemental composition by ICP/AES analysis of a solution obtained by dissolving a portion of each material. Some samples were also analyzed for leachable anions and carbon. The combination of data from the measurements made on these samples permitted assignment of the particulate debris to several types of ferrous and non-ferrous metal corrosion products. This information is being used by Wisconsin Electric Power Co. to understand observations their staff made during maintenance operations at their Point Beach Plant and, thereby, to improve plant performance.

19. Quality Assurance Laboratory Support to the U.S. Army Corps of Engineers

In October 1997, the U.S. Army Corps of Engineers (USACE) assumed responsibility for the Formerly Utilized Sites Remedial Action Program, which had been the responsibility of the DOE since 1974. The objectives of this program are to study and remediate sites having radioactive materials from DOE and its predecessors' operations, dating back in some cases to the Manhattan Project. In late 1998, the Buffalo and Baltimore Districts of the USACE requested the ACL to serve as a Quality Assurance Laboratory for the analysis of ambient matrix samples (e.g., soil, sediment, ground or surface water) from various remediation sites. In this role, the ACL receives and analyzes split samples for organic, inorganic, and radiological parameters to provide reference data that may be used to corroborate analysis results previously obtained by the primary production laboratories on samples from the same locations. All organic and inorganic analytes are determined using existing ACL facilities and procedures and methods described in the U.S. EPA laboratory manual *Test Methods for Evaluating Solid Waste, Physical/Chemical Methods* (SW-846), in accordance with instructions from the USACE. Radiological measurements are carried out according to U.S. EPA methods and established ANL methods and procedures.

In 1998, the ACL received samples from two sites under the jurisdiction of the Buffalo District: the Luckey Site in Ohio, which was a magnesium and beryllium processing facility that received radiologically contaminated scrap metal from the Atomic Energy Commission, and the Ashland 2 site in Tonawanda, New York, which was used from 1974 to 1982 to store soil containing low-level radioactive residues. Samples from the Colonie site in New York, which is under the jurisdiction of the Baltimore District, were also received. Analysis has begun on these samples and will be completed in early 1999.

20. Characterization of Top-of-Rail Lubricant Byproduct

The Energy Technology Division is collaborating with Tranergy Inc. and Texaco in testing several proprietary lubricants developed by Texaco to reduce friction between the rail tracks and locomotive wheels. The reduction in friction should lead to lower energy consumption by the locomotive engines and less wear on the rail hardware. When the engines are in front of the train, the lubricant is applied on the rail tracks behind the engines to allow normal traction between the tracks and the wheels of the engine, while friction between the tracks and the rail cars is minimized. The automated system that applies the lubricant calculates the amount of lubricant needed based on the weight of the rail cars and the length of the train. The lubricant is expected to significantly lose its lubrication power during use by a train before the next train uses the same tracks.

One of the tasks of the project is to identity volatile and semivolatile byproducts produced during use of the lubricants. A device built by Tranergy Inc. that allows accurate measurement of friction between a simulated track and wheel system was used in applying lubricant and collecting residue from the tracks after a defined period of use. The ACL analyzed samples of lubricant before and after application; GC/MS was used to identify major components of the proprietary lubricant. In preliminary work, only minor semivolatile byproducts have been detected in the lubricant after its use in the test apparatus constructed by Energy Technology personnel for this project. Identification of these compounds is in progress. A device is under construction to collect VOCs that may be produced during use of the lubricants.

VIII

Publications and Presentations—1998

The Division's publications and oral presentations for 1998 were entered into a bibliographic data base. The pages that follow are a printout of this information sorted into six categories: (1) journal articles, books, and book chapters, (2) patents, (3) ANL progress and topical reports, as well as contributions to reports published by organizations other than ANL, (4) abstracts and papers published in proceedings of conferences, symposia, workshops, etc., (5) oral presentations at scientific meetings and seminars not referenced in the fourth category, and (6) papers accepted for publication but not yet published.

Chemical Technology Division Publications and Presentations—1998

A. Journal Articles, Books, and Book Chapters

Modeling of a Zeolite Column for the Removal of Fission Products from Molten Salt
R. K. Ahluwalia, H. K. Geyer, C. Pereira, and J. P. Ackerman
Ind. Eng. Chem. Res. **37**(1), 145–153 (1998)

New Process for Low Temperature Preparation of $LiNi_{1-x}Co_xO_2$ Cathode Material for Lithium Cells
K. Amine, H. Yasuda, and Y. Fujita
Annales de Chimie, Science des Materiaux **23**, 37–42 (1998)

New Process for Loading Highly Active Platinum on Carbon Black Surface for Application in Polymer Electrolyte Fuel Cell
K. Amine, K. Yasuda, and H. Takenaka
Annales de Chimie, Science des Materiaux **23**, 331 (1998)

Review of *Biotechnology for Waste and Wastewater Treatment*, by N. P. Cheremisinoff
J. E. Banaszak
Environ. Prog. **17**(1), S9–S10 (1998)

Speciation-Dependent Toxicity of Neptunium(V) towards *Chelatobacter heintzii*
J. E. Banaszak, D. T. Reed, and B. E. Rittmann
Environ. Sci. Technol. **32**(8), 1085–1091 (1998)

A Switchable Radioactive Neutron Source: Proof-of-Principle
D. L. Bowers, E. A. Rhodes, and C. E. Dickerman
J. Radioanal. Nucl. Chem. **233**(1–2), 161–165 (1998)

Investigation of the Vibrational Properties of OCN^- on a Silver Electrode by *In-Situ* Synchrotron Far Infrared Spectroscopy and Visible-Infrared Sum Frequency Generation Spectroscopy
G. A. Bowmaker, J. M. Leger, A. LeRille, C. A. Melendres, and A. Tadjeddine
J. Chem. Soc., Faraday Trans. **94**(9), 1309–1313 (1998)

Microstructural Characterization of an HDS-Active Co_6S_8-Pillared Molybdenum Sulfide
J. R. Brenner, C. L. Marshall, L. Ellis, N. A. Tomczyk, J. Heising, and M. Kanatzidis
Chem. Mater. **10**(5), 1244–1257 (1998)

Materials Derived from Synthetic Organo-Clay Complexes as Novel Hydrodesulfurization Catalyst Supports
K. A. Carrado, C. L. Marshall, J. R. Brenner, and K. Song
Microporous Mesoporous Mater. **20**, 17–26 (1998)

The Role of pE, pH, and Carbonate on the Solubility of UO_2 and Uraninite under Nominally Reducing Conditions

I. Casas, J. de Pablo, J. Gimenez, M. E. Torrero, J. Bruno, E. Cera, R. J. Finch, and R. C. Ewing

Geochim. Cosmochim. Acta **62**, 2223–2231 (1998)

Use of Sol-Gel Systems for Solid/Liquid Separation

D. J. Chaiko, J. P. Kopasz, and A. J. G. Ellison

Ind. Eng. Chem. Res. **37**, 1071–1078 (1998)

The U.S. Department of Energy—Investing in Clean Transportation

S. G. Chalk, J. Milliken, J. F. Miller, and S. R. Vankateswaran

J. Power Sources **71**, 26–35 (1998)

Oxygen Atom Transfer from μ-Oxo-bis[1,4,8,11,15,18,22,25-octakis(trifluoromethyl)phthalocyaninato] dirhodium(III): Evidence for an Fe(IV) = O Intermediate

M. J. Chen, D. E. Fremgen, and J. W. Rathke

J. Porphyrins Phthalocyanines **2**, 473–482 (1998)

Recent Advances in Metallaphthalocyanine-Catalyzed Carbon-Hydrogen Bond Activation

M. J. Chen and J. W. Rathke

Trends in Inorganic Chemistry **5**, 29–41 (1998)

Paramagnetic Rh(III) Complexes from Reactions of Phosphines with Hydride-Bridged and Nonbridged Rhodium Phthalocyanine Dimers: Metal-to-Ligand Charge Transfer Induced by Phosphines

M. J. Chen, L. M. Utschig, and J. W. Rathke

Inorg. Chem. **37**(22), 5786–5792 (1998)

Assessment of Complete Basis Set Methods for Calculation of Enthalpies of Formation

L. A. Curtiss, K. Raghavachari, P. C. Redfern, and B. B. Stefanov

J. Chem. Phys. **108**(2), 692–697 (1998)

Assessment of Gaussian-2 and Density Functional Theories for the Computation of Ionization Potentials and Electron Affinities

L. A. Curtiss, P. C. Redfern, K. Raghavachari, and J. A. Pople

J. Chem. Phys. **109**(1), 42–55 (1998)

A Novel Fermentation Pathway in an *Escherichia coli* Mutant Producing Succinic Acid, Acetic Acid, and Ethanol

M. I. Donnelly, C. S. Millard, D. P. Clark, M. J. Chen, and J. W. Rathke

Appl. Biochem. Biotechnol. **70–72**, 187–198 (1998)

Outlier Detection in Multivariate Analytical Chemical Data

W. J. Egan and S. L. Morgan

Anal. Chem. **70**(11), 2372–2378 (1998)

$LiMn_{2-x}Cu_xO_4$ Spinels ($0 \leq x \leq 0.5$)—A New Class of 5 V Cathode Materials for Lithium Batteries: I. Electrochemical, Structural and Spectroscopic Studies

Y. Ein-Eli, W. F. Howard, S. H. Lu, S. Mukerjee, J. McBreen, J. T. Vaughey, and M. M. Thackeray

J. Electrochem. Soc. **45**(4), 1238–1244 (1998)

Reactions of Hexafluorides of Uranium, Neptunium, and Plutonium with Nitrogen Oxides and Oxyfluorides. Synthesis and Characterization of $(NO)[N_pF_6]$ and $(NO)[PuF_6]$

P. G. Eller, J. G. Malm, B. I. Swanson, and L. R. Morss

J. Alloys Compounds **269**, 50–56 (1998)

Structural Relations among Schoepite, Metaschoepite and "Dehydrated Schoepite"

R. J. Finch, F. C. Hawthorne, and R. C. Ewing

Can. Mineral. **36**, 831–845 (1998)

Pyrolysis Gas Chromatography/Mass Spectrometry Investigation of a Thermally Cured Polymer

R. C. Galipo, W. J. Egan, J. F. Aust, M. L. Myrick, and S. L. Morgan

J. Anal. Appl. Pyrolysis **45**(1), 23–40 (1998)

In Situ Imaging of Charge Carriers in an Electrochemical Cell

R. E. Gerald, R. J. Klingler, J. W. Rathke, G. Sandí, and K. Woelk

In Chapter 9 of *Spatially Resolved Magnetic Resonance*, Eds., P. Blümler, B. Blümich, R. Botto, and E. Fukushima, Wiley-VCH, New York, pp. 111–119 (1998)

Analytical Electron Microscopy Study of Surface Layers Formed on the French SON68 Nuclear Waste Glass During Vapor Hydration at 200°C

W. L. Gong, L. M. Wang, R. C. Ewing, E. Vernaz, J. K. Bates, and W. L. Ebert

J. Nucl. Mater. **254**, 249–265 (1998)

Chemistry and Management Education

D. W. Green

Managing the Modern Laboratory **3**(2), 29A–31A (1998)

Forum on Hiring the Right Person the First Time

D. W. Green

Managing the Modern Laboratory **3**(1), 11A–16A (1998)

Management Style—What is It?

D. W. Green

Managing the Modern Laboratory **3**(3), 45A–46A (1998)

Missed Communication

D. W. Green

Managing the Modern Laboratory **3**(1), 4A–6A (1998)

Pore-Structure Determinations of Silica Aerogels by ^{129}Xe NMR Spectroscopy and Imaging
D. M. Gregory, R. E. Gerald, and R. E. Botto
J. Magn. Reson. A **131**(2), 327–335 (1998)

^{129}Xe MRM Characterization of Pore Structures in Silica Aerogels
D. M. Gregory, R. E. Gerald, D. J. Clifford, and R. E. Botto
In Chapter 13 of *Spatially Resolved Magnetic Resonance*, Eds., P. Blümler, B. Blümich, R. Botto, and E. Fukushima, Wiley-VCH, New York, pp. 163–177 (1998)

A Comparison of Two Aluminizing Methods for Corrosion Protection in the Wet Seal of Molten Carbonate Fuel Cells
J. E. Indacochea, I. Bloom, M. Krumpelt, and T. G. Benjamin
J. Mater. Res. **13**(7), 1834–1839 (1998)

Ceramic Breeder Materials: Status and Needs
C. E. Johnson, K. Noda, and N. Roux
J. Nucl. Mater. **258–263**, 140–148 (1998)

Spectroscopic Study of the Proton Dynamics in Manganese Dioxide Electrode Materials
C. S. Johnson, M. M. Thackeray, J. C. Nipko, and C.-K. Loong
Physica B **241–243**, 1252–1254 (1998)

Hydrogen Activation in Oxo Catalysis
R. J. Klingler and J. W. Rathke
The Chemist **75**(3), 23–28 (1998)

Hermetic Holder for X-ray Powder Diffraction of Air-Sensitive Differential Scanning Calorimetry Samples
D. Lexa
Rev. Sci. Instrum. **69**(12), 4249–4250 (1998)

Analysis of X-ray Absorption Spectra of Some Nickel Oxycompounds Using Theoretical Standards
A. N. Mansour and C. A. Melendres
J. Phys. Chem. **102**(1), 65–81 (1998)

In-Situ X-ray Absorption Spectroscopic Study of Electrodeposited Nickel Oxide Films during Redox Reactions
A. N. Mansour, C. A. Melendres, and J. Wong
J. Electrochem. Soc. **145**(4), 1121–1125 (1998)

Evaluation of Stainless Steel-Zirconium Alloys as High-Level Nuclear Waste Forms
S. M. McDeavitt, D. P. Abraham, and J. Y. Park
J. Nucl. Mater. **257**(1), 21–34 (1998)

Synchrotron Infrared Spectroscopy of Electrode Surfaces and Interfaces
C. A. Melendres
Synchrotron Radiation News **11**(3), 39–46 (1998)

In-Situ Synchrotron Far Infrared Spectroscopy of Surface Films on a Copper Electrode in Aqueous Solutions
C. A. Melendres, G. A. Bowmaker, J. M. Leger, and B. Beden
J. Electroanal. Chem. **449**(1–2), 215–218 (1998)

The Formation of the Transition and Inner-Transition Metal to Transition and Inner-Transition Metal Bond
L. R. Morss
Inorganic Reactions and Methods, Ed., J. D. Atwood, Wiley-VCH, New York, Vol. 14, pp. 3–16 (1998)

Argonne "Green" Magnets Pick Up More than Nails
L. Nuñez and J. M. Andrew
Pollution Prevention Advisor **8**(1), 2 (1998)

Magnetically Assisted Chemical Separation Process
L. Nuñez and M. D. Kaminski
Filtr. Sep. **35**(4), 349–352 (1998)

Separating Metals Using Coated Magnetic Particles
L. Nuñez and M. D. Kaminski
CHEMTECH **28**(9), 41–46 (1998)

Review of *Hazardous Waste Planning*, by J. A. Soesilo and S. R. Wilson
J. B. Rajan
Environ. Prog. **17**(1), S7 (1998)

Reduction of Np(VI) and Pu(VI) by Organic Chelating Agents
D. T. Reed, S. B. Aase, D. G. Wygmans, and J. E. Banaszak
Radiochim. Acta **82**, 109–114 (1998)

FTIR and Hyphenated FTIR Techniques for the Analysis of Foods
G. T. Reedy and M. M. Mossoba
Chapter 7 in *Spectral Methods in Food Analysis, Instrumentation and Applications*, Ed., M. M. Mossoba, Marcel Dekker, Inc., New York, pp. 325–396 (1998)

Ceramic Breeder Development
N. Roux, S. Tanaka, and C. E. Johnson
Fusion Eng. Des. **41**, 31–38 (1998)

Electrochemical and Spectroscopic Studies of Novel Carbonaceous Materials Used in Lithium Ion Cells
G. Sandi, R. E. Winans, K. A. Carrado, C. S. Johnson, and P. Thiyagarajan
J. New Mater. Electrochem. Syst. **1**, 83–88 (1998)

Structural Features of Low-Temperature $LiCoO_2$ and Acid-Delithiated Products
Y. Shao-Horn, S. A. Hackney, C. S. Johnson, A. J. Kahaian, and M. M. Thackeray
J. Solid State Chem. **140**(1), 116–127 (1998)

Microstructural Features of α-MnO_2 Electrodes for Lithium Batteries
Y. Shao-Horn, S. A. Hackney, C. S. Johnson, and M. M. Thackeray
J. Electrochem. Soc. **145**(2), 582–589 (1998)

Coprocessing Reactions of Illinois 6 Coal With Hondo Resid
Y. Shi, T. A. Cutler, and E. M. Eyring
Prepr. Pap. Am. Chem. Soc., Div. Fuel Chem. **43**, 344 (1998)

Kinetic Analysis of the Complexation of Aqueous Lanthanide(III) Ions by Arsenazo III
Y. Shi, E. M. Eyring, and R. van Eldik
J. Chem. Soc., Dalton Trans., 967 (1998)

Kinetics and Mechanism of Complexation of Aqueous Lanthanide Ions and UO_2^{2+} by PAR and PAN
Y. Shi, R. van Eldik, and E. M. Eyring
J. Chem. Soc., Dalton Trans., 3565 (1998)

Electrochemically Generated $CaCO_3$ Deposits on Iron Studied with FTIR and Raman Spectroscopy
L. J. Simpson
Electrochim. Acta **43**(16–17), 2543–2547 (1998)

Radiostrontium Analysis Using Sorbent Disks
L. L. Smith, F. Markun, J. S. Alvarado, K. A. Orlandini, K. M. Hoffmann, D. C. Seely, and R. T. Shannon
Current Protocols in Field Analytical Chemistry, Vol. I, John Wiley & Sons, Inc. (1998)

Li^+-Diglyme Complexes: Barriers to Lithium Cation Migration
A. Sutjianto and L. A. Curtiss
J. Phys. Chem. A **102**(6), 968–974 (1998)

Structural Fatigue in Spinel Electrodes in High Voltage (4 V) $Li/Li_x[Mn_2]O_4$ Cells
M. M. Thackeray, Y. Shao-Horn, A. J. Kahaian, K. D. Kepler, E. Skinner, J. T. Vaughey, and S. A. Hackney
Electrochem. Solid-State Lett. **1**(1), 7–9 (1998)

Counting Holes in Ni Complexes Using Integrated X-ray L Absorption Spectra
H. Wang, P. Ge, C. G. Riordan, S. Brooker, C. G. Woomer, T. Collins, C. A. Melendres, O. Graudejus, N. Bartlett, and S. P. Cramer
J. Phys. Chem. **102**, 8343 (1998)

On the Mechanism of Hematite Deposition on a Metal Surface under Nucleate Boiling Conditions
L. Wen and C. A. Melendres
Colloids Surf. A **132**(2-3), 315–319 (1998)

Imaging Diffusion with Non-Uniform B_1 Gradients

K. Woelk, B. L. J. Zwank, J. Bargon, R. J. Klingler, R. E. Gerald, and J. W. Rathke

In Chapter 8 of *Spatially Resolved Magnetic Resonance*, Eds., P. Blümler, B. Blümich, R. Botto, and E. Fukushima, Wiley-VCH, New York, 103–110 (1998)

Application of Instrumental Radioanalytical Techniques to Nuclear Waste Testing and Characterization

S. F. Wolf

J. Radioanal. Nucl. Chem. **235**(1–2), 207–212 (1998)

Chemical Studies of H Chondrites—IX. Volatile Trace Element Composition and Petrographic Classification of Equilibrated H Chondrites

S. F. Wolf and M. E. Lipschutz

Meteor. Planet. Sci. **33**, 303–312 (1998)

An Assessment of Density Functional Methods for Studying Molecular Adsorption in Cluster Models of Zeolites

S. A. Zygmunt, R. M. Mueller, L. A. Curtiss, and L. E. Iton

J. Mol. Struct. (Theochem.) **430**, 9–16 (1998)

B. Patents and Inventions

Fluid Clathrate System for Continuous Removal of Heavy Noble Gases from Mixtures of Lighter Gases

K. C. Gross, F. Markun, and M. T. Zawadzki

Patent No. 5,743,944, issued April 28, 1998

High Power Bipolar Battery/Cells with Enhanced Overcharge Tolerance

T. D. Kaun

Patent No. 5,736,275, issued April 7, 1998

Porous Silicon with Embedded Tritium as a Stand Alone Prime Power Source for Optoelectronic Applications

S.-W. Tam

Patent No. 5,765,680, issued June 16, 1998

Method for Treating Electrolyte to Remove Li_2O

Z. Tomczuk, W. E. Miller, G. K. Johnson, and J. L. Willit

Patent No. 5,711,019, issued January 20, 1998

Method for Encapsulating and Isolating Hazardous Cations, Medium for Encapsulating and Isolating Hazardous Cations

S. R. Wasserman, K. B. Anderson, K. Song, S. E. Yuchs, and C. L. Marshall

Patent No. 5,743,842, issued April 28, 1998

C. Reports

Practical Superconductor Development for Electrical Power Applications, Annual Report for FY 1998
U. Balachandran, T. R. Askew, Y. S. Cha, S. E. Dorris, J. T. Dusek, J. E. Emerson, B. L. Fisher, K. C. Goretta, K. E. Gray, J. R. Hull, D. S. Kupperman, M. T. Lanagan, M. Lelovic, S. Majumdar, V. A. Maroni, R. L. McDaniel, N. N. Merchant, D. J. Miller, R. C. Niemann, J. J. Picciolo, J. P. Singh, and A. S. Wagh
ANL-98/32 (October 1998)

Subsurface Interactions of Actinide Species and Microorganisms: Implications for the Bioremediation of Actinide-Organic Mixtures
J. E. Banaszak, B. E. Rittmann, and D. T. Reed
ANL-98/26 (October 1998)

Hydrogen-Fueled Polymer Electrolyte Fuel Cell Systems for Transportation
E. D. Doss, R. K. Ahluwalia, and R. Kumar
ANL-98/16 (August 1998)

Corrosion Behavior of Environmental Assessment Glass in Product Consistency Tests of Extended Duration
W. L. Ebert, E. C. Buck, J. S. Luo, S.-W. Tam, and J. K. Bates
ANL-98/27 (September 1998)

Formulation of a Candidate Glass for Use as an Acceptance Test Standard Material
W. L. Ebert, D. M. Strachan, and S. F. Wolf
ANL-98/10 (April 1998)

Data Needs for Long-Term Dry Storage of LWR Fuel
R. E. Einziger, D. L. Baldwin, and S. G. Pitman
TR-108757 (April 1998)

Yucca Mountain Project—Argonne National Laboratory, Annual Progress Report, FY 1997
P. A. Finn, D. J. Wronkiewicz, R. J. Finch, J. C. Hoh, C. J. Mertz, J. W. Emery, E. C. Buck, J. Fortner, S. F. Wolf, L. A. Neimark, and J. K. Bates
ANL-98/12 (June 1998)

Guideline for Gloveboxes, Second Edition
A. A. Frigo, R. F. Malecha, M. A. Slawecki, R. L. Tollner, S. G. Wiedmeyer, et al.
American Glovebox Society Report AGS-G001-1998 (July 1998)

Standard of Practice for the Application of Linings to Gloveboxes
A. A. Frigo, R. F. Malecha, S. G. Wiedmeyer, et al.
American Glovebox Society Report AGS-G003-1998 (July 1998)

Standard of Practice for the Design and Fabrication of Glovebags
A. A. Frigo, R. F. Malecha, S. G. Wiedmeyer, et al.
American Glovebox Society Report AGS-G002-1998 (July 1998)

Initial Results from Dissolution Rate Testing of N-Reactor Spent Fuel over a Range of Potential Geologic Repository Aqueous Conditions
W. J. Gray and R. E. Einziger
PNNL-11894, DOE/SNF/REP-022 (April 1998)

Analytical Chemistry Laboratory Progress Report for FY 1998
D. W. Green, A. S. Boparai, D. L. Bowers, D. G. Graczyk, and P. C. Lindahl (with contributions from ACL staff)
ANL/ACL-98/2 (December 1998)

Chemical Technology Division Annual Technical Report, 1997
J. J. Laidler et al.
ANL-98/13 (June 1998)

Natural Analogues of Nuclear Waste Glass Corrosion
J. S. Luo, T. A. Abrajano, and W. L. Ebert
ANL-98/22 (September 1998)

Nondestructive NMR Technique for Moisture Determination in Radioactive Materials Progress Report
L. Nuñez, R. E. Gerald, E. S. Growney, M. D. Kaminski, and S. E. Aumeier
ANL-98/19 (July 1998)

Gas Production Due to Alpha Particle Degradation of Polyethylene and Polyvinylchloride
D. T. Reed, J. C. Hoh, J. W. Emery, S. Okajima, and T. R. Krause
ANL-97/7 (July 1998)

A Data Base and a Standard Material for Use in Acceptance Testing of Low-Activity Waste Products
S. F. Wolf, W. L. Ebert, J. S. Luo, and D. M. Strachan
ANL-98/9 (April 1998)

D. Abstracts and Proceedings Papers

Metal Waste Forms from Treatment of EBR-II Spent Fuel
D. P. Abraham, D. D. Keiser, and S. M. McDeavitt
Proc. of the Int. Conf. on Decommissioning and Decontamination and on Nuclear and Hazardous Waste Management, Spectrum '98, Denver, CO, September 13–18, 1998, Vol. 2, p. 783 (1998)

Waste Form Development and Characterization in Pyrometallurgical Treatment of Spent Nuclear Fuel
J. P. Ackerman, S. M. McDeavitt, C. Pereira, and L. J. Simpson
Abstracts, Third Topical Meeting on DOE Spent Nuclear Fuel and Fissile Materials Management, Am. Nucl. Soc., Charleston, SC, September 8–11, 1998

Catalytic Partial Oxidation Reforming of Hydrocarbon Fuels
S. Ahmed, M. Krumpelt, R. Kumar, S. H. D. Lee, J. D. Carter, R. Wilkenhoener, and C. L. Marshall
Abstracts, Fuel Cell Seminar, Palm Springs, CA, November 16–19, 1998, pp. 242–245 (1998)

Thermodynamics of the Li_4SiO_4/H_2O System
C. Alvani, S. Casadio, and C. E. Johnson
Proc. of the Sixth Int. Workshop on Ceramic Breeder Blanket Interactions, Mito, Japan, October 22–24, 1997, pp. 7–14 (1998)

β-FeOOH, A New Positive Electrode Material for Lithium Secondary Batteries
K. Amine, H. Yasuda, and M. Yamachi
Proc. of the Ninth Int. Conf. on Lithium Batteries, Edinburgh, Scotland, United Kingdom, July 12–17, 1998, p. 14 (1998)

New Iron Oxide Positive Active Material for Lithium Secondary Batteries
K. Amine, H. Yasuda, and M. Yamachi
Abstracts, Fall Meeting of the Materials Research Soc., Boston, MA, November 30–December 4, 1998, Vol. 1, p. 371 (1998)

The Corrosion Behavior of a Pu Ceramic—Static Corrosion Test Results
A. J. Bakel, E. C. Buck, D. B. Chamberlain, S. F. Wolf, and B. B. Ebbinghaus
Proc. of the AIChE Spring National Meeting, New Orleans, LA, March 8–12, 1998

The Behavior of Different Elements during the Corrosion of Pu Titanate Ceramics
A. J. Bakel, E. C. Buck, B. B. Ebbinghaus, D. B. Chamberlain, and S. F. Wolf
Abstracts, 215th Am. Chem. Soc. National Meeting, Dallas, TX, March 29–April 2, 1998

Comparison of the Corrosion Behavior of Two Proposed Pu Immobilization Materials
A. J. Bakel, C. J. Mertz, E. C. Buck, J. Fortner, and D. B. Chamberlain
Abstracts, 18th Int. Congress on Glass, San Francisco, CA, July 5–10, 1998

X-ray Absorption Spectroscopy Studies of Electrochemically Deposited Thin Oxide Films
M. Balasubramanian, C. A. Melendres, A. N. Mansour, and S. Mini
Mater. Res. Soc. Symp. Proc. **524** (1998)

First-Principles Calculation of Atomic Structure and Electrochemical Potential of $Li_{1+x}V_3O_8$
R. Benedek, M. M. Thackeray, and L. H. Yang
Book of Abstracts, Ninth Int. Meeting on Lithium Batteries, Edinburgh, Scotland, United Kingdom, July 12–17, 1998

Structure and Electrochemical Potential Simulation for the Cathode Material $Li_{1+x}V_3O_8$
R. Benedek, M. M. Thackeray, and L. H. Yang
Mater. Res. Soc. Symp. Proc. **496**, 115 (1998)

MCFC Component Development at ANL
I. Bloom, T. D. Kaun, M. T. Lanagan, and M. Krumpelt
Abstracts, Fuel Cell Seminar, Palm Springs, CA, November 16–19, 1998, pp. 166–169 (1998)

Retention of Neptunium in Uranyl Alteration Phases Formed during Spent Fuel Corrosion
E. C. Buck, R. J. Finch, P. A. Finn, and J. K. Bates
Mater. Res. Soc. Symp. Proc. **506**, 87–94 (1998)

The Incorporation of Technetium into a Representative Low-Activity Waste Glass
W. L. Ebert, A. J. Bakel, D. L. Bowers, E. C. Buck, and J. W. Emery
Ceram. Trans. **87**, 431–440 (1998)

Dissolution Tests for Low-Activity Waste Product Acceptance
W. L. Ebert and S. F. Wolf
Proc. of the Spectrum '98 Meeting, Am. Nucl. Soc., Denver, CO, September 13–18, 1998, pp. 721–724 (1998)

Evaluation of a Standard Test Method and Material for Low-Activity Waste Product Acceptance
W. L. Ebert, S. F. Wolf, and D. M. Strachan
Proc. of the 18th Int. Glass Conf., Am. Ceram. Soc., San Francisco, CA, July 5–10, 1998

Oxidative Corrosion of UO_2 in High S/V Batch Experiments
R. J. Finch, S. F. Wolf, J. M. Hanchar, and J. K. Bates
Proc. of the Eighth Annual Int. High-Level Radioactive Waste Management Conf., Am. Nucl. Soc., Las Vegas, NV, May 11–14, 1998, pp. 619–620 (1998)

Corrosion Mechanisms of Spent Fuel under Oxidizing Conditions
P. A. Finn, R. J. Finch, E. C. Buck, and J. K. Bates
Mater. Res. Soc. Symp. Proc. **506**, 123–131 (1998)

Concentration of Uranium and Plutonium in Unsaturated Spent Fuel Tests
P. A. Finn, R. J. Finch, S. F. Wolf, and J. K. Bates
Proc. of the Third Topical Meeting on DOE Spent Nuclear Fuel and Fissile Materials Management, Am. Nucl. Soc., Charleston, SC, September 8–11, 1998, pp. 693–696 (1998)

Radionuclide Release in Vapor Tests by Means of Thin-Film Flow
P. A. Finn, S.-W. Tam, and J. K. Bates
Proc. of the Eighth Annual Int. High-Level Radioactive Waste Management Conf., Am. Nucl. Soc., Las Vegas, NV, May 11–14, 1998, pp. 622–624 (1998)

Terra Incognito: Spectra from Edges and Elements Not in the EELS Atlas
J. Fortner and E. C. Buck
Proc. of the Microscopy and Microanalysis '98 Conf., Atlanta, GA, July 12–16, 1998, Vol. 4, pp. 532–533 (1998)

Extended Electron Loss Fine Structure Analysis of Silicon-K Edges Using an Imaging Filter
J. Fortner, E. C. Buck, D. M. Strachan, and N. J. Hess
Proc. of the Microscopy and Microanalysis '98 Conf., Atlanta, GA, July 12–16, 1998, Vol. 4, pp. 706–707 (1998)

Heat-Shield Design for Glovebox Applications
A. A. Frigo, D. E. Preuss, and J. L. Bailey
Proc. of the Eleventh Annual Conf. and Exhibition of the Am. Glovebox Soc., Orlando, FL, July 13–15, 1998, pp. 34-51 (1998)

Toroid Cavity NMR Detector: Application to Electrochemical Systems
R. E. Gerald, R. J. Klingler, J. W. Rathke, G. Sandí, and K. Woelk
Program and Abstracts, 40th Rocky Mountain Conf. on Anaytical Chemistry, Denver, CO, July 25–August 1, 1998, p. 119 (1998)

In Situ NMR Analysis of Charge Carriers in Polymer Electrolytes
R. E. Gerald, R. J. Klingler, J. W. Rathke, G. Sandí, and K. Woelk
Program and Abstracts, 40th Rocky Mountain Conf. on Analytical Chemistry, Denver, CO, July 25–August 1, 1998, p. 46 (1998)

Applications of NMR for Nondestructive Evaluation of Nuclear Materials
E. S. Growney, R. E. Gerald, R. J. Klingler, J. W. Rathke, L. Nuñez, and S. E. Aumeier
Program and Abstracts, 40th Rocky Mountain Conf. on Analytical Chemistry, Denver, CO, July 25–August 1, 1998, p. 130 (1998)

Ceramic Waste Form Powder Preparation Techniques
M. C. Hash, C. Pereira, V. N. Zyryanov, M. A. Lewis, G. L. Burns, J. J. Smith, J. P. Thalacker, and J. P. Ackerman
Environmental Issues and Waste Management Technologies in the Ceramic and Nuclear Industries III, Eds., D. K. Peeler and J. C. Marra, Proc. of the Am. Ceram. Soc. Conf., p. 399 (1998)

Status of Shipping Provisions for Large Lithium Batteries

G. L. Henriksen

Proc. of the 15th Int. Seminar and Exhibit on Primary and Secondary Batteries, Fort Lauderdale, FL, March 2–5, 1998

Advanced Cell Technology for High Performance Li-Al/FeS_2 Secondary Batteries

G. L. Henriksen, A. N. Jansen, T. D. Kaun, J. Prakash, and D. R. Vissers

Proc. of the Eleventh Int. Symp. on Molten Salts, 193rd Electrochem. Soc. Meeting, San Diego, CA, May 3–8, 1998, Vol. 98-11, pp. 302–315 (1998)

Development of High Power Lithium Ion Battery

A. N. Jansen, A. J. Kahaian, K. D. Kepler, P. A. Nelson, K. Amine, D. W. Dees, D. R. Vissers, and M. M. Thackeray

Proc. of the Ninth Int. Conf. on Lithium Batteries, Edinburgh, Scotland, United Kingdom, July 12–17, 1998, p. 83 (1998)

Structural and Electrochemical Analysis of Layered Compounds from Li_2MnO_3

C. S. Johnson, S. D. Korte, T. E. Bofinger, Y. Shao-Horn, S. A. Hackney, J. T. Vaughey, and M. M. Thackeray

Book of Abstracts, Ninth Int. Meeting on Lithium Batteries, Edinburgh, Scotland, United Kingdom, July 12–17, 1998, Vol. 1, p. 170 (1998)

In-Situ Synchrotron Spectroscopy of Lithium Battery Positive Electrode Materials

C. S. Johnson, A. J. Kropf, J. T. Vaughey, and M. M. Thackeray

Abstracts, Fall Meeting of the Materials Research Soc., Boston, MA, November 30–December 4, 1998, Vol. 1, p. 568 (1998)

Microporous Titanium Oxide Anodes for Rechargeable Lithium Batteries

C. S. Johnson, L. D. Noailles, J. T. Vaughey, and M. M. Thackeray

Abstracts, 194th Electrochem. Soc. Meeting, Boston, MA, November 1–6, 1998, Vol. 98-2, p. 149 (1998)

Layered Lithium-Manganese Oxide Electrodes Derived from Rock-Salt $Li_xMn_yO_z$ (x+y=z) Precursors

C. S. Johnson, J. T. Vaughey, M. M. Thackeray, T. E. Bofinger, and S. A. Hackney

Abstracts, 194th Electrochem. Soc. Meeting, Boston, MA, November 1–6, 1998, Vol. 98-2, p. 161 (1998)

Electrometallurgical Treatment of Oxide Spent Fuel—Engineering-Scale Development

E. J. Karell and K. V. Gourishankar

Proc. of the Third Topical Meeting on DOE Spent Nuclear Fuel and Fissile Materials Management, Am. Nucl. Soc., Charleston, SC, September 8–11, 1998, pp. 682–688 (1998)

Resistivity of Bipolar Plate Materials at the Cathode Interface in Molten Carbonate Fuel Cells

T. D. Kaun, A. C. Schoeler, I. Bloom, M. T. Lanagan, and M. Krumpelt

Abstracts, 194th Electrochem. Soc. Meeting, Boston, MA, November 1–6, 1998, Vol. 98–2, Abstract No. 307 (1998)

Phase Development in As-Cast Zirconium-Based Alloys Containing Type 304 Stainless Steel and Pu

D. D. Keiser and S. M. McDeavitt

Light Metals, 1998, Ed., B. J. Welch, Proc. of the Technical Sessions Presented by the TMS Aluminum Committee at the 127th Annual Meeting of the Minerals, Metals, and Materials Soc., San Antonio, TX, February 15–19, 1998, pp. 1373–1378 (1998)

Copper-Tin Anodes for Rechargeable Lithium Batteries: An Example of the Matrix Effect in an Intermetallic System

K. D. Kepler, J. T. Vaughey, and M. M. Thackeray

Book of Abstracts, Ninth Int. Meeting on Lithium Batteries, Edinburgh, Scotland, United Kingdom, July 12–17, 1998, Vol. 1, p. 129 (1998)

Design, Integration, and Trade-Off Analyses of Gasoline-Fueled Polymer Electrolyte Fuel Cell Systems for Transportation

R. Kumar, R. K. Ahluwalia, E. D. Doss, H. K. Geyer, and M. Krumpelt

Abstracts, Fuel Cell Seminar, Palm Springs, CA, November 16–19, 1998, pp. 226–229 (1998)

Removal of CO from Reformate for PEFC Application

S. H. D. Lee, R. Kumar, and M. Krumpelt

Abstracts, Fuel Cell Seminar, Palm Springs, CA, November 16–19, 1998, pp. 578–581 (1998)

Sample Consistency Testing of the Glass-Sodalite Ceramic Waste Form

M. A. Lewis, C. W. Vander Kooi, and L. J. Simpson

Abstracts, Fall Meeting of the Materials Research Soc., Boston, MA, November 30–December 4, 1998

The Activity of Cobalt and Silicon in the Co-Si System with Special Focus on the α-Co Solid Solution

D. Lexa, R. J. Kematick, and C. E. Myers

Metall. Trans. A **28A**, 909–915 (1997)

Self-Radiation Induced Anisotropic Structure Damage in ^{244}Cm-Doped Orthophosphate $LuPO_4$

G. K. Liu, J. S. Luo, S. T. Li, C.-K. Loong, M. M. Abraham, J. V. Beitz, J. K. Bates, and L. A. Boatner

Mater. Res. Soc. Symp. Proc. **506**, 921 (1998)

Examination of Subaerially Altered Basaltic Glass with TEM and EELS

J. S. Luo and W. L. Ebert

Proc. of the 100th Am. Ceram. Soc. Annual Meeting, Cincinnati, OH, May 3–6, 1998

Temperature Dependence of Bi-2223 Phase Formation in a Silver Sheath

V. A. Maroni, M. Teplitsky, and M. W. Rupich

Extended Abstract, Int. Workshop on Superconductivity, Okinawa, Japan, July 12–15, 1998, pp. 161–164 (1998)

The Development of Stable Ceramic Materials for the Containment of Molten Zirconium and Uranium Alloys

S. M. McDeavitt and G. W. Billings

Light Metals, 1998, Ed., B. J. Welch, Proc. of the Technical Sessions Presented by the TMS Aluminum Committee at the 127th Annual Meeting of the Minerals, Metals, and Materials Soc., San Antonio, TX, February 15–19, 1998, p. 1365 (1998)

X-ray Absorption Spectroscopy Studies of the Structure of Electrodeposited Metal Oxide Films and Some Applications

C. A. Melendres, M. Balasubramanian, A. N. Mansour, and S. Mini

Extended Abstracts, 193rd Electrochem. Soc. Meeting, San Diego, CA, May 3–8, 1998, Vol. 98–1, Abstract No. 265 (1998)

Lithium Insertion into Hollandite-Type TiO_2

L. D. Noailles, C. S. Johnson, J. T. Vaughey, and M. M. Thackeray

Book of Abstracts, Ninth Int. Meeting on Lithium Batteries, Edinburgh, Scotland, United Kingdom, July 12–17, 1998, Vol. 1, p. 85 (1998)

Reformer Technology Challenges

W. F. Podolski

Proc. of the Fuel Cell Reformer Conf., South Coast Air Quality Management District, Diamond Bar, CA, November 20, 1998, pp. 70–76 (1998)

Supercritical Hydroformylation Catalysis

J. W. Rathke, R. J. Klingler, and M. J. Chen

Proc. of the Fourth DOE/BES Research Conf. on Homogeneous Catalysis and Organometallic Chemistry, Baltimore, MD, June 3–7, 1998, pp. 17–19 (1998)

Carbons for Lithium Ion Cells Prepared using Sepiolite as an Inorganic Template

G. Sandí, K. A. Carrado, R. E. Winans, C. S. Johnson, and K. D. Kepler

Abstracts, 194th Electrochem. Soc. Meeting, Boston, MA, November 1–6, 1998, Vol. 98-2, p. 103 (1998)

Studies of Electrolyte Penetration in Carbon Anodes by NMR Techniques

G. Sandí, R. E. Gerald, R. J. Klingler, J. W. Rathke, K. A. Carrado, and R. E. Winans

Extended Abstracts, 194th Electrochem. Soc. Meeting, Boston, MA, November 1–6, 1998, Abstract No. 154, p. 186 (1998)

Computational, Electrochemical and ^7Li NMR Studies of Lithiated Disordered Carbon Electrodes in Lithium Ion Cells

G. Sandí, R. E. Gerald, L. G. Scanlon, K. A. Carrado, and R. E. Winans

Mater. Res. Soc. Symp. Proc. **496**, 95 (1998)

Anomalous Chondrites from the Sahara

A. S. Sexton, P. A. Bland, S. F. Wolf, I. A. Franchi, R. M. Hough, A. J. T. Jull, S. E. Klandrud, F. J. Berry, and C. T. Pillinger

Abstracts, Meteoritics and Planetary Science **33**, A143 (1998)

The Stability of Lithium Manganese Oxide Structures in 4V Lithium Ion Cells

Y. Shao-Horn, S. A. Hackney, A. J. Kahaian, K. D. Kepler, E. Skinner, J. T. Vaughey, and M. M. Thackeray

Abstracts, Fall Meeting of the Materials Research Soc., Boston, MA, November 30–December 4, 1998, Vol. 1, p. 566 (1998)

Structural Fatigue of Spinal Electrodes in 4V $Li/Li_{1+\delta}Mn_{2-\delta}O_4$ Cells ($0<d<0.1$)

Y. Shao-Horn, S. A. Hackney, A. J. Kahaian, K. D. Kepler, E. Skinner, J. T. Vaughey, and M. M. Thackeray

Book of Abstracts, Ninth Int. Meeting on Lithium Batteries, Edinburgh, Scotland, United Kingdom, July 12–17, 1998, Vol. 1, p. 171 (1998)

Accelerated Test Behavior of the Glass Zeolite Ceramic Waste Form

L. J. Simpson

Book of Abstracts, Presented at the 215th Am. Chem. Soc. National Meeting, Dallas, TX, March 29–April 2, 1998

Corrosion Testing for Qualification of the Glass-Zeolite Ceramic Waste Form

L. J. Simpson

Book of Abstracts, 100th Am. Ceram. Soc. Annual Meeting, Cincinnati, OH, May 3–6, 1998

Corrosion Behavior from Flow-Through Tests with a Glass-Sodalite Ceramic Waste Form

L. J. Simpson, C. K. Vander Kooi, and W. K. Hoashi

Abstracts, Fall Meeting of the Materials Research Soc., Boston, MA, November 30–December 4, 1998

Methods and Criteria Development for Qualification of the Glass-Zeolite Ceramic Waste Form

L. J. Simpson, D. J. Wronkiewicz, and S. F. Wolf

Ceram. Trans. **87**, 471 (1998)

Waste Minimization in Analytical Chemistry through Innovative Sample Preparation Techniques

L. L. Smith, J. H. Aldstadt, J. S. Alvarado, L. L. Chromizky, C. S. Sabau, B. Szostek, and J. A. Tinklenberg

Proc. of the Pollution Prevention Conf. XIV, Seattle, WA, June 1–4, 1998 (www.hanford.gov/polprev/conference/proceedings.htm)

Study of Alteration Phases in Glass Bonded Zeolite and Sodalite Using Vapor Hydration Tests

D. Sun, D. J. Wronkiewicz, and L. J. Simpson

Abstracts, Fall Meeting of the Materials Research Soc., Boston, MA, November 30–December 4, 1998

Stabilization of Insertion Electrodes for Lithium Batteries

M. M. Thackeray, C. S. Johnson, A. J. Kahaian, K. D. Kepler, J. T. Vaughey, Y. Shao-Horn, and S. A. Hackney

Book of Abstracts, Ninth Int. Meeting on Lithium Batteries, Edinburgh, Scotland, United Kingdom, July 12–17, 1998, Vol. 1, p. 12 (1998)

Composite Electrodes for Lithium Batteries

M. M. Thackeray, K. D. Kepler, J. T. Vaughey, A. J. Kahaian, C. S. Johnson, Y. Shao-Horn, and S. A. Hackney

Abstracts, Twelveth Int. Battery Assoc. (IBA) Grenoble-Annecy Meeting, Imperial Palace, Annecy, France, September 27–October 2, 1998, Vol. 1, p. 23 (1998)

New Materials for Advanced Thermal Barrier Coatings

R. Vassen, F. Tietz, G. Kerkhoff, R. Wilkenhoener, and D. Stoever

Proc. of the Sixth Liege Conf., Part III, Materials for Advanced Power Engineering, Liege, Belgium, October 5–7, 1998, 1627–1635 (1998)

Crystallographic and Elecrochemical Studies of $Li_4Ti_5O_{12}$

J. T. Vaughey, K. D. Kepler, A. N. Jansen, C. S. Johnson, A. J. Kahaian, K. Amine, D. R. Vissers, and M. M. Thackeray

Abstracts, Fall Meeting of the Materials Research Soc., Boston, MA, November 30–December 4, 1998, Vol. 1, p. 568 (1998)

Intermetallic Anodes for Lithium Batteries

J. T. Vaughey, K. D. Kepler, and M. M. Thackeray

Abstracts, Fall Meeting of the Materials Research Soc., Boston, MA, November 30–December 4, 1998, Vol. 1, p. 571 (1998)

Flow and Rheological Studies Using Toroid-Cavity NMR

K. Woelk, R. E. Gerald, P. Trautner, B. L. J. Zwank, J. Bargon, R. J. Klingler, and J. W. Rathke

Program and Abstracts, 40th Rocky Mountain Conf. on Analytical Chemistry, Denver, CO, July 25–August 1, 1998, pp. 157–158 (1998)

Application of ICP-MS for the Measurement of Long-Lived Fission Products and Actinides in Solutions from Durability Testing of Spent Nuclear Fuel

S. F. Wolf, P. A. Finn, and J. K. Bates

Abstracts, Second Symp. on Applications of ICP-MS to Radionuclide Determinations, 49th Pittsburgh Conf. and Exposition on Analytical Chemistry and Applied Spectroscopy, New Orleans, LA, March 1–6, 1998, Abstract No. 707 (1998)

E. Papers Presented at Scientific Meetings

Influence of Zirconium Content on Fission Product Distributions in Stainless Steel-Zirconium Waste Forms

D. P. Abraham and S. M. McDeavitt

Presented at the Symp. on Hazardous & Radioactive Waste, Dallas, TX, March 29–April 2, 1998

Corrosion Testing of Stainless Steel-Zirconium Metal Waste Forms

D. P. Abraham, L. J. Simpson, M. J. DeVries, and S. M. McDeavitt

Presented at the Fall Meeting of the Materials Research Soc., Boston, MA, November 30–December 4, 1998

Iron Oxide Positive Active Material for Lithium Battery

K. Amine

Presented at the Fall Meeting of the Materials Research Soc., Boston, MA, November 30–December 4, 1998

Corrosion Testing: Examples from the FMD Program

A. J. Bakel

Presented at the Plutonium Immobilization Meeting, Argonne, IL, October 26–28, 1998

The Effects of Impurities on the Corrosion Behavior and Phase Distribution of Titanate Ceramics for Plutonium Immobilization

A. J. Bakel, E. C. Buck, C. J. Mertz, and D. B. Chamberlain

Presented at the Fall Meeting of the Materials Research Soc., Boston, MA, November 30–December 4, 1998

Corrosion Behavior of Pyroclore-Rich Titanate Ceramics for Plutonium Disposition: Impurity Effects

A. J. Bakel, V. N. Zyryanov, C. J. Mertz, E. C. Buck, and D. B. Chamberlain

Presented at the Fall Meeting of the Materials Research Soc., Boston, MA, November 30–December 4, 1998

Fate of Neptunium in an Anaerobic, Methanogenic Microcosm

J. E. Banaszak, S. M. Webb, B. E. Rittmann, J.-F. Gaillard, and D. T. Reed

Presented at the Fall Meeting of the Materials Research Soc., Boston, MA, November 30–December 4, 1998

Study of Effect of Spectral Resolution on Pattern Recognition Results Using Passive FTIR Sensor Data

A. S. Bangalore, A. S. Boparai, and G. W. Small

Presented at the 49th Pittsburgh Conf. and Exposition on Analytical Chemistry and Applied Spectroscopy, New Orleans, LA, March 1–6, 1998

Hydration of Glass in an Unsaturated Waste Repository Environment

J. K. Bates

Presented at the 63rd Annual Meeting of the Soc. for Am. Archaeology, Seattle, WA, March 25–29, 1998

Exploratory Battery Program of the U.S. Department of Energy
V. S. Battaglia, R. Sutula, and F. F. McLarnon
Presented at the 194th Electrochem. Soc. Meeting, Boston, MA, November 1–6, 1998

Evaluation of FT-Raman and FTIR Techniques for Screening of Semivolatile Organic Compounds in an Inorganic Salt Matrix
A. S. Boparai, D. Fimmen, Y. Tsai, K. J. Parish, and M. J. Schipma
Presented at the 49th Pittsburgh Conf. and Exposition on Analytical Chemistry and Applied Spectroscopy, New Orleans, LA, March 1–6, 1998

The Application of Analytical Transmission Electron Microscopy in Titanate "Synroc" Ceramic Development
E. C. Buck
Presented at the Plutonium Immobilization Meeting, Argonne, IL, October 26–28, 1998

Interpreting Uranyl Mineral Diffraction Patterns
E. C. Buck
Presented at the Microscopy-Microanalysis '98 Conf., Atlanta, GA, July 12–16, 1998

Intergrowth Structures in Synthetic Pyrochlores
E. C. Buck, D. B. Chamberlain, and R. Giere
Presented at the Fall Meeting of the Materials Research Soc., Boston, MA, November 30–December 4, 1998

Use of Sol-Gel Systems for Solid/Liquid Separation
D. J. Chaiko and J. P. Kopasz
Presented at the 72nd Colloid and Surface Science Symp., Am. Chem. Soc., University Park, PA, June 21–24, 1998

Solid/Liquid Separation Using Sol-Gel Systems
D. J. Chaiko, J. P. Kopasz, and A. J. G. Ellison
Presented at the 72nd Colloid & Surface Science Symp., University Park, PA, June 21–24, 1998

FMD Activities at Argonne National Laboratory
D. B. Chamberlain
Presented at the Plutonium Immobilization Meeting, Argonne, IL, October 26–28, 1998

Corrosion Testing of Ceramic Materials for the Immobilization of Plutonium
D. B. Chamberlain, A. J. Bakel, E. C. Buck, J. Fortner, and C. J. Mertz
Presented at the Third Topical Meeting on DOE Spent Nuclear Fuel and Fissile Materials Management, Am. Nucl. Soc., Charleston, SC, September 8–11, 1998

Rh(III) Complexes of Singly and Doubly-Reduced Phthalocyanine Ligands Generated by Chemical and Electrochemical Reduction

M. J. Chen and J. W. Rathke

Presented at the Second Int. Symp. on Phthalocyanines, Edinburgh, Scotland, United Kingdom, September 21–23, 1998

In Situ X-ray Diffraction Study on $RuO_2(100)$ Single Crystal

Y. S. Chu, J. A. Tanzer, T. E. Lister, H. You, and Z. Nagy

Presented at the Am. Phys. Soc. Meeting, Los Angeles, CA, March 16–20, 1998

Progress in Developing Processes for Converting ^{99}Mo Production from High- to Low-Enriched Uranium—1998

C. Conner, M. W. Liberatore, A. Mutalib, J. Sedlet, D. E. Walker, and G. F. Vandegrift

Presented at the 21st Int. Meeting on Reduced Enrichment for Research and Test Reactors (RERTR), Sao Paulo, Brazil, October 18–23, 1998

Measurement of Low Levels of Alpha in ^{99}Mo Product Solutions

C. Conner, M. W. Liberatore, J. Sedlet, and G. F. Vandegrift

Presented at the AIChE Spring National Meeting, New Orleans, LA, March 8–12, 1998

Lithium Polymer Electrolytes: Li Cation Coordination and Migration Barriers

L. A. Curtiss, A. G. Baboul, A. Sutjianto, and J. W. Halley

Presented at the 215th Am. Chem. Soc. National Meeting, Dallas, TX, March 29–April 2, 1998

Ab Initio and Density Functional Studies of Hydrocarbon Adsorption in Zeolites

L. A. Curtiss, S. A. Zygmunt, and L. E. Iton

Presented at the 12th Int. Zeolite Conf., Baltimore, MD, July 5–10, 1998

Aquo Ions of Some Trivalent Actinides, XANES and EXAFS Data, Thermodynamic Consequences

F. David, R. Revel, B. Fourest, S. Hubert, J. F. Le Du, C. Den Auwer, C. Madic, and L. R. Morss

Presented at the Workshop on Speciation, Techniques, and Facilities for Radioactive Materials at Synchrotron Light Sources, Grenoble, France, October 4–6, 1998

Comparison of Infrared and Mass Spectroscopy as Methods of Continuous Emission Monitoring

J. C. Demirgian and C. T. Snyder

Presented at the 49th Pittsburgh Conf. and Exposition on Analytical Chemistry and Applied Spectroscopy, New Orleans, LA, March 1–6, 1998

Release of ^{99}Tc during Aqueous Corrosion of a Borosilicate Glass

W. L. Ebert and A. J. Bakel

Presented at the 19th U.S. Department of Energy Low-Level Radioactive Waste Management Conf., Salt Lake City, UT, November 10–12, 1998

Release of ^{99}Tc Aqueous Corrosion of a Borosilicate Glass
W. L. Ebert, A. J. Bakel, and J. C. Cunnane
Presented at the 100th Am. Ceram. Soc. Annual Meeting, Cincinnati, OH, May 3–6, 1998

Dissolution Test for Low-Activity Waste Product Acceptance
W. L. Ebert and S. F. Wolf
Presented at the Spectrum '98 Conf., Denver, CO, September 13–18, 1998

Extending Dry Storage of Spent LWR Fuel for 100 Years
R. E. Einziger, M. A. McKinnon, and A. J. Machiels
Presented at the Int. Symp. on Storage of Spent Fuel from Power Reactors, Vienna, Austria, November 9–13, 1998

Synthesis and Characterization of $Ba[(UO_2)_5(MoO_6)(OH)_6]\cdot nH_2O$
R. J. Finch and E. C. Buck
Presented at the Fall Meeting of the Materials Research Soc., Boston, MA, November 30–December 4, 1998

Oxidative Corrosion of Spent UO_2 Fuel in Vapor and Dripping Groundwater at 90°C
R. J. Finch, E. C. Buck, P. A. Finn, and J. K. Bates
Presented at the Fall Meeting of the Materials Research Soc., Boston, MA, November 30–December 4, 1998

Rare-Earth Elements in Zircon: The Roles of Phosphorous and Lithium
R. J. Finch, J. M. Hanchar, P. W. O. Hoskin, and P. C. Burns
Presented at the Annual Meeting of the Geological Society of America, Toronto, Canada, October 26–29, 1998

UO_2 Corrosion in High Surface-Area-to-Volume Batch Experiments
R. J. Finch, S. F. Wolf, J. M. Hanchar, and J. K. Bates
Presented at the Eighth Annual Int. High-Level Radioactive Waste Management Conf., Am. Nucl. Soc., Las Vegas, NV, May 11–14, 1998

Corrosion Testing of High-Level Waste Glass (and Other Materials)
J. Fortner
Presented at the Plutonium Immobilization Meeting, Argonne, IL, October 26–28, 1998

XANES Analysis of Plutonium and Uranium Edges from Titanate Ceramics for Fissile Materials Disposal
J. Fortner, S. B. Aase, A. J. Kropf, D. T. Reed, M. C. Hash, and D. B. Chamberlain
Presented at the Ninth Users Meeting for the Advanced Photon Source, Argonne, IL, October 13–15, 1998

Structural Analysis of a Completely Amorphous ^{238}Pu-Doped Zircon by Neutron Diffraction
J. Fortner, Y. Badyal, D. C. L. Price, J. M. Hanchar, and W. J. Weber
Presented at the Fall Meeting of the Materials Research Soc., Boston, MA, November 30–December 4, 1998

Gas Phase Micelles as Microreactors for Catalysis
D. E. Fremgen, R. J. Klingler, and J. W. Rathke
Presented at the Spring Symp. of the Catalysis Club of Chicago, Chicago, IL, May 8, 1998

Proposed Quality Assurance Levels for Nuclear Facilities
A. A. Frigo
Presented at the Argonne National Laboratory Quality Assurance Representatives' Meeting, Argonne, IL, April 1998

Quality Assurance Applied to Glovebox Design, Fabrication, Installation, Operation, and Decommissioning
A. A. Frigo
Presented at the Eleventh Annual Conf. and Exhibition of the Am. Glovebox Soc., Orlando, FL, July 13–15, 1998

Quality Assurance Levels Utilized by Argonne and Outside Organizations
A. A. Frigo
Presented at the Argonne National Laboratory Quality Assurance Representatives' Meeting, Argonne, IL, March 1998

Development of Electrorefiners to Separate Pure Metals from Spent Nuclear Fuel
E. C. Gay
Presented at the 25th Annual National Organization of Black Chemists and Chemical Engineers Conf., Dallas, TX, April 11–18, 1998

Chemical Imaging
D. W. Green
Presented at the 49th Pittsburgh Conf. and Exposition on Analytical Chemistry and Applied Spectroscopy, New Orleans, LA, March 1–6, 1998

News from Argonne
D. W. Green
Presented at the 16th Annual DOE Analytical Managers' Association Meeting, Cincinnati, OH, August 18–20, 1998

The Spectrum of Analytical Needs
D. W. Green
Presented at the DOE Office of Environmental Management National Analytical Management Program (NAMP '98) Workshop on Addressing Analytical Needs into the 21st Century, Bethesda, MD, June 2–5, 1998

Boundary Element Technique for Calculations of Field and Spectral Distortions
E. S. Growney, G. Friedman, R. E. Gerald, R. J. Klingler, and J. W. Rathke
Presented at the Workshop on Computational Electromagnetics in Magnetic Resonance, College Station, TX, May 30–June 1, 1998

Rare-Earth Element and Cathodoluminescence Variations in a "Gem" Quality Zircon from the Mud Tank Carbonatite, Australia

J. M. Hanchar, R. J. Finch, and P. W. O. Hoskin

Presented at the Annual Meeting of the Geological Soc. of America, Toronto, Ontario, Canada, October 26–29, 1998

Development of Nuclear Waste Forms at Argonne National Laboratory

M. C. Hash

Presented at the Am. Ceram. Soc. Meeting, Chicago-Milwaukee Section, Westmont, IL, October 20, 1998

FMD Ceramic Form Development, Fabrication Activities

M. C. Hash

Presented at the Plutonium Immobilization Meeting, Argonne, IL, October 26–28, 1998

Hot Isostatic Pressing of Sodalite-Glass Composites

M. C. Hash, G. L. Burns, J. P. Thalacker, D. R. Simon, C. Pereira, M. A. Lewis, and R. H. Woodman

Presented at the 215th Am. Chem. Soc. National Meeting, Dallas, TX, March 29–April 2, 1998

The Evaluation of Sintered Sodalite-Glass Composites

M. C. Hash, J. P. Thalacker, D. R. Simon, G. L. Burns, and R. H. Woodman

Presented at the 100th Am. Ceram. Soc. Annual Meeting, Cincinnati, OH, May 3–6, 1998

Air System Technology Overview

G. L. Henriksen

Presented at the Soc. of Automotive Engineers Fuel Cell Topical Meeting, Boston, MA, March 18–19, 1998

Lithium Insertion into Hollandite-Type TiO_2

C. S. Johnson, L. D. Noailles, J. Vaughey, and M. M. Thackeray

Presented at the Second Nagoya New Battery Conf. with Exhibition, Nagoya, Japan, August 26–28, 1998

Extractant-Coated Magnetic Microparticles Application to Industrial Waste Minimization

M. D. Kaminski and L. Nuñez

Presented at the 216th Am. Chem. Soc. National Meeting, Boston, MA, August 23–27, 1998

Extractant-Coated Magnetic Particles for Cobalt and Nickel Recovery from Acidic Solution

M. D. Kaminski and L. Nuñez

Presented at the Second Int. Conf. on the Scientific and Clinical Applications of Magnetic Carriers, Cleveland, OH, May 28–30, 1998

Engineering-Scale Testing of the Lithium Reduction Process

E. J. Karell and K. V. Gourishankar

Presented at the 22nd Annual Actinide Separations Conf., Chattanooga, TN, April 20–23, 1998

High Pressure *In-Situ* NMR Spectroscopy of Phosphine Modified Cobalt Carbonyl Oxo Catalysts

K. W. Kramarz, R. J. Klingler, and J. W. Rathke

Presented at the Shell Oil Company, Houston, TX, January 19, 1998

Nuclear Magnetic Resonance (NMR) Spectroscopy in High-Pressure/High-Temperature Catalysis

K. W. Kramarz, R. J. Klingler, and J. W. Rathke

Presented at the 215th Am. Chem. Soc. National Meeting, Dallas, TX, March 29–April 2, 1998

X-ray Absorption Near-Edge Spectroscopy of Plutonium Solid Species

A. J. Kropf, D. T. Reed, and S. B. Aase

Presented at the Tenth Int. Conf. on X-ray Absorption Fine Structure, Chicago, IL, August 10–14, 1998

Partial Oxidation Reformer Development

M. Krumpelt, S. Ahmed, R. Kumar, S. H. D. Lee, J. D. Carter, R. Wilkenhoener, and C. L. Marshall

Presented at the Annual National Laboratory R&D Meeting of the DOE Fuel Cells for Transportation Program, Los Alamos, NM, July 28–29, 1998

Supporting R&D of Industrial Fuel Cell Developers

M. Krumpelt, T. D. Kaun, X. Wang, and M. T. Lanagan

Presented at the Joint DOE/EPRI/GRI Workshop on Fuel Cell Technology, San Francisco, CA, May 18–20, 1998

Automotive Fuel Cell Systems Modeling

R. Kumar, R. K. Ahluwalia, E. D. Doss, H. K. Geyer, and M. Krumpelt

Presented at the Annual National Laboratory R&D Meeting of the DOE Fuel Cells for Transportation Program, Los Alamos, NM, July 28–29, 1998

Developing New Solvent Extraction Processes

R. A. Leonard and C. Conner

Presented at the AIChE Spring National Meeting on Extraction in Practice, New Orleans, LA, March 8–12, 1998

Audit and Performance Evaluation Management—Overview of IPEP

P. C. Lindahl and W. E. Streets

Presented at the DOE Office of Environmental Management National Analytical Management Program (NAMP '98) Workshop on Addressing Analytical Needs into the 21st Century, Bethesda, MD, June 2–5, 1998

DOE's Integrated Performance Evaluation Program (IPEP)—A Resource for Promoting Excellence in EM Sampling and Analysis Operations throughout the DOE Complex

P. C. Lindahl, W. E. Streets, J. R. Dahlgran, J. S. Morton, and L. Ekman

Presented at the Tenth National Technology Information Exchange Workshop, Willowbrook, IL, October 27–29, 1998

Investigation of Microscopic Radiation Damage in Waste Forms Using ODNMR and AEM Techniques

G. K. Liu, J. S. Luo, S. T. Li, and J. V. Beitz

Presented at the DOE Environmental Management Science Program Workshop, Rosemont, IL, July 27–30, 1998

Application of Amperometric Oxygen Sensors in Trace Concentration Range

J. Liu and W. Weppner

Presented at the 193rd Electrochem. Soc. Meeting, San Diego, CA, May 3–8, 1998

The Electronic Property Study of $La_{0.72}Sm_{0.08}Sr_{0.02}Ga_{0.08}Mg_{0.02}O_{3-d}$ by Polarization Measurements

J. Liu and W. Weppner

Presented at the 193rd Electrochem. Soc. Meeting, San Diego, CA, May 3–8, 1998

Interfacial Reaction in Subaerially Altered Basaltic Glass: An Electron Energy Filtered Imaging and EELS Study

J. S. Luo, W. L. Ebert, and J. K. Bates

Presented at the 100th Am. Ceram. Soc. Annual Meeting, Cincinnati, OH, May 3–6, 1998

Radiation Damage in ^{244}Cm-Doped Orthophosphate Crystals: An Analytical Electron Microscopy Study

J. S. Luo and G. K. Liu

Presented at the 215th Am. Chem. Soc. National Meeting, Dallas, TX, March 29–April 2, 1998

What is a Cee-M-Tee 1470 Series Glovebox?

R. F. Malecha, E. F. Bielick, and B. A. Size

Presented at the Eleventh Annual Conf. and Exhibition of the Am. Glovebox Soc., Orlando, FL, July 13–15, 1998

Using Imaging Raman Microscopy to Explore Phase Evolution in Composite Ceramic Superconductors

V. A. Maroni, A. K. Fischer, and K. T. Wu

Presented at the 215th Am. Chem. Soc. National Meeting on Applications of Spectroscopy to Superconducting Materials, Dallas, TX, March 29–April 2, 1998

Probing the Origins of the SEIRA Effect

V. A. Maroni, S. A. Johnson, T. R. Jensen, and R. P. Van Duyne

Presented at the Eastern Analytical Symp., Somerset, NJ, November 15–20, 1998

Improved Catalysts for the Removal of Sulfur from Heavy Hydrocarbons

C. L. Marshall

Presented at the University of Illinois at Chicago, Department of Chemical Engineering, Chicago, IL, November 13, 1998

Improved Catalysts for the Removal of Sulfur from Heavy Hydrocarbons
C. L. Marshall
Presented at Dartmouth College, Dartmouth, NH, November 5, 1998

Ab Initio Calculations of the Hydrodesulfurization Process
C. L. Marshall, J. R. Brenner, J. L. Tilson, S. Harris, and M. R. Palmer
Presented at the Gordon Research Conf. on Catalysis, New London, NH, June 22, 1998

Ab Initio Calculations of the Hydrodesulfurization Process
C. L. Marshall, J. R. Brenner, J. L. Tilson, and M. R. Palmer
Presented at the 215th Am. Chem. Soc. National Meeting, Dallas, TX, March 29–April 2, 1998

In-Situ Spectro-electrochemical Studies of Radionuclide Contaminated Surface Films on Metals
C. A. Melendres, M. Balasubramanian, S. Mini, and A. N. Mansour
Presented at the DOE Environmental Management Science Program Workshop, Rosemont, IL, July 27–30, 1998

Chemical and Microstructural Aspects of the Coated-Wire-in-Tube Ag/Bi-2223 Composite Conductor
N. N. Merchant, S. E. Dorris, T. Truchan, K. T. Wu, and V. A. Maroni
Presented at the TMS Annual Meeting and Exhibition, San Antonio, TX, February 15–19, 1998

Phase Stability and Grain Growth in an Ag/Bi-2223 Composite Conductor Prepared Using Fine-Grained Bi-2223 as a Precursor
N. N. Merchant, D. J. Miller, V. A. Maroni, R. D. Parrella, Q. Li, M. W. Rupich, W. L. Carter, and G. N. Riley
Presented at the Applied Superconductivity Conf., Palm Desert, CA, September 13–18, 1998

Interaction Corrosion Testing
C. J. Mertz, A. J. Bakel, J. Fortner, and D. B. Chamberlain
Presented at the Plutonium Immobilization Meeting, Argonne, IL, October 26–28, 1998

Dynamic Light Scattering of Waste Form Colloids
C. J. Mertz and J. K. Bates
Presented at the 215th Am. Chem. Soc. National Meeting, Dallas, TX, March 29–April 2, 1998

Colloids and Their Characterization
C. J. Mertz, J. K. Bates, E. C. Buck, J. Fortner, and S. F. Wolf
Presented at the Plutonium Immobilization Meeting, Argonne, IL, October 26–28, 1998

The Chemical Behavior of Neptunium and Its Importance in Nuclear Waste Disposition

L. R. Morss

Presented at the 216th Am. Chem. Soc. National Meeting, Boston, MA, August 23–27, 1998

Full-Scale Demonstration of the Cintichem Process for the Production of Mo-99 Using a Low-Enriched Target

A. Mutalib, B. Purwadi, H. G. Adang, L. Hotman, Moeridoen, Kadarisman, A. Sukmana, Sriyono, A. Suripto, H. Nasution, D. L. Amin, A. Basiran, A. Gogo, D. Sunaryadi, T. Taryo, G. F. Vandegrift, G. L. Hofman, C. Conner, J. Sedlet, D. E. Walker, R. A. Leonard, E. L. Wood, T. C. Wiencek, and J. L. Snelgrove

Presented at the 21st Int. Meeting on Reduced Enrichment for Research and Test Reactors (RERTR), Sao Paulo, Brazil, October 18–23, 1998

Reformate Post-Processing for CO Cleanup

D. J. Myers, S. H. D. Lee, J. D. Carter, R. Kumar, and M. Krumpelt

Presented at the Annual National Laboratory R&D Meeting of the DOE Fuel Cells for Transportation Program, Los Alamos, NM, July 28–29, 1998

Trace Anion Catalysis of Elementary Heterogeneous Charge-Transfer Reactions

Z. Nagy

Presented at the Gordon Research Conf. on Electrochemistry, Ventura, CA, January 18–23, 1998

Applications of NMR for Nondestructive Evaluation of Nuclear Packaging Material

L. Nuñez, R. E. Gerald, and S. E. Aumeier

Presented at the Third Topical Meeting on DOE Spent Nuclear Fuel and Fissile Materials Management, Am. Nucl. Soc., Charleston, SC, September 8–11, 1998

Nondestructive Evaluation of Nuclear Packaging Materials by Toroid NMR

L. Nuñez, R. E. Gerald, and S. E. Aumeier

Presented at the Third Topical Meeting on DOE Spent Nuclear Fuel and Fissile Materials Management, Am. Nucl. Soc., Charleston, SC, September 8–11, 1998

Magnetically Assisted Chemical Separation (MACS)

L. Nuñez and M. D. Kaminski

Presented at the Argonne National Laboratory Visitors Reception Center, Argonne, IL, April 13–17, 1998

Multilayer Morphology of Porous Anodic Oxides of Silicon

V. Parkhutik, Y. S. Chu, H. You, Z. Nagy, and P. A. Montano

Presented at the Porous Semiconductors: Science and Technology Conf., Mallorca, Spain, March 16–20, 1998

Incorporation of Radionuclides from the Electrometallurgical Treatment of Spent Fuel into a Ceramic Waste Form

C. Pereira, M. C. Hash, M. A. Lewis, M. K. Richmann, and J. K. Basco

Presented at the Fall Meeting of the Materials Research Soc., Boston, MA, November 30–December 4, 1998

Fuel Cell Development Challenges
W. F. Podolski
Presented at the NAEVI '98 Conf., Phoenix, AZ, December 3, 1998

First Principles Calculations for Lithiated Manganese Oxides
R. Prasad, R. Benedek, M. M. Thackeray, J. M. Wills, and L. H. Yang
Presented at the Fall Meeting of the Materials Research Soc., Solid State Ionics Session, Boston, MA, November 30–December 4, 1998

Biodegradation of Organics in Radionuclide-Organic Mixtures: Extension of *In-Situ* Bioremediation Methods to the Cleanup of DOE Nuclear Waste Sites
D. T. Reed, J. E. Banaszak, and B. E. Rittmann
Presented at the Subsurface Barrier Technologies Conf., Tucson, AZ, January 26–27, 1998

Radiolytic Gas Generation under Conditions Relevant to TRU Waste
D. T. Reed, T. R. Krause, J. C. Hoh, J. W. Emery, and D. G. Wygmans
Presented at the Fall Meeting of the Materials Research Soc., Boston, MA, November 30–December 4, 1998

Ceramic Waste Form Development for Spent Nuclear Fuel
J. E. Saienga, J. B. Dobson, and S. A. Slater
Presented at the Argonne Symp. for Undergraduates in Science, Engineering, and Mathematics, Argonne, IL, November 6–7, 1998

Mechanical Properties and Sintering Behavior of New Developed P/M Steels
A. C. Schoeler
Presented at Argonne National Laboratory, Energy Technology Division Seminar, Argonne, IL, August 25, 1998

Solution Exchange Corrosion Testing with the Glass-Zeolite Ceramic Waste Form in Demineralized Water at 90°C
L. J. Simpson, C. W. Vander Kooi, and V. N. Zyryanov
Presented at the 100th Am. Ceram. Soc. Annual Meeting, Cincinnati, OH, May 3–6, 1998

Using Electrochemical Separation to Reduce the Volume of High-Level Nuclear Waste
S. A. Slater and E. C. Gay
Presented at the Soc. of Women Engineers National Convention, Houston, TX, June 15–20, 1998

Utility Connections—Maintaining the Barrier
M. A. Slawecki
Presented at the Eleventh Annual Conf. and Exhibition of the Am. Glovebox Soc., Orlando, FL, July 13–15, 1998

Electrochemical Production of Lithium Metal from Lithium Oxide in Molten Lithium Chloride
J. L. Smith
Presented at the TMS Annual Meeting and Exhibition, San Antonio, TX, February 15–19, 1998

The Characterization and Testing of Candidate Immobilization Forms for the Disposal of Plutonium

D. M. Strachan, A. J. Bakel, E. C. Buck, D. B. Chamberlain, J. Fortner, C. J. Mertz, S. F. Wolf, B. B. Ebbinghaus, H. F. Shaw, R. A. Van Konynenburg, B. P. McGrail, J. D. Vienna, J. C. Marra, and D. K. Peeler

Presented at the Waste Management '98 Conf., Tucson, AZ, March 1–5, 1998

The Dependence of Long-Term Dissolution on Glass Composition

D. M. Strachan and T. L. Croak

Presented at the Eighth Annual Int. High-Level Radioactive Waste Management Conf., Am. Nucl. Soc., Las Vegas, NV, May 11–14, 1998

Enhanced Use of Performance Evaluation Program Data in Support of the Department of Energy's Environmental Management Activities

W. E. Streets and P. C. Lindahl

Presented at the Fifth Great Lakes Conf. on Applied Statistics, Kalamazoo, MI, October 21–23, 1998

Integrated Performance Evaluation Program (IPEP)

W. E. Streets and P. C. Lindahl

Presented at the Radiological and Environmental Sciences Laboratory, Idaho National Engineering and Environmental Laboratory, Idaho Falls, ID, August 11–12, 1998

PEM Fuel Cell Technology: Status of the DOE Fuel Cells for Transportation Program

W. M. Swift

Presented at the DOE/AIST Technology Transfer Meeting, Palm Springs, CA, November 20, 1998

Investigation of Rhodium Films Electrodeposited on Au(111) Single Crystals Using X-ray Synchrotron Techniques

J. A. Tanzer, H. You, T. E. Lister, Y. S. Chu, Z. Nagy, and A. Wieckowski

Presented at the Gordon Research Conf. on Electrodeposition, New London, NH, August 9–14, 1998

Thermodynamic and Nonstoichiometric Behavior of the $GdBa_2Cu_3O_x$ System via EMF Measurements

M. Tetenbaum, D. Diana, B. S. Tani, and M. Blander

Presented at the Gordon Research Conf. on Solid State Chemistry, New London, NH, July 26–31, 1998

Thermodynamic and Nonstoichiometric Behavior of the $GdBa_2Cu_3O_x$ System

M. Tetenbaum, D. Diana, B. S. Tani, and M. Blander

Presented at the First China Int. Conf. on High Performance Ceramics, Beijing, China, October 31–November 3, 1998

Prospects for Manganese Oxides in Rechargeable Lithium Batteries

M. M. Thackeray

Presented at the First Hawaii Battery Conf., Kona, HI, January 5–7, 1998

Spinel Electrodes for Rechargeable Lithium Batteries
M. M. Thackeray
Presented at the 100th Am. Ceram. Soc. Annual Meeting, Cincinnati, OH, May 3–6, 1998

Kilogram Scale Preparation of Uranium Trichloride
Z. Tomczuk
Presented at the 22nd Annual Actinide Separations Conf., Chattanooga, TN, April 20–23, 1998

Converting ^{99}Mo Production from High- to Low-Enriched Uranium
G. F. Vandegrift
Presented at the Mallinckrodt Medical B.V. Meeting, Petten, The Netherlands and I.R.E., April 7, 1998

Modification of Targets and Processes for Conversion of ^{99}Mo Production from High- to Low-Enriched Uranium
G. F. Vandegrift, C. Conner, R. A. Leonard, J. Sedlet, D. E. Walker, and J. L. Snelgrove
Presented at the 216th Am. Chem. Soc. National Meeting, Boston, MA, August 23–27, 1998

Progress in Converting ^{99}Mo Production from High- to Low-Enriched Uranium
G. F. Vandegrift, C. Conner, J. Sedlet, D. E. Walker, and J. L. Snelgrove
Presented at the 22nd Annual Actinide Separations Conf., Chattanooga, TN, April 20–23, 1998

Electrometallurgical Treatment of Aluminum-Based Fuels
J. L. Willit, S. A. Slater, A. G. Raraz, and E. C. Gay
Presented at the Third Topical Meeting on DOE Spent Nuclear Fuel and Fissile Materials Management, Am. Nucl. Soc., Charleston, SC, September 8–11, 1998

Computational Studies of Catalytic Cracking in Large Cluster Models of Zeolite H-ZSM-5
S. A. Zygmunt, L. A. Curtiss, and L. E. Iton
Presented at the 215th Am. Chem. Soc. National Meeting, Dallas, TX, March 29–April 2, 1998

A Computational Study of Hydrocarbon Cracking in Zeolites
S. A. Zygmunt, L. A. Curtiss, and L. E. Iton
Presented at the 12th Int. Zeolite Conf., Baltimore, MD, July 5–10, 1998

F. Papers Accepted for Publication

β-FeOOH, A New Positive Electrode Material for Lithium Secondary Batteries
K. Amine, H. Yasuda, and M. Yamachi
To be published in J. Power Sources

New Iron Oxide Positive Active Material for Lithium Secondary Batteries
K. Amine, H. Yasuda, and M. Yamachi
To be published in Mater. Res. Bull.

Local Structure of Chromium Incorporated into Electrodeposited Nickel Hydroxide Films
M. Balasubramanian and C. A. Melendres
To be published in J. Synchrotron Radiat.

Selective Site Occupancy Exhibited by Cr^{3+} and Cr^{6+} Incorporated into Electrochemically Deposited Nickel Hydroxide Films
M. Balasubramanian and C. A. Melendres
To be published in Electrochem. Solid State Lett.

X-ray Absorption Specroscopy Study of the Local Structure of Heavy Metal Ions Incorporated into Electrodeposited Nickel Oxide Films
M. Balasubramanian, C. A. Melendres, and A. N. Mansour
To be published in J. Electrochem. Soc.

An X-ray Absorption Study of the Local Structure of Cerium in Electrochemically Deposited Thin Films
M. Balasubramanian, C. A. Melendres, and A. N. Mansour
To be published in Thin Solid Films

Evaluation of Glass Corrosion Mechanisms through Laboratory Tests and Analysis
J. K. Bates, W. L. Ebert, and D. M. Strachan
To be published in Nuclear Technology—A Journal of the American Nuclear Society

Methanol Fuel Cell Model: Anode
S. F. Baxter, V. S. Battaglia, and R. E. White
To be published in J. Electrochem. Soc.

The Development of $LiFeO_2$-$LiCoO_2$-NiO Cathodes for Molten Carbonate Fuel Cells
I. Bloom, M. T. Lanagan, M. Krumpelt, and J. L. Smith
To be published in J. Electrochem. Soc.

Barriers to Improved Resid Hydroprocessing
J. R. Brenner, C. L. Marshall, L. Ellis, P. Thiyagarajan, N. A. Tomczyk, and R. E. Winans
To be published in Energy & Fuels

Microanalysis of Colloids and Suspended Particles from Nuclear Waste Glass Alteration
E. C. Buck and J. K. Bates
To be published in Applied Geochemistry

Behavior of Dinonylnaphthalene Sulfonate Monolayers at the Air/Water Interface
D. J. Chaiko and K. Osseo-Asare
To be published in Colloids Surf.

Development of Solid Oxide Fuel Cells That Operate at 500°C
R. Doshi, V. L. Richards, J. D. Carter, X. Wang, and M. Krumpelt
To be published in J. Electrochem. Soc.

Refinement of the Crystal Structure of Rutherfordine
R. J. Finch, M. A. Cooper, F. C. Hawthorne, and R. C. Ewing
To be published in Can. Miner.

Rare-Earth Elements in Zircon. Part 1: Synthesis and Rare-Earth Element Doping
J. M. Hanchar, E. B. Watson, D. Cherniak, R. J. Finch, and A. Marinoni
To be published in Am. Mineral.

Advanced Cell Technology for High Performance Li-Al/FeS_2 Secondary Batteries
G. L. Henriksen, A. N. Jansen, T. D. Kaun, J. Prakash, and D. R. Vissers
To be published in the Proc. of the Eleventh Int. Symp. on Molten Salts, 193rd Electrochem. Soc. Meeting, San Diego, CA, May 3–8, 1998

Corrosion Performance of Ferrous and Refractory Metals in Molten Salts under Reducing Conditions
J. E. Indacochea, J. L. Smith, K. R. Litko, and E. J. Karell
To be published in J. Mater. Res.

Application of Nuclear Shielding Surfaces to the Fundamental Understanding of Adsorption and Diffusion in Microporous Solids
C. J. Jameson, A. K. Jameson, A. C. de Dios, R. E. Gerald, H. M. Lim, and P. Kostikin
To be published in Chapter XX of *Modeling NMR Chemical Shifts: Gaining Insights into Structure and Environment*, Eds., J. C. Facelli and A. C. de Dios, Am. Chem. Soc., New York

Development of High Power Lithium Ion Battery
A. N. Jansen, A. J. Kahaian, K. D. Kepler, P. A. Nelson, K. Amine, D. W. Dees, D. R. Vissers, and M. M. Thackeray
To be published in J. Power Sources

Tritium Behavior in Lithium Ceramics
C. E. Johnson
To be published in J. Nucl. Mater.

Structural and Electrochemical Analysis of Layered Compounds from Li_2MnO_3
C. S. Johnson, S. D. Korte, J. T. Vaughey, M. M. Thackeray, T. E. Bofinger, Y. Shao-Horn, and S. A. Hackney
To be published in J. Power Sources

Extractant Coated Magnetic Particles for Cobalt and Nickel Recovery from Acidic Solutions
M. D. Kaminski and L. Nuñez
To be published in J. Magn. Magn. Mater.

Resistivity of Bipolar Plate Materials at the Cathode Interface in Molten Carbonate Fuel Cells
T. D. Kaun, A. C. Schoeler, I. Bloom, M. T. Lanagan, and M. Krumpelt
To be published in the Proc. of the 194th Electrochem. Soc., Boston, MA, November 1–6, 1998

Toroid NMR Probes for the *In Situ* Examination of Homogeneous Cobalt Hydroformylation Catalysts at High Pressures and Temperatures
K. W. Kramarz, R. J. Klingler, D. E. Fremgen, and J. W. Rathke
To be published in Catalysis Today

Design Rules for Solvent Extraction
R. A. Leonard
To be published in Solvent Extraction and Ion Exchange

Developing and Testing an Alkaline-Side Solvent Extraction Process for Technetium Separation from Tank Waste
R. A. Leonard, C. Conner, M. W. Liberatore, P. V. Bonnesen, D. J. Presley, B. A. Moyer, and G. J. Lumetta
To be published in Sep. Sci. Technol.

The Enthalpy of Occlusion of the LiCl-KCl Eutectic Salt in Zeolite 4A
D. Lexa
To be published in J. Chem. Thermodyn.

A Hermetic Sample Enclosure for Simultaneous Differential Scanning Calorimetry/Synchrotron Powder X-ray Diffraction
D. Lexa
To be published in Rev. Sci. Instrum.

Preparation and Physical Characteristics of a Lithium-Beryllium-Substituted Fluorapatite
D. Lexa
To be published in Metall. Mater. Trans. A

An *In-Situ* X-ray Absorption Spectroscopy Study of Charged $LiNiO_2$ Cathode Material
A. N. Mansour, J. McBreen, and C. A. Melendres
To be published in J. Electrochem. Soc.

Using Imaging Raman Microscopy to Explore Phase Evolution in Composite Ceramic Superconductors

V. A. Maroni, A. K. Fischer, and K. T. Wu

To be published as a Chapter in *Applications of Spectroscopy to Superconductors*, Proc. of the 215th Am. Chem. Soc. National Meeting, Dallas, TX, March 29–April 2, 1998

An Environmental Scanning Electron Microscope Study of the Ag/Bi-2223 Composite Conductor from 25 to 840°C

V. A. Maroni, M. Teplitsky, and M. W. Rupich

To be published in Physica C

In-Situ Observation of Halide Ion Adsorption on a Gold Electrode Using Synchrotron Far Infrared Spectroscopy

C. A. Melendres and F. Hahn

To be published in J. Electroanal. Chem.

In-Situ Observations of Adorption and Film Formation on Metal Electrodes by Synchrotron Far Infrared Reflectance Spectroscopy

C. A. Melendres, F. Hahn, J. M. Leger, and G. A. Bowmaker

To be published in Passivity of Metals and Semiconductors

Phase Stability and Grain Growth in an Ag/Bi-2223 Composite Conductor Prepared Using Fine-Grained Bi-2223 as a Precursor

N. N. Merchant, D. J. Miller, V. A. Maroni, R. D. Parrella, Q. Li, M. W. Rupich, W. L. Carter, and G. N. Riley

To be published in IEEE Trans. on Applied Superconductivity

Lithium Insertion into Hollandite-Type TiO_2

L. D. Noailles, C. S. Johnson, J. T. Vaughey, and M. M. Thackeray

To be published in J. Power Sources

Superconducting Open Gradient Magnetic Separation for the Pretreatment of Mixed Waste Vitrification Feeds

L. Nuñez, R. D. Doctor, M. D. Kaminski, and A. E. Visser

To be published in Sep. Sci. Technol.

NMR Spectroscopy

J. W. Rathke, R. J. Klingler, R. E. Gerald, D. E. Fremgen, K. Woelk, and C. J. Elsevier

Book Chapter to be published in *Chemical Synthesis Using Supercritical Fluids*

Impact of Clean Air Act on Fuel Production and Use

J. G. Reynolds, D. C. Cronauer, and M. R. Khan

To be published in *Designing Transportation Fuels for a Cleaner Environment*

Structural Characterization of Layered $LiMnO_2$ Electrodes by Electron Diffraction and Lattice Imaging

Y. Shao-Horn, S. A. Hackney, A. R. Armstrong, P. G. Bruce, R. L. Gitzendanner, C. S. Johnson, and M. M. Thackeray

To be published in J. Electrochem. Soc.

Pyrite Removal by $CrCl_2$ Reduction and Pyrite Effect on the Coprocessing of Illinois 6 Coal with Waste Automotive Oil

Y. Shi, E. C. Orr, L. Shao, and E. M. Eyring

To be published in Fuel Processing Technology

Electrochemical Separation of Aluminum from Uranium for Research Reactor Spent Nuclear Fuel Applications

S. A. Slater, A. G. Raraz, J. L. Willit, and E. C. Gay

To be published in Sep. Purif. Technol.

The Isotopic Composition of Atmospheric Methane and Its Sources

C. M. Stevens and M. Wahlen

To be published in *Atmospheric Methane*, Ed., M. A. K. Khalil, Springer-Verlag

Thermodynamic and Nonstoichiometric Behavior of the $GdBa_2Cu_3O_x$ System

M. Tetenbaum, D. Diana, B. S. Tani, and M. Blander

To be published in the Proc. of the First China Int. Conf. on High Performance Ceramics, Beijing, China, Tsingua University Press

The Li-Mn-O Phase Diagram and Its Importance for Rechargeable Lithium/Spinel Cells

M. M. Thackeray

To be published in ITE Battery Letters

Stabilization of Insertion Electrodes for Lithium Batteries

M. M. Thackeray, C. S. Johnson, A. J. Kahaian, K. D. Kepler, J. T. Vaughey, Y. Shao-Horn, and S. A. Hackney

To be published in J. Power Sources

Composite Electrodes for Lithium Batteries

M. M. Thackeray, K. D. Kepler, J. T. Vaughey, A. J. Kahaian, C. S. Johnson, Y. Shao-Horn, and S. A. Hackney

To be published in Prog. Batteries Battery Mater.

Stabilization of Rocky Flats Pu-Containing Ash within Chemically-Bonded Phosphate Ceramics

A. S. Wagh, R. V. Strain, S.-Y. Jeong, D. T. Reed, T. R. Krause, and D. Singh

To be published in J. Nucl. Mater.

L-Edge X-ray Absorption Spectroscopy of Some Ni Oxycompounds: Ni Oxidation States

H. Wang, M. Balasubramanian, C. A. Melendres, and S. P. Cramer

To be published in J. Phys. Chem.

Distribution for ANL-99/10

Internal:

D. P. Abraham
J. P. Ackerman (75)
S. Ahmed
K. Amine
J. M. Andrew
J. G. Asbury
A. J. Bakel
J. E. Battles
P. R. Betten (5)
S. K. Bhattacharyya
I. D. Bloom
A. S. Boparai
D. L. Bowers
L. M. Boxberger
E. C. Buck
J. D. Carter
D. J. Chaiko
D. B. Chamberlain
Y. I. Chang
L. S. H. Chow
J. C. Cunnane
D. W. Dees
L. W. Deitrich
H. Drucker
B. D. Dunlap
W. L. Ebert
R. E. Einziger
P. A. Finn
J. Fortner
S. C. Foster
F. Y. Fradin
E. C. Gay
M. M. Goldberg
K. V. Gourishankar
D. G. Graczyk
D. W. Green
D. M. Gruen
J. E. Harmon (3)
J. E. Helt
G. L. Henriksen
D. J. Hill
L. R. Johnson
E. J. Karell
T. D. Kaun
J. P. Kopasz
T. R. Krause
M. Krumpelt
R. Kumar
J. J. Laidler
L. Leibowitz
R. A. Leonard
M. A. Lewis
M. J. Lineberry
J. S. Luo
V. A. Maroni
S. M. McDeavitt
W. D. McFall
J. F. Miller
W. E. Miller
D. J. Myers
L. Nuñez
W. H. Perry
W. F. Podolski
R. B. Poeppel
J. W. Rathke
D. T. Reed
M. K. Richmann
W. W. Schertz
D. K. Schmalzer
D. L. Smith
M. J. Steindler
W. M. Swift
S.-W. Tam
M. Thackeray
M. C. Thurnauer
Z. Tomczuk
G. F. Vandegrift
D. C. Wade
L. C. Walters
R. W. Weeks
C. L. Wilkinson
J. L. Willit
S. F. Wolf
A. M. Wolsky
R. D. Wolson
TIS Files

External:

DOE-OSTI (2)
ANL-E Library
ANL-W Library
A. Bindokas, DOE-CH
P. M. Ferrigan, DOE-CH
J. C. Haugen, DOE-CH
S. Ludwig, DOE-CH
R. L. San Martin, DOE-CH
A. L. Taboas, DOE-CH
J. R. LaFevers, DOE-UC

Chemical Technology Division Review Committee Members:

H. U. Anderson, University of Missouri-Rolla, Rolla, MO
E. R. Beaver, Monsanto Company, St. Louis, MO
A. L. Bement, Purdue University, West Lafayette, IN
M. V. Koch, University of Washington, Seattle, WA
R. A. Osteryoung, North Carolina State University, Raleigh, NC
V. P. Roan, University of Florida, Palm Beach Gardens, FL
G. R. St. Pierre, Ohio State University, Columbus, OH
R. C. Alkire, University of Illinois, Champaign, IL
R. A. Bajura, USDOE, Federal Energy Technology Center, Morgantown, WV
S. Barker, Lockheed Martin Hanford Company, Richland, WA
S. E. Berk, USDOE, Office of Fusion Energy, Germantown, MD
A. L. Boldt, Lockheed Martin Hanford Company, Richland, WA
G. G. Boyd, USDOE, Office of Science and Technology, Washington, DC
S. A. Butter, USDOE, Office of Basic Energy Sciences, Washington, DC
L. Camara, MC Power Corporation, Burr Ridge, IL
M. H. Campbell, MACTECH, Richland, WA
K. A. Chacey, USDOE, Office of Environmental Management, Germantown, MD
S. G. Chalk, USDOE, Office of Transportation Technologies, Washington, DC
H. Cost, Chrysler Corporation, Auburn Hills, MI
P. Davis, USDOE, Office of Transportation Technologies, Washington, DC
C. Donnelly, 3M Center, St. Paul, MN
J. Dunning, GM EV, Troy, MI
T. Dvong, USDOE, Office of Transportation Technologies, Washington, DC
J. J. Eberhardt, USDOE, Office of Transportation Technologies, Washington, DC
R. E. Erickson, USDOE, Office of Environmental Management, Germantown, MD
G. Escobar, LATO Office Rocky Flats Plant, Golden, CO
R. C. Ewing, University of Michigan, Ann Arbor, MI
R. J. Fiskum, USDOE, Office of Building Energy Research, Washington, DC
M. W. Frei, USDOE, Office of Waste Management, Germantown, MD
T. Fryberger, Pacific Northwest National Laboratory, Richland, WA
D. R. Funk, USDOE, Office of Nuclear Energy, Germantown, MD
D. Geiser, USDOE, Office of Technology Development, Germantown, MD
M. R. Ghate, USDOE, Federal Energy Technology Center, Morgantown, WV
R. Gilchrist, Pacific Northwest National Laboratory, Richland, WA
T. J. Gross, USDOE, Office of Transportation Technologies, Washington, DC
H. Haskins, Ford Motor Company, Dearborn, MI
K. L. Heitner, USDOE, Office of Transportation Technologies, Washington, DC
T. M. Hohl, COGEMA Engineering Corporation, Richland, WA
N. Iyer, Westinghouse Savannah River Company, Aiken, SC
G. Jansen, Lockheed Martin Hanford Company, Richland, WA
L. J. Jardine, Lawrence Livermore National Laboratory, Livermore, CA
E. F. Johnson, Princeton University, Princeton, NJ
E. Jones, Pacific Northwest National Laboratory, Richland, WA
F. Kane, University of Idaho, Moscow, ID
R. D. Kelley, USDOE, Office of Basic Energy Sciences, Germantown, MD
C. Kincaid, USDOE, Office of Nonproliferation and National Security, Washington, DC

R. Kinney, 3M Industrial and Electronic Sector Research Laboratory, St. Paul, MN
R. S. Kirk, USDOE, Office of Transportation Technologies, Washington, DC
B. Knutson, Lockheed Martin Hanford Company, Richland, WA
L. J. Krause, 3M Industrial and Electronic Sector Research Laboratory, St. Paul, MN
K. Krist, Gas Research Institute, Chicago, IL
S. C. T. Lien, USDOE, Office of Technology Development, Germantown, MD
P. Loscoe, USDOE, Richland Operations Office, Richland, WA
G. J. Lumetta, Pacific Northwest National Laboratory, Richland, WA
W. D. Magwood, USDOE, Office of Nuclear Energy, Washington, DC
P. Marpin, USDOE, Office of Science, Germantown, MD
B. P. McGrail, Pacific Northwest National Laboratory, Richland, WA
J. Milliken, USDOE, Office of Transportation Technologies, Washington, DC
A. C. Muscatello, Rocky Flats Plant, Golden, CO
R. J. Nowak, DARPA/DSO Defense Sciences Office, Arlington, VA
J. B. O'Sullivan, Electric Power Research Institute, Palo Alto, CA
A. L. Olson, Lockheed Idaho Technology Company, Idaho Falls, ID
J. Owendoff, USDOE, Office of Environmental Management, Washington, DC
P. G. Patil, USDOE, Office of Transportation Technologies, Washington, DC
R. Paur, Army Research Office, Research Triangle Park, NC
D. Pepson, USDOE, Office of Waste Management, Germantown, MD
R. Person, USDOE, Materials Disposition, Washington, DC
L. Petrakis, Brookhaven National Laboratory, Upton, NY
S. T. Picraux, Sandia National Laboratories, Albuquerque, NM
G. Reddick, Lockheed Martin Hanford Company, Richland, WA
S. Rogers, USDOE, Office of Transportation Technologies, Washington, DC
P. S. Schaus, Lockheed Martin Hanford Company, Richland, WA
L. H. Schwartz, National Institute of Standards and Technology, Gaithersburg, MD
A. W. Searcy, Lawrence Berkeley Laboratory, Berkeley, CA
R. W. Shivers, USDOE, Office of Conservation, Washington, DC
W. A. Siegel, USDOE, Office of Transportation Technologies, Washington, DC
M. I. Singer, USDOE, Advanced Research/Special Technologies, Washington, DC
S. Singhal, Westinghouse Electric Corporation, Pittsburgh, PA
E. Slaathug, Lockheed Martin Hanford Company, Richland, WA
C. Sloane, GM Research and Development Center, Warren, MI
D. Stahl, Framatome Cogema Fuels, Las Vegas, NV
R. B. Stout, Lawrence Livermore National Laboratory, Livermore, CA
J. P. Strakey, USDOE, Federal Energy Technology Center, Pittsburgh, PA
R. A. Sutula, USDOE, Office of Transportation Technologies, Washington, DC
R. Swaroop, Electric Power Research Institute, Palo Alto, CA
T. A. Thornton, Framatome Cogema Fuels, Las Vegas, NV
J. A. Turi, USDOE, Office of Environmental Management, Germantown, MD
University of California, Government Documents Department, Berkeley, CA
M. Williams, USDOE, Federal Energy Technology Center, Morgantown, WV
R. E. York, General Motors Corporation, Warren, MI
C. Zeh, USDOE, Federal Energy Technology Center, Morgantown, WV
S. Zimmer, Chrysler Corporation, Auburn Hills, MI
R. J. Harrison, Atomic Energy of Canada, Ltd., Chalk River, Ontario, CANADA
M. Ozawa, PNC Tokai-Works, Ibaraki-ken, JAPAN